Investigating the Genetic Basis of Autoimmune Disease



Rose Hodgson

Nuffield Department of Medicine
St John's College
University of Oxford

Supervisors:
Richard Cornall
Katherine Bull

DPhil in Clinical Medicine
Michaelmas 2021

Acknowledgements

Firstly, I would like to thank Katherine Bull and Richard Cornall for their endless support. Richard has been a constant supply of enthusiasm and dad jokes, full of infinite ideas for the next experiment, but also for support of the path that was right for me. Katherine has offered me so much more than scientific conversations and direction, she has provided a shoulder to lean on as both a supervisor and a friend and has shared so much of her experience, perspective and advice.

I would also like to extend huge gratitude to past and present Cornall and Bull lab members; thank you to Mukta, who always went above and beyond the role of post-doc, who has endless patience for listening and explaining, and provides sunshine in everything she does. Also, to Consuelo for your enthusiasm and insight that definitely wasn't limited to immunology and to Tanya for all the advice, in the lab and in life. Thank you to Aneesha for always taking the bone marrows, to Jenny for netball conversations, to Xijin for getting me through second year, to Robot for dealing with #7 and to Jianwei for your endless generosity. Thank you also to Lucy, Tom and Marsha from the Davison/O'Callaghan lab, for your expertise across coding, life choices and tea break snacks, and to Jie, Chris, Martin, Betina, Eleanor and Belinda for making the Cornall/Bull labs such a lovely place.

Particular thanks go to Emily, Jess and Mary for reminding me you're only an espresso martini away from forgetting that failed experiment. To Melis, Janine, Lucy and Issy; we've dragged each other through all the failings that accompanied the successes, of which I am so proud of us for. To Chris, Saj, Harrold and the extended Shadwell crew for all the laughs that popped the Oxford bubble each week.

I hugely appreciate all the love and support that my Mum, Dad, Dill, and even sometimes my brother, Joe have given. Thank you for grounding me, brightening my world and for being on the

end of the line at 2am when it all got too much on the FACS machine. Also to my grandparents, on both sides, who are amazing role models and have provided careers to aspire to.

Last but not least, to my amazing partner, Alex. What is there to say, except for thank you for always being my boulder, through the highs and the many lows, for always loving me at the end of the day, and for learning how to describe B cell anergy to all our friends.

Abstract

The maintenance of immune tolerance is essential to prevent the initiation of inappropriate and potentially harmful responses by autoreactive lymphocytes. Autoimmune diseases are ultimately caused by a loss of tolerance to self; this can be driven by rare genetic variants; however, the aetiologies are more often complex, covering an incompletely understood combination of environmental, immunological and common genetic risk factors. Since rare monogenic disorders can illuminate mechanisms relevant to common disease, furthering our knowledge of the inherited mechanisms that affect tolerance loss may help to advance treatment options across many immune disorders, beyond current strategies of broad immunosuppression with limited efficacy and significant side effects. Using forward and reverse genetics approaches and engineered *in vivo* models, this thesis aims to establish whether two genes, N-myc Downstream-Regulated Gene 1 (*Ndrg1*) and *Pepd*, with apparent roles in the maintenance of immune tolerance, do alter the threshold for autoimmunity and begin to explore how this is mediated.

NDRG1 is a tumour suppressor that has previously been implicated as a $CD4^+$ T-cell clonal anergy factor, induced by T cell receptor (TCR) signalling and negatively regulated by co-stimulation. By RNA Sequencing (RNA-Seq), the Cornall lab previously identified *Ndrg1* as the third highest differentially expressed gene in anergic B cells compared to naïve follicular B cells. In this thesis, I show that *Ndrg1* is upregulated by activation of the B cell receptor (BCR) (signal one) and suppressed by positive co-stimulation (signal two), initially suggesting that NDRG1 may also play an important role in B cell tolerance. To analyse the function of NDRG1 in B cells, I describe here the generation of a $Ndrg1^{-/-}$ knockout mouse model using directed clustered regularly interspaced short palindromic repeats (CRISPR)/CRISPR-associated nuclease (Cas9) mutagenesis. NDRG1-deficient mice have a neurological defect characteristic of Charcot-Marie-Tooth Type 4d (CMTD4d) disease but a normal primary and secondary immune response, and induction of anergy is normal.

This work shows that NDRG1 is not required for the maintenance of B cell tolerance and does not play a role in downstream responses during re-stimulation of *in vivo* antigen-experienced $CD4^+$ T cells.

In contrast to reverse genetics targeting of suspected immune-involved genes, phenotype-driven screening programmes provide an alternative way to discover novel genes and regulatory pathways involved in maintaining immunological tolerance. A novel mouse model with hallmarks of autoimmunity identified within an autoimmune screening programme presents potential to provide insight into the pathogenesis of prolidase deficiency (PD). Patients with PD present with a multi-system disorder including symptoms concurrent with immunodeficiency, though many also have autoimmune characteristics and 6% meet the criteria to be diagnosed with systemic lupus erythematosus (SLE). PD is known to be caused by mutations in the *PEPD* gene, but is unclear whether prolidase directly regulates immune tolerance or whether autoimmunity is a secondary complication, in addition to a primary immunodeficiency. A murine *Pepd* null mouse provides a tool to explore the immunological basis of this disease and more general adaptive tolerance mechanisms.

Deep characterisation of the mouse model of PD in this thesis demonstrates that *Pepd* loss is associated with autoimmunity, with some elevation of anti-nuclear antibodies (ANAs), increased serum IgA and a histological phenotype reminiscent of human immune complex nephropathy in SLE patients, with glomerular IgA, IgG and C1q deposition. Deep immunophenotyping using flow cytometry and multimodal single cell RNA sequencing (scRNA-Seq) demonstrates that prolidase modulates $CD8^+$ T cell fate, characterised by accumulation of $CD8^+$ effectors expressing a transcriptional signature concurrent with chronic exhaustion, whilst resting populations are reduced. Mixed chimeras confirm that this phenotype is intrinsic, and *in vivo* labelling suggests that more proliferating cells adopt this exhausted phenotype independent of TCR specificity or antigenic

stimulation, which results in the accumulation of these populations in sites of likely breakdown. These mechanistic insights shed light how prolidase regulates self-tolerance as well as pathways involved in $CD8^+$ T cell differentiation, highlighting the potential of studying rare genetic variants implicated in human disease.

Table of Contents

Acknowledgements ***2***

Abstract ***4***

Acronyms & Abbreviations ***10***

List of Figures ***13***

List of Tables ***16***

List of Appendices ***16***

1. Introduction ***17***

1.1 Overview; tolerance maintains immune homeostasis to prevent autoimmune disease **17**

1.2 Central tolerance during lymphocyte development; antigen receptors are tested at several checkpoints **18**

1.2.1 The BCR is positively and negatively tested for antigen binding in the bone marrow 18

1.2.3 Central T cell tolerance in the thymus 21

1.3 Maintaining tolerance in the periphery **23**

1.3.1 Peripheral B cell subset differentiation 24

1.3.2 Peripheral T cell subset differentiation 25

1.3.3 The two-signal hypothesis of lymphocyte activation and anergy 26

1.3.4 The role of regulatory T cells in peripheral tolerance 29

1.3.5 Maintaining tolerance in the germinal centre 30

1.4 Understanding the mechanisms of autoimmune disease **32**

1.4.1 Genetic basis of autoimmunity 33

1.4.2 External triggers of autoimmune disease 35

1.5 Modelling mechanisms of autoimmunity using *in vivo* models **36**

1.5.1 Targeted gene editing approaches to exploring disease pathogenesis 38

1.5.2 Forward genetics; phenotype-driven studies 40

1.5.3 Transgenic mouse models; tools to study mechanisms of immune tolerance 43

1.6 Summary and aims of thesis **44**

2. Materials and Methods ***47***

2.1 Animal work **47**

2.1.1 Breeding and maintenance 47

2.1.2 CRISPR-Cas9 mutagenesis-creation of *Ndrg1*$^{-/-}$ mouse model 48

2.1.3 Immunisation 49

2.1.4 Irradiation BM chimeras 49

2.1.5 Sample processing 50

2.2. Cellular assays **50**

2.2.1 *Ex vivo* cell sorting, culture and stimulation 50

2.2.2 Flow cytometry 51

2.2.3 Phospho-FLOW and intracellular staining 51

2.2.4 Fluorescent activated cell sorting (FACS) 52

2.2.5 In vivo T cell anergy experiments 52
2.2.6 Mass cytometry immunophenotyping 53

2.3 Transcriptomic profiling 57
2.3.1 Bulk RNA-Seq 57
2.3.2 Single cell RNA and ADT proteomic sequencing 58
2.3.3 Quantitative real-time PCR 60

2.4 Molecular analyses 61
2.4.1 Western blot 61
2.4.2 ELISA 61
2.4.3 Anti-nuclear antibody staining 62

2.5 Histology 62
2.5.1 Tissue fixation and sectioning 62
2.5.2 H & E staining 63
2.5.3 Immunohistochemistry 63

2.6 Statistical analysis 64

3. NDRG1, a tumour suppressor protein involved in regulating growth and apoptosis . 65

3.1 Chapter introduction 65

3.2 Results 67
3.2.1 *Ndrg1* expression is associated with B cell anergy 67
3.2.1.2 *Ndrg1* is induced by BCR signalling but suppressed by positive co-stimulation 69
3.2.2 A mouse model of NDRG1 deficiency 70
3.2.3 Investigating the role of NDRG1 in B cell anergy 74
3.2.4 NDRG1 loss does not affect B cell anergic responses in the periphery 80

3.3 Summary of chapter 83

4. Investigating the role of Ndrg1 in T cells 85

4.1 Chapter introduction 85

4.2 Results 86
4.2.1 NDRG1 is not required for development of the pre-immune T cell repertoire .. 86
4.2.2 NDRG1 loss does not affect primary T cell responses to foreign antigen 87
4.2.3 Exploring the role of NDRG1 in T cell tolerogenic assays 87

4.3 Summary of chapter 91

5. A rare genetic disorder with features of human monogenic lupus-like disease 93

5.1 Introduction to chapter 93

5.2 Results 96
5.2.1 Prolidase deficiency causes loss of immune tolerance characterised by raised serum IgA titres and SLE-like renal immune complex deposition 97
5.2.2 Immunophenotyping of *Pepd*$^{-/-}$ lymphocyte populations identifies an altered B cell phenotype and increases in activated T cell populations 98
5.2.3 Multimodal scRNA-Seq analysis shows that loss of prolidase is associated with an accumulation of exhausted effector CD8^{+} T cells and loss of *Ly6c2*$^{+}$ memory precursor effector cell (MPEC)-like populations 103

5.2.4 Cytometric approaches confirm splenic CD8+ T cell phenotype associated with prolidase deficiency 114
5.3 Summary of chapter 118
6. Drivers of CD8+ exhausted effector T cell accumulation with Pepd loss 120
6.1 Introduction to chapter 120
6.2 Results 121
6.2.1 Cell intrinsic prolidase loss drives the activated T cell phenotype 121
6.2.3 The T cell phenotype associated with prolidase loss is driven by increased differentiation of proliferating cells into exhausted effectors 127
6.2.4 *Pepd*-/- exhausted populations accumulate in the liver in an intrinsic manner 129
6.2.4 The accumulation of exhausted CD8+ T cells associated with prolidase loss is antigen-independent 131
6.3 Summary of chapter 135
7. Discussion 137
7.1 The role of *Ndrg1* in tolerance is relevant for the development of anti-cancer therapies. 137
7.1.1 NDRG1 represents a redundant biomarker of chronically stimulated lymphocytes 138
7.1.2 Understanding the association of NDRG1 expression in lymphocyte anergic responses 139
7.1.3 Limitations of the gene-editing approaches used to model the role of NDRG1 in lymphocyte anergy 142
7.1.4 Modelling adaptive tolerance requires appropriate models and controls 143
7.2 Prolidase deficiency drives autoimmunity 145
7.2.1 The role of prolidase in T cell differentiation and associated disease relevance 146
7.2.2 *Pepd* deficiency in the regulation of humoral immunity and renal immune complex deposition 150
7.2.3 Future insights into modelling prolidase deficiency 152
7.3 The future of human autoimmune disease models 154
7.3.1 Modelling human genetics; limitations of genetic targeting approaches 155
7.3.2 Validating and translating findings from mouse models of human autoimmune disease to the clinic 157
7.4 Conclusions 159
References 160
Appendix 200

Acronyms & Abbreviations

3i	Infection and Immunity Immunophenotyping
ACPAs	anti-citrullinated protein antibodies
ADT	antibody-derived tag
AIRE	autoimmune regulator gene
ANA	anti-nuclear antibody
ANOVA	Analysis of variance
APC	antigen presenting cell
Ars/A1	arsonate model of B cell anergy
APS-1	autoimmune polyglandular syndrome type 1
BAFF	B cell activating factor
Bcl2	B cell lymphoma 2
BCR	B cell receptor
Bim	Bcl-2 interacting mediator of cell death
BM	bone marrow
BrdU	bromodeoxyuridine
Cas9	CRISPR-associated (Cas)-9
CLR	centered log ratio
CI	confidence interval
CyTOF	time of flight mass cytometry
CMTD	Charcot Marie Tooth Disease
CRISPR	clustered regularly interspaced short palindromic repeats
crRNA	CRISPR RNA
cTEC	cortical thymic epithelial cells
CTLA4	cytotoxic T-lymphocyte antigen 4
CTV	cell trace violet
DC	dendritic cell
DN	double negative
Dock8	Dedicator of cytokinesis 8
DP	double positive
dsDNA	double stranded DNA
DW	distilled water
DZ	dark zone
ETP	early thymic precursor

ENU	N-ethyl-N-nitrosourea
ES	embryonic stem
EUCOMM	European Conditional Mouse Mutagenesis
FACS	Fluorescence-activated cell sorting
FCS	fetal calf serum
FGSEA	fast gene set enrichment analysis
GC	germinal centre
GVHD	graft versus host disease
GWAS	genome-wide association studies
HC	heavy chain
HEL	hen-egg lysozyme
HEL-SRBC	HEL conjugated to SRBC
HLA	human leukocyte antigen
HSC	haemopoietic stem cell
HTO	hashtag information
ICOS	inducible T cell costimulator
IMPC	International Mouse Phenotyping Consortium
ITAM	immunoreceptor tyrosine based activation motifs
KOMP	National Institutes of Health Knockout Mouse
LC	light chain
LZ	light zone
MAPK	mitogen activated protein kinase
MD4/IgHEL	HEL-specific BCR
MHC	major histocompatibility complex
mTEC	medullary thymic epithelial cells
MVA	modified vaccinia Ankara virus
MZ	marginal zone
NDRG1	N-myc Downstream-Regulated Gene 1
NFAT	Nuclear factor of activated T-cells
OT-I	Ovalbumin-specific TCR transgene
OVA	Ovalbumin
PAM	protospacer adjacent motif
PAMR	predictive association model
PD1	programmed cell death protein 1
RNA-Seq	RNA-Sequencing
PI3K	phosphoinositol 3-kinase

PRR	pattern recognition receptor
pT_{reg}	peripherally derived Tregs
RA	rheumatoid arthritis
RAG	recombination activating gene
RBC	red blood cell
RNA-Seq	RNA sequencing
SAP	SLAM-associated protein
scRNA-Seq	single cell RNA-Seq
SE	suicidal emperipolesis
sgRNA	single-guide RNA
sHEL	soluble HEL
SHM	somatic hypermutation
SLAM	signalling lymphocytic activation molecule
SLE	Systemic Lupus Erythematosus
SNP	single nucleotide polymorphism
SP	Single positive
SRBC	sheep red blood cells
T1DM	Type 1 Diabetes Mellitus
TCR	T cell receptor
T_{FH}	T follicular helper cells
T_{FR}	T follicular regulatory T cells
Tg	transgenic
TLR	Toll-like receptor
tracrRNA	trans-activating CRISPR RNA
T_{reg}	regulatory T cells
TREX1	3'repair exonuclease 1
tSNE	t-distributed stochastic neighbour embedding
tT_{reg}	thymically derived regulatory cells
UMAP	uniform manifold approximation and projection
WNN	weighted nearest neighbour

List of Figures

Figure 1.1 Tolerance checkpoints during lymphocyte development in central lymphoid organs. 20
Figure 1.2 Peripheral tolerance maintenance prevents autoimmunity 26
Figure 3.1 NDRG1 is induced by stress and hypoxia signals and is proposed to regulate multiple signalling pathways. 66
Figure 3.2 Ndrg1 is associated with B cell anergy 69
Figure 3.3 Ndrg1 expression is regulated by the signal one/signal two axis in B cells 70
Figure 3.4 Creation of a $Ndrg1^{-/-}$ mouse model by directed CRISPR/Cas9 mutagenesis 71
Figure 3.5 Normal B cell development in the absence of NDRG1 73
Figure 3.6 $Ndrg1^{-/-}$ mice respond normally to foreign antigen 74
Figure 3.7 NDRG1 loss is not associated with loss of tolerance at baseline 75
Figure 3.8 Intrinsic B cell tolerance is intact in the absence of NDRG1 75
Figure 3.9 Anergy induction during development is normal during NDRG1 loss 77
Figure 3.10 Chronic self-antigen exposure mediated inhibition of TLR-signalling is equivalent in $Ndrg1^{-/-}$ anergic B cells 78
Figure 3.11 Anergic B cells lacking NDGR1 survive and compete normally in a polyclonal repertoire 79
Figure 3.12 NDRG1 deficiency does not provide an advantage in the presence of competing clonal anergic B cells 80
Figure 3.13 NDRG1-deficient B cells exposed to self-antigen in the periphery are subject to follicular exclusion and cell death 82
Figure 3.14 NDRG1 loss does not affect BCR-mediated apoptosis 83
Figure 4.1 T cell development is normal in $Ndrg1^{-/-}$ mice 86
Figure 4.2 $Ndrg1^{-/-}$ $CD4^{+}$ and $CD8^{+}$ T cells show normal activation in response to foreign antigen. 87
Figure 4.3 Antigen-experienced T cells respond normally in the absence of NDRG1 88
Figure 4.4 Antigen-experienced $CD4^{+}$ T cells proliferate more in the last 24h culture than naïve $CD4^{+}$ regardless of assay readout 89
Figure 4.5 Ag-experienced $CD4^{+}$ T cells intrinsically produce elevated IL-2 and IFNy than naïve $CD4^{+}$ T cells 91
Figure 5.1 Proposed molecular functions of prolidase 94
Figure 5.2 Pepd deficiency is associated with loss of immune tolerance in mice 97

Figure 5.3 Pepd$^{-/-}$ mice are smaller than WT controls 97
Figure 5.4 Serum IgA levels are specifically raised with loss of prolidase 98
Figure 5.5 Loss of prolidase is associated with SLE-like renal immune complex deposition 98
Figure 5.6 Pepd loss is associated with an altered B cell phenotype 100
Figure 5.7 B cell anergy is intact in the absence of prolidase expression..... 101
Figure 5.8 Pepd$^{-/-}$ mice have a peripherally activated T cell phenotype 102
Figure 5.9 Pepd$^{-/-}$ mice have an activated T cell phenotype through development..... 103
Figure 5.10 Multimodal proteomic and transcriptomic sequencing of WT and Pepd$^{-/-}$ splenic T cell populations; quality control and filtering..... 104
Figure 5.11 ADT clustering identifies enrichment of Pepd$^{-/-}$ CD8^{+} effector cells..... 106
Figure 5.12 Pepd$^{-/-}$ CD8^{+} effector cells have an altered transcriptional phenotype..... 108
Figure 5.13 WNN-mediated analysis of CD8^{+} populations identifies enrichment of exhausted CD8^{+} effectors and loss of resting populations with Pepd deficiency 109
Figure 5.14 Trajectory analysis and differential gene expression demonstrate Pepd loss drives altered differentiation 113
Figure 5.15 Confirmation of the CD8^{+} phenotype associated with Pepd deficiency..... 115
Figure 5.16 Cytofkit profiling confirms loss of Ly6c-expressing CD8^{+} and trend increases in activated CD8^{+} populations in Pepd$^{-/-}$ mice compared to WT populations 116
Figure 5.17 Citrus CyTOF analysis highlights altered surface phenotype of CD8^{+} Pepd$^{-/-}$ populations 117
Figure 6.1 The T lymphocyte phenotype is driven by intrinsic loss of Pepd expression in mixed BM chimeras 122
Figure 6.2 The B lymphocyte phenotype is driven by intrinsic loss of Pepd expression in mixed BM chimeras 123
Figure 6.3 Quality control of multimodal scRNAseq of chimeric CD45.2^{+} WT and Pepd$^{-/-}$ T cells 124
Figure 6.4 scRNAseq demonstrates exhausted CD8^{+} T cell phenotype is intrinsically driven by prolidase deficiency 126
Figure 6.5 Bcl2 expression at the protein level is not affected by prolidase loss 127
Figure 6.6 Proliferating pepd-deficient T cell populations are more likely to adopt an exhausted phenotype 128
Figure 6.7 Exhausted CD8^{+} effectors accumulate in the liver on prolidase loss 130

Figure 6.8 Cell-intrinsic loss of Pepd leads to hepatic accumulation of $CD8^+$ $PD1^+$ effectors with equivalent survival and apoptosis markers 130
Figure 6.9 The T cell phenotype partially rescued by transgenic TCR expression 132
Figure 6.10 The $Pepd^{-/-}$ $CD8^+$ phenotype is antigen-independent 133
Figure 6.11 TCR-mediated proliferation is unaffected by Pepd deficiency 134
Figure 6.12 $Pepd^{-/-}$ $CD8^+$ OT-I cells compete and produce comparable cytokine amounts in response to antigenic stimulation 134

List of Tables

Table 2.1 CyTOF antibody panel 55

Table 3.1 Anergic B cells lacking NDGR1 survive and compete normally in a polyclonal repertoire 78

List of Appendices

Appendix A. Antibodies used for flow cytometry 200

Appendix B. Top differentially expressed genes between anergic and naïve follicular B cells 203

Appendix C RNA cluster markers of ADT-marker defined splenic T cell clusters (Figure 5.11) 218

Appendix D RNA cluster markers of WNN-clustered splenic $CD8^+$ populations (Figure 5.13) 221

Appendix E Differential gene expression analysis between splenic $CD8^+$ CEM populations, 2.$Ly6c2^+$CEM and 3.CEM as visualised in Figure 5.13E 223

Appendix F Differential gene expression analysis between splenic $CD8^+$ effector populations, 4.Exhausted effector and 5.Terminal effector as visualised in Figure 5.13F 229

Appendix G Differential surface phenotype of CD8+ populations identified by Citrus clustering analysis 232

Appendix H RNA cluster markers of WNN-clustered $CD8^+$ $CD45.2^+$ chimeric subsetted populations visualised in Figure 6.4 233

Appendix I Differential gene expression analysis between $CD45.2^+$ chimeric splenic $CD8^+$ effector populations, 4.Exhausted effector and 6.Terminal effector as visualised in Figure 6.4D 236

1. Introduction

1.1 Overview; tolerance maintains immune homeostasis to prevent autoimmune disease

Autoimmune diseases, such as rheumatoid arthritis (RA), thyroiditis, coeliac disease and type 1 diabetes (T1DM), affect around 5-10% of the world's population (Marson, Housley and Hafler, 2015; Laxminarayana, 2017). These auto-inflammatory syndromes are ultimately explained by a loss of self-tolerance, although the genetic, immunological and environmental drivers are not fully understood. Consequently, most treatment options are based on broad spectrum immunosuppression, and better mechanistic understanding is needed in order to develop more targeted or preventative treatment options (Vojdani, Pollard and Campbell, 2014; Marson, Housley and Hafler, 2015; Chung and Shum, 2016). Rare cases are monogenic, but most have a complex genetic component to risk, evidenced by heritability in families and by genome wide association studies (Vyse and Todd, 1996; Jiang, Stanley and Vinuesa, 2020). Study of rare variants with large effect sizes can provide a tractable way to discover novel genes and regulatory pathways involved in maintaining immunological tolerance, to ultimately improve therapeutic options for patients with both rare and complex common forms of disease.

This thesis describes approaches to explore how two genes, *Ndrg1* and *Pepd*, are implicated in regulating immune tolerance with the aim of furthering the understanding of mechanisms driving autoimmune disease. Two *in vivo* genetic knockout models are characterised here in combination with established transgenic (tg) murine tools, to explore how loss of *Ndrg1* or *Pepd* modulates the balance between the recognition of self and non-self within the immune system.

1.2 Central tolerance during lymphocyte development; antigen receptors are tested at several checkpoints

Whereas the innate arm of our immune response is restricted to respond to a pre-defined set of molecular patterns using germline-encoded receptors, the adaptive response coordinates huge receptor diversity through gene recombination and lymphocyte selection events. Divergence of the jawed fish was accompanied by the emergence of the recombination-activating gene (RAG) transposon, recombinases which drive the rearrangement of non-germline encoded antigen receptors, forming the basis for adaptive immunity (Flajnik and Kasahara, 2010). As a result, in addition to pattern recognition receptors (PRR), B and T lymphocytes recognise specific antigens via the B cell receptor (BCR) and T cell receptor (TCR), respectively (Elhanati *et al.*, 2015). Each lymphocyte expresses receptors of a single specificity; however, the adaptive immune system spans a hugely diverse repertoire due to random gene-shuffling recombination events and diversification during lymphocyte development (Briney and Crowe, 2013). Inevitably, some self-reactive antigen receptors are produced, hence tolerance mechanisms are essential throughout lymphocyte development to prevent the development of autoimmunity (Yarkoni, Getahun and Cambier, 2010; Xing and Hogquist, 2012). Self-reactivity of antigen receptors is tested at several points of lymphocyte development, with lymphocytes positively and negatively selected on the basis of their binding properties.

1.2.1 The BCR is positively and negatively tested for antigen binding in the bone marrow

During B cell development in the mouse bone marrow (BM), multiple tolerance checkpoints must be passed, as summarised in figure 1.1. Positive selection first tests for successful rearrangements of heavy chain (HC) immunoglobulin (Ig) upon its incorporation and expression as the pre-BCR on the surface of large pre-B cells. First initiated in the pro-B cell by transcriptional programming, RAG genes drive recombination of μ HC immunoglobin, which is expressed with a germline encoded invariant light chain (LC), either VpreB1 or 2 and λ5 to assemble the pre-BCR (Karasuyama, Kudo and Melchers, 1990; Tsubata and Reth, 1990; Mårtensson and Ceredig, 2000). Once expressed,

progression to the small pre-B cell stage relies on productive pre-BCR signalling feedback through associated invariant signalling proteins, CD79α and CD79β immunoreceptor tyrosine-based activation motifs (ITAM), from interaction with the BM environment (Murphy, Kenneth; Travers, Paul; Walport, 2008; Nemazee, 2017). Unproductive signalling from inefficient HC rearrangement promotes continued HC rearrangement and receptor editing to alter BCR specificity. Successful signalling induces proliferation and halts further HC rearrangement, preventing receptors of multiple specificities being co-expressed in a process called allelic exclusion (Pernis *et al.*, 1965; Alt *et al.*, 1984; Boekel, Melchers and Rolink, 1995) (Vettermann and Schlissel, 2010) .

Once at the small pre-B cell stage, LC rearrangement is initiated to ultimately express mature cell surface Ig of class IgM, that again associates with CD79α and CD79β signalling chains to form the mature BCR complex on the surface of immature B cells. Tonic signalling from productively rearranged BCRs in response to BM ligands inhibits further LC recombination, and drives development into an immature B cell expressing a BCR of a single specificity (Monroe, 2006). Strongly self-binding B cells can re-engage in receptor editing, or rarely die by clonal deletion if editing is unsuccessful (Fig. 1.1). This is directed by BCR-mediated increase in B cell lymphoma 2 (Bcl-2) interacting mediator of cell death (Bim) expression, combined with neglect by insufficient survival factors, including B cell activating factor (BAFF)(Goodnow *et al.*, 2005). B lymphocytes encountering low avidity forms of self-antigen in the BM can be intrinsically induced to express an altered phenotypical, biochemical and genetic profile termed anergy, suppressing their ability to respond to self-antigen (Fig. 1.1)(Goodnow *et al.*, 1988; Ferry *et al.*, 2006; Yarkoni, Getahun and Cambier, 2010).

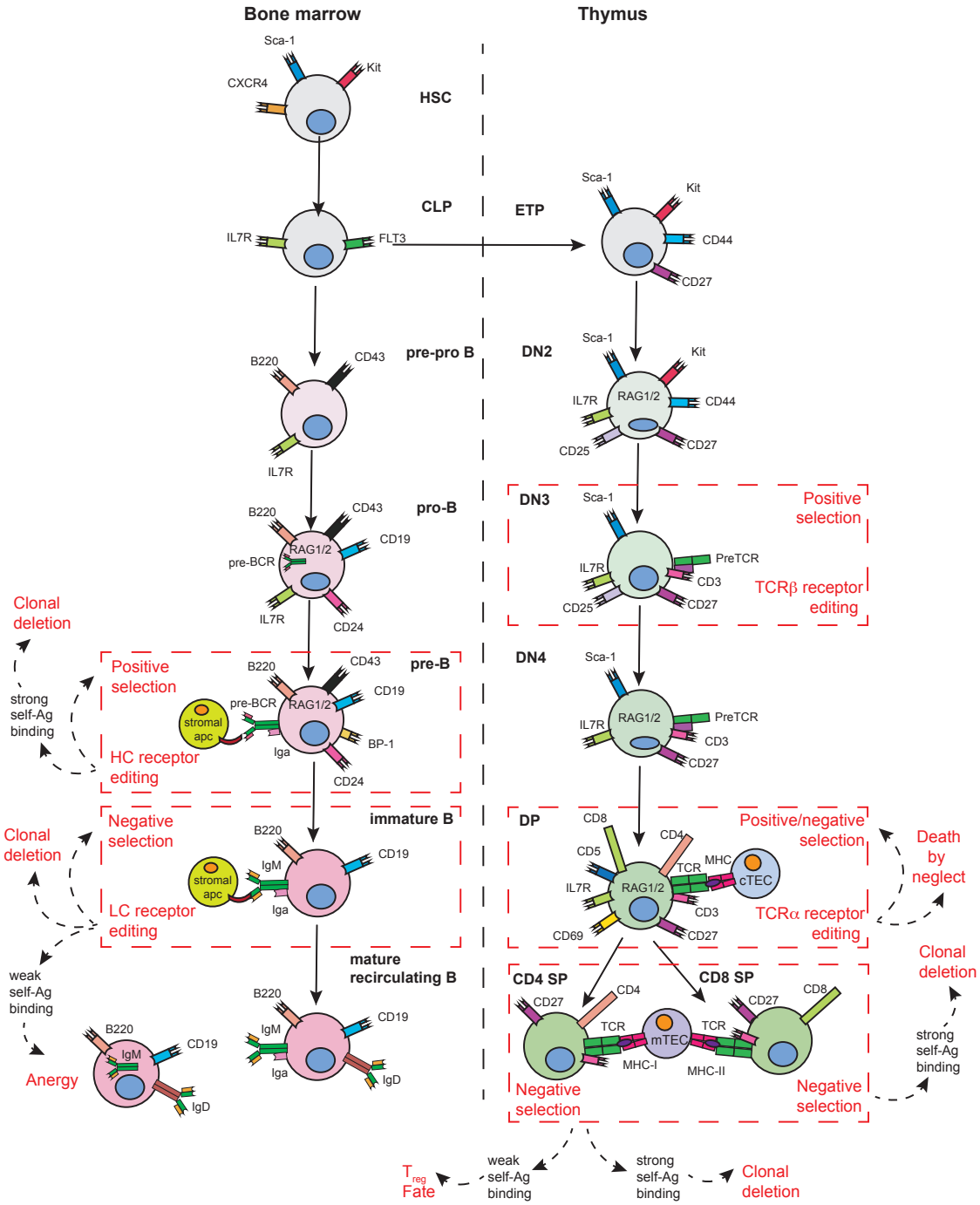


Figure 1.1 Tolerance checkpoints during lymphocyte development in central lymphoid organs.

B and T Lymphocytes developing in the BM and thymus respectively, are subject to multiple tolerance checkpoints dependent on antigen receptor binding and interactions with the surrounding microenvironment. Acronyms previously unused are as follows: Early T cell precursor (ETP), haemopoietic stem cell (HSC), common lymphoid progenitor (CLP), double negative (DN), double positive (DP), single positive (SP), antigen-presenting cell (apc), cortical thymic epithelial cell (cTEC) and medullary TEC (mTEC).

Anergic B lymphocytes emerging into the periphery have an increased threshold for activation due to proximal blockade of BCR-signalling and selective inhibition of IgM trafficking to the cell surface

(Goodnow *et al.*, 1988; Cooke *et al.*, 1994; Cambier *et al.*, 2007). Continual low avidity autoreactive BCR-signalling in the absence of co-stimulation results in chronically low oscillations of calcium, yielding activation of ERK and NFAT dependent pathways (Healy *et al.*, 1997; Barrington *et al.*, 2006; Borde *et al.*, 2006) , but proximal blockade of BCR-dependent signalling and a specific block in JNK, Card11, NF-kB (Healy *et al.*, 1997; Healy and Goodnow, 1998; Weintraub *et al.*, 2000; O'Neill *et al.*, 2011) and pathways downstream of TLRs (Rui *et al.*, 2003, 2006; Cambier *et al.*, 2007). The resultant negative regulatory programme diminishes both responses to stimulation and capacity for cytokine production. Furthermore, an increased dependence on cytokine, BAFF along with raised expression of pro-apoptotic Bim means that anergic B cells have a shortened lifespan in a mixed, non-anergic repertoire (Cyster and Goodnow, 1995; Enders *et al.*, 2003; Lesley *et al.*, 2004). However, anergic B cells can be recruited into the immune response by foreign antigen through high avidity stimulation of the BCR and the provision of antigen-specific T cell help (Fulcher *et al.*, 1996; Cook, Basten and Fazekas De St. Groth, 1998), inducing their differentiation and proliferation.

Despite the presence of these central tolerance mechanisms, receptor editing, allelic exclusion, clonal deletion and anergy, many self-reactive B cells escape BM checkpoints and peripheral tolerance mechanisms are required to limit the actions of these escapees.

1.2.3 Central T cell tolerance in the thymus

In the thymus, T cells with functional TCRs able to recognise peptides expressed with major histocompatibility complex (MHC) molecules must be positively selected, alongside negatively selecting those autoreactive cells that strongly recognise MHC-presented self-peptides, as summarised in figure 1.1. Microenvironmental spatial and temporal changes, and qualitive differences in signalling strength and affinity, help mediate the decision between positive and negative selection (Klein *et al.*, 2014). Progression through the double negative (DN) stages of T cell development is characterised by sequential gain and loss of CD44 and CD25 expression, accompanied by the recombination of the pre-TCR in a scenario that mirrors the pro to pre-B

transition (Rothenberg, 2014). Successful expression of a rearranged TCRβ chain with a surrogate pTα chain promotes T cell survival through feedback via arrangement with the CD3 signalling apparatus, promoting the expression of both CD4 and CD8 during transition to the double positive (DP) stage, where the TCRα chain is rearranged and single positive (SP) fate of the T cell is again controlled by TCR signalling (Singer, Adoro and Park, 2008; Klein *et al.*, 2014).

Mature T cells must recognise antigens presented by MHC molecules on the surface of antigen presenting cells (APCs). Therefore, the SP final T cell lineage is driven by positive selection by thymic cortical epithelial cells presenting peptide in either MHC-I or MHC-II molecules. DP T cells that recognise MHC-I molecules are positively selected to become mature $CD8^+$ SP T cells, whereas those that bind MHC-II lose CD8 expression to become $CD4^+$SP T cells (Singer, Adoro and Park, 2008). During selection, T cells upregulate activation markers including CD69, as well as inhibitory receptor CD5, in titrated amounts based on self-antigen binding in an intrinsic tolerance measure to alter the threshold of TCR signalling (Wong *et al.*, 2001; Goodnow *et al.*, 2005). Over 90% of DP T cells die before becoming SP cells, many from neglect as they do not receive the essential survival signals that are mediated by production of an effective TCR. A substantial amount of DP cell loss also arises from negative selection, again mediated by thymic cortical epithelial cells (cTEC); T cells presenting a strongly autoreactive TCR undergo apoptosis driven by TCR-induced Bim expression (Stritesky *et al.*, 2013; Klein *et al.*, 2014).

Subsequently SP T cells transition to the medulla where they interact with medullary thymic epithelial cells (mTECs) that also mediate negative selection (fig. 1.1), inducing the clonal deletion of $CD4^+$ or $CD8^+$ T cells that strongly recognise self-peptide MHC complexes (Burkly et al., 1993). Crucially to maintain self-tolerance, T cells must encounter self-antigens that would normally be restricted to tissues, within MHC molecules in the thymus. Thus the autoimmune regulator gene (AIRE) drives transcription of tissue specific antigens within mTECs, which process the antigens to

be presented directly by cTEC, mTEC or by other thymic APCs (Anderson *et al.*, 2005). AIRE deficiency causes autoimmune polyglandular syndrome type 1 (APS-1), where self-reactive T cells that would normally be removed by negative selection, continue to the periphery to attack self-proteins expressed on tissues, demonstrating the critical importance of negative selection in the thymus (Anderson and Su, 2011).

Strong binding of the SP TCR to self-peptide-MHC complexes elicits clonal deletion, again via Bim upregulation, or in a subset of $CD4^+$T cells, regulatory T (T_{reg}) cell differentiation (Takaba and Takayanagi, 2017). How this decision is made is not fully understood, but strong affinity or avidity of TCR binding may favour deletion (Wirnsberger, Hinterberger and Klein, 2011; Klein *et al.*, 2014). In addition to direct TCR binding, thymic antigen presenting cells may also tip the tolerogenic balance by secretion of tolerogenic cytokines including IL-2 and TGF-β. TGF-β signalling drives expression of FoxP3, the key transcription factor that characterises T_{reg} development and function, whilst IL-2 is required for the survival of $CD25^+FoxP3^-$ T_{reg} precursors (Wirnsberger, Hinterberger and Klein, 2011; Shevach and Thornton, 2014). Thus divergence to the T_{reg} fate in the thymus complements clonal deletion as T_{reg} cells migrate to the periphery to act as a suppressive brake on immune responses (Breed, Lee and Hogquist, 2018).

1.3 Maintaining tolerance in the periphery

Successfully selected B and T lymphocytes leave primary lymphoid organs, following chemokine gradients to migrate and recirculate between particular zones of peripheral lymphoid organs, where they differentiate into specialised subsets and wait to encounter cognate antigen in order to initiate adaptive immunity (Hardy *et al.*, 1982; Stein and Nombela-Arrieta, 2005). Since central tolerance, particularly in B cells, is imperfect, peripheral checkpoints are required to prevent autoreactivity. In this section, I briefly review peripheral B and T cell differentiation, and then discuss peripheral tolerance mechanisms, including anergy, which are summarised in figure 1.2.

1.3.1 Peripheral B cell subset differentiation

Immature B cells begin to mature through transitional stages of B cell development in either the BM or upon release into the periphery. Transitional 2-like cells upregulate CD23 and BAFF-R, and begin to co-express IgD of the same specificity through alternative splicing of the Ig constant region (Hardy *et al.*, 1982; Loder *et al.*, 1999; Allman *et al.*, 2001). Immature and transitional B cells migrating to enter secondary lymphoid organs require survival signals including BAFF and BCR tonic signalling and many clones with lower affinity or specificity die by neglect due to competition for antigen (Fig. 1.2) (Allman *et al.*, 2001; Kraus *et al.*, 2004; Goodnow *et al.*, 2005; Cambier *et al.*, 2007). Factors including BCR specificity, the strength of BCR interactions, BAFF-R-driven NF-kB signalling and Notch signalling, dictate the differentiation of B cells into B cell subsets; namely B-2 follicular, B-2 marginal zone (MZ) and B-1 cell populations (Loder *et al.*, 1999; Saito *et al.*, 2003; Hozumi *et al.*, 2004; Rodig *et al.*, 2005; Pillai and Cariappa, 2009)

Conventional B-2 follicular B cells recirculate through the BM, blood and secondary lymphoid organs searching for cognate antigen. Upon antigen engagement, activated B cells upregulate chemokine receptor CCR7 and migrate to T cell rich zones to interact with T helper cells in order to differentiate into germinal centre (GC), memory and plasma cells during T-dependent immune responses (Loder *et al.*, 1999; Reif *et al.*, 2002). B-2 MZ cells represent a more innate-like B cell subset able to mediate T-independent responses to pathogens and rapidly divide into short-lived plasma cells on antigen exposure (Oliver *et al.*, 1997). MZ B cells express high levels of complement receptor CD21 and non-classical MHC, CD1d, and reside in the marginal sinus area of the spleen, due to their high expression of sphingosine1-phosphate receptors (Cinamon *et al.*, 2004) and elevated expression of integrins, LFA-1 (αLβ2) and α4β1, whose ligands are highly expressed in the marginal zone (Lu and Cyster, 2002). On the other hand, $B220^{lo}CD19^{+}CD43^{+}$ B1 populations can originate from fetal BM and fetal liver HSCs, then migrate to take up residence in pleural, splenic and peritoneal cavities where they can self-renew. B1 cells represent an innate-like population,

which express a restricted BCR repertoire that can be activated without BCR ligation to produce poly-reactive natural antibody in the form of soluble IgM (Hardy *et al.*, 1994; Kantor *et al.*, 1997; Cunningham *et al.*, 2014).

1.3.2 Peripheral T cell subset differentiation

Naïve T cells migrating from the thymus also rely on survival signals in the form of IL-7 and MHC-mediated tonic signalling to maintain and restrict T cell proliferative homeostasis (Fig. 1.2) (Tan *et al.*, 2001; Barthlott, Kassiotis and Stockinger, 2003). Once in the periphery, like B cells, naïve T cells circulate secondary lymphoid organs and the blood in search of their cognate antigen. Differential cytokine microenvironments, innate immune interactions and the type of antigen dictate the induction of transcriptional programs that drive maturation into defined T cell subsets, each conferring a distinct effector role (Seder and Ahmed, 2003; Golubovskaya and Wu, 2016).

Proinflammatory cytokines including IFN-α and IL-12 drive cytotoxic killer T cell ($CD8^+$ T cell) development by inducing *Tbet*, granzyme B, IFNγ and expression of other genes responsible for cytolytic functions including Fas-mediated killing of antigen-expressing cells (Mescher *et al.*, 2006; Golubovskaya and Wu, 2016). Meanwhile $CD4^+$T subsets are classified by the transcription factors they express and the cytokines they produce in response to classes of pathogens; T_H1 $CD4^+$cell responses are characterised by *Tbet* expression, which is induced by IL-12 and IFNγ proinflammatory cytokines in order to target intracellular pathogens, including viruses by release of IFNγ (Szabo *et al.*, 2000; Zhu, Yamane and Paul, 2010; Caza and Landas, 2015), whereas T_H2 $CD4^+$T cells express *Gata3* and secrete IL-4 and IL-5 to provide B cell help and target helmiths and extracellular bodies when induced by IL-4 (Zheng and Flavell, 1997; Seder and Ahmed, 2003; Caza and Landas, 2015). Depending on the context, IL-6 can induce T follicular helper (T_{FH}) $CD4^+$ differentiation to support humoral immunity, or drive T_H17 differentiation when combined with TGF-β1, which induces transcription factor, *RORγt* in order to respond to extracellular pathogens

through IL-17 production (Ivanov *et al.*, 2006; Yosef *et al.*, 2013; Crotty, 2014). TGF-β1 alone can drive peripheral T regulatory (pT_{reg}) development by induction of *Foxp3* transcription factor (Chen *et al.*, 2003), which acts as an essential tolerance mechanism as described below to balance the inflammatory axis by producing suppressive cytokines and dampening immune responses (Shevach and Thornton, 2014).

1.3.3 The two-signal hypothesis of lymphocyte activation and anergy

Central tolerance is imperfect; many self-reactive B cells and few self-reactive T cells escape negative selection checkpoints, and peripheral tolerance mechanisms are therefore essential to prevent autoimmune reactions as summarised in figure 1.2.

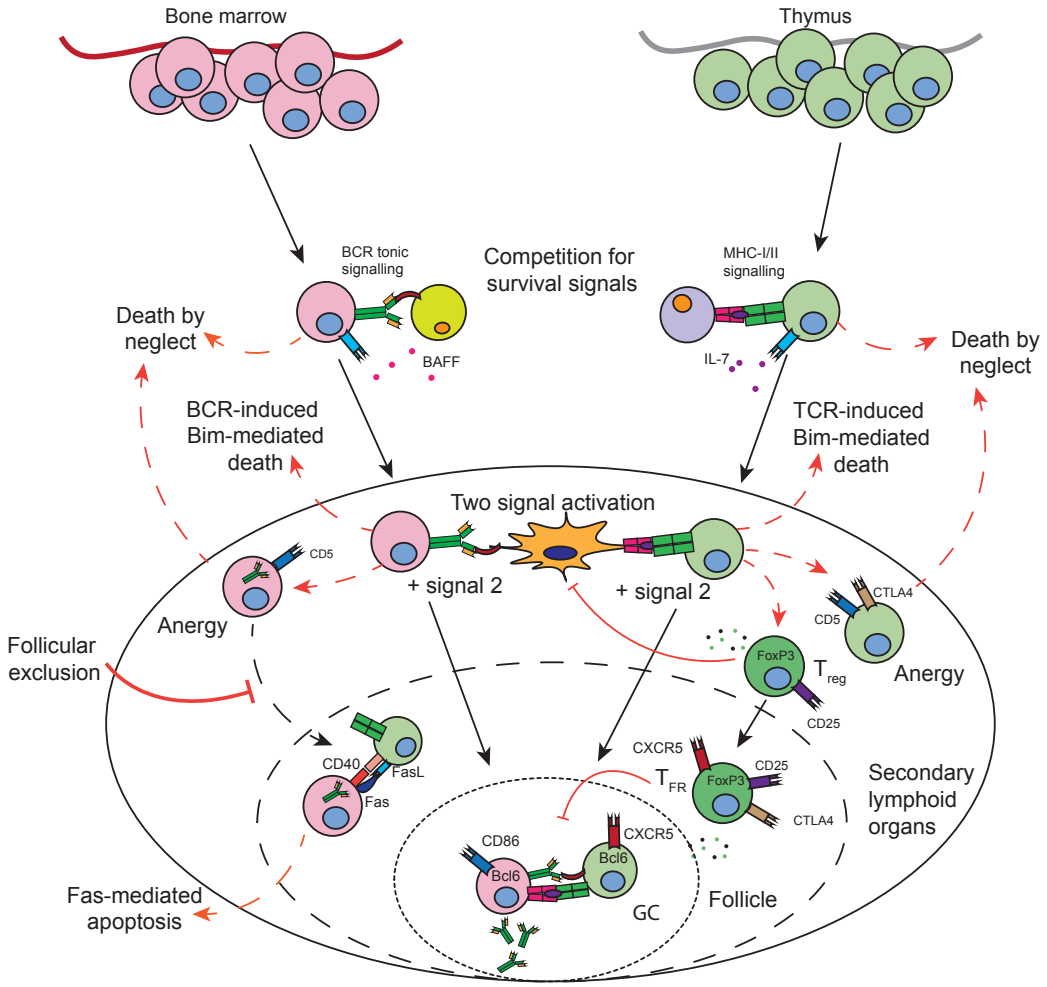


Figure 1.2 Peripheral tolerance maintenance prevents autoimmunity

Several cell-extrinsic and cell autonomous tolerance mechanisms act within peripheral lymphoid organs and during active immune responses to prevent the development of antibody-mediated autoimmune disease. Acronyms used are as follows: T follicular regulatory cell (T_{FR}), germinal centre (GC).

Central to the fate decision between induction of a tolerogenic or immunogenic response in the periphery is Bretscher and Cohn's two signal model of cell activation (Bretscher and Cohn, 1970); full activation of B and T lymphocytes typically requires two distinct signals: antigen-engagement of the BCR or TCR respectively (signal one), which leads to limited initiation of intracellular signalling cascades, and co-stimulation by PRRs or $CD4^+$ T cell help (signal two), which triggers the remaining pathways required for productive activation (Bretscher, 1999; Baxter and Hodgkin, 2002). If signal two is not received within a temporally-defined window of signal one, this leads to induction of a unresponsive state called anergy, in order to limit inappropriate responses (Fulcher *et al.*, 1996; Bretscher, 1999; Ferry *et al.*, 2006). Similar to that seen in immature B cells in the BM, induced lymphocyte anergy is a cell-intrinsic form of tolerance, classically described when mature B or T cells become functionally unresponsive upon antigen receptor binding by self-antigen in the absence of accessory signals in the periphery (Borde *et al.*, 2006; Ferry *et al.*, 2006).

As in the BM, peripherally-tolerised anergic B cells are characterised by low surface IgM, demonstrate altered localisation, reduced lifespan and an acquired cell autonomous inability to respond to T cell help (Cambier *et al.*, 2007; Yarkoni, Getahun and Cambier, 2010). Furthermore, like self-reactive T cells, B cells expressing BCRs with some level of self-reactivity also upregulate inhibitory surface receptor CD5 in an intrinsic mechanism to increase the threshold of BCR activation, limiting clonal expansion of autoreactive populations (Hippen, Tze and Behrens, 2000).

1.3.3.2 Peripheral T cell tolerance and clonal T cell anergy

Compared to B cell tolerance, central T cell tolerance by thymic clonal deletion or anergy induction is robust; however not all self-antigens are presented in the thymus and peripheral tolerance plays an important role in preventing autoimmunity (Johnson and Jenkins, 1994; Borde *et al.*, 2006; Xing and Hogquist, 2012). As with the two signal model in B cells, Productive activation of T cells requires secondary costimulatory signals (signal 2) from the MHC-antigen (signal1) presenting cell

(Bretscher, 1999; Schwartz, 2003); while TCR signalling activates phosphorylation cascades eliciting calcium influx, mitogen activated protein kinase (MAPK), phosphoinositide 3-kinase (PI3K) and Akt signalling to drive complete T cell activation (Borde *et al.*, 2006). Amongst other costimulatory receptors, CD28 activation by B7.1 and B7.2 expressed on APCs primarily augments TCR signalling cascades to overcome the signalling threshold for productive T cell activation (Acuto and Michel, 2003). Sub-optimal T cell activation can lead to several outcomes, which include cell death from neglect due to insufficient pro-survival factors, development into peripheral T_{reg} populations driven by suppressive TGF-β, or activation of the cell-intrinsic anergy program (Schwartz, 2003; Liu *et al.*, 2008; Shevach and Thornton, 2014). Self-reactive peripheral T cells also upregulate inhibitory receptors including CD5, as well as cytotoxic T-lymphocyte antigen 4 (CTLA4), which competes with the CD28 co-stimulator, thus raising the threshold for responding to both signal one and two respectively (Van Der Merwe *et al.*, 1997; Goodnow *et al.*, 2005; Arruvito *et al.*, 2007; Ise *et al.*, 2010).

The term T cell anergy has been used to describe two related but distinct tolerogenic, autonomous mechanisms induced by suboptimal T cell activation; *in vivo* peptide-induced T cell anergy defines the inactivated state induced in peripheral T cells that have experienced antigen stimulation in the absence of co-stimulation, while T cell clonal anergy arises on the restimulation of previously activated T cells, solely with signal one *in vitro* (Perez *et al.*, 1997; Schwartz, 2003). Whereas clonally anergic T cells *in vitro* principally demonstrate IL-2-reversible growth-arrest, *in vivo* peptide-induced anergised T cells are characterised by their inability to proliferate or produce cytokines upon restimulation, a state that is not reversible by IL-2 treatment (Beverly *et al.*, 1992; Pape *et al.*, 1998; Schwartz, 2003). The two anergic states present with biochemically distinct profiles; the Ras/MAPK pathway is selectively blocked in clonal anergy, whereas proximal TCR signalling including Zap70 kinase activity is impaired in adaptive tolerance, leading to chronically low calcium-dependent signalling, sufficient to activate NFAT and associated factors (Kimura *et al.*, 2000;

Macián *et al.*, 2002; Jeon *et al.*, 2004a; Safford *et al.*, 2005; Chiodetti *et al.*, 2006; Baine, Abe and Macian, 2009), echoing the pattern in anergised B cells. Thus alongside the shared unresponsive and functionally inactivated phenotype, the signalling patterns that characterise peptide-induced anergic $CD4^+$ T cells and tolerised B cells also have parallels that suggest shared pathways, and may provide novel targeting opportunities for therapeutics.

1.3.4 The role of regulatory T cells in peripheral tolerance

In addition to cell autonomous modes of tolerance, regulatory T cell populations play an essential, external suppressive role in preventing autoimmune diseases in both mice and humans (Li *et al.*, 2007; Van Der Vliet and Nieuwenhuis, 2007; Yadav, Stephan and Bluestone, 2013; Hadaschik *et al.*, 2015), by producing suppressive cytokines and dampening immune responses (Fig. 1.2)(Kronenberg and Rudensky, 2005; Shevach and Thornton, 2014). There are two distinct lineages of regulatory T cells; whereas $FoxP3^+$ thymically derived regulatory cells (tT_{reg}) contribute the majority of the population, peripherally derived T_{reg} (pT_{reg}) are produced from conventional $FoxP3^-$ cells that are subjected to TGF-β1 signalling in the absence of other cytokines, under conditions similar to those reported for T cell anergy (Schwartz, 2003; Shevach and Thornton, 2014). In fact, the phenotypical and biochemical similarities between regulatory T cell populations and anergic T cell populations mean the two phenomena are hard to distinguish, suggesting some lineage and functional overlap across these regulatory states (Schwartz *et al.*, 1989; Itoh *et al.*, 1999).

Mechanisms of T_{reg}-mediated immunosuppression include release of inhibitory cytokines including TGF-β and IL-10 (Annacker *et al.*, 2003; Li, Wan and Flavell, 2007), direct cytolysis of cytotoxic T cells by granzyme release (Cao *et al.*, 2007), direct CTLA-4-mediated extrinsic suppression of T cell activation (Friedline *et al.*, 2009; Schmidt *et al.*, 2009), metabolic starvation of actively dividing effector subsets by over-consumption of survival cytokines including IL-2 (Pandiyan *et al.*, 2007; Vignali, Collison and Workman, 2008), and modulation of dendritic cell (DC) populations to limit T

cell activation (Tadokoro *et al.*, 2006; Vignali, Collison and Workman, 2008). Key specialised subsets of regulatory T cell population have also been described in situations such as GC response regulation, where they contribute key control of humoral immunity (Chung *et al.*, 2011; Linterman *et al.*, 2011; Wollenberg *et al.*, 2011; Stebegg *et al.*, 2018).

Consistent with these functions, direct transfer of $CD25^+$ T_{reg} populations can prevent graft versus host disease (GVHD) in mouse models (Sakaguchi *et al.*, 1995; Nguyen *et al.*, 2007) and some success has been described in T_{reg} transfers preventing GVHD after allogenic haematopoietic cell transplant human patients (Jones, Murphy and Korngold, 2003; Brunstein *et al.*, 2011). The multicentre ONE study has recently demonstrated regulatory cell therapy may be effective in preventing infection and restoring immune homeostasis post-kidney transplant, reducing the requirement for immunosuppression in these patients (Sawitzki *et al.*, 2020).

1.3.5 Maintaining tolerance in the germinal centre

During infection, GC formation and accompanying antigen-driven production of novel, high-affinity BCRs present new challenges for the maintenance of immunological tolerance. On activation by APCs, peripheral antigen-specific B cells upregulate CCR7 and CD86 and travel via chemokine gradients across B cell follicles to present cognate peptide in MHC-II molecules in order to receive co-stimulation within the T cell zones from helper T cells (Okada *et al.*, 2005; Victora *et al.*, 2010). Productive co-stimulation from helper T cells stimulates survival and proliferative signals and the activated B cells can thus differentiate into plasmablasts, producing early waves of pathogen-specific antibody, or into early memory B cells, or subsequently, on the induction of transcription factor *Bcl6*, may enter the GC reaction (Ye *et al.*, 1997; Brink and Phan, 2018; Stebegg *et al.*, 2018). By contrast, without T cell help, the activated B cell will die in accordance with the two-signal hypothesis via Bim-mediated apoptosis (Enders *et al.*, 2003). Though able to transverse the GC, anergic B cells generally cannot engage in GC reactions even in the context of subsequent cognate

T cell help, as CD40 engagement by CD40L on T helper cells in the absence of BCR feedback from the anergic B cell, instead drives upregulation of B cell Fas death receptor. Thus T helper-driven FasL signalling initiates Fas-mediated apoptosis, preventing self-reactive T cells from inappropriately engaging in GC reactions and producing autoantibody (Fig. 1.2)(Rathmell *et al.*, 1995; Brink and Phan, 2018).

Once in the germinal centre, activated B cells shuttle between the light zone (LZ) and dark zone (DZ), sections which are defined based on expression of CXCR5 and CXCR4 respectively (Allen *et al.*, 2004). B cells in the DZ (known as centroblasts) express activation-induced cytidine deaminase to drive random recombination of the BCR (Nagaoka *et al.*, 2000; Stebegg *et al.*, 2018). On migration to the LZ, BCRs are positively selected by testing against antigen-expressing follicular DCs and specialised T_{FH} cells (Allen *et al.*, 2004; Brink and Phan, 2018). Antigen-specific T_{FH} cells arise from naïve $CD4^{+}$T cell priming by antigen-presenting DCs, inducing a *Bcl6*-driven transcriptional programme, in which upregulation of CXCR5 and downregulation of CCR7 promote migration to the T:B cell zones (Hardtke, Ohl and Förster, 2005; Yu *et al.*, 2009). Once here, SLAM-associated protein (SAP)-dependent B cell-mediated co-stimulation finalises T_{FH} differentiation, allowing T_{FH} cells to support GCs by acting in the LZ to promote and regulate positive selection of foreign antigen-specific somatic hypermutating-cycling GC B cells (Qi *et al.*, 2008; Stebegg *et al.*, 2018).

Because somatic hypermutation of foreign-specific GC B cells can result in the production of novel self-reactive BCRs, further GC-specific tolerance mechanisms are required to prevent autoimmune disease. The Goodnow lab described the phenomenon of clonal redemption in humans, where clonally anergic B cells can mutate away from self-reactivity during an active immune response (Reed *et al.*, 2016). Additionally, a specialised subset of T_{reg}, called T follicular regulatory T cells (T_{FR}), reside in the B cell follicle and regulate GC responses (Fig. 1.2). Derived from $FoxP3^{+}$ T_{reg}, T_{FR} cells express CXCR5 in a Bcl6, SAP, CD28 and B cell-driven manner, allowing localisation to the GC (Chung

et al., 2011; Linterman *et al.*, 2011; Wollenberg *et al.*, 2011). T_{FR} cells act to suppress the GC response by restricting the engagement of non-antigen specific GC B cells and by limiting T_{FH} cell expansion, through mechanisms involving secretion of TGF-β and IL10 as well as high CTLA-4 expression (Linterman *et al.*, 2011; Wing *et al.*, 2014; Stebegg *et al.*, 2018). Together, these T cell-dependent and B cell intrinsic tolerance mechanisms are essential for preventing GC-derived autoimmunity (Fig 1.2).

1.4 Understanding the mechanisms of autoimmune disease

Autoimmune disease describes the heterogenous group of chronic autoinflammatory disorders that develop on the loss of self-tolerance. Direct targeting of self-reactive immune populations can result in tissue-specific organ damage such as pancreatic islet beta cell destruction in T1DM (Chen, Mathews and Driver, 2018), or multiple organs can be affected, often by combinations of direct and indirect mechanisms that result in chronic inflammation, such as cytokine production, neutrophil NETosis, complement activation, T cell effector activity and immune complex deposition in patients with SLE (Tsokos *et al.*, 2016). Thus, the pathogenesis of autoimmunity is highly complex and heterogeneous and dysregulation of many aspects of the innate and adaptive systems has been described. For example, deficiencies in components of the complement pathway are associated with SLE, alongside enhanced IFNα production and dysregulated apoptosis (Bengtsson *et al.*, 2000; Mok and Lau, 2003; Niewold *et al.*, 2008), whereas subtypes of RA have been demonstrated to be triggered by abnormal production of antibodies against citrullinated proteins (ACPAs)(Sebbag *et al.*, 1995; Aggarwal *et al.*, 2009).

More research into the shared and specific mechanisms of loss of tolerance and the genetic and environmental triggers of these altered pathways is essential for the development of safer and more efficacious therapeutics across these diseases. Furthermore, the emergence of autoimmune side effects associated with cancer immunotherapy, and the characterisation of the modulatory

role of the tolerogenic microenvironment between tumour and immune cells in cancer patients, highlights the requirement for better understanding of the mechanisms that maintain the balance of tolerance, and the genetic and environmental factors that disrupt these to introduce novel therapeutic targets across disease boundaries (Collier *et al.*, 2021; Hiam-Galvez, Allen and Spitzer, 2021).

1.4.1 Genetic basis of autoimmunity

The influence of a genetic component in autoimmunity was first identified by the high rate of concordance of diseases such as multiple sclerosis in twin pairs and first degree family members compared to incidence in the rest of the population (Sadovnick, Baird and Ward, 1988; Sadovnick *et al.*, 1993; Marson, Housley and Hafler, 2015). The study of familial aggregation of inherited monogenic disorders, combined with genetic linkage analyses of simple traits have provided invaluable insights into normal and disease physiology (Rioux and Abbas, 2005). However, most common autoimmune diseases have complex genetic aetiologies, composed of combinations of many variants, which each confer a modest risk with modest individual effect size. Linkage disequilibrium mapping techniques identified the MHC superlocus, human leukocyte antigen (HLA)-DRB1-HLA-DQA1-HLA-DQB1 region on chromosome 6 as conferring over 50% of the genetic predisposition to insulin-dependent diabetes mellitus (Rich, Weitkamp and Barbosa, 1984; Todd, Bell and McDevitt, 1987; Gutierrez-Arcelus, Rich and Raychaudhuri, 2016), as well as representing strong susceptibility loci in SLE (Gaffney *et al.*, 1998), RA (Raychaudhuri *et al.*, 2012) and multiple sclerosis (Gourraud *et al.*, 2012).

Understanding of the genetic causes of complex disorders using classical linkage analysis lacks power due to weaker familial aggregation of polygenic disorders, with incomplete penetrance and small effect sizes. However, the development of genome-wide association studies (GWAS) has enabled identification of common variants and genetic loci covering immunoregulatory regions

that each contribute increased risk of disease, by studying large populations (Vyse and Todd, 1996; Rioux and Abbas, 2005; Marson, Housley and Hafler, 2015). Many GWAS-identified common variants within risk loci overlap multiple autoimmune diseases; TNFAIP3 single nucleotide polymorphisms (SNPs) are associated with increased risk to RA, psoriasis and SLE (Graham *et al.*, 2008; Nair *et al.*, 2009; Cotsapas *et al.*, 2011), and PTPN22 SNPs modulate risk to multiple autoimmune diseases including SLE, RA, T1DM and Hashimoto thyroiditis (Criswell *et al.*, 2005). More than 90 loci have been identified to be SLE-associated genes by GWAS (Wang *et al.*, 2021), however these variants each contribute small individual risk and polygenic risk scores have been used to explore how disease pathogenesis relates to cumulative genetic risk (Reid *et al.*, 2020). GWAS analyses highlight the shared immune deregulatory mechanisms of tolerance loss, however identification of causative variants specific for disease and their functional consequences is limited by the huge heterogeneity of human genetic disease, and the non-coding location of most GWAS SNPs (Tam *et al.*, 2019).

Rare monogenic diseases thus provide a tractable way to discover novel individual genes and regulatory pathways essential for maintaining immunological tolerance. Linkage analysis and genetic mapping of patients with distinct Mendelian immune dysregulation syndromes has identified highly penetrant mutations that disrupt immune homeostasis (Teare and Barrett, 2011), which can be further studied with experimental mouse genetic models. For example, study of patients with APS-1 identified the role of AIRE in thymic central tolerance (Farid *et al.*, 1980; Aaltonen *et al.*, 1997; Nagamine *et al.*, 1997), whereas deficiencies in C1q, a key PRR that initiates the classical complement pathway, result in a monogenic form of SLE (Nishino *et al.*, 1981; Arnett and Reveille, 1992). Similarly, the importance of pathways such as the nucleic acid sensing and degradation pathway in maintaining immune tolerance have been identified due to causal rare variants of monogenic lupus (Jiang, Stanley and Vinuesa, 2020), for example mutations in 3'repair exonuclease 1 (TREX1), which cause Aicardi-Goutieres syndrome (Crow *et al.*, 2006).

Although monogenic syndromes are rare, the clinical importance and insight of single-gene variants is not limited only to disease-sufferers; key pathways revealed by rare Mendelian syndromes of autoimmunity may be shared with more common, complex autoimmune diseases. For example, while autosomal-dominant mutations in immune checkpoint molecule, CTLA-4 causes severe multiorgan autoimmune disease in humans (Schubert *et al.*, 2014) and a lethal autoimmune phenotype is present in CTLA-4-deficient mice (Tivol *et al.*, 1995), common non-penetrant CTLA-4 variants confer modest increased risk in complex autoimmune diseases such as Grave's disease and T1DM (Marson, Housley and Hafler, 2015; Onengut-Gumuscu *et al.*, 2015). Identification of CTLA-4 as a key molecule regulating T cell co-stimulation has led to the development of CTLA modulatory therapies for both autoimmune disease and cancer (Lenschow *et al.*, 1992; Tivol *et al.*, 1995; Wei *et al.*, 2019).

1.4.2 External triggers of autoimmune disease

Ultimately, most autoimmune disease is caused by the complex interplay of genetic susceptibility, immunological and biological fluctuations combined with environmental exposures (Wei *et al.*, 2019). In individuals primed to loss of self-tolerance by their genetic make-up, external triggers may push immune homeostasis over the breaking point, eliciting autoimmunity. Such environmental factors may include chemicals and therapeutics, diet and nutrition, or infections by bacterial or viral pathogens. Long term exposure to drugs such as hydralazine, chlorpromazine and procainamide are associated with drug-induced lupus, with this risk enhanced by certain HLA variants, demonstrating this interplay between genetic and environmental factors (Mok and Lau, 2003; Vojdani, Pollard and Campbell, 2014).

Infections have been strongly linked to the induction of autoimmunity; explanatory hypotheses include general induction of an inflammatory environment, infectious agents mimicking self-

antigens (Cusick, Libbey and Fujinami, 2012; Root-Bernstein and Fairweather, 2014), and by epitope spreading where chronic or repeat infections result in diversification of the epitopes targeted by immune cells, which can ultimately result in self-antigen targeting (Lehmann *et al.*, 1992; Vanderlugt and Miller, 2002). Guillain-Barre syndrome can in some cases be directly triggered following *Campylobacter jejuni* infection, due to the production of antibodies against microbial liposaccharides that share structure similarities with cell surface gangliosides expressed throughout the central nervous system (Wim Ang, Jacobs and Laman, 2004). Several microorganisms have been associated with RA disease severity, including *Porphyromonas gingivalis*, *Proteus mirabilis* and *Escherichia coli* (Yinshi Yue, 2013). In these cases, the contribution of infection to loss of tolerance may be indirect through altered inflammatory or immunosuppressive conditions that ultimately affect immune homeostasis (Kuhn and Stappenbeck, 2013; Belkaid and Hand, 2014).

1.5 Modelling mechanisms of autoimmunity using *in vivo* models

Experimental model systems are a crucial complement to human datasets in furthering our understanding of autoimmune disease pathogenesis. Studies of samples derived from affected human patients can be important for understanding effects of risk variants, but are limited by difficulties accessing appropriate human tissue samples, and are further complicated by potential confounding effects from patient treatment history, genetic background, as well as accompanying disease-dependent and -independent infections (Vojdani, Pollard and Campbell, 2014). *In vitro* genetic modification of established cell lines, induced pluripotent stem cells induced to form organoids, tissue-on-a-chip, or other model *in vitro* systems can circumvent these issues, but despite major advances in gene editing and cell differentiation, such systems remain technically challenging, and read outs may have limited relevance to complex physiology and clinical outcomes.

Thus, animal models remain a key methodology to study autoimmune disease pathogenesis *in vivo*; the tractable nature of murine strains combined with the short time scale to study disease on a homogenous genetic background, and availability of established antigen-specific tg models provides vast opportunities to explore and manipulate immune homeostasis in the absence of the confounding factors associated with human samples. To probe individual aspects and mechanisms of disease pathogenesis, many autoimmune *in vivo* models have been described over the decades. Mouse models of disease can be split into induced, for example by treatment with chemicals such as TLR7 agonist, imiquimod, spontaneous, driven by a combination of genetic background risk and environmental triggers, or genetically modified, which covers tg, mutant and knockout or gene-edited systems (Morel, 2004; Yokogawa *et al.*, 2014; Richard and Gilkeson, 2018; Dawes and Uren, 2021). These models not only support mechanistic studies, but also provide valuable tools for testing new therapeutic targets and pharmaceuticals.

A number of spontaneous (Makino *et al.*, 1980; Kotzin, 1996; Rozzo *et al.*, 1996) and induced models (Brand, Latham and Rosloniec, 2007; Schroeder and DiPersio, 2011; Yokogawa *et al.*, 2014; Klarquist and Janssen, 2015; Wirth *et al.*, 2020) of autoimmune disease mimic the immune dysregulation and resulting organ damage seen in human disorders, but in order to understand how a specific gene acts in maintaining tolerance, genetically engineered strains are required. Knockout, knock-ins, tg and more recently CRISPR/Cas9 precision-edited murine strains can permit directed investigation into the role of individual genes on tolerance in a process called reverse genetics (Morel, 2004; Wang *et al.*, 2013), whereas forward genetics describes the identification of genes contributing to a known phenotypic effect (Cordes, 2005). Additionally, tg models introducing antigen receptors with fixed specificity, or neo-antigens expressed as self-proteins, can be bred to a murine strain with a modified gene of interest providing elegant tools to control and challenge aspects of tolerance development (Boyton and Altmann, 2002)

1.5.1 Targeted gene editing approaches to exploring disease pathogenesis

The direct targeting of specific genetic regions has been a powerful tool to explore the role of individual genes of interest in immunological processes. This approach requires prior hypotheses and knowledge of genes potentially implicated in disease; it has been particularly useful in exploring and functionally validating candidate genes identified by the study of rare human monogenic disease. Researchers have an increasingly sophisticated set of tools suitable for genetic manipulation in the mouse. Conventionally, homologous recombination within embryonic stem (ES) cells can be directed by injected DNA constructs designed to target the gene of interest, resulting in a genetic knockout or knockin (Waterston *et al.*, 2002; Skarnes *et al.*, 2011). Advancements in gene targeting technologies enable researchers to custom-design alterations in genes, whether introducing large deletions, chromosomal rearrangements, SNPs and variants replicating patient genotypes of loss-of- or gain-of- function mutations (Wang *et al.*, 2013; Li *et al.*, 2020).

In combination with genome-wide strategies, the majority of the coding genes in the mouse genome have been targeted in large scale efforts to create a complete ES-targeted cell resource of reporter-tagged null alleles by programs including the European Conditional Mouse Mutagenesis (EUCOMM), National Institutes of Health Knockout Mouse (KOMP)(Austin *et al.*, 2004; Consortium *et al.*, 2007; Skarnes *et al.*, 2011). The large scale creation of knockout mouse libraries has been accompanied by mass phenotyping pipelines such as the International Mouse Phenotyping Consortium (IMPC), aiming to attribute impairments in molecular processes to individual genes (Muñoz-Fuentes *et al.*, 2018).

The development of CRISPR/Cas9 technology has allowed more accessible and efficiently directed reverse genetics, reducing the production time of genetically engineered mouse models significantly, and improving the efficacy of introducing targeted precise mutations (H. Kim *et al.*,

2018). For production of a knockout, this approach relies on the interaction of two components; a Cas9 nuclease and a single guide RNA (sgRNA). The sgRNA is created by fusion of trans-activating CRISPR RNA (tracrRNA) and CRISPR RNA (crRNA), the latter of which contains a 20 nucleotide long sequence complementary to the target genomic DNA region, known as the protospacer, that must be followed by a protospacer adjacent motif (PAM; conventionally 5'NGG) to direct nuclease cleavage (Sander and Joung, 2014). Direct injection of oocytes with Cas9 mRNA and sgRNA can efficiently direct DNA manipulation, producing mutant mouse lines within one generation, compared to the several required using traditional genome engineering of ES cells (Hsu, Lander and Zhang, 2014; Cebrian-Serrano *et al.*, 2017). In mice, about 25% of gene knockouts are incompatible with life, so CRISPR/Cas9 precision editing to produce hypomorphic alleles, and mouse models expressing conditional alleles using the Cre-LoxP site-specific recombination system are important to overcome limitations of embryonically lethality, enabling replication of human variants and gene function, and study of genes during development and later in adult life and spatially in different tissues (Testa *et al.*, 2004; Skarnes *et al.*, 2011).

Tg overexpression of key pathway molecules under cell type specific promoters provide another valuable tool for rescue experiments. For example B cell-specific overexpression of the pro-survival Bcl-2 molecule by transgenesis has been useful for separating survival defects from developmental problems (Strasser, Harris and Cory, 1991; Strasser, Harris, Corcoran, *et al.*, 1994; Strasser, Harris, Von Boehmer, *et al.*, 1994). Additionally, tg mouse models expressing humanised forms of drug targets, such as immune receptors, have been engineered for the receptor to interact within murine immunological signalling pathways, whilst able to respond to anti-human monoclonal antibodies. Humanised CTLA-4 or programmed cell death protein 1 (PD1) tgs are successfully used as pre-clinical *in vivo* strategies to assess therapeutic targets, mechanisms and efficacies for human diseases (Richard and Gilkeson, 2018; Zhu *et al.*, 2019).

Reverse genetics has enabled powerful molecular investigation into how specific mutations contribute to disease phenotype, particularly in delineating the causality of other candidate genes and risk alleles identified by GWAS as disease-associated loci in complex genetic disease (Ermann and Glimcher, 2012). For example, the molecular role of LRRK2 in modulating immune tolerance via NFAT regulation in inflammatory bowel disease has been dissected using directed mouse models to distinguish causal SNP variants from those inherited by linkage disequilibrium (Liu *et al.*, 2011). Study of tg mice over-expressing LRRK2 demonstrated high risk alleles causing increased expression of LRRK2 drive autoimmunity via enhanced activation of the NF-κB pathway, in addition to inhibition of autophagy, which ultimately drives increased inflammation resulting in colitis (Takagawa *et al.*, 2018).

1.5.2 Forward genetics; phenotype-driven studies

Reverse approaches model known or candidate disease genes and allelic variants, but to discover novel genetic contributions to immune function, screening or 'forward genetic' strategies are necessary, which require no prior knowledge of gene function for targeting (Stottmann and Beier, 2014). This unbiased approach identifies disease-associated genes by the direct association with altered phenotype and subsequent genetic mapping (Bull *et al.*, 2013). For example, development of a spontaneous, fatal lymphoproliferative disorder in mice named *Scurfy*, lead to subsequent mapping to identify the *Foxp3* gene and the essential role of T_{reg} in maintaining peripheral tolerance (Godfrey, Wilkinson and Russell, 1991; Brunkow *et al.*, 2001; Khattri *et al.*, 2017). Corresponding *Foxp3* mutations and clinical disease phenotypes are present in human patients with immune dysregulation polyendocrinopathy enteropathy, X-linked syndrome, hence *Scurfy* mice provided a key model to study this monogenic autoimmune disorder (Bennett *et al.*, 2001).

Phenotype-driven gene linkage studies such as the WGS500 project, where the genomes of patients and family members across a wide spectrum of rare diseases were sequenced to identify shared

variants in the affected families, also represented a powerful approach to identify novel causative genes before the mainstream application of whole genome sequencing transformed the exploration of the genetic basis of such disorders (Taylor *et al.*, 2015). This study helped paved the way for the Genomics England 100,000 genomes project, where the whole genomes of 100,000 patients with rare diseases or cancers were sequenced alongside their families in order to advance clinical diagnoses and treatments of such disorders whilst furthering the understanding of genetic disease (Caulfield *et al.*, 2017).

Classical forward genetics approaches in mice have been based on random genome-wide mutagenesis; ES cells are subjected to mutagenesis, whether by introduction of chemicals, genetic constructs or X-ray-mediated and resulting mutant offspring can be screened for the presence of phenotype (Stanford, Cohn and Cordes, 2001; Consortium *et al.*, 2007; Nguyen *et al.*, 2011; Skarnes *et al.*, 2011). Sequencing and positional cloning of the resultant mutant mice, crossed to another strain for linkage or subsequently rapid next generation sequencing based linkage, can directly attribute an immunological phenotype to mapped genotype (Nelms and Goodnow, 2001; Bull *et al.*, 2013). The chemical mutagen, N-ethyl-N-nitrosourea (ENU) is an alkylating agent used in several large mutagenesis programmes such as the International Mouse Knockout Consortium (Consortium *et al.*, 2007), as it specifically introduces point mutations into DNA sequence by alkylating oxygen molecules in nitrogenous DNA bases at extremely high efficiency (Russell *et al.*, 1979; Stottmann and Beier, 2014). Single base changes better mimic natural genetic variants and have the advantage of producing hypomorphic, hypermorphic and null alleles, including inactivation or alterations of specific protein functions rather than simply inducing the complete loss of the protein through genetic knockouts, hence creating more realistic models of human genetic variants in disease (Nelms and Goodnow, 2001; Nguyen *et al.*, 2011; Bull *et al.*, 2013).

Large-scale screening of mutants requires sensitive assays to detect those that cause immune dysregulation. Autoantibodies to nuclear epitopes (ANAs), a sensitive hallmark of autoimmune disease in humans, provide a scalable tool for autoimmune screening in mice (Vinuesa and Goodnow, 2004). Though autoantibodies are also found in 2.5% of healthy human adults (Wandstrat *et al.*, 2006) and 16% wildtype C57BL/6 mice, differential ANAs targeting specific autoantigens are associated with certain disorders: for example, anti-double stranded DNA (dsDNA) and anti-Sm ANAs are strongly associated with SLE (Arbuckle *et al.*, 2003), whereas RA patients have a high incidence of anti-ACPA (Aggarwal *et al.*, 2009) and ANAs targeting centromeres and Scl-70 act as a classical marker of systemic sclerosis (Spencer-Green, Alter and Welch, 1997). Hence, ANAs can serve as an indicator of loss of tolerance in screens for autoimmunity, and were used in an ENU mutagenesis screen in the first identification of the ubiquitin ligase family member, Roquin (*Rc3h1*) as a key repressor of T_{FH} cell development and function, acting to prevent autoantibody responses (Vinuesa *et al.*, 2005; Nguyen *et al.*, 2011). Sanroque homozygous mice *(san/san)* develop a SLE-like syndrome from 6 weeks of age, presenting with ANAs against dsDNA, chronic immunological inflammation and glomerulonephritis with IgG immune complex deposition (Vinuesa *et al.*, 2005). This work recognised the role of Roquin in regulating the expression of inducible T cell co-stimulator (ICOS) molecule on T_{FH} cell surfaces through *Icos* mRNA suppression, thus ultimately identifying a novel key regulatory pathway of post-transcriptional T cell activation (Vinuesa *et al.*, 2005; Di Yu *et al.*, 2007).

Similarly, ANA quantification contributed to detection of impaired immunological tolerance in the more recent high-throughput phenotype-driven screen, the Infection and Immunity Immunophenotyping (3i's) consortium project (Abeler-Dörner *et al.*, 2020). Baseline and challenge immunological phenotyping on over 550 knockout mouse lines generated by the Wellcome Sanger Institute identified 140 knockout models with immune phenotypes, including 80 genes not previously associated with the immune system (Abeler-Dörner *et al.*, 2020). Such large-scale

immunophenotyping pipelines contribute to identification of novel protein-coding immunoregulatory genes and provide a starting resource for investigating genetic mechanisms of loss of tolerance.

1.5.3 Transgenic mouse models; tools to study mechanisms of immune tolerance

The explosion of genetically engineered models of human autoimmune disease has been complemented by simultaneous development of tg mouse models, used to elucidate the precise molecular mechanisms driving loss of immune tolerance and, most importantly, lymphocytes of defined specificity. Classically, antigen receptor tg models were used to explore lymphocyte anergy, where a rearranged BCR or TCR is inserted into the germline murine sequence, fixing the specificity of all respective B or T cells to a single epitope (Boyton and Altmann, 2002). These tg mouse lines allow fine control and study of lymphocyte selection and development, as they can be crossed to mouse lines expressing their cognate antigen as an endogenous protein or a self-antigen expressed ubiquitously, or in a tissue-, temporal- or cell-specific manner.

TCR tg models have been key to our understanding of the relationship between strength of TCR signal to T cell selection, including clonal deletion, anergy and positive selection, and in determining at what specific stage of development these checkpoints occur in normal physiology (Strasser, Harris, Von Boehmer, *et al.*, 1994; Clarke *et al.*, 2000; Miyagawa *et al.*, 2010). The phenomenon of B cell anergy was discovered and characterised using BCR transgenics based on the anti-hen-egg lysozyme (HEL)-specific (Ig^{HEL}) model in combination with several HEL-expressing mouse cell lines (Goodnow *et al.*, 1988; Ferry *et al.*, 2003; Fields and Erikson, 2003). By crossing BCR and TCR tg mice to knockout strains, immunological defects can be better pinpointed to individual selection stages of immune tolerance, and the role of antigen exposure explored.

1.6 Summary and aims of thesis

This thesis uses two models and complementary approaches to explore the role of candidate immune modifiers, *Ndrg1* and *Pepd,* in the maintenance of self-tolerance.

In 2015, Oh and colleagues described in a Nature Communications paper that the tumour suppressor N-myc downstream regulated gene 1 (*NDRG1*) is induced by antigen receptor signalling in $CD4^{+}$T cells, and proposed that it played an important role in the maintenance of peripheral T cell tolerance (Oh *et al.*, 2015). NDRG1 is also a therapeutic target in cancer, where it has pleiotropic and context-specific roles dependent on cell and tissue type, and inherited mutations in *NDRG1* are the cause of peripheral nerve damage known as Charcot-Marie-Tooth Disease Type 4D (CMTD4d). The discovery that NDRG1 deficiency might also contribute to T cell-mediated autoimmune disease, raised questions about its broader functions and its relevance in onco-therapy. Identification by Xijin Xu in the Cornall lab that *Ndrg1* is highly differentially expressed in murine anergic B cells compared to follicular naïve B cells (Xu, 2018) suggested that NDRG1 might be a B lymphocyte anergy factor.

In chapter 3 of this thesis, I demonstrate that the transcriptional regulation of *Ndrg1* in B cells mirrors the findings in T cells; it is induced by antigen receptor signalling but inhibited by co-stimulation. I describe a series of experiments, using a CRISPR/Cas9-generated mouse model of *Ndrg1* deficiency and the Ig^{HEL} and soluble HEL (sHEL) models of self-tolerance, in which I show that B cell anergy in the central and peripheral repertoire is intact in the absence of NDRG1.

Chapter 4 revisits the earlier published report of T cell anergy. I describe replication of the ovalbumin (OVA) peptide-induced anergy model and demonstrate that T cell responses are in fact normal in the absence of NDRG1. These findings provide a possible explanation for the previous assertion that *Ndrg1* was a T cell anergy factor.

Having taken a reverse genetics type approach to investigate the role of NDRG1 in lymphocyte anergy, the discovery of an association of the metallopeptidase, prolidase, in regulating immune tolerance was phenotype-driven. Patients with Prolidase Deficiency (PD) present with a varied multisystem immunodeficiency disorder, in some cases accompanied by features of autoimmunity. In a high-throughput immunological screen of knockout mouse lines, prolidase-deficient mice also presented with hallmarks of autoimmunity, including ANA production, and further analysis of this model in our hands demonstrated increased glomerular immune complex deposition, indeed indicating that prolidase deficiency is associated with autoimmune disease. The study of this model identified intrinsic modulation of T cell activation and fate and begins to shed light into how prolidase might act to prevent the loss of immune tolerance.

The experiments detailed in **chapter 5** aim to deeply immunophenotype a mouse model of PD using high-dimensional cytometry and single cell sequencing techniques. Prolidase-deficient mice present with a SLE-like renal phenotype characterised by immune complex deposition and enhanced IgA serum levels, conclusively demonstrating for the first time that *Pepd* loss is strongly associated with autoimmunity. Furthermore, prolidase loss is associated with an altered B cell phenotype and perturbed T cell differentiation; *Pepd*$^{-/-}$ mice have enlarged populations of CD8^{+} effectors expressing an inflammatory, exhausted profile, in addition to losses of Ly6c-expressing CD62L^{+} populations.

Chapter 6 begins to explore how prolidase loss leads to altered T cell differentiation and exhaustion. Here, I describe how intrinsic prolidase deficiency is responsible for driving altered T cell differentiation, an important conclusion as prolidase is ubiquitously expressed and reportedly functions both intra- and extracellularly. Unlike the reduction in Ly6c-expressing populations, the associated increase in CD8^{+} exhausted populations was independent of TCR specificity, and is likely

to be due to increased differentiation of proliferating cells into this phenotype independent of self or foreign antigenic signalling downstream of the TCR. These exhausted populations collect in organs responsible for the removal of autoimmune-associated cells, and are likely to drive enhanced inflammation by accumulating in these areas. Chapter 5 and 6 therefore highlight the important role of prolidase in maintaining immune tolerance and regulating a cell-intrinsic mechanism of $CD8^+$ T cell differentiation.

2. Materials and Methods

2.1 Animal work

All procedures involving animals were performed in accordance with the Animals (Scientific Procedures) Act 1986, amended 2012, with procedures reviewed by the clinical medicine animal care and ethical review body (AWERB) and conducted under Home Office Project License, P79A4C5BA.

All experiments included age and sex matched control animals and controls were co-housed littermates wherever possible.

I would like to acknowledge all the staff at the Functional Genetics Facility for all their help with colony maintenance, and particularly to Peter and Luke for their help with irradiation and procedures.

2.1.1 Breeding and maintenance

I would like to gratefully acknowledge Lucie Abeler-Dörner and the rest of the 3i's team for sharing data from previous phenotyping of the *Pepd*$^{-/-}$ mouse.

C57BL/6JOlaHsd mice were purchased from Envigo and bred in specific pathogen-free individually ventilated cages under PPL P79A4C5BA at the Wellcome Trust Centre for Human Genomics. B6SJL-CD45.1(Ly5^{a}) mice were bred at Biomedical Services, OX1 3RQ. Ig^{HEL} (C57BL/6-Tg(MD4)4Ccg/J), soluble HEL (sHEL) tg mice (C57BL/6-Tg(ML5)5Ccg/J), OT-I mice (C57BL/6-Tg(TcraTcrb)1100Mjb/J) and OT-II tg mice (C57BL/6-Tg(TcraTcrb) 425Cbn/Crl) have been described previously and were maintained on a C57BL/6 background (Goodnow *et al.*, 1988; Hogquist *et al.*, 1994; Barnden *et al.*, 1998; Clarke *et al.*, 2000; Ferry *et al.*, 2003). *Pepd* mice (*Pepd* tm1a(KOMP)Wtsi) have been previously described (Abeler-Dörner *et al.*, 2020) (https://www.immunophenotype.org/threei/home) and were ordered from KOMP IMPC (https://www.mousephenotype.org/data/genes/MGI:97542#order). Genotyping was performed

by PCR from genetic material using the primers below, then visualised by agarose gel electrophoresis. Some PCR products were also subsequently sent for Sanger Sequencing to confirm the sequence:

Ig^{HEL} genomic PCR;	forward-1 5' gcgactccatcaccagcgat 3'
	forward-2 5' ctggagccctagccaaggat 3'
	reverse 5' accacagaccagcaggcaga 3'
sHEL genomic PCR	forward 5' gagcgtgaactgcgcgaaga 3'
	reverse 5' tcggtacccttgcagcggtt 3'
Pepd genomic PCR	forward 5' cccaggctatctcaaagctacg 3'
	reverse 5' aatggctccaagacccacag 3'
OT-I genomic PCR	oIMR1321 5' cagcagcaggtgagacaaagt 3'
	oIMR1322 5' ggctttataattagcttggtcc 3'
	internal positive control forward; oIMR8744 5' caaatgttgcttgtctggtg 3'
	internal positive control reverse; oIMR8745 5' gtcagtcgagtgcacagttt 3'

2.1.2 CRISPR-Cas9 mutagenesis-creation of *Ndrg1*$^{-/-}$ mouse model

Ndrg1$^{-/-}$ mice were generated by CRISPR/Cas9 directed mutagenesis on the Ig^{HEL} background as described in Fig.3.4 in collaboration with Dr Ben Davies, Transgenics Core, Wellcome Centre for Human Genetics. CRISPR/Cas9 nuclease guide (5'gatgacaggacggttgcccttgg) was designed against exon 4 of the *Ndrg1* gene (ENSMUSG00000005125) using the design tool at MIT (crispr.mit.edu). Exon 4 is the most upstream exon of the *Ndrg1* gene for which, if exon skipping occurred despite mutagenesis, the resulting transcript would still contain a missense mutation, leading to nonsense mediated decay. Complementary oligos of the guide sequence (5' caccgatgacaggacggttgccct 3', 5' aaacagggcaaccgtcctgtcatc 3') were annealed, creating a compatible linker for cloning into a pre-BbsI digested CRISPR/Cas9 vector, pX330-Puro. Guide-RNA was prepared using EnGen sgRNA synthesis kit (NEB) and purified using Megaclear Clean-up kit (Ambion). Guide-RNA efficiency and specificity was tested by lipofection into murine melanocyte, B16F10 line. C57BL/6J oocytes derived from *Tg(IghelMD4)4Ccg/J* studs were microinjected with 20ng/μl guide-RNA and 20ng/μl Cas9 mRNA before reimplantation into pseudo-pregnant foster mothers at the two-cell stage.

Founder mice harbouring an indel mutation in *Ndrg1* were identified by PCR and Sanger sequencing using the following primers, *Ndrg1* genomic set 1 for PCR and Sanger Sequencing; forward 5' ggactgtgcttgtatgacattc 3', reverse; 5'gtgtccatagtcagtgggtcag 3', *Ndrg1* genomic set 2 PCR; forward 5' ccaaactcacggttcatgcc 3', reverse 5' caggtgatgggcctctgtct 3', amplifying a 522bp region and 151 bp region of *Ndrg1* exon 4, respectively. Founder mice were then backcrossed for 7 generations with wild-type (WT) C57BL6/J mice, and intercrossed to generate homozygotes, selecting both *Ndrg1*$^{-/-}$ Ig^{HEL} tg and *Ndrg1*$^{-/-}$ non-tg animals for experiments. The following primers sets were used for PCR and Sanger sequencing of *Ndrg1* mRNA, mRNA set 1 spanning whole CDS; forward 5' atgtcccgagagctacatg *3'* and reverse *5'* ttagcaggacacctccatgg 3' and mRNA set 2; forward 5' atgtcccgagagctacatg 3' and reverse 5' agttgaagaggggttgtag *3'.*

2.1.3 Immunisation

HEL conjugated to sheep red blood cells (HEL-SRBC) was prepared by incubating SRBC in Alsevers solution (FirstLink) with 20mg HEL per 10ml 10% SRBC in conjugation buffer (0.35M Mannitol, 0.01M NaCl in HBSS) and later addition of 100mg EDCI (Sigma Aldrich). After washing with HBSS, 200μl 2x10^9 HEL-SRBC was injected intraperitoneally into each mouse.

Modified vaccinia virus ankara (MVA)-immunisation was performed under anaesthesia, each mouse received 1x10^6 PFU either intradermally or intramuscularly, and was monitored and weighed daily for 10 days or until weight was fully recovered.

2.1.4 Irradiation BM chimeras

For BM chimeras, sHEL and non-tg CD45-1$^+$ heterozygous or homozygous recipients were irradiated with two doses of 4.5 Gy, spaced by 3 hours and then intravenously injected with at least 5x10^6 donor BM cells. All chimeras were given water treated with 1% baytril antibiotic (Enrofloxacin) for at least the first 3 weeks of reconstitution. BM chimeras were allowed to reconstitute for at least 7 weeks before immunisation or analysis. Specified mice received BrdU for 7 days in their drinking

water at a final concentration of 0.8mg/ml. The water was supplemented with 1% sucrose to ensure palatability.

2.1.5 Sample processing

All mice were euthanised by Schedule 1. Whole blood was extracted and spun at 17,000xg for 10 minutes for serum isolation, which was subsequently removed from the cell pellet, spun a second time and then extracted and stored at -20°C. Tissues were harvested on ice and processed to single cell suspensions for BM, spleen, thymus, peritoneal cavity, liver, peyer's patches and MLNs in R2 media (RPMI media containing 2% fetal calf serum (FCS), 10-20mM Hepes) for subsequent analyses. Cell counting was performed using white blood cell counting fluid (1.5% acetic acid, 0.5% methyl violet in water) and a haemocytometer. If required for downstream applications, splenic, liver and thymic cell preparations were treated with red blood cell (RBC) lysis. Harvested kidneys were processed immediately for protein or RNA lysates (as described below). Organs for histology were stored in 10% neutral-buffered formalin for 24h before replacing with 70% ethanol for paraffin embedding, or stored at -80°C post-freezing in liquid nitrogen for later OCT embedding.

2.2. Cellular assays

2.2.1 *Ex vivo* cell sorting, culture and stimulation

Total B cells were isolated from RBC-lysed splenocyte suspensions by positive selection using Miltenyi Biotec MACS LS columns and CD45R (B220) microbeads. Total T cells were isolated from processed and ACK-treated spleens using magnetic sorting and Miltenyi Biotec Pan T cell isolation kit II, mouse (130-095-130) by protocol.

Cells were cultured at a final density of 1-2x10^5 cells/mL in complete R10 (RPMI media with 10% FCS plus non-essential amino acids, 1mM Sodium Pyruvate and 50µM 2-β-Mercaptoethanol, 20mM Hepes, 2mM L-Glutamine, 10units/mL penicillin, 10µg/mL Streptomycin and 20µg/ml neomycin/mL) at 37°C, 5%$C0_2$. For RNA extraction, cells were washed with PBS after 24h culture

and pelleted for later RNA extraction as described below. For proliferation analysis, 10^6-10^7 cells were labelled with 2.5µM CellTraceViolet (CTV) Dye before culturing for 72-96 hours then analysed by flow cytometry. Stimuli were prepared as indicated in complete R10; anti-IgM, µ-chain specific (Jackson ImmunoResearch; 115-005-075), LPS from Salmonella species (Sigma Aldrich; L7770), hen egg lysozyme (Sigma Aldrich; L6876-5G), and LEAF purified anti-CD40 (Biolegend; 102908), LEAF purified CD3e (Biolegend; 100331), LEAF-purified anti-CD28 (Biolegend; 122004) and recombinant mouse IL-4 (Biolegend; 715004).

2.2.2 Flow cytometry

Briefly, 0.5-1x10^6 cells were aliquoted and washed twice with 200µl FACS buffer (PBS with 2%FCS, 20mM Hepes, 0.05% sodium azide). Cells were resuspended in 25-50µl antibody staining cocktail for 20-30 minutes on ice in the dark then washed twice with 200µl FACS buffer and resuspended in FACS buffer to be acquired for analysis on a BD FACS CANTO10c. HEL-binding cells were detected by pre-incubation with 200ng/ml HEL on ice, washed with FACS buffer, then counterstained with HyHEL9 (a kind gift from Jason Cyster) conjugated to pacific blue or FITC. Antibodies used for both surface and intracellular staining are detailed in appendix A.

2.2.3 Phospho-FLOW and intracellular staining

2-5x10^6 splenocytes were stimulated with 1µg/ml sHEL or 10µg/ml anti-IgM $F(ab)_2$ (Jackson Immunoresearch) at 37°C for 5 minutes and then subsequently fixed and permeabilised using the BD Cytofix/Cytoperm kit in combination with Cytofix and Perm Wash buffer (BD Biosciences; 554655, 554722, 557885) before staining in intracellular antibody staining cocktail.

For recall of antigen-specific T cells in the peripheral lymphoid organs of immunised mice, 2-5x10^6 splenocytes were stimulated with epitopes from MVA, B8R peptide (sequence TSYFKESV, 2µg/ml) or $CD8^+$ OT-I-specific OVA peptide (SIINFEKL, 2µg/ml) for 5h in R10 medium at 37°C in the presence of GolgiPlug (BD Biosciences; #555029 1:1000) and GolgiStop (BD Biosciences; #554724 1:1500).

Cells were then washed with FACS buffer, surface stained and cytokine production was measured by intracellular staining following fixation and permabilisation with cytofix/cytoperm as described above.

To detect BrdU incorporation, surface-stained cells, fixed using BD Cytofix/Cytoperm, were washed, then treated with BD Cytoperm Permeabilization Buffer Plus (BD Biosciences; 561651) by protocol, and re-fixed before treatment with 30μg DNase/10^6 cells for 1 hour at 37°C. Following washing, cells were incubated with fluorescent anti-BrdU, followed by washing and acquisition.

2.2.4 Fluorescent activated cell sorting (FACS)

I would like to acknowledge Ruddy Montandon in the WTCHG flow cytometry facility for help sorting samples.

$1x10^6$ live $CD45.1^-CD45.2^+$ T cells were sorted on a FACSAria Fusion Cell sorter at the WTCHG flow cytometry facility from magnetically-isolated splenic T cells stained with live/dead (APC-Cy7 640-780/60-A), anti-CD45.1 (PB 405-450/50-A), anti-CD45.2 (PE 561-582/15-A) with negative dump channel, AlexaFluor700 (640-730/45-A) containing anti-B220 and anti-CD19 and negative dump channel APC (640-670/30-A) containing CD11b, MHC-II, CD11c and CD49b.

2.2.5 In vivo T cell anergy experiments

Protocol as previously described by Oh et al (Oh et al., 2015); briefly $CD4^+$ T cells were isolated from WT $OT\text{-}II^+$ or $Ndrg1^{-/-}$ $CD45.2^+$ OT-II+ tg mice and adoptively transferred to $CD45.1^+$ non-tg congenic recipients, with subsequent intravenous injection of 500μg OVA peptide on day 1 (Insight Biotech; 21-51023-G (323-339)). 5 days later, total splenic $CD4^+$ cells were magnetically isolated from recipient mice and naïve unstimulated WT or $Ndrg1^{-/-}$ $OT\text{-}II^+$ control mice, before loading with CTV viable dye. As determined by flow cytometry, $4x10^4$ $CD45.2^+V\alpha2^+OT\text{-}II^+$ cells were cultured *in vitro* at 37°C with a titration of OVA peptide for 72h and $4x10^5$ irradiated splenocytes. In some experiments, 10μM BrdU was added at 48h after the setup of the culture. Proliferation of

CD45.2^{+}Vα2^{+} OT-II^{+} CD4^{+} T cells was then detected by flow cytometry by CTV dilution or BrdU incorporation.

2.2.6 Mass cytometry immunophenotyping

I gratefully acknowledge Michalina Mazurczyk and Giorgio Napolitani for their help with performing the CyTOF experiments, as well as for their insights into analysis.

2.2.6.1 Antibody Conjugation

100μg of each of anti-Bcl2, anti-HIF1a, anti-CXCR3, anti-CXCR4, anti-CXCR5, anti-Bcl6, anti-ICOS, anti-FoxP3, anti-CD45.1 and anti-CD95 were conjugated in house using Maxpar X8 antibody labelling kits according to manufacturer instructions (Fluidigm cat #PRD002 Version7, Fluidigm; 141Pr# 201141A, 147Sm # 201147A, 153Eu # 201153A, 154Eu # 201154B, 163Dy #201163A, 164Dy #201164A, 165Ho #201165A, 174Yb #201174B, 166Er #201166B, 173Yb #201173A). Single use X8 polymer tubes were preloaded with L-buffer (#S00007) and the specified Ln metal solution for 40 minutes at 37°C, then transferred to a 3kDa filter containing L-buffer and spun at 12,000xg for 25 minutes. 400μl C-buffer (S00003) was added to the filter and centrifuged for 30 minutes at 12,000xg. 100μg of antibody was added to a separate 50kDa filter and spun for 10 minutes at 12,000xg, adjusted to 400μl with R-buffer (#S00001) and spun again. 100μl 4mM Tris(2-carboxyethyl)phosphine hydrochloride (TCEP; Sigma #646547) prepared in R-buffer was added to the 50kDa filter unit after flow-through discard and incubated for 30 minutes at 37°C. 300μl C-buffer was added to the 50kDa filter and centrifuged for 10 minutes at 12,000xg then repeated with 400μl C-buffer following discard of flow through. The polymer was then transferred into the 50kDa filter containing the antibody and incubated for 90minutes at 37°C, then washed with 400μl W-buffer (#S00005) and centrifuged for 10 minutes at 12,000xg three times over. The yield was determined using a NanoDrop spectrophotometer and adjusted to 0.5mg/ml using antibody stabiliser PBS and titrated using the staining protocol below.

2.2.6.2 Maxpar cell surface antigen staining protocol

Centrifugation steps were performed at 400xg for 5 minutes pre-fixation, then 800xg for 5 minutes post-fixation. 10% $CD45.1^+$ splenocytes were spiked into $CD45.2^+$ samples for batch correction across samples. $2x10^6$ cells were washed with Maxpar cell staining buffer (CSB; fluidigm #201068), then resuspended in total 0.1μm filtered 100μl antibody cocktail using the antibodies in table 2.1 at the specified titration in CSB and incubated at RT for 30 minutes before 1μl Cisplatin (Fluidigm #201064) prior diluted 100x in PBS was added for an additional 5 minutes incubation. Samples were washed with 2ml of CSB three times and then resuspended in 1ml pre-diluted Nuclear Antigen Staining Buffer (#201063) and incubated for 30 minutes at RT. Cells were washed with 2ml of Nuclear antigen staining perm wash three times, then resuspended in intracellular antibody cocktail, prepared in the permeabilisation buffer used for washes then incubated for 30-45 minutes at RT. Samples were washed three times and then resuspended in 1ml 1.6% formaldehyde prepared in PBS, washed three times with 2ml CSB and resuspended in 1ml 72.5nM Cell-ID Intercalator-Ir (#201192A) in PBS, and incubated overnight at 4°C. Cells were washed twice with CSB, twice with water and then adjusted to $1x10^6$/ml with water, 10% EQ beads were added and filtered into cell strainer tubes for acquisition on a Helios mass cytometer.

Table 2.1 CyTOF antibody panel

Antibodies in yellow denote intracellular stains. Titrations are provided for 100µl.

	Intracellular	Titration	Clone	Supplier	Catalog
141Pr	Bcl2	0.5	BCL/10C4	Biolegend	633502
142Nd	CD4	0.25	RM4-5	In house	
143Nd	CD19	0.25	6D5	In house	
144Nd	CD8a	0.5	53-6.7	In house	
145Nd	IgD	0.25	11-26c.2a	In house	
146Nd	Ly6C	0.25	HK1.4	In house	
147Sm	HIF1a	1	241812	R&D systems	MAB1935
148Nd	I-A/I-E	0.25	M5/114.15.2	In house	
149Sm	CD11b	0.5	M1/70	In house	
150Nd	CD44	0.25	IM7	In house	
151Eu	CD5	0.5	53-7.3	In house	
152Sm	IL-17	1	TC11-18H10.1	In house	
153Eu	CXCR4	1	L276F12	Biolegend	146502
154Sm	CXCR5	0.5	L138D7	Biolegend	145502
155Gd	CD62L	0.5	MEL-14	In house	
156Gd	CD69	0.5	H1.2F3	In house	
158Gd	IgM	0.5	RMM-1	In house	
159Tb	Tcrb	0.5	H57-597	In house	
160Gd	B220	0.5	RA3-6B2	In house	
161Dy	CD3	0.5	145-2C11	In house	
162Dy	CD27	0.5	LG.3A10	In house	
163Dy	Bcl6	0.25	IGI9IE/A8	Biolegend	648302
164Dy	CXCR3	0.25	CXCR3-173	Biolegend	126502
165Ho	ICOS	1	C398.4A	Biolegend	313502
166Er	CD45.1	0.25	A20	Biolegend	110702
167Er	F4/80	0.5	BM8	In house	
168Er	Ki-67	0.25	B56	In house	
169Tm	NK1.1	0.5	PK136	In house	
170Er	PD-1	0.5	RMP1-30	In house	
171Yb	CD25	1	3C7	In house	
172Yb	CD103	0.5	2E7	In house	
173Yb	CD95	1	SA367H8	Biolegend	152602
174Yb	FoxP3	1	MF-14	Biolegend	126402
175Lu	Ly6G	0.5	1A8	In house	
176Yb	CD127	0.5	A7R34	In house	
209Bi	CD11c	0.5	N418	In house	
89Y	CD45	0.5	30F11	In house	

2.2.6.3 CyTOF compensation protocol

For compensation, one drop of OneComp eBeads compensation beads (#01-1111-42) was stained with 1µl of each antibody for 15 minutes at RT, then washed three times with 200µl CSB, then pooled into one tube and fixed with 1.6% PFA for 1h at RT. After washing twice with PBS and twice with water, beads were resuspended in water and acquired on a Helios mass cytometer.

2.2.6.4.CyTOF data analysis

Files were processed following at event duration minimum 10 to maximum 75 and at Fluidigm recommendation, including randomization and normalization using EQ Beads signal. FCS files were compensated for spillover between metal isotopes using the CATALYST tool, employing NLS compensation (Chevrier *et al.*, 2018) and the panel was updated using cytofCORE (). FlowJo was used to gate out beads, then on cells that were singlets, alive and $CD45^+$ that are $CD45.1^+$. Clustering was performed using Cytofkit analysis by providing 10,000 cells per sample and all markers except CD45 and CD45.1. T-distributed stochastic neighbour embedding (tSNE) analysis was used for visualisation employing the transformation method, cytofAsinh (Chen *et al.*, 2016).

For downstream analysis, CD8-expressing populations were manually gated in flowJo and downsampled to the smallest number of $CD8^+$ cells in a sample (9,500 events). For Cytofkit analysis, $CD8^+$ cells were clustered at a resolution of 15 clusters in FlowSOM using the following markers; CD3e, CD27, CXCR3, Ki-67, PD-1, CD5, CXCR4, CD62L, CD69, ICOS, CD8a, Ly6c, CD44, Bcl2, HIF1a, IL-17, CXCR5, TCRB, CD25, CD103, CD95, FoxP3 and CD127, transforming with cytofAsinh. Clusters were visualised by uniform manifold approximation and projection (UMAP) and cluster identities were determined by heatmaps of the mean expression values of markers per cluster. For Citrus analysis of $CD8^+$ populations on the Cytobank platform (Bruggner *et al.*, 2014), files were assigned to their experimental groups and the Nearest Shrunken Centroid (PAMR) association model was

performed with the following specifications for analysis; minimum cluster size of 1, cross validation folds of 5, false discovery rate of 1 with equal event sampling and clustering characterisation by medians. The PAMR method was used as it represents a predictive model that incorporates a false discovery rate. The following markers were used for clustering; CD3e, CD27, CXCR3, Ki-67, PD-1, CD5, CXCR4, CD62L, CD69, CD8a, Ly6c, CD44, HIF1a, IL-17, CXCR5, CD95, CD127 and Bcl2, and the median statistic channels tested for differences were CD27, Ki-67, PD-1, CD5, CD69, CD62L, Ly6c, CD44, Bcl2, HIF1a, CD95 and CD127.

2.3 Transcriptomic profiling

2.3.1 Bulk RNA-Seq

Raw RNA-Seq data produced by Xijin Xu was previously deposited in the Gene Expression Omnibus (https://www.ncbi.nlm.nih.gov/geo/) under accession code GSE135650 (Xu *et al.*, 2020). This RNA-Seq data was initially processed by Xijin Xu using CGAT Pipelines and tools (https://github.com/CGATOxford/CGATPipelines) as described before (Xu, 2018; Xu *et al.*, 2020); briefly, reads were aligned to the mm10 mouse genome using hisat2 v.2.1.0 (Kim *et al.*, 2019), and reads were quantified over feature annotations from GRCm39 assembly using featureCounts v.1.4.6 in the Subread software package (Liao, Smyth and Shi, 2014).

DESeq2 v.1.28.1 was used for differential expression analysis between follicular and anergic B cell populations (Love, Huber and Anders, 2014). A gene was considered differentially expressed if the log2 fold change was ±1 and adjusted p value < 0.05. Differential gene expression was visualised using EnhancedVolcano v.1.8.0 (Blighe, Rana and Lewis, 2019), and pheatmap v.1.0.12 (https://github.com/raivokolde/pheatmap) was used to visualise variance stabilising transformed counts between anergic and naïve follicular B cells. Gene ontogeny enrichment analysis was performed on the differentially expressed gene list using ClusterProfiler v.3.16.1(Yu *et al.*, 2012), using a p value cut-off of 0.05 for subontology, 'BP', employing ensembl annotation from

org.Mm.eg.db v.3.11.4(Carlson, 2019). GO results were visualised using EnrichPlot v.1.8.1 (https://github.com/YuLab-SMU/enrichplot).

2.3.2 Single cell RNA and ADT proteomic sequencing

2.3.2.1 Sample submission

Thank you to the Oxford Genomics Centre for performing scRNA-Seq on samples and for initial processing of the data for downstream analysis.

Experiment 1. Magnetically isolated T cell populations from 3 WT and 3 *Pepd*$^{-/-}$ mice aged 30-42 weeks were incubated with FC block, then washed and hashtagged by sample using Biolegend TotalSeq-B hashing antibodies (B0301 #155831, B0302 #155833, B0303 #155835, B0304 #155837, B0305 #155839, B0306 #155841) by protocol. After washing, samples were pooled and stained using Biolegend TotalSeq-A antibodies as protocol (anti-CD4 A-0001 #100569, anti-CD8a A-0002 #100773, anti-CD279 (PD-1) A-0004 #109123, anti-CD44 A-0073 #103063, anti-CD62L A-0112 #104451, anti-CD45.1 A-0178 #110753, anti-CD45.2 A-0157 #109853, anti-CD25 A-0097 #102055, anti-CD127 (IL7R) A-0198, #135045, anti-ICOS A-0171 #313555, anti-CD69 A-0197 #104546, anti-CD27 A-0191 #124235, anti-CD5 A-0111, #100637, anti-KLRG1 A-0250 #138431, anti-CD95 A-0917 #152614). After washing, cells were resuspended at 1-2M/ml and loaded into the chromium controller (10X-Genomics) chip and sequenced as previously described (Kendal *et al.*, 2020).

Experiment 2. Magnetically isolated T cell populations from 4 WT:WT and 4 WT: *Pepd*$^{-/-}$ BM chimeric mice were hashtagged by sample as above with the addition of B0307 (#155843) and B0308 (#155845), washed then pooled and CD45.2^{+} cells were isolated by FACS. The sample was then labelled with TotalSeq-A antibodies as above, minus A-0178 and A-0157, washed and submitted for sequencing.

2.3.2.2 scRNA-Seq bioinformatic analysis

I would like to thank the Oxford Biomedical Data Science Training Course team for guidance and support in bioinformatics and data processing.

The raw single cell sequencing data were mapped and quantified with 10X-Genomics CellRanger count v3.1.0, using transcriptome mm10-1.2.0 (experiment 1) or mm10-3.0.0 (experiment 2) for the gene expression matrices. The EmptyDroplets algorithm was used to call cells based on the gene expression library, then a Seurat object was created from the three libraries, gene expression (RNA), hashtag information (HTO) and surface antibody-derived information (ADT) by filtering on cell barcodes identified in the gene expression assay by CellRanger. The following steps were performed in Seurat v3.1.2. After centered log ratio transformation (CLR)-normalisation of the HTO assay, samples were demultiplexed using htodemux, which also identifies doublets and negative cells that were later removed from the object.

Samples were filtered based on the gene expression assay for mitochondrial genes and numbers of features and counts. The ADT assay was CLR-normalised and scaled for initial dimensionality reduction and clustering using the FindNeighbours and FindClusters functions. For clustering and dimensionality reduction, the RNA assay was normalised using the SCTransform function, though for differential expression and visualization, Log-normalised RNA counts were used. Seurat v4.0.3 or Seurat v3.9.9 was used for weighted nearest neighbor (WNN) assay integration, clustering and downstream analysis (Stuart *et al.*, 2019; Hao *et al.*, 2021). Trajectory analysis used Slingshot v1.8.0 (Street *et al.*, 2018); the clustered, log-normalized Seurat object was split by genotype and these objects were provided as input for the trajectory inference step, with naïve cells specified as the start cluster.

Based on subpopulations identified by Seurat unbiased clustering, differential expression analysis between clusters was performed using Seurat FindMarkers function and visualised in Seurat and

EnhancedVolcano plots (Blighe, Rana and Lewis, 2019). For differential expression between WT and *Pepd*$^{-/-}$ cells, pseudobulk differential state analysis was performed using muscat v1.4.0 (Crowell *et al.*, 2020), with data visualised using the scater package (McCarthy *et al.*, 2016). Pseudobulk analysis created an aggregated pseudo-bulk RNA-Seq object for each cluster by sample, and sample-level differential gene expression was calculated across groups from a submitted design matrix (Crowell *et al.*, 2020). Fast gene set enrichment analysis (FGSEA) of published gene sets identified in https://www.gsea-msigdb.org/gsea/index.jsp was performed using fgsea v1.14.0 (Korotkevich *et al.*, 2016) using a ranked expression matrix as input. Thresholds for significance are defined within figure legends.

2.3.3 Quantitative real-time PCR

RNA was extracted from homogenised murine kidney lysates or 10^6-10^7 pelleted cells using the Qiagen RNeasy Plus kit (Qiagen; 74134) or using TRIzol extraction (Life Technologies; 12183555) by protocol. Equivalent quantities of RNA were then reverse transcribed to cDNA using SuperScript II Reverse Transcriptase (ThermoFisher Scientific; 18064014), priming with Oligo(dT12-18) primer (ThermoFisher; 18418012). Expression of *Ndrg1* and *Gapdh* mRNA was quantified by qPCR using SYBR Green PowerUp Master Mix (ThermoFisher Scientific; A25776) with the following primers *Ndrg1* qPCR forward 5' accctgagatggtagagggtctc 3', reverse 5'ccaatttagaattgcattccacc 3', *Gapdh* qPCR forward 5' tgtgtccgtcgtggatctga 3', reverse 5'ttgctgttgaagtcgcaggag 3', and run on a Bio-Rad CFX96 detection system. Standard curve construction demonstrated equivalent efficiencies of *Ndrg1* and *Gapdh* cDNA amplification, therefore changes to *Ndrg1* mRNA levels were directly calculated relative to endogenous *Gapdh* expression using the following equation: 1/(2^(*Ndrg1* C_t – *Gapdh* C_t))*100.

2.4 Molecular analyses

2.4.1 Western blot

Kidney protein lysates were produced by homogenisation in lysis buffer containing 50mM Tris HCl pH7.4, 0.5%NP40, 150mM NaCl, 20mM $MgCl_2$, protease and phosphatase inhibitors (Sigma Aldrich; 4906837001/5892970001), or in supplemented RIPA buffer (Santa Cruz; sc-24948). As measured by Pierce BCA assay (ThermoFisher #23225), 1-25μg protein lysate was reduced by addition of SDS-containing reducing buffer containing 0.1M DTT and denatured by boiling at 95°C for 5 minutes and loaded onto 4-12% Tris-HCl gels (ThermoFisher; NP0323BOX. Proteins were transferred to a nitrocellulose membrane, blocked with 5% BSA or 5% non-fat milk and probed with indicated antibodies. Antibodies; anti-NDRG1 D6C2 mAb #9408 (1:1000) and anti-rabbit IgG, HRP-linked antibody #7074 were ordered from cell signalling technologies. Monoclonal anti-β-actin-peroxidase A3854 (Sigma 1:10000) was used as a loading control and Amersham ECL prime (RPN2232) was used for detection.

2.4.2 ELISA

Serum HEL-specific IgM^a ELISA was performed as previously described (Xu *et al.*, 2020). Briefly, for HEL-specific ELISAs, half-area high binding Greiner plates were coated with 10μg/ml HEL in carbonate buffer pH9.6 (20mM Na_2CO_3, 35mM $NaHCO_3$), incubated overnight at 4°C, washed with PBS/Tween20, then blocked with PBS, 1%BSA for 1h. After washing, serially diluted serum samples were added to wells in PBS/0.1%BSA in duplicate. After incubation at 37°C for 2 hours and washing, plates were incubated with 0.5μg/mL biotinylated anti-IgMa (BD Pharmigen, #553515; clone DS-1) or anti-IgG-HRP (Bethyl laboratories) in ICE-T buffer (1%FCS, 1% milk powder, 0.1% Tween20 and NaN_3 in PBS) at 37°C for 1 hour then washed. Avidin-alkaline phosphate (A7294) was added to the wells at 1:3000 in PBS/0.1%BSA and incubated at 37°C for 1 hour. After washing with PBS/Tween20, triple distilled water (DW) and NPP buffer (50mM Na_2CO_3, 0.5mM $MgCl_2$ pH9.8.), wells were developed with addition of 1mg/ml Sigma 104 phosphatase substrate (#104105) in NPP buffer and absorbance measured at 405nm using a Bio-Rad model 550 Microplates reader. Absorbance

measured at 405nm using a Bio-Rad model 550 Microplates reader. Background absorbance values were subtracted from absorbance readings before interpolation to standard curve using Hyperbola (X is concentration).

Bethyl laboratories mouse IgG (E90-131), IgM (E90-101) and IgA (E90-103) quantification kits were used by protocol with serum titration of samples as follows: IgG 1:4000, IgM 1:2000, IgA 1:2000 or 1:4000, developed using TMB substrate (Life Technologies; 00-4201-56) and detected at 450nm. Il-2 concentration in the supernatant was quantified by Mouse Ready-Set-Go IL-2 ELISA kit (eBioscience; 88-7024) and developed using TMB substrate as above.

2.4.3 Anti-nuclear antibody staining

ANA titres were detected as previously described and the positive control was pooled from positive samples from the 3i's cohort (Abeler-Dörner *et al.*, 2020). Briefly, serum samples were diluted at 1:100 in PBS and stored at -20C before incubation on Hep-2 cell coated slides (A.Menarini; 37806) for 30 minutes at room temperature, in a humidifying chamber. Slides were washed with PBS, then water and then incubated with FITC-conjugated, goat anti-mouse IgG (ThermoFisher; 62-6511) for 20 minutes at room temperature in a humidifying chamber. Slides were washed, then mounted and stored at 4C, before imaging on Nikon wide-field TE20000U Microscope or a Deltavision Elite wide field system (GFP channel: 20x, 400ms). Images were analysed using multi-parametric analyses in Fiji and intensity scored from 0-4 based on control samples, including FITC-QC slide (A.Menarini; 1900). Positive scoring samples (2+) were manually cross-checked by eye before scoring.

2.5 Histology

2.5.1 Tissue fixation and sectioning

Formalin-fixed tissues stored in 70% ethanol were dehydrated further using an automated tissue processor by moving to two baths of 70% ethanol, two 90% ethanol, three 100% ethanol and three

baths of melted wax, then embedded in paraffin blocks. Sections were cut from 3-10μm using a microtome.

For cryosections, frozen tissue was embedded in OCT (CellPath; KMA-0100-00A) then 5um sections were cut on a Leica Ultracut UCT ultramicrotome then let dry before storing at -20°C.

2.5.2 H & E staining

Paraffin slides were rehydrated in xylene for 5 minutes twice, then transferred for 5 minutes to 100% ethanol, 5 minutes in 95% ethanol, 5 minutes in 70% ethanol and then 5 minutes in 50% ethanol before 5 minutes in DW. Slides were then transferred to neat haematoxylin for 10 sec, then rinsed in running DW for 5 minutes. Slides were dipped in acid alcohol (5ml concentrated HCl (34.5-38%) in 0.5L 70% ethanol), then rinsed in DW for 5 minutes. Slides were dehydrated through 5 minute changes in 50% ethanol, 5 minutes in 70%, 5 minutes in 95% ethanol then 1 minute in 0.5% eosin 95% ethanol before a quick rinse in 100% ethanol. Slides were then transferred to xylene for 5 minutes twice, then mounted with DPX for imaging on an Aperio SlideScanner at 40X magnification.

For H&E staining of cryosections, slides were fixed in two baths of ice-cold acetone for 10 minutes, then washed and stained from the haematoxylin stage as above.

2.5.3 Immunohistochemistry

Frozen sections were fixed in two ice-cold baths of acetone, with washes with TBST (20mM TrisHCL ph 7.4, 150mM NaCl) in between, then washed three times with TBST. Slides were blocked in goat serum (10%) in a humidified chamber for 1h at 37°C. After three TBST washes, primary antibody was added in Ab dilutent (1%BSA, 0.05%tween20 in TBST), overnight at 4C. After three washes with TBST, fluorescently-tagged secondary antibody was added for 45-60 minutes at 37°C, then washed three times and counterstained with DAPI for 3 minutes at room temperature. Slides were washed,

then mounted with Vectashield aqueous medium (Vectorlabs; H-1000-10). Antibodies used were as follows: anti-mouse IgG alexaFluor-488 (ThermoFisher; 62-6511), anti-mouse C1q (HyCult; HM1096-100UG) and secondary; goat anti-mouse IgG alexaFluor-647 (Life Technologies; A21235), goat anti-mouse IgA (Cambridge BioScience; A90-103A) and secondary; donkey anti-goat IgG alexaFluor-488, (ThermoFisher; A11055).

2.6 Statistical analysis

GraphPad Prism Software was used for statistical analyses of graphical data, and unpaired, two tailed Student's t tests, multiple t tests or two-way ANOVA were used for statistical comparison between groups, unless otherwise specifically mentioned. Multiple testing was adjusted for using either Holm-Sidak (multiple T test) or Sidak (ANOVA) method.

3. NDRG1, a tumour suppressor protein involved in regulating growth and apoptosis

3.1 Chapter introduction

Lymphocyte anergy is defined as an autonomous suppressive state induced on suboptimal antigen receptor signalling in the absence of co-stimulation. The mechanisms that drive anergy induction and maintenance in both B and T lymphocytes are still not fully understood, and experiments identifying novel candidate factors are key to deepening our knowledge of how lymphocytes balance activating versus tolerogenic responses (Macián *et al.*, 2002). In 2015, anti-cancer therapeutic target, NDRG1, was identified as a novel $CD4^+$ anergy factor upregulated by TCR-dependent *Egr2/3* activation alone in naïve and anergic $CD4^+$ T cells, and down-regulated in a proteasome-dependent manner by co-stimulation. The loss of NDRG1 *in vivo* was described as partially rescuing peptide-induced T cell tolerance, and *in vitro* induction of NDRG1 expression led to a hyporesponsive state in $CD4^+$ T cells consistent with clonal $CD4^+$ T cell anergy (Oh *et al.*, 2015).

NDRG1 is a stress and hypoxia-inducible 43kDa protein associated with regulation of cell growth and differentiation, (Van Belzen *et al.*, 1997; Piquemal *et al.*, 1999; Stein *et al.*, 2004; Ellen *et al.*, 2008; Sahni *et al.*, 2014) and reported to be necessary but not essential for p53-mediated caspase activation and apoptosis (Stein *et al.*, 2004). Though ubiquitously expressed in human tissues, the amount and subcellular localization of NDRG1 expression varies by cell type, with relatively higher staining in kidney, prostate, ovary, small and large intestines and brain tissues, and particular localization to the cytoplasm of Schwann cells in peripheral nerve tissue (Pascale Lachat, Philip Shaw, Sandra Gebhard, Nico van Belzen, 2002). Indeed, NDRG1 mutations cause a form of CMTD4d in both mice and humans; this autosomal recessive demyelinating distal neuropathy is thought to be due to impaired vesicular trafficking of lipids for Schwann cell myelination caused by NDRG1 loss (Echaniz-Laguna *et al.*, 2007; Pietiäinen *et al.*, 2013; Li *et al.*, 2017). *Ndrg1*$^{-/-}$ mast cells also

show impaired exocytosis and degranulation, in addition to reduced maturation and differentiation, further evidence of NDRG1's role in regulating vesicular transport (Taketomi *et al.*, 2007). Figure 3.1 illustrates the currently described roles and functions of NDRG1 .

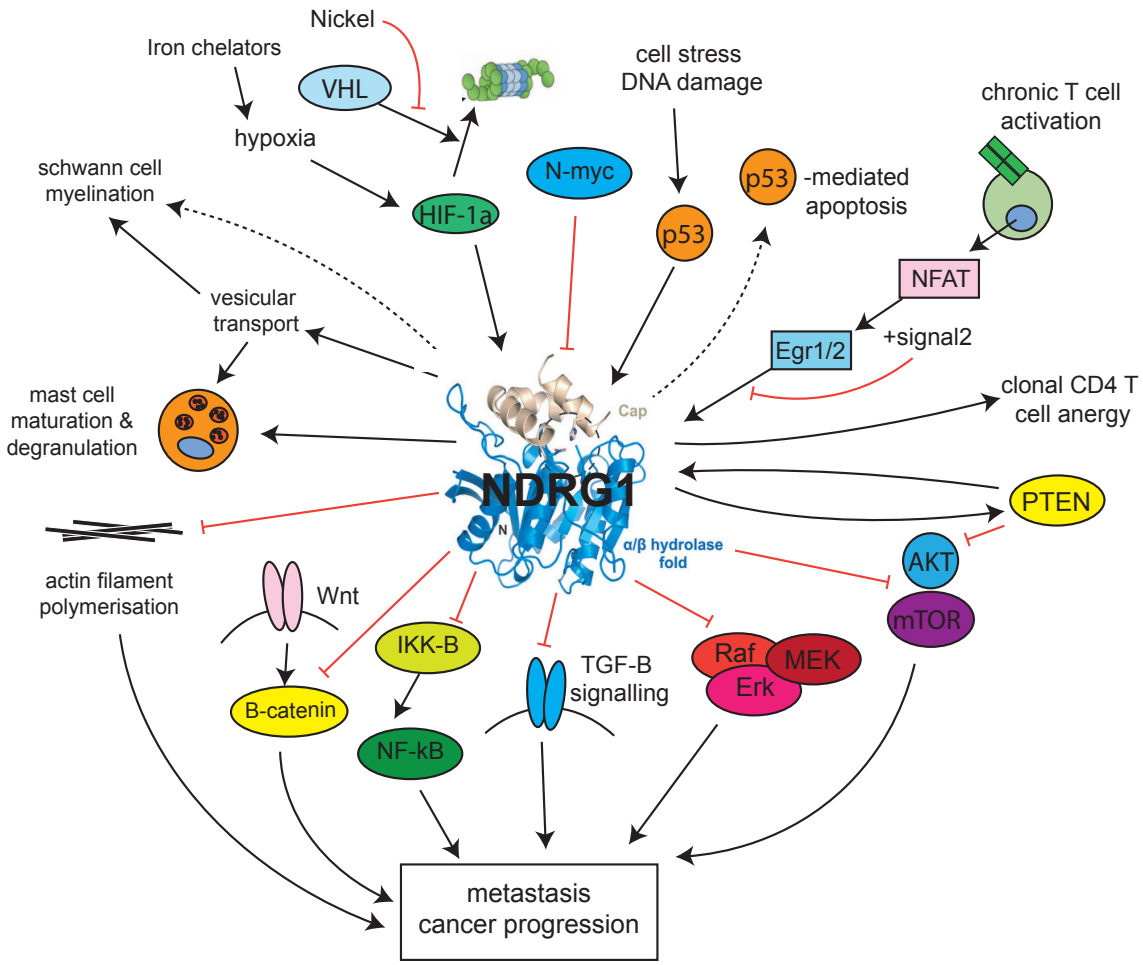


Figure 3.1 NDRG1 is induced by stress and hypoxia signals and is proposed to regulate multiple signalling pathways.

NDRG1 reportedly interacts with key signalling pathways and has been implicated in multiple biological outcomes. Crystal structure source; https://febs.onlinelibrary.wiley.com/doi/full/10.1111/febs.15660

The role of NDRG1 within cancer biology has been extensively studied, where its functions appear to be highly pleiotropic in a cell type and context-specific manner. NDRG1 expression is suppressed via N-myc and the locus is hypermethylated in many cancer tissues including gastric, colon, pancreatic, prostate and some breast cancers (Van Belzen *et al.*, 1997; Bandyopadhyay *et al.*, 2003, 2004; Angst *et al.*, 2011; Chang *et al.*, 2016). In such tissues, NDRG1 has been reported to possess potent anti-metastatic activity, through several of the signalling pathways summarised in fig. 3.1,

including antagonism of EMT-associated TGF-β signalling, the Raf/MEK1/ERK axis, NF-κB canonical and non-canonical signalling, PI3K/AKT/mTOR molecular pathways and inhibition of F-actin polymerisation-mediated migration in cancer cells (Kurdistani *et al.*, 1998; Chen *et al.*, 2012; Sun *et al.*, 2013; Fang *et al.*, 2014). NDRG1-mediated inhibition of tumour growth and metastasis may explain the anti-cancer effects of iron chelating agents such as Dp44mT (Chen *et al.*, 2012, 2018; Sun *et al.*, 2013). However positive correlation between tumour tissue NDRG1 levels and cancer progression in some human studies suggests differential functions of NDRG1 (Ring *et al.*, 2006; Chua *et al.*, 2007; Li *et al.*, 2019), with silencing of NDRG1 inhibiting migration, invasion and viability of hepatocellular cancer and sarcoma cell lines (Luo *et al.*, 2021; Zhao *et al.*, 2021). Therefore, both NDRG1 activation and inhibition have been proposed as anti-cancer treatments. The potential for pharmacological targeting of NDRG1 in cancer highlights the importance of understanding the role of NDRG1 within adaptive immunity.

The Cornall lab's discovery that NDRG1 is highly differentially expressed gene in anergic B cells compared to the naïve follicular B population by RNA-Seq (Xu, 2018), alongside the previous report proposing that NDRG1 acts as a T cell anergy factor (Oh *et al.*, 2015), implicated NDRG1 as a general regulator of lymphocyte anergy, necessitating further experiments to explore this hypothesis fully. The work in the following chapter demonstrates that the transcriptional regulation of *Ndrg1* parallels that described in stimulated $CD4^+$ T cells (Oh *et al.*, 2015), but experiments using a *Ndrg1*$^{-/-}$ mouse model demonstrate that NDRG1 is not required for the tolerogenic responses downstream of self-antigen engagement in B cells.

3.2 Results

3.2.1 *Ndrg1* expression is associated with B cell anergy

Acknowledgement: The RNA-Seq data was generated, and the experiments to generate the samples for RNA-Seq in this chapter performed, by Xijin Xu in the Cornall lab and was made

available in the Gene Expression Omnibus under accession code GSE135650. From the aligned and mapped counts tables previously created by Xijin Xu (Xu, 2018), the author performed DESeq for differential gene expression analysis and visualisation of the data, that analysis is presented here in figure 3.2.

The CRISPR/Cas9 generation of the *Ndrg1*$^{-/-}$ mouse strain was designed by Consuelo Anzilotti, and performed by Ben Davies and the transgenics core at the Wellcome Centre for Human Genetics. Eleanor Cawthorne and Tanya Cheetham helped with the identification of mutants by PCR and Sanger sequencing for subsequent breeding. Both also helped with the screening of serum for ANAs. Martin Wilcock engineered the A20 B cell line to express the Ig^{HEL} BCR, as described in his thesis (Wilcock, 2018). All other work presented in this chapter was performed by Rose Hodgson.

3.2.1.1 Ndrg1 is the 3rd most highly DE gene in anergic B cells

To investigate the pathways underlying B cell anergy, RNA-Seq was performed on B220^{+}CD19^{+}CD21^{mid}CD23^{hi} naïve and B220^{+}IgM^{lo}IgD^{a+} anergic splenic B cell subsets sorted respectively from Ig^{HEL} tg, and double tg mice expressing Ig^{HEL} and sHEL as a self-antigen (Ig^{HEL}/sHEL)(Goodnow *et al.*, 1988; Xu, 2018)(Fig. 3.2A). Differential gene expression analysis revealed significant upregulation of anergy-associated transcription factors *Egr2* and *Egr3,* with *Egr2* coactivator/corepressor, Ngfi-A binding protein 2*, Nab2* and calcium-regulator neurogranin *(Nrgn),* in anergic compared to naïve B cells, presenting a pattern of expression consistent with the NFAT signalling reported in anergic cells (Fig. 3.2A and B, appendix B) (Merrell *et al.*, 2006; Collins *et al.*, 2008). Of 868 significantly differentially expressed transcripts, *Ndrg1* was identified as the third most highly differentially expressed transcript in anergic B cells by $\log_2$ fold change of 7.378, and eleventh highest by adjusted p value, 7.41×10^{-117} (appendix B, Fig. 3.2A). NDRG1 has been previously reported as a CD4^{+} T cell anergy factor downstream of *Egr2/3* (Oh *et al.*, 2015), which together with these findings suggested it might be a common participant in the regulation of

lymphocyte tolerance. Significant differential expression of *Ndrg1* was confirmed by qPCR of mRNA extracted from Ig^{HEL} or Ig^{HEL}/sHEL $B220^+$ cells (Fig. 3.2C), confirming the association between NDRG1 and B cell anergy.

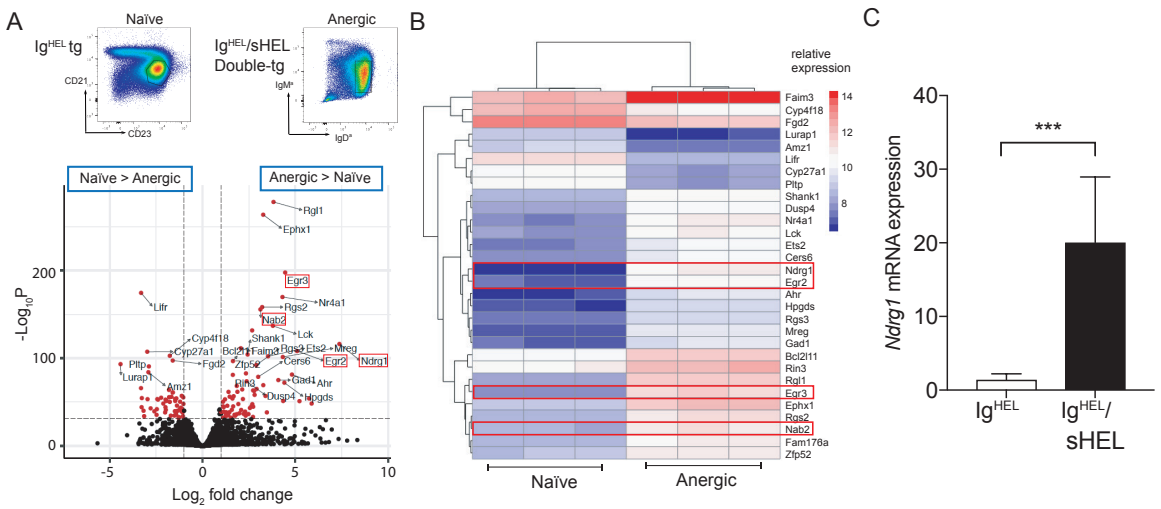


Figure 3.2 Ndrg1 is associated with B cell anergy

*A. Differential gene expression between Ig^{HEL} naïve follicular ($B220^+CD19^+IgMa^+CD93^-CD21^{mid}CD23^{hi}$) and Ig^{HEL}/sHEL anergic ($B220^+IgMa^{lo}IgDa^+$) splenic B cell populations, represented in FACS plots above, gated on $B220^+$. Genes differentially expressed >1 and <1 log_2FC and below a significance threshold of adjusted p value, 10^{e-32} for visualisation, are shown in red, with the top 30 differentially expressed genes filtered by adjusted p value labelled. B. Heatmap of the relative abundance of the top 30 differentially expressed genes filtered by adjusted p value between naïve (left) and anergic (right) B cells as in (A). Columns represent samples from individual mice. C. Expression of Ndrg1 mRNA calculated relative to Gapdh expression in Ig^{HEL} or Ig^{HEL}/sHEL primary B lymphocytes. Significance is calculated by unpaired t test *** p <0.001.*

3.2.1.2 *Ndrg1* is induced by BCR signalling but suppressed by positive co-stimulation

In $CD4^+$ T lymphocytes, NDRG1 has been proposed as an anergy factor, and is induced by signal one stimulation and inhibited by signal two. To investigate whether *Ndrg1* shared a similar pattern of molecular regulation, qPCR was performed on mRNA isolated from primary Ig^{HEL} B cells stimulated *ex vivo* via the BCR by anti-IgM or the cognate antigen sHEL (signal one), in the presence or absence of co-stimulation by anti-CD40 or LPS (signal two) for 24h. Consistent with the transcriptional control pattern of other anergy factors (Powell *et al.*, 1998; Yarkoni, Getahun and Cambier, 2010), *in vitro* antigen receptor signalling via signal one alone induced *Ndrg1* mRNA expression in primary B cells, but signal two stimulation was associated with a dose-dependent suppression of *Ndrg1* mRNA (Fig. 3.3A). This pattern of *Ndrg1* expression was also observed *in vitro* using the A20 B cells

engineered to express the Ig^{HEL} BCR (Fig. 3.3B), supporting the possibility that NDRG1 may play a role in the induction or maintenance of B cell anergy in central or peripheral tolerance.

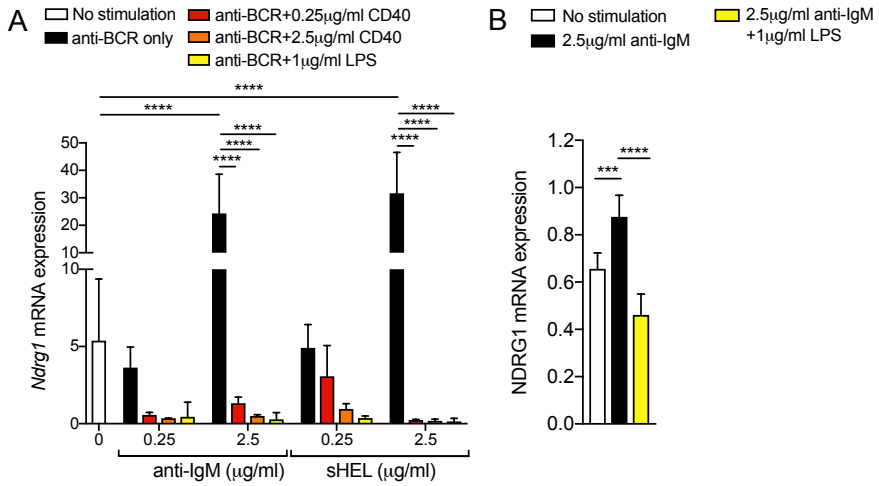


Figure 3.3 Ndrg1 expression is regulated by the signal one/signal two axis in B cells

*A. Ndrg1 mRNA expression calculated relative to Gapdh expression in Ig^{HEL} primary B lymphocytes stimulated ex vivo with the indicated concentrations of anti-IgM or sHEL, with or without anti-CD40 or LPS for 24h at 37°C. B. Ndrg1 mRNA expression calculated relative to Gapdh expression in murine A20 Ig^{HEL} tg B cells cultured for 24h at 37°C with anti-IgM and with or without LPS. Columns show means with 95% confidence interval (CI) error bars. Data presented is from two to four replicate qPCR readings for each condition and is representative of 3 independent experiments using Ig^{HEL} or non-tg (A) or from two A20 (B) independent experiments. Significance was determined using a two-way ANOVA with post-hoc Tukey's testing, *** p <0.001 and **** p<0.0001.*

3.2.2 A mouse model of NDRG1 deficiency

3.2.2.1 Creation of a mouse model by CRISPR/Cas9

Having confirmed the positive correlation of NDRG1 expression with anergy, and to establish if it has a role in B cell immune function, a *$Ndrg1^{-/-}$* mouse model was created using CRISPR/Cas9-directed mutagenesis (Fig. 3.4A). The gene targeting produced an 11bp deletion within exon 4 of the *Ndrg1* gene in oocytes causing a frameshift mutation *Ndrg1 null* allele, which was propagated further to produce homozygote *$Ndrg1^{-/-}$* mice at expected ratios from heterozygous parents (Fig. 3.4B). PCR-amplification and subsequent Sanger sequencing of cDNA reverse-transcribed from RNA isolated from WT kidney and splenic B cell lysates demonstrated the RNA transcript is expressed in both tissues (Fig. 3.4C-D), with the 11bp deletion detectable within the transcript amplified from *$Ndrg1^{-/-}$* kidney and B cell samples with no exon skipping or repair (Fig. 3.4C-D). Although NDRG1 protein was not expressed at detectable levels in WT splenocyte or thymocyte samples,

immunoblot analysis of WT and *Ndrg1*$^{-/-}$ kidney lysates using a N-terminal binding antibody confirmed the complete loss of NDRG1 protein expression, likely a result of nonsense-mediated decay of the altered transcript (Fig. 3.4E).

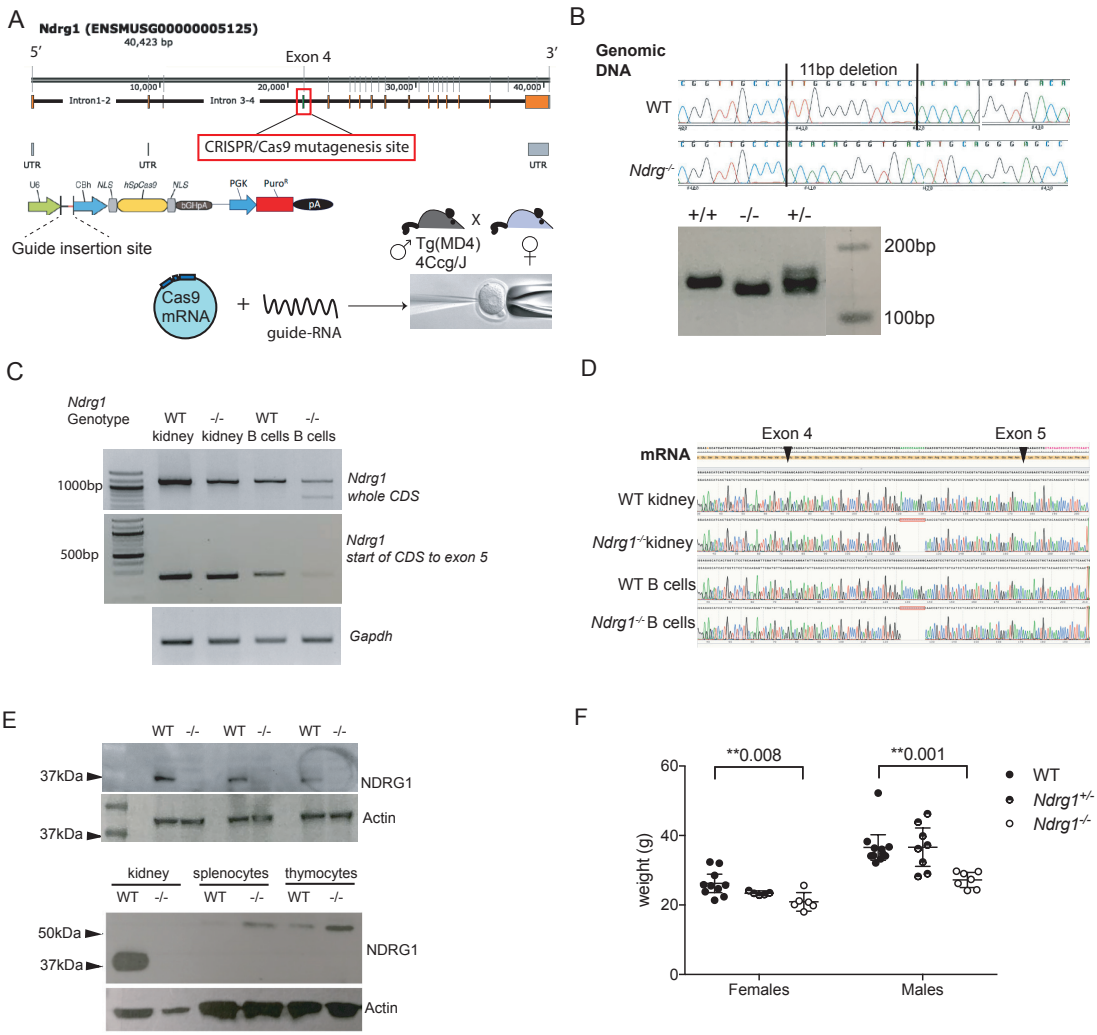


Figure 3.4 Creation of a Ndrg1$^{-/-}$ mouse model by directed CRISPR/Cas9 mutagenesis

A. Design of CRISPR/Cas9 guide RNAs targeting exon 4 (green; ENSMUSE00001241456) of the Ndrg1 gene (ENSMUSG00000005125, upper panel). Cloning of complementary oligos of the guide sequences into pX330-Puro vector and microinjection with Cas9 mRNA into embryos derived from super-ovulated C57BL/6J females mated with Ig^{HEL} tg studs (lower panel). B. Sanger sequencing trace of genomic DNA at the mutagenesis site comparing WT and Ndrg1$^{-/-}$ mice (upper panel) using genomic primer set 1, and agarose gel electrophoresis of PCR-amplified genomic DNA at the CRISPR-mutagenesis site of Ndrg1 gene (lower panel) using genomic primer set 2, cropped for presentation. C. Gel electrophoresis of PCR-amplified Ndrg1 transcripts reverse transcribed from WT and Ndrg1$^{-/-}$ kidney or splenic B cell samples. Top panel; bands amplified using mRNA set 1 primers spanning the entire Ndrg1 coding sequence, the lower band in Ndrg1$^{-/-}$ B cells represents genomic DNA (Wdr70) contamination as confirmed by Sanger sequencing. Middle panel; bands amplified using mRNA set 2 primers spanning the start of the Ndrg1 coding sequence to exon 5. Lower panel: Gapdh expression. Gel images are cropped for presentation. D. Sanger sequencing of PCR products amplified in (C) (second panel) using the same primers. Sequences are aligned to Ndrg1 mRNA sequence with exon starts labelled in orange. E. Western blot of protein lysates from WT and Ndrg1$^{-/-}$ samples using N-terminal binding antibody; top blot shows kidney samples from 3 mice per group. NDRG1

detected at 37kDa, Bottom blot shows kidney, splenocyte and thymocyte lysates, highlighting NDRG1 protein below the threshold of detection in splenocyte and thymocyte samples, Bands > 50ka are attributed to non-specific antibody binding. Actin was used as loading control for both blots (lower panels). Gel images are cropped for presentation. F. Weights of WT, Ndrg1$^{+/-}$ and Ndrg1$^{-/-}$ adult mice aged 14 - 25 weeks of age, where circles are individual mice, bars represent mean and 95% CI.

In humans, *Ndrg1* mutations are one of the causes of hereditary motor and sensory peripheral neuropathy-type Lom, also known as CMTD4d (Kalaydjieva *et al.*, 2000). Consistent with previous reports, our *Ndrg1*$^{-/-}$ animals displayed a shaking, tremorous phenotype with muscle weakness and abnormal clasping of the hind limbs (Okuda *et al.*, 2004; King *et al.*, 2011), providing further evidence that the protein had been correctly targeted. *Ndrg1*$^{-/-}$ mice were also significantly smaller than their WT littermate controls, as previously described (Fig. 3.4F)(Watari *et al.*, 2016).

3.2.2.2 NDRG1 is not required for development of the pre-immune B cell repertoire or B cell antigenic responses

Immunophenotyping of *Ndrg1*$^{-/-}$ mice by flow cytometry demonstrated normal development of B cells in the BM (Fig. 3.5A and D), and no difference in the development, distribution or absolute numbers of peripheral B populations within the spleen or absolute B cell numbers in the mesenteric lymph nodes (MLNs)(Fig. 3.5B and E). Peritoneal B1 B cell populations were also comparable (Fig. 3.5C), indicating that NDRG1 deletion has no effect on development or distribution of basal B cell populations, and serum IgM, IgG and IgA titres were equivalent in *Ndrg1*$^{-/-}$ and WT mice (Fig. 3.5F).

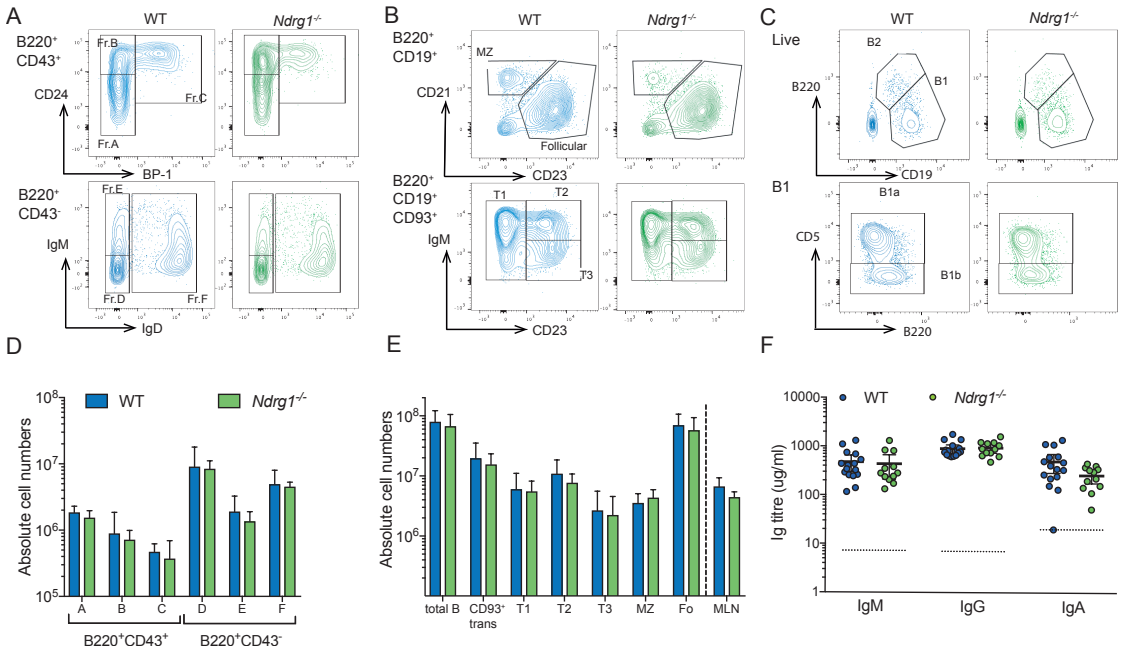


Figure 3.5 Normal B cell development in the absence of NDRG1

A. Representative flow cytometry plots of adult WT (blue) and Ndrg1$^{-/-}$ (green) mice, showing Hardy B cell fractions in BM (A), splenic (B) and peritoneal (C) B cells. D. Quantification of absolute BM B cell numbers as gated in (A). E. Quantification of B cell subsets, transitional (trans), transitional populations (T1-T3), marginal zone and follicular (Fo) numbers in the spleen and total B cells in MLNs as gated in (B). Columns represent means with 95% CI error bars and are representative of three independent experiments, each with 3-6 mice per group between 8-20 weeks of age. F. Serum Ig levels from WT and Ndrg1$^{-/-}$ mice determined by ELISA. Bars represent means with 95% CI error bars with 12-16 mice per group. Dotted line represents 1.5x interpolated background absorbance.

To investigate the requirement for NDRG1 during the response to stimulation by foreign antigens, *Ndrg1*$^{-/-}$ and WT B cells were cultured under a range of stimulatory conditions for 24h and 72h. The absence of NDRG1 did not alter the *in vitro* upregulation of activation markers CD69, CD86 or CD25 (Fig. 3.6A), or the extent of proliferation and class-switching in response to TLR ligands (Fig. 3.6B-D).

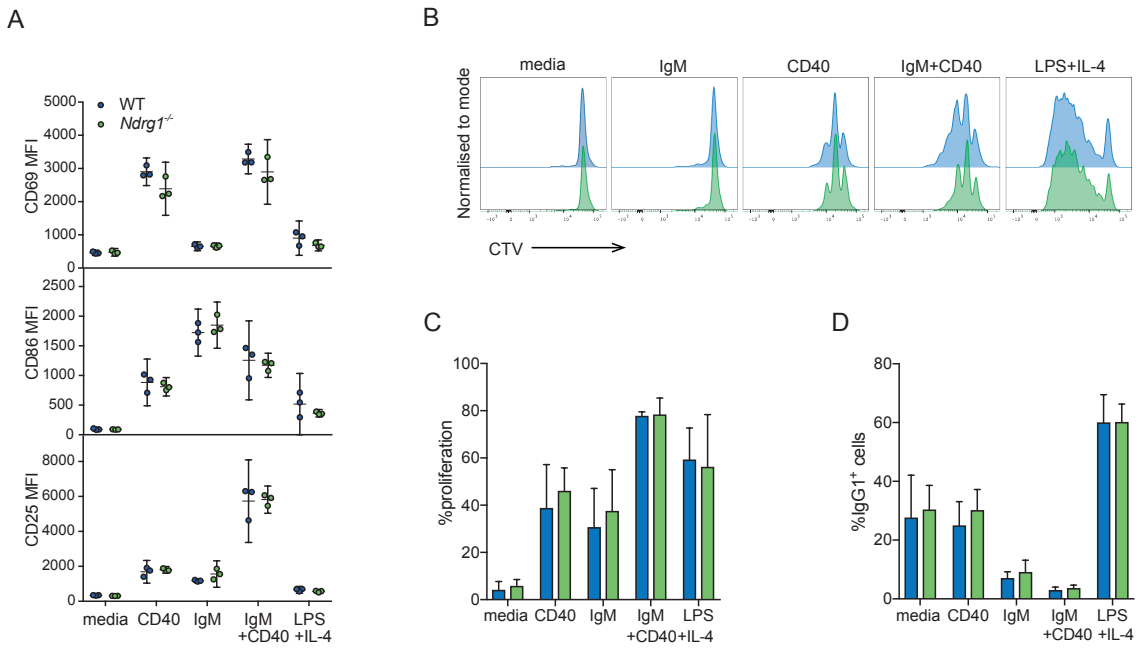


Figure 3.6 Ndrg1$^{-/-}$ mice respond normally to foreign antigen

A. Median fluorescence intensities (MFIs) of activation marker expression on WT and Ndrg1$^{-/-}$ primary B220^{+} splenic B cells stimulated with media alone, or combinations of anti-CD40 2.5μg/ml, anti-IgM 2.5μg/ml, LPS 10μg/ml and IL-4 10ng/ml for 24 hours at 37°C ex vivo. B-C. Flow cytometric plots of CTV dilution in B220^{+} splenocytes stimulated with the same conditions as (A) for 72 hours, (B) with quantification of proliferation (C) and class-switching (D). Results are representative of two independent experiments: circles represent individual mice and columns are means with 95% CI error bars.

3.2.3 Investigating the role of NDRG1 in B cell anergy

3.2.3.1 Loss of NDRG1 does not affect central tolerance or anergy induction during development

To explore whether loss of NDRG1 is sufficient to break tolerance to self-antigen at resting state, adult WT and *Ndrg1*$^{-/-}$ mouse sera were tested for anti-nuclear antibodies (ANAs), a sensitive hallmark of autoimmune disease in both mice and humans (Vinuesa and Goodnow, 2004). ANAs were not detected in the absence of NDRG1 expression (Fig. 3.7).

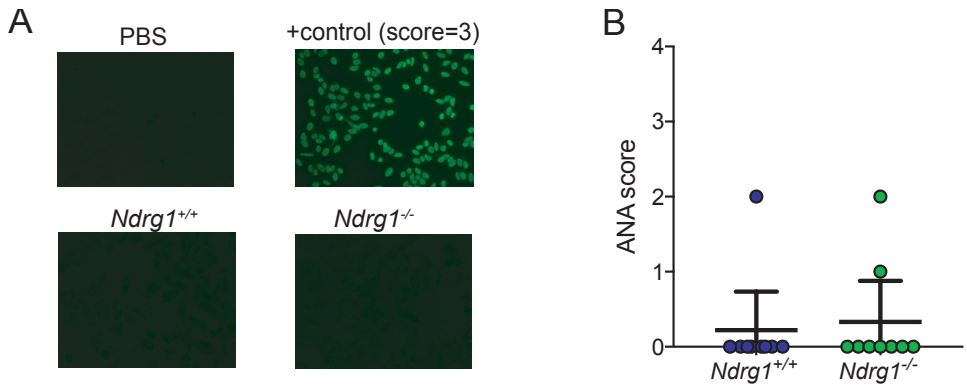


Figure 3.7 NDRG1 loss is not associated with loss of tolerance at baseline

A. Representative microscopy images of ANA staining on Hep2 cells from serum of WT and Ndrg1$^{-/-}$ mice. Sera were scored from 0-4, PBS represents negative control. B Serum ANA scores of WT and Ndrg1$^{-/-}$ mice, where circles represent individual mice, and bars are means with 95% CI. Scores >= 2 are considered positive.

To isolate and test for a specific defect in B cell tolerance, we investigated whether the provision of T cell help might be sufficient to induce autoantibodies to endogenous self-antigen in the absence of NDRG1. Accordingly, WT or *Ndrg1*$^{-/-}$ non-tg and WT or *Ndrg1*$^{-/-}$ sHEL mice were primed with HEL-conjugated to SRBC (HEL-SRBC) and then boosted with HEL-SRBC at 30 days (Fig. 3.8A). There was no difference in the humoral immune response between WT or *Ndrg1*$^{-/-}$ mice in these experiments. As expected, the sHEL expressing mice generated lower anti-HEL-specific IgG titres than non-tg mice (Goodnow *et al.*, 1988), despite equivalent germinal centre formation across groups (Fig. 3.8B), indicating that B cell tolerance to self-antigen remained intact during humoral challenge despite loss of NDRG1 (Fig. 3.8C).

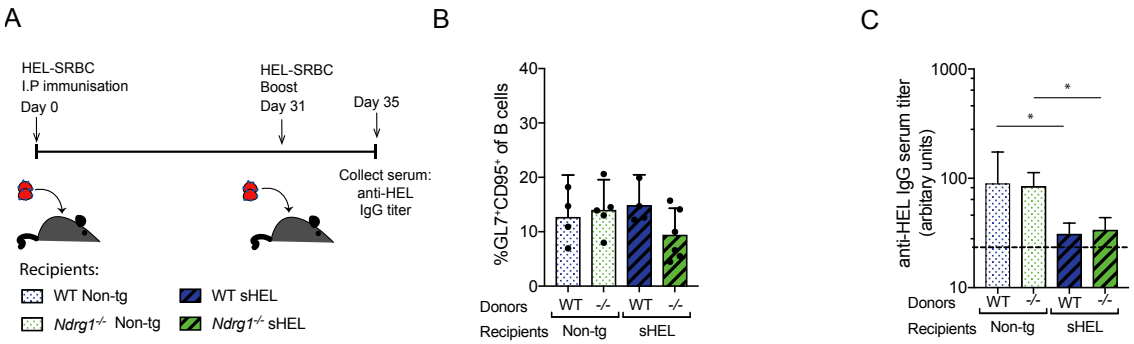


Figure 3.8 Intrinsic B cell tolerance is intact in the absence of NDRG1

A. Experimental schematic: WT and Ndrg1$^{-/-}$ non-tg or sHEL-tg recipients were immunised with HEL-SRBC at day 0 and then boosted with HEL-SRBC again at day 31 before serum was collected on day 35. B. GC

*formation on day 35 from mice in (A) as determined by gating on GL7$^+$CD95$^+$ of B220$^+$CD19$^+$ cells. C. Serum anti-HEL IgG titres from mice in (A) on day 35. Data are from one experiment with 4-6 mice per group, columns are means and 95% CI error bars. Dotted line represents unimmunised background titre level. Significance was determined using a two-way ANOVA, * p = <0.05.*

To investigate whether NDRG1 might play a role in tolerance and anergy induction during B cell development in the context of self-antigen, we took further advantage of the Ig^{HEL} and sHEL tg models. Lethally irradiated CD45.1$^+$ non-tg and sHEL mice were reconstituted with WT or *Ndrg1*$^{-/-}$ CD45.2$^+$ Ig^{HEL} BM (Fig. 3.9A). Irrespective of NDRG1, flow cytometric analysis showed down-modulation of surface IgM^a on mature recirculating B cells in the BM and spleens of sHEL recipients, which is typical of anergy (Fig. 3.9B and C); and *ex vivo* stimulation of the same cells with sHEL showed a block in BCR signalling evidenced by absent phosphorylation of downstream proteins ERK, BLINK, SYK and PLCy2 (Fig. 3.9D). Anti-HEL specific IgM^a was also equivalently suppressed in sHEL recipients reconstituted with WT or *Ndrg1*$^{-/-}$ Ig^{HEL} BM (Fig. 3.9E). These findings show that NDRG1 is dispensable for the IgM modulation, and for the block in proximal BCR signalling and plasma cell differentiation, characteristic of anergic B cells.

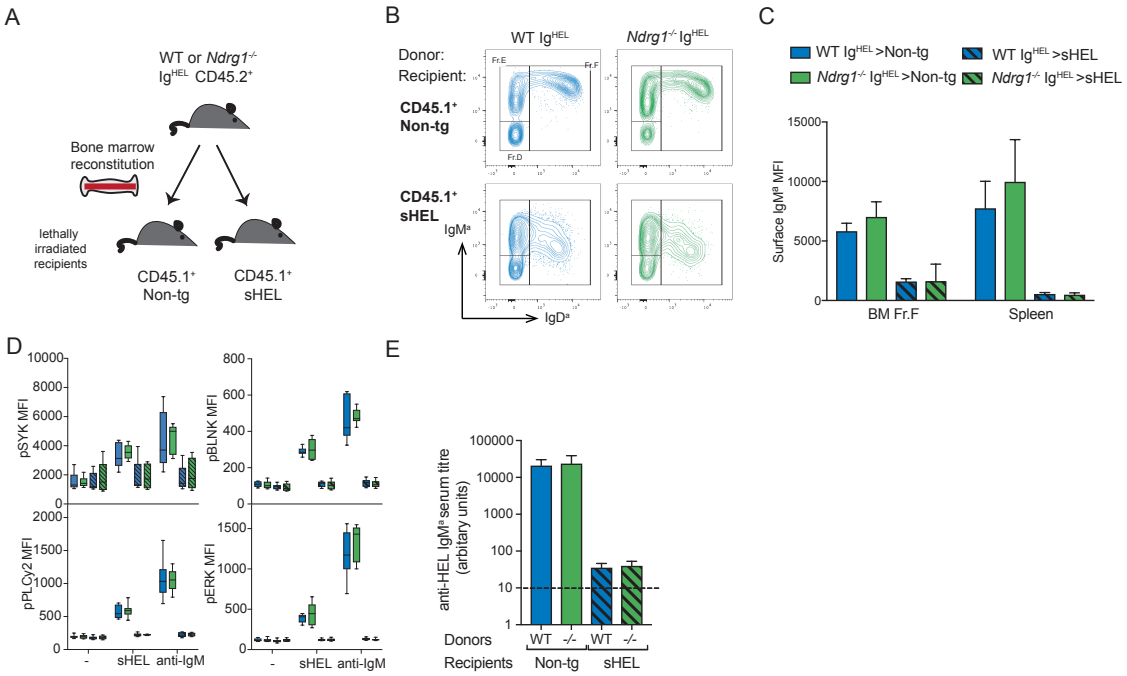


Figure 3.9 Anergy induction during development is normal during NDRG1 loss

A. Experimental schematic: lethally irradiated sHEL or non-tg CD45.1$^+$ recipients were reconstituted with WT or Ndrg1$^{-/-}$ CD45.2$^+$ Ig^{HEL} tg BM for 8 weeks. B. Representative flow cytometry plots of B220$^+$CD43$^-$ BM cells from mice in (A). C. IgM^a surface expression on mature recirculating B cells in the BM (B220$^+$CD43$^-$ IgD$^+$), and on splenic B220$^+$CD19$^+$ B cells from mice in (A), quantified by flow cytometry as MFI. Results are representative of three independent experiments (2-4 mice per group) and bars show means with 95% CI error bars. D. MFIs of phospho-flow intracellular staining of pSyk, pPLCγ2, pBLNK and pERK in splenic B220$^+$CD19$^+$ Ig^{HEL} B cells from WT and Ndrg1$^{-/-}$ mice in (A), after stimulation ex vivo with media alone, 1μg/ml sHEL or 10μg/ml IgM. Results are pooled from 3 independent experiments with 2-4 mice per group. Box plots show mean with min to max. E. Serum levels of anti-HEL IgM^a from mice in (A). Columns show means with 95% CI error bars and are representative of two independent experiments. Dotted line shows 1.5x interpolated background.

3.2.3.2 Self-antigen mediated inhibition of TLR signalling-induced proliferation is intact in the absence of NDRG1

Persistent self-antigen stimulation of the BCR in anergic B cells also has the effect of inhibiting proliferative responses to LPS, an essential checkpoint to prevent autoimmunity during exposure to external co-stimulation such as with bacterial infection (Rui *et al.*, 2006). To exclude the possibility that NDRG1 might be induced to mediate the inhibition of co-stimulation by LPS, CTV-labelled WT and *Ndrg1*$^{-/-}$ Ig^{HEL} naïve and Ig^{HEL}/sHEL double tg anergic splenic B cells *ex vivo* were stimulated with LPS and increasing amounts of sHEL as self-antigen. Proliferation was equivalently inhibited in *Ndrg1*$^{-/-}$ anergic B cells compared to WT, indicating that the refractory mechanisms in

place to inhibit autoreactive B cell responses to LPS do not depend upon NDRG1 expression (Fig. 3.10).

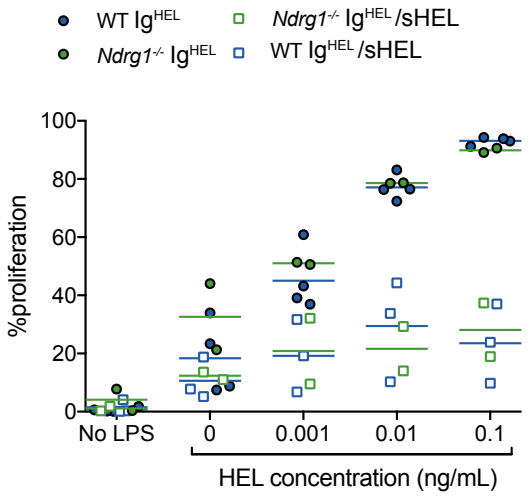


Figure 3.10 Chronic self-antigen exposure mediated inhibition of TLR-signalling is equivalent in Ndrg1$^{-/-}$ anergic B cells

Ex vivo proliferation of magnetically positively sorted CTV-labelled WT and Ndrg1$^{-/-}$ Ig^{HEL} naïve and Ig^{HEL}/sHEL double tg anergic B220^{+} splenocytes quantified by CTV dilution in response to media alone, or 500ng/ml LPS plus sHEL titration for 72h at 37°C. Results are pooled from 2-3 independent experiments per group, each point represents one mouse.

3.2.3.3 NDRG1 deficiency does not provide a competitive advantage to anergic B cells within a polyclonal repertoire

The antigen-induced differential signalling pathways in anergic B cells cause a shortened lifespan in a polyclonal repertoire, due to an inability to compete with non-anergic cells for BAFF, and increased expression of the proapoptotic protein, Bim (Cyster and Goodnow, 1995; Enders *et al.*, 2003). Since NDRG1 has been implicated in the induction of apoptosis (Stein *et al.*, 2004), I hypothesised that NDRG1 might act downstream of signal one to modulate the threshold for survival in a diverse B cell repertoire. To test this, I reconstituted lethally irradiated non-tg or sHEL CD45.1^{+} mice with 80:20 mixtures of *Ndrg1*$^{-/-}$ or WT CD45.2^{+} Ig^{HEL} BM and WT non-tg CD45.1^{+} BM (Fig. 3.11A)(Cyster, Hartley and Goodnow, 1994; Cyster and Goodnow, 1995). Analysis of the reconstituted mice showed equivalent numbers of *Ndrg1*$^{-/-}$ and WT Ig^{HEL} B cells in a mixed repertoire (Fig. 3.11B, table 3.1) and an equivalent increase in turnover in the presence of self-antigen, as judged by BrdU labeling *in vivo* (Fig. 3.11C). These data show that NDRG1 is not required to maintain

the rapid turnover of anergic B cells that have developed in the presence of self-antigen due to competition with non-autoimmune cells for BAFF (Cyster, Hartley and Goodnow, 1994; Cyster and Goodnow, 1995).

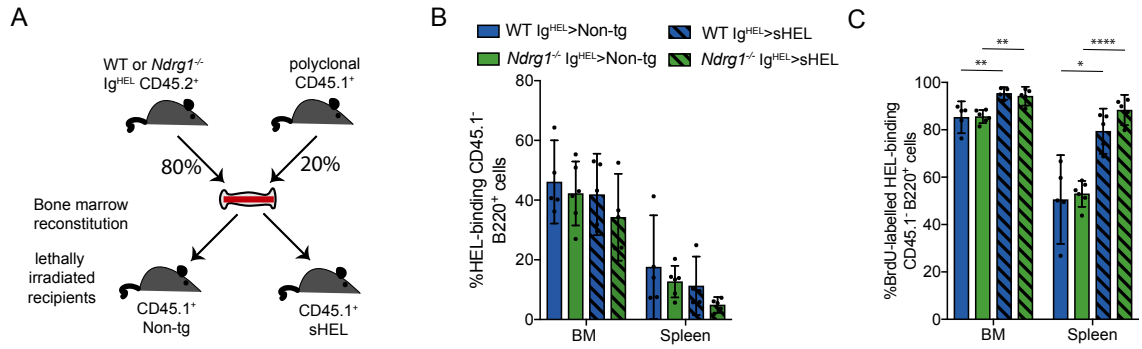


Figure 3.11 Anergic B cells lacking NDGR1 survive and compete normally in a polyclonal repertoire

A. Experimental schematic; lethally irradiated WT CD45.1⁺ recipients were reconstituted with 80:20 mixtures of WT or Ndrg1⁻/⁻ IgHEL CD45.2⁺ BM and WT non-tg CD45.1⁺ BM. B. Percentage of total HEL-binding B220⁺ cells in the BM and spleen of mice in (A). C. Percentage of HEL-binding B220⁺CD45.2⁺ cells labelled with BrdU after one week. Dots are individual mice from one experiment with 4-6 mice per group, columns show means and 95% CI error bars.

Table 3. 1 Anergic B cells lacking NDGR1 survive and compete normally in a polyclonal repertoire

Numbers of total B220⁺ (Total B) and HyHEL9⁺CD45.1⁻ B220+ (IgHEL) cells in the BM and spleen of Non-tg or sHEL recipients reconstituted with 80% WT or Ndrg1⁻/⁻ IgHEL CD45.2⁺ BM and 20% non-transgenic polyclonal WT CD45.1⁺ BM cells. Data reported are means (and SD) from one experiment, with 4-6 mice per group.

Tissue	BM (x10⁶)				Spleen (x10⁶)			
Recipient	Non-tg		sHEL		Non-tg		sHEL	
BM donor	WT IgHEL	Ndrg1⁻/⁻ IgHEL	WT IgHEL	Ndrg1⁻/⁻ IgHEL	WT IgHEL	Ndrg1⁻/⁻ IgHEL	WT IgHEL	Ndrg1⁻/⁻ IgHEL
Total B	5.86 (1.8)	8.49 (2.5)	8.27 (3.9)	9.17 (1.9)	42.31 (10.9)	71.49 (18.5)	40.95 (14.06)	63.22 (28.1)
IgHEL	2.67 (0.8)	3.45 (1.0)	3.48 (1.7)	3.09 (0.9)	6.56 (3.7)	9.06 (4.3)	4.32 (2.3)	2.82 (1.4)

Similarly, NDRG1 deficiency did not produce an altered anergic response or survival advantage in B cells exposed to self-antigen in the presence of directly competing IgHEL anergic B cells. Flow cytometric analysis of CD45.1⁺ sHEL recipients reconstituted with equal parts WT CD45.1⁺ IgHEL BM and either WT or *Ndrg1⁻/⁻* CD45.2⁺ IgHEL BM demonstrated NDRG1 loss did not provide a competitive advantage in the presence of self-antigen (Fig. 3.12A-B). Self-antigen induced downregulation of

surface IgM (Fig. 3.12C and D) and upregulation of Bim were equivalent between *Ndrg1*$^{-/-}$ and WT mature B cell populations in the chimeric mice (Fig. 3.12E).

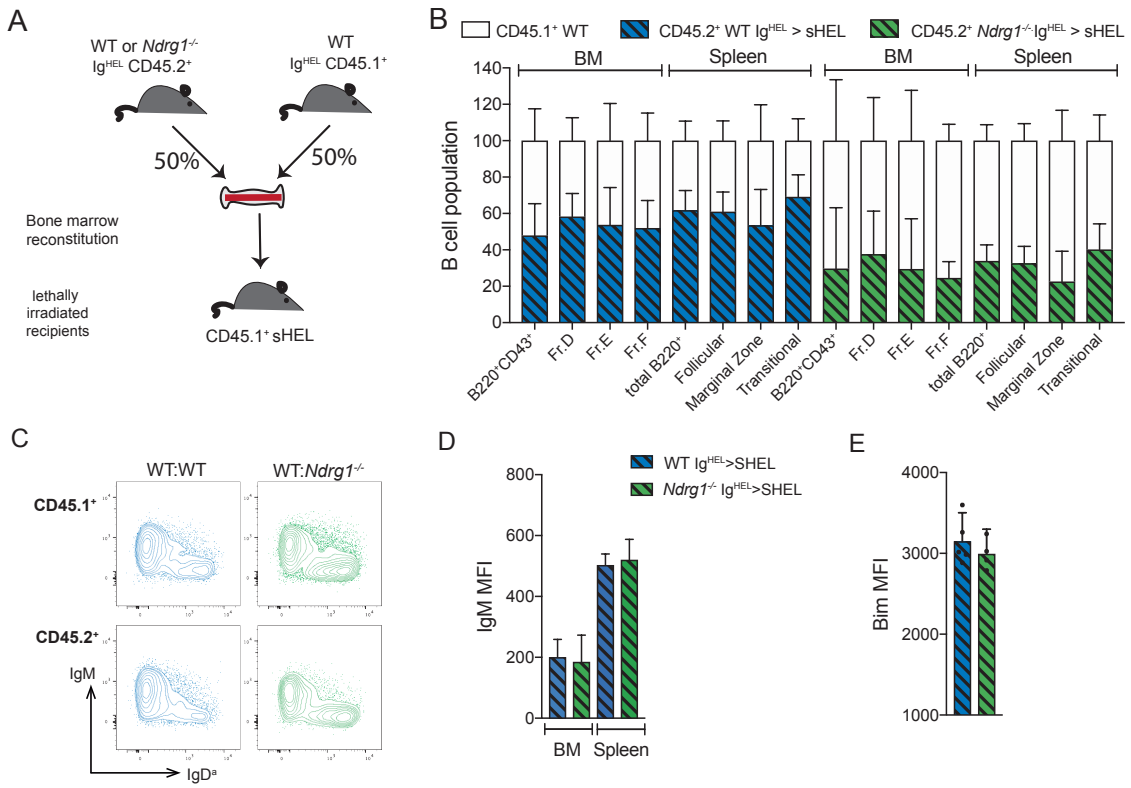


Figure 3.12 NDRG1 deficiency does not provide an advantage in the presence of competing clonal anergic B cells

A. Experimental schematic; lethally irradiated sHEL CD45.1^{+} recipients were reconstituted with 50:50 mixtures of WT CD45.1^{+} and either WT CD45.2^{+} Ig^{HEL} or Ndrg1$^{-/-}$ CD45.2^{+} Ig^{HEL} BM. B. Relative proportions of reconstituted BM and splenic B cell populations from (A) gated as in Fig.3.5 A-B, then gated based on CD45.1 and CD45.2 expression. C. Representative flow cytometry plots of B220^{+}CD43^{-} B cells from BM of sHEL mice reconstituted with 50:50 mixtures of WT CD45.1^{+} BM with either WT or Ndrg1$^{-/-}$ Ig^{HEL} CD45.2^{+} BM. D. Surface IgM expression on B cell populations from (A). E. Intracellular Bim quantification in B220^{+}CD19^{+}IgD^{a+}splenocytes from (A). Columns represent means and 95% CI error bars. Data points are individual mice from one experiment (4-5 per group).

3.2.4 NDRG1 loss does not affect B cell anergic responses in the periphery

3.2.4.1 NDRG1 is not required for the localization of naïve B cells in response to foreign antigen

The experiments in section 3.2.3 demonstrated that NDRG1 is dispensable for the induction and maintenance of anergy when B cells develop in the presence of self-antigen and when challenged with signal two alongside chronic BCR stimulation; however, this does not exclude a role for NDRG1 unique to migration and re-localisation of antigen-stimulated B cells, which is linked to their ability

to find and interact with T cell help. When naïve B cells first bind antigen, they relocate to the outer periarteriolar lymphoid sheath where they require signal two in the form of T cell help for survival and entry into the follicle to initiate a productive germinal centre (Cyster, Hartley and Goodnow, 1994; Cyster and Goodnow, 1995; Craxton *et al.*, 2005). Similarly, in the context of self-antigen and competing naïve cells anergic B cells also relocate to the T cell rich cortical zones, where they may be rescued by T cell help; but in this situation typically die from a combination of insufficient engagement with BAFF and increased Bim-dependent apoptosis (Rathmell *et al.*, 1995; Craxton *et al.*, 2005).

To exclude a possible role for NDRG1 in these interactions, equal ratios of WT CD45.1$^+$ Ig^{HEL} and WT or *Ndrg1*$^{-/-}$ Ig^{HEL} CD45.2$^+$ splenocytes were labelled with CTV dye and transferred into non-tg or sHEL CD45.2$^+$ recipients (Fig. 3.13A). After 48h, the total number of transferred CTV$^+$ HEL-binding Ig^{HEL} B cells were significantly reduced in sHEL compared to non-tg recipients (Fig. 3.13A and B), but ratios of CD45.1$^+$:CD45.2$^+$ surviving HEL-binding splenocytes were equivalent for WT and *Ndrg1*$^{-/-}$ donor populations (Fig. 3.13C). These findings show that NDRG1 does not play a role in the elimination of BCR-activated B cells in the periphery. This conclusion is supported by the equivalent induction of CD95, BAFF-R, Bcl2 and Bim proteins in the CD45.1$^+$ WT and CD45.2$^+$ *Ndrg1*$^{-/-}$ antigen-experienced B cells (Fig. 3.13D). In sHEL recipients, IgM^a downmodulation, and upregulation of the activation marker CD86 were similar in CD45.1$^+$ WT and CD45.2$^+$ *Ndrg1*$^{-/-}$ Ig^{HEL} B cells (Fig. 3.13D). Levels of localisation markers CD23 and CXCR5 were also reduced equivalently on exposure to sHEL in CD45.2$^+$ *Ndrg1*$^{-/-}$ antigen experienced B cells, suggesting follicular exclusion is also unlikely to depend on NDRG1 expression (Fig. 3.13D).

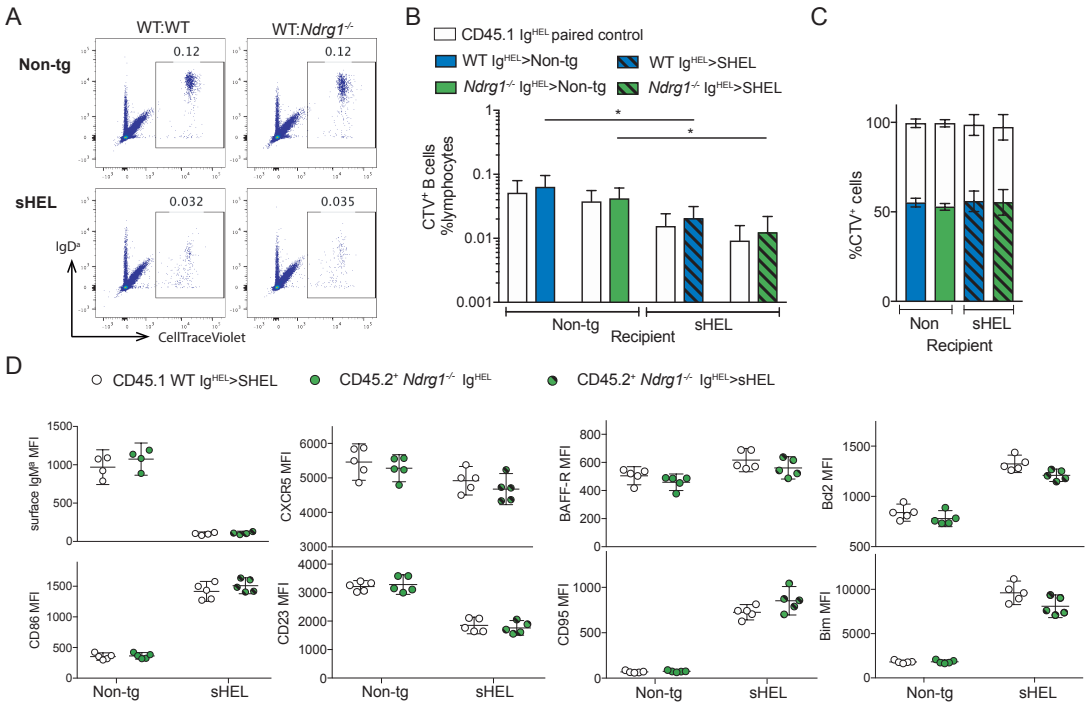


Figure 3.13 NDRG1-deficient B cells exposed to self-antigen in the periphery are subject to follicular exclusion and cell death

A. Representative flow cytometry plots of 50:50 mixtures of WT CD45.1$^+$ Ig^{HEL} and WT or Ndrg1$^{-/-}$ CD45.2$^+$ Ig^{HEL} splenocytes labelled with CTV dye and transferred by i.v. injection into non-tg or sHEL-tg CD45.2$^+$ recipients for 48h, showing live B220$^+$CD19$^+$ gated populations and % transferred CTV$^+$ cells B. Percentage of total lymphocytes that were either CD45.1$^+$ or CD45.2$^+$ CTV$^+$ as gated in (A), with white bars showing paired CD45.1$^+$ Ig^{HEL} cells from donor, coloured bars are CD45.2$^+$. C. Ratio of CTV$^+$ cells as gated in (A) that were CD45.1$^+$ (white) or CD45.2$^+$. D. MFI of surface marker expression CD86, CD23, CXCR5, IgMa, BAFFR and CD95 and intracellular Bim and Bcl2 in transferred Ig^{HEL} B cells, gated as in (A). Bars are means with 95% CI error bars and data are representative from 1-3 independent experiments with 4-6 mice per group, columns show means and bars 95% CI error bars.

3.2.4.2 BCR-induced apoptosis is intact in the absence of NDRG1

To further establish that NDRG1 has no role in inducing apoptosis downstream of signal one in the absence of signal two, mixed cultures of WT CD45.1$^+$ and WT or *Ndrg1*$^{-/-}$ CD45.2$^+$ non-tg B cells were stimulated with a titration of plate-bound anti-IgM for 16h *in vitro*. The ratio of CD45.1$^+$:CD45.2$^+$ B cells was not altered by increasing concentrations of anti-IgM in cultures (Fig. 3.14A), despite equal dose-dependent antigenic engagement as measured by CD86 upregulation (Fig. 3.14B), supporting the conclusion that NDRG1 does not induce B cell death in response to signal one in the absence of signal two.

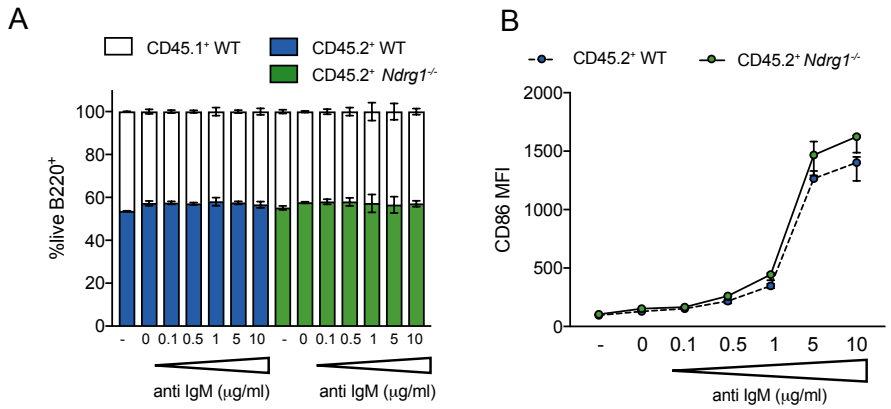


Figure 3.14 NDRG1 loss does not affect BCR-mediated apoptosis

A. Ratio of B220⁺ cells surviving from 50:50 mixtures of WT CD45.1⁺ and WT or Ndrg1⁻/⁻ CD45.2⁺ non-tg B cells stimulated with anti-IgM at the indicated concentrations for 16h at 37°C ex vivo. B. CD86 surface expression as MFI on the CD45.2⁺ B220⁺ cells from (A). Data are representative of 3 independent experiments with columns or circles as means with 95% CI error bars.

3.3 Summary of chapter

Previously, the Cornall lab identified *Ndrg1* as the third most differentially expressed gene in anergic B cells compared to naïve follicular B cells. When combined with the evidence for shared genetic regulation of *Ndrg1* by the signal one and two costimulatory axis in T cells (Oh *et al.*, 2015) and B cells as shown in this chapter, this suggested NDRG1 could represent a potential central factor regulating lymphocyte tolerance downstream of *Egr2/3* and NFAT activation.

In this chapter, experiments employing a CRISPR/Cas9-generated NDRG1-deficient mouse demonstrated NDRG1 is either dispensable, or acts redundantly within B cell tolerance mechanisms during B cell development and activation. NDRG1 deficiency did not affect induction and maintenance of B cell anergy tested using the Ig^{HEL}>sHEL BM chimeric model system, nor did it alter the maintenance of cell-intrinsic tolerance to self-antigen at resting state, upon immunisation or during direct competition. We hypothesised that NDRG1 action may be limited to specific properties of B cell tolerance such as influencing the threshold for breakdown of tolerance in response to external stimulation, as *Ndrg1* expression is closely regulated by signal two in B and T lymphocytes; however, the characteristic inhibition of signal two was intact in *Ndrg1*$^{-/-}$ anergic B

cells. Furthermore, the loss of NDRG1 had no effect on the response of splenic B cells exposed to self-antigen, or the induction of cell death due to the absence of rescue by signal two. There was no requirement for NDRG1 in these aspects of B cell tolerance, despite clear regulation of NDRG1 by the signal one/signal two axis in lymphocytes.

In summary, I have shown in this chapter that the association of NDRG1 expression in B cells may represent a biomarker of anergic or activated naïve cells, stimulated by the BCR in the absence of signal two, and reminiscent of other cell types under conditions of cell stress (Piquemal *et al.*, 1999; Okuda *et al.*, 2004; Stein *et al.*, 2004; Ellen *et al.*, 2008; Sun *et al.*, 2013; Sahni *et al.*, 2014; Merlot *et al.*, 2019).

4. Investigating the role of *Ndrg1* in T cells

4.1 Chapter introduction

NDRG1 has been previously identified as a clonal $CD4^+$ anergy factor upregulated by TCR-dependent *Egr2/3* activation alone in naïve and anergic $CD4^+$ T cells, and down-regulated in a proteasome-dependent manner by co-stimulation (Oh *et al.*, 2015). In their Nature Communications report in 2015, Oh *et al* showed that *Ndrg1*$^{-/-}$ $CD4^+$ T cells have normal reactivity at baseline in un-aged mice, though NDRG1-deficient $CD4^+$ T cells were resistant to clonal anergy induction *in vitro*, indicating the blockade in IL-2 production is lost in *Ndrg1*$^{-/-}$ $CD4^+$T cells in response to *in vitro* anergising stimuli. These findings appeared to partially translate to the *in vivo* form of T cell peripheral tolerance, peptide-induced anergy, where loss of NDRG1 rescued the proliferative block observed in anergised T cells, though IL-2 effector functions were still partially impaired in NDRG1-deficient cells during *in vivo* adaptive tolerance experiments.

As previously discussed in section 1.3.3.2, *in vivo* peptide-induced T cell anergy and clonal T cell anergy represent biochemically distinct phenomena. The former, *in vivo* adaptive tolerance, has been reported in murine TCR-tg models on injection of soluble peptide or in double TCR-tg models similar to the classical use of Ig^{HEL}/sHEL models to study B cell anergy, as exemplified in chapter 3. Peptide-induced anergy models include the OT-II/OVA model where OT-II^+ $CD4^+$ T cells are introduced into non-tg recipients, which are then immunised with cognate antigen, OVA intravenously. On restimulation with OVA presented by APCs *in vitro,* in addition to reduced proliferation, less IL-2 can be detected in the supernatants after 2 days compared to that of naïve T cells stimulated in culture, or T cells isolated from mice immunised with adjuvant (Kearney *et al.*, 1994; Oh *et al.*, 2015). In contrast to *in vivo* adaptive tolerance, clonal anergy arises on the re-stimulation of previously fully activated T cell clones solely with signal one alone, and generally is limited to *in vitro* conditions (Schwartz, 2003; Chiodetti *et al.*, 2006).

The finding in chapter 3 that NDRG1 is transcriptionally controlled in the same signal one/signal two manner as seen in T cells, suggests this is a generalised pattern, related to the shared *NFAT/Egr2/Egr3* axis induced by chronic calcium signalling in sub-optimally-activated lymphocytes (Macián *et al.*, 2002; Safford *et al.*, 2005; Oh *et al.*, 2015). However, as a result of the finding that NDRG1 is either dispensable or acts redundantly for the induction and maintenance of B cell anergy, I revisited the role of NDRG1 in T cells, reassessing the evidence for NDRG1-regulation of peptide-induced T cell anergy.

4.2 Results

4.2.1 NDRG1 is not required for development of the pre-immune T cell repertoire

As previously reported, immunophenotyping of un-aged *Ndrg1*$^{-/-}$ non-tg mice by flow cytometry demonstrated normal development of T cells in the thymus (Fig. 4.1A and C), and no difference in the development, distribution or absolute numbers of peripheral T populations within the spleen (Fig. 4.1B and D) (Oh *et al.*, 2015).

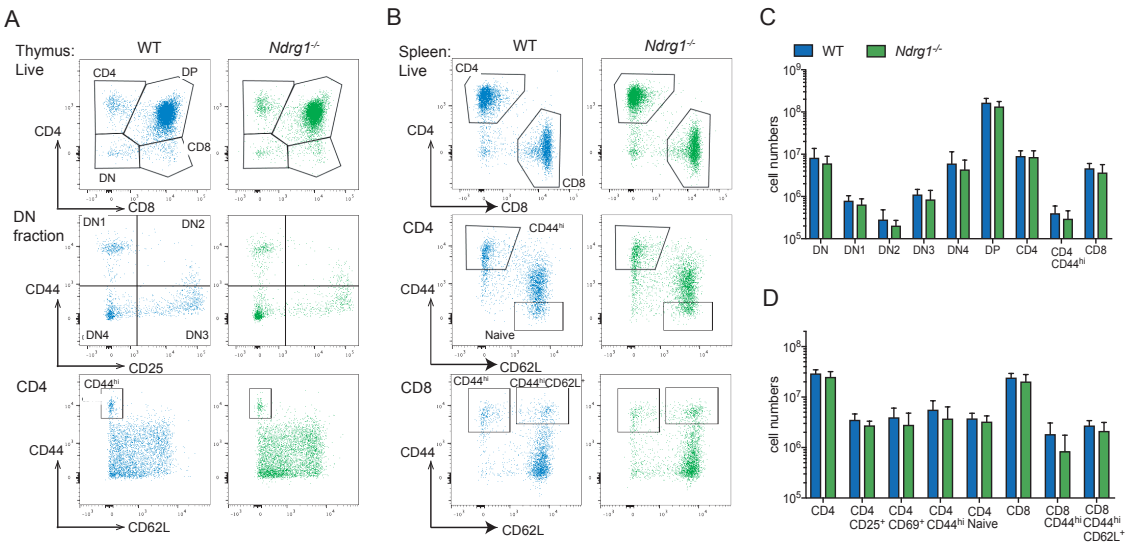


Figure 4.1 T cell development is normal in Ndrg1$^{-/-}$ mice

A. Representative flow cytometry plots of WT and Ndrg1$^{-/-}$ T cell development in the thymus, and B. peripheral T cell populations in the spleen. C. Quantification of WT and Ndrg1$^{-/-}$ thymic T cell subsets as gated in (A). D. Numbers of WT and Ndrg1$^{-/-}$ splenic T cell populations as gated in (B). Results are representative of three independent experiments, each with 3-6 mice per group between 8-20 weeks of age, where columns show means and bars 95% CI.

4.2.2 NDRG1 loss does not affect primary T cell responses to foreign antigen

Stimulation of *Ndrg1*$^{-/-}$ non-tg T cells demonstrated no difference in the initial response to productive TCR signalling compared to WT cultures. The absence of NDRG1 did not alter the *in vitro* upregulation of activation markers CD69, CD25 or OX40 in either CD4^{+} or CD8^{+} T cell populations (Fig. 4.2).

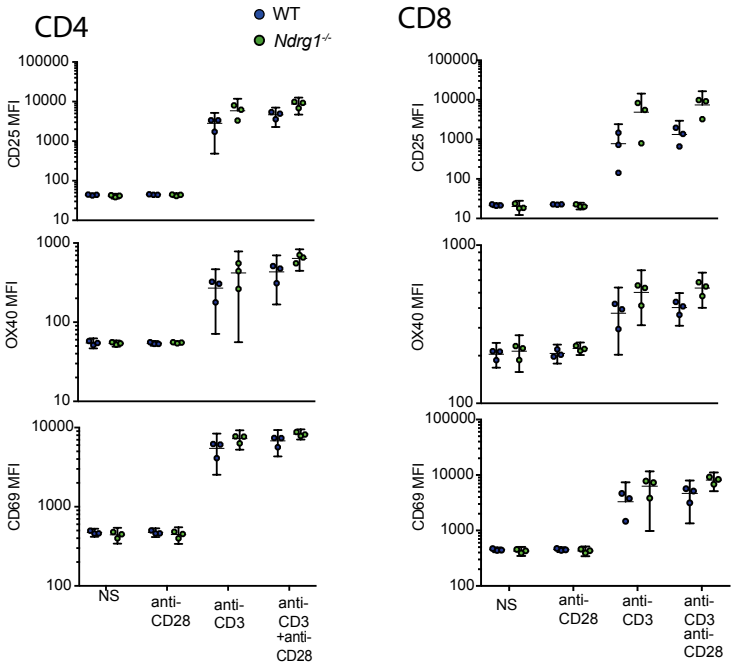


Figure 4.2 Ndrg1$^{-/-}$ CD4^{+} and CD8^{+} T cells show normal activation in response to foreign antigen.

MFIs of activation marker expression on WT and Ndrg1$^{-/-}$ primary CD4^{+} or CD8^{+} splenic T cells stimulated with media alone, or combinations of anti-CD28 at 2μg/ml and anti-CD3 at 3μg/ml for 24 hours at 37°C ex vivo. Results are representative of 2-3 independent experiments: the circles are representative of individual mice and columns are means with 95% CI error bars.

4.2.3 Exploring the role of NDRG1 in T cell tolerogenic assays

4.2.3.1 NDRG1 deficiency does not affect the response of in vivo antigen-experienced CD4^{+} T cells exposed to antigen in vivo

To confirm that NDRG1 acts as a T cell-specific anergy regulator, we recapitulated the *in vivo* peptide-induced T cell anergy assay previously described (Oh *et al.*, 2015) using our mouse model of NDRG1 deficiency. In the following experiments, CD45.2^{+} OVA-specific CD4^{+} OT-II^{+} TCR tg T cells were isolated from WT or *Ndrg1*$^{-/-}$ OT-II^{+} tg mice and adoptively transferred into CD45.1^{+} congenic recipients, with subsequent intravenous injection of OVA peptide (Fig. 4.3A). After 5 days, naïve

and challenged splenic WT and *Ndrg1*$^{-/-}$ OT-II^{+} CD4^{+} cells were harvested and stimulated *in vitro with OVA peptide plus irradiated splenocytes as APCs*.

In contrast to the result reported previously using a thymidine incorporation assay, flow cytometric analysis of CTV dilution demonstrated a significantly enhanced proliferation response in antigen-experienced T cells compared to naïve T cells, regardless of NDRG1 expression ($p = < 0.01$ at all concentrations of OVA; Fig. 4.3B), as would be expected during a recall response to antigen rather than peptide-induced *in vivo* T cell anergy. Furthermore, although the concentration of IL-2 in culture supernatant was lower from antigen-experienced CD4^{+} T cells compared to naïve cells, we could not replicate the reported raised IL-2 production in antigen-experienced *Ndrg1*$^{-/-}$ T cells compared to WT (Fig. 4.3C)(Oh *et al.*, 2015).

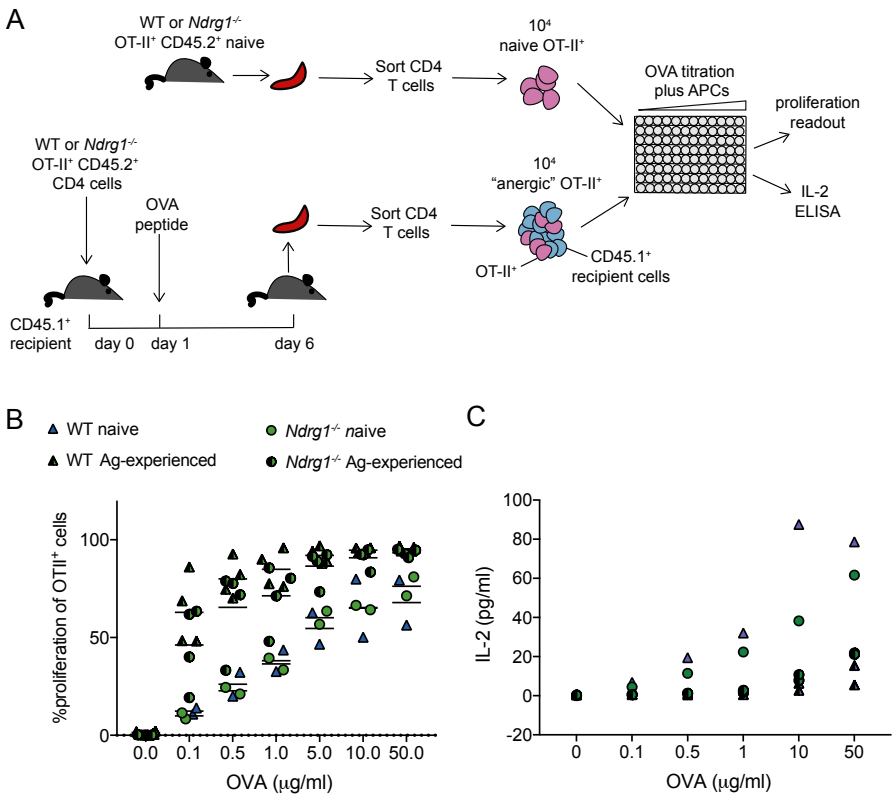


Figure 4.3 Antigen-experienced T cells respond normally in the absence of NDRG1

A. Experimental schematic; OVA-specific CD4^{+} OT-II^{+} T cells were isolated from CD45.2^{+} WT or Ndrg1$^{-/-}$ OT-II^{+} tg mice and adoptively transferred to CD45.1^{+} non-tg recipients, with subsequent intravenous injection of 500μg OVA peptide. After 5 days, splenic CD4^{+} cells were isolated from recipient mice and naïve unstimulated WT or Ndrg1$^{-/-}$ OT-II^{+} tg mice and loaded with CTV. Equal numbers of Vα2^{+} CD45.2^{+}OT-II^{+} cells were cultured in vitro with a titration of OVA peptide for 72h at 37°C with irradiated APCs. B. Proliferation of CD4^{+}Vα2^{+} CD45.2^{+}OT-II^{+} T cells measured by CTV dilution by flow cytometry. C. IL-2 concentration in

culture supernatants in (A). Results are pooled from two independent experiments (B) or one experiment (C); points are individual mice, averaged from technical replicates and bars represent means and 95% CI.

4.2.3.2 Can temporal or bystander effects explain the findings in the T cell anergy assay?

To understand why our results contrasted from those results previously reported (Oh *et al.*, 2015), and explore the apparent discord between enhanced proliferation and reduced IL-2 concentration in the culture supernatants of antigen-experienced cells, I tested variations on the *in vivo* $CD4^+$ T cell anergy experiment described in section 4.2.3.1.

I hypothesised that antigen-experienced cells are primed and hence may start to proliferate earlier than naïve populations and then run out of growth nutrients later in the time course. This theory could explain why measuring solely the period of 48-72h post-stimulation may capture more proliferation in the naïve populations as reported by Oh *et al* using thymidine incorporation assays. To replicate this readout, I added BrdU into the cultures at 48h post re-stimulation, in addition to CTV staining at the start of the 72h protocol immediately before re-stimulation. Flow cytometric detection of BrdU incorporation as a percentage of total cells mirrored the enhanced proliferative response seen in antigen-experienced cells compared to naïve populations using CTV dilution in the same populations (figure 4.4), indicating time differences in readout between experiments do not explain the discrepancies between these results and those previously reported (Oh *et al.*, 2015).

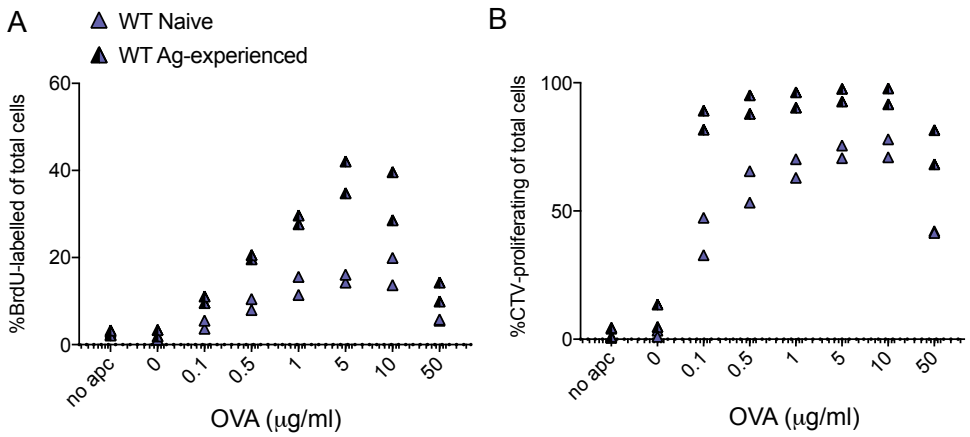


Figure 4.4 Antigen-experienced $CD4^+$ T cells proliferate more in the last 24h culture than naïve $CD4^+$ regardless of assay readout

The T cell anergy assay was set up with WT naïve and WT Ag-experienced as described in Fig. 4.3, with the addition of BrdU at 48h post in vitro assay set up. A. BrdU incorporation of total cells between 48-72h was

detected by flow cytometry. B. Proliferation as a percentage of total cells was detected by CTV dilution in the same wells as (A). Results are from one experiment; points are individual mice, averaged from technical replicates.

Due to the setup of the experiment, wells containing Ag-experienced T cells will also contain bystander non Ag-specific cells from the recipient mice, in contrast to the naïve cells. To determine whether the presence of these non-OT-II tg cells affected either the proliferative response of Ag-specific cells or the level of IL-2 in the supernatant, $CD45.1^+$ bystander cells isolated from mice immunised with OVA were added into the naïve OT-II tg samples. The addition of bystander cells did not explain the observation of reduced proliferation in experienced cells described by Oh *et al* (Fig. 4.5A) (Oh *et al.*, 2015), furthermore the pattern of IL-2 concentration in the supernatants was not affected by the added presence of bystander cells in the wells of naïve populations (Fig. 4.5B).

We then hypothesised that the reduced IL-2 concentration in the supernatants of wells containing antigen-experienced cells may not reflect the intrinsic cellular production of cytokines, and instead IL-2 may be being used up more rapidly due to the enhanced rate of proliferation. To test this, IL-2 and IFNγ cytokine production was directly measured by intracellular staining. In contrast to that measured in the supernatant by ELISA, Ag-experienced populations produced more IL-2 and IFNγ in a dose-dependent manner than naïve $CD4^+$ T cells, a result that was unaffected by NDRG1 deficiency (*= 0.0407 at 0.1μg/ml OVA; Fig. 4.5C,D). $CD45.1^+$ bystander cells, depicted in red, did not produce cytokines in wells containing either Ag-experienced or naïve cells (Fig. 4.5C).

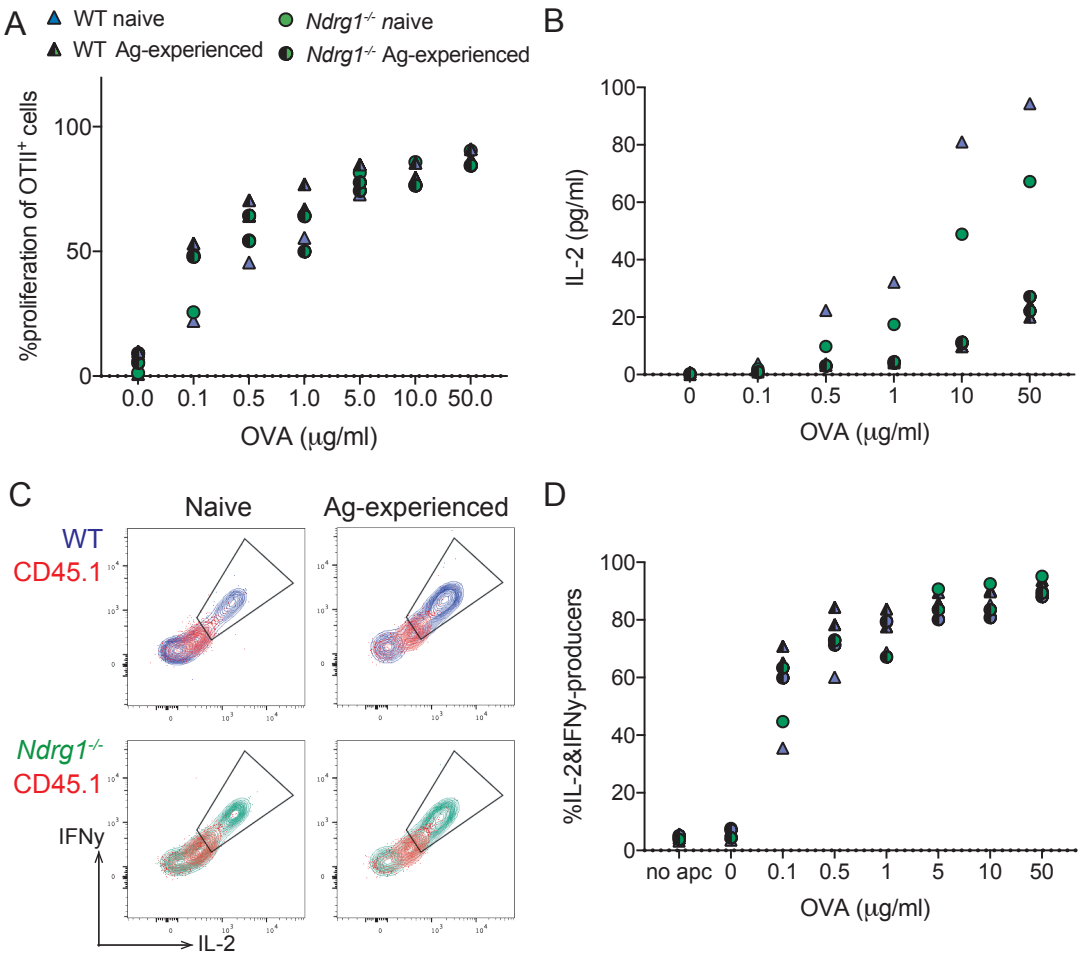


Figure 4.5 Ag-experienced CD4⁺ T cells intrinsically produce elevated IL-2 and IFNγ than naïve CD4⁺ T cells

The T cell anergy assay was set up with WT and Ndrg1$^{-/-}$ naïve and WT and Ndrg1$^{-/-}$ Ag-experienced as described in Fig. 4.3, though CD45.1⁺ bystander cells from a mouse immunised with OVA peptide were added into naïve samples before isolation of CD4⁺ T cells and in vitro set up. A. Proliferation of CD4⁺ CD45.2⁺ T cells measured by CTV dilution by flow cytometry. B. IL-2 concentration in culture supernatants from (A) measured by ELISA. C. Representative flow cytometry plots at 0.1μg/ml OVA of WT naïve or Ag-experienced (blue) or Ndrg1$^{-/-}$ naïve or Ag-experienced (green) CD4⁺ CD45.2⁺ T cells, CD4⁺ CD45.1⁺ cells from each culture are overlaid in red, quantified in (D). Results are from one experiment (C); points are individual mice, averaged from technical replicates.

4.3 Summary of chapter

To strengthen the findings from our mouse model of NDRG1 deficiency, and with the aim of demonstrating that NDRG1 functions specifically in CD4⁺ T cell tolerance, we recapitulated an experimental design to show the role of NDRG1 in *in vivo* peptide-induced T cell anergy (Oh *et al.*, 2015). In contrast to the results reported previously, regardless of NDRG1 deficiency we saw increased proliferation of antigen-experienced pre-stimulated CD4⁺ T cells, as would be expected

during re-stimulation rather than anergic responses. The reported reduction in IL-2 amounts in culture supernatant upon re-stimulation of antigen-experienced $CD4^+$ T cells was reproducible, but NDRG1 deficiency did not affect this phenomenon. Furthermore, the intracellular levels of IL-2 and IFNγ were by contrast higher in the antigen experienced cells, consistent with a recall response to stimulation. It is possible that antigen-experienced cells use IL-2 at a faster rate due to their enhanced proliferation rate on re-stimulation, potentially explaining the reduction of IL-2 detected in the culture supernatants of these cells. Together, these experiments demonstrate that this experimental system does not test for peptide-induced $CD4^+$ T cell unresponsiveness and better experimental models of *in vivo* clonal T anergy are needed.

In conclusion, chapters 3 and 4 of this thesis demonstrate no non-redundant role for NDRG1 during B or T lymphocyte responses. In addition to regulation by chronic anergic signalling in lymphocytes, NDRG1 is reportedly induced by stress, DNA damage and hypoxia across multiple other cell types, and has been implicated in p53-mediated apoptosis and senescence (Van Belzen *et al.*, 1997; Piquemal *et al.*, 1999; Stein *et al.*, 2004; Ellen *et al.*, 2008; Sahni *et al.*, 2014)(Lu, Chua and So, 2014). Hence, NDRG1 may be regulated by signals that themselves drive suppressive, regulatory states including anergy, senescence or apoptosis. At least in the case of lymphocytes, NDRG1 either acts redundantly or solely as a biomarker during the response to anergising antigen receptor-mediated stimuli.

5. A rare genetic disorder with features of human monogenic lupus-like disease

5.1 Introduction to chapter

Rare genetic variants provide a tractable way to discover novel genes and regulatory pathways involved in maintaining immunological tolerance. Individuals with missense or loss-of-function mutations in the prolidase (*Pepd*) gene present with a wide range of clinical manifestations, including massive imidodipeptiduria, facial dysmorphism, developmental delay, lower limb skin ulcerations and recurrent respiratory infections. Many have autoimmune features; 45% patients are reported with splenomegaly, 39% with hematologic abnormalities such as anaemia, and over 20% report immune defects including hypergammaglobulinemia and ANA positivity. 15% patients are formally diagnosed with an autoimmune disorder, with 6% of patients meeting the criteria for SLE (Rossignol *et al.*, 2021). Prolidase deficiency (PD) is a rare, autosomal recessive condition; less than 100 patients with a molecular or genetic diagnosis have been described in the literature, which contribute to a total of 160 cases of PD that reported up to 2021 (Spodenkiewicz *et al.*, 2020; Rossignol *et al.*, 2021). The incidence has been estimated at around 1 in 1 million births (Renaud, J. & Dagenais, 2009; Ferreira and Wang, 2015), however it may be more frequent in some populations due to potential founder variants, such as that seen within the Druze community of Northern Israel and in some US-based Amish populations (Wang *et al.*, 2006; Falik-Zaccai *et al.*, 2010).

Though immune involvement is regularly reported in PD, these features are often in the context of recurrent respiratory infections, hence it has been unclear if loss of immunological tolerance results from prolidase loss or is triggered by chronic microbial exposure, secondary to chronic infection and inflammation (Kurien *et al.*, 2013; Spodenkiewicz *et al.*, 2020). A high degree of incidence of autoimmune disease has been reported in patients with primary immunodeficiencies (Fischer *et al.*, 2017), which can be driven by direct genetic deficiency or may be contributed to by secondary

mechanisms resulting from a pro-inflammatory environment such as alterations to the T_{reg}/T_H17 axis (Fischer *et al.*, 2017), or enhanced antigen exposure leading to bystander activation through the presence of chronically unresolved recurrent infections (Boyman, 2010; Amaya-Uribe *et al.*, 2019). Therefore, further research is required to understand whether autoimmunity directly results from prolidase loss or from the secondary effects of primary immunodeficiency.

Prolidase is a ubiquitously-expressed metallopeptidase that is uniquely required for the hydrolysis of dipeptides containing C-terminal proline or hydroxyproline, and hence the breakdown of proline-rich substrates including collagen (Lupi *et al.*, 2008). PD diagnosis is reached via detection of massive imidodipeptiduria (10-30mmol/day) in addition to measurement of reduced prolidase enzymatic activity in patient-derived cell populations (Ferreira and Wang, 2015). However, prolidase also possesses enzymatic-independent functions; the biological roles of *Pepd* are summarised in figure 5.1. Prolidase enzymatic action is reported to drive stabilisation of HIF-1a

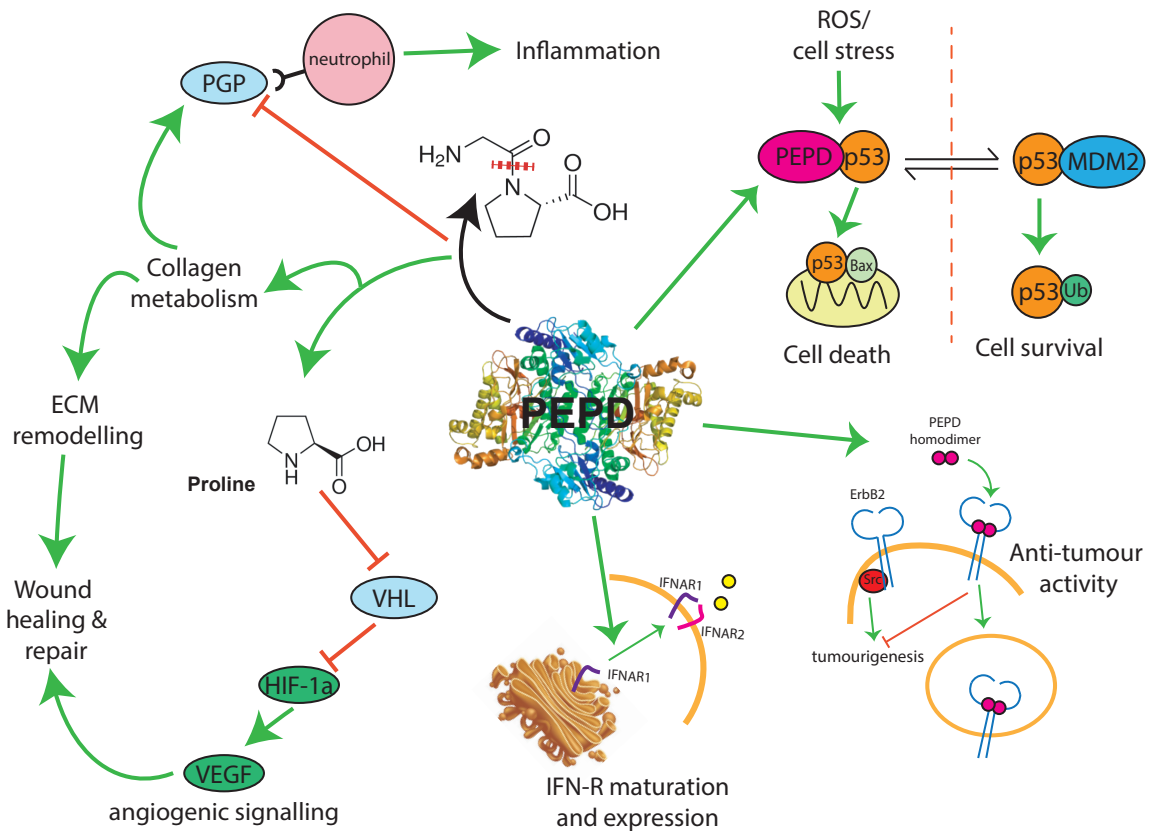


Figure 5.1 Proposed molecular functions of prolidase

Pepd, encoding the metallopeptidase, prolidase is reported to act with multiple biological pathways in both enzymatic-dependent and independent manners. Abbreviations; vascular endothelial growth factor (VEGF), hypoxia-inducible factor 1α (HIF1α), Von Hippel Lindau (VHL), Interferon receptor (IFN-R), extracellular matrix (ECM), proline-glycine-proline (PGP), reactive oxygen species (ROS), mouse double minute 2 (MDM2), Bcl2-associated X protein (Bax).

(Surazynski *et al.*, 2008) and regulate neutrophil chemotaxis through chemoattractant metabolism (Kurien *et al.*, 2013). Independent of imidodipeptide metabolism, prolidase has been demonstrated to regulate p53 availability during cell stress and apoptosis by nuclear localisation, despite generally being described as detected in the cytoplasm (Anna Lupi *et al.*, 2006; Yang *et al.*, 2016, 2017). Additionally, prolidase has been reported to act as an extracellular ligand of ErbB2 to inhibit tumourigenesis, though the mechanism of how *Pepd* enters the extracellular milieu is unknown as it has not demonstrated to be secreted from cells (Yang, Li and Zhang, 2014; Yang *et al.*, 2017). Reports also describe prolidase as required for effective IFN type I signalling, as *Pepd* is essential for the maturation and surface expression of IFN α/β receptor subunit, IFNAR1, a role which is independent of prolidase enzymatic function (Lubick *et al.*, 2015)

Despite this literature describing the multiple roles for prolidase, the mechanism by which Pepd deficiency leads to loss of immune tolerance is not defined. Impaired neutrophil chemotaxis has been reported in some PD patients (Cleary et al., 1994; Shrinath et al., 1997), which has been speculated to drive an increase in autoantigen-sampling by impairing inflammation resolution (Kurien et al., 2013). On the other hand, alterations in the complement pathway have been hypothesised to drive PD-related SLE-like symptoms due to the proline-rich nature of C1q, however C1q levels are normal in most patients, where reported, despite records of hypocomplementemia in others (Kurien et al., 2013; Spodenkiewicz et al., 2020; Rossignol et al., 2021). One paper has described decreased IFNAR expression in fibroblasts isolated from prolidase-deficient patients, accompanied by reduced responses to IFN-β stimulation, which could contribute to impaired resolution of viral infections in these patients (Lubick *et al.*, 2015). Alternatively, the build-up of imidodipeptides or reduced availability of proline, in addition to the prolidase enzymatic-

independent regulation of p53, could hypothetically dysregulate apoptosis in *Pepd*-deficient cells, again increasing exposure to self-antigens (Yang et al., 2017; Misiura and Miltyk, 2020). Previously, mice with a 4bp deletion in exon 14 of *Pepd* have been described to have pigmented fur, cardiomyopathy and a skeletal phenotype due to abnormal apoptosis, however immune phenotyping has not been reported for this model (Besio et al., 2015). Thus, more research using controlled experimental models is required to interpret how the loss of immunological tolerance is driven by prolidase deficiency, to ultimately delineate the contributions of prolidase, separate from the confounding variables of the inflammatory environment of PD patients.

During a large immunophenotyping screening platform designed to detect genes involved in immune homeostasis, loss of the *Pepd* gene was shown to be associated with breakdown of immune tolerance (Abeler-Dörner *et al.*, 2020). Initial screening of prolidase-deficient mice demonstrated increased incidence of ANAs compared to control mice (WT; 17.36% positive (n=386), $Pepd^{-/-}$; 42.9% (n=14) p=*0.0267), indicating *Pepd* loss is associated with autoimmunity. These findings suggested that $Pepd^{-/-}$ mice might offer a useful model to explore the role of *Pepd* in T cell function and immune tolerance. $Pepd^{-/-}$ mice were rederived in an independent mouse facility and in the following chapters of this thesis, I describe the immune characterisation of this murine model of PD, including deep immune proteomic and transcriptomic characterisation of $Pepd^{-/-}$ lymphocyte populations to begin to establish how prolidase deficiency leads to loss of self-tolerance.

5.2 Results

Acknowledgement: Eleanor Cawthorne and Tanya Cheetham helped with the identification of mutants by PCR for subsequent breeding and Tanya Cheetham and Aneesha Bhandari helped to test murine serum for ANAs.

5.2.1 Prolidase deficiency causes loss of immune tolerance characterised by raised serum IgA titres and SLE-like renal immune complex deposition

Rederivation of the *Pepd*$^{-/-}$ mouse model of PD in the Wellcome Trust functional genomics facility recapitulated a similar trend increase in ANA positivity within *Pepd*$^{-/-}$ mice compared to controls (Figure 5.2). Furthermore, as previously reported, prolidase-deficient mice were smaller than their WT counterparts (Figure 5.3) (Besio *et al.*, 2015).

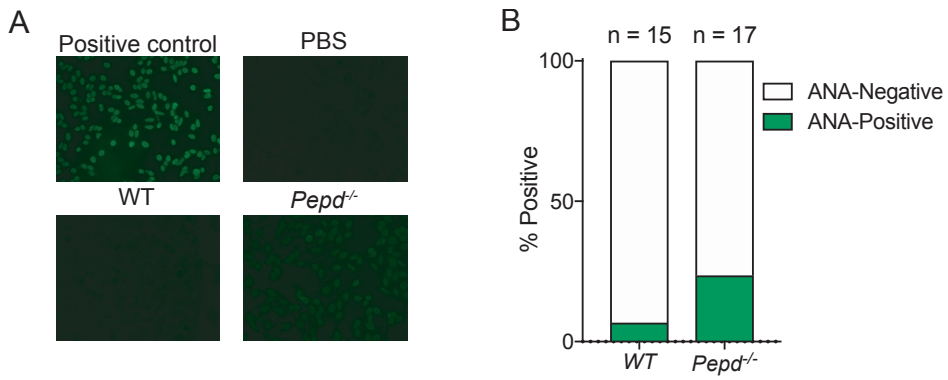


Figure 5.2 Pepd deficiency is associated with loss of immune tolerance in mice

A. Serum ANA testing of WT and Pepd$^{-/-}$aged-matched female mice between 8-26 weeks on HepB2 cells, quantified in (B) as % positive of samples tested. Significance was determined using a fisher's exact test (p 0.3382).

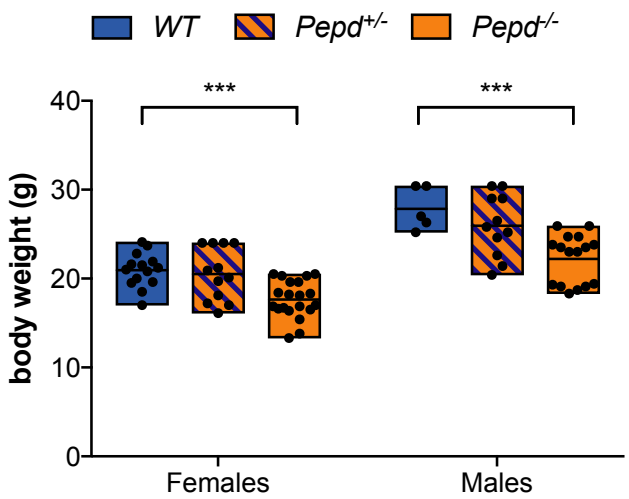


Figure 5.3 Pepd$^{-/-}$ mice are smaller than WT controls

*Weights of mice of different genotypes between 8-12 weeks. Each point represents one mouse. Weights were collected over time and pooled. Significance was determined with a multiple t test *** p= <0.001.*

PD patients are also frequently reported to have hypergammaglobulinemia (Spodenkiewicz *et al.*, 2020); IgA was specifically increased in the serum of *Pepd*$^{-/-}$ mice for all forms of the complex (Figure

5.4), and IgA, with C1q and IgG were deposited in the renal glomeruli, a pattern consistent with the immune complex mediated disease seen in human SLE (Figure 5.5).

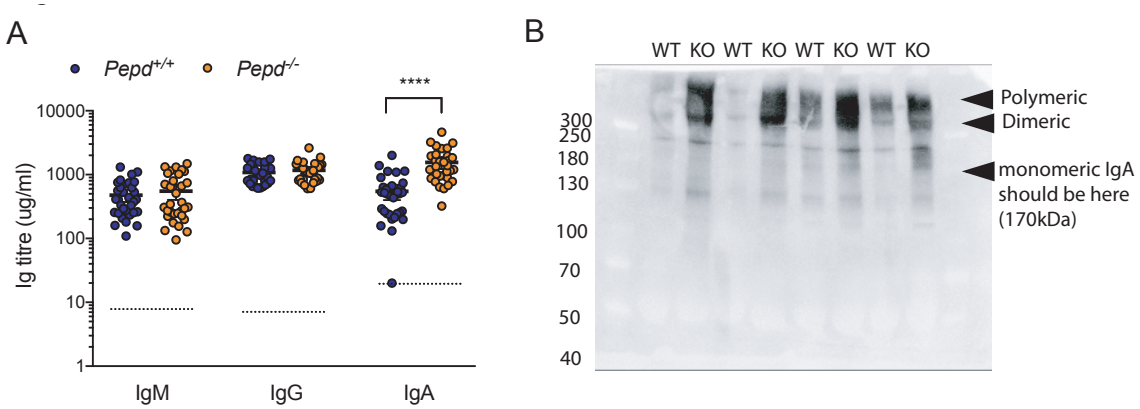


Figure 5.4 Serum IgA levels are specifically raised with loss of prolidase

*A. Serum immunoglobulin levels from WT and Pepd$^{-/-}$ mice. Dotted line represents 1.5x interpolated background absorbance, each point is one mouse. Significance was determined with a multiple t test **** p=<0.0001. B. Non-reduced SDS-PAGE and western blot of serum from WT or Pepd$^{-/-}$ (KO) mice, detecting IgA species.*

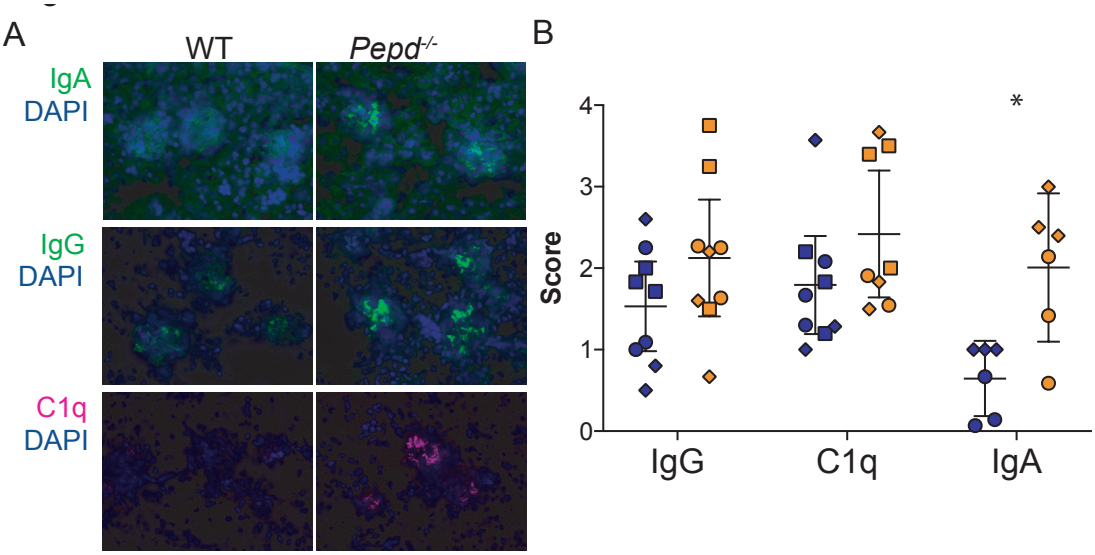


Figure 5.5 Loss of prolidase is associated with SLE-like renal immune complex deposition

*A. Representative fluorescent immunostaining of WT and Pepd$^{-/-}$ kidney sections with antibodies against IgG, IgA and C1q in green or pink, nuclei are counter-stained with DAPI (blue). Images are representative of 3 independent experiments with 3-4 mice per group. B. Images were blinded and scored by eye then averaged across at least 3 images per sample at 40x magnification. Significance was determined using an unpaired t test, adjusted for multiple testing. IgG ns = 0.15, C1q ns = 0.15, IgA * = 0.02.*

5.2.2 Immunophenotyping of *Pepd*$^{-/-}$ lymphocyte populations identifies an altered B cell phenotype and increases in activated T cell populations

5.2.2.1 Pepd loss is associated with an altered B cell surface phenotype

Deep immunophenotyping of prolidase-deficient lymphocyte populations identified equivalent development and distribution of B2 cell subsets in the bone marrow, periphery or B1 populations in the peritoneum (Figure 5.6A-F). However, prolidase deficiency is associated with significantly altered surface phenotype of mature B cell populations in the BM, spleen and MLN, characterised

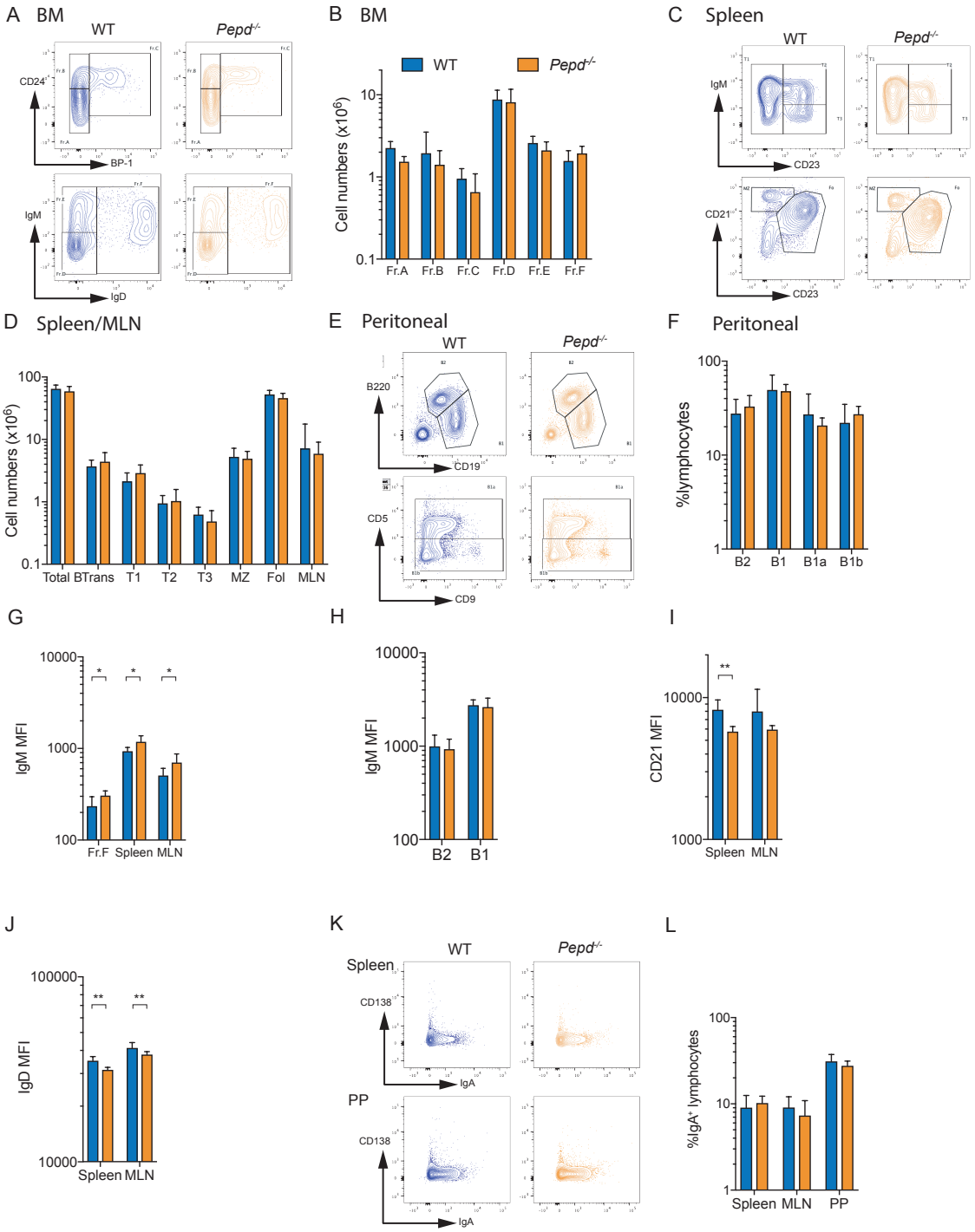


Figure 5.6 Pepd loss is associated with an altered B cell phenotype

*A. Representative flow cytometry plots of B cell development through Hardy fractions in the BM of WT and Pepd$^{-/-}$ mice. B. Quantification of bone marrow B cell numbers as gated in (A). C. Representative flow cytometry plots of splenic B cell populations of WT and Pepd$^{-/-}$ mice, quantified as cell numbers in (D). E. Representative flow cytometry plots of B populations in the peritoneum of WT and Pepd$^{-/-}$ mice, quantified as %peritoneal lymphocytes in (F). G. Surface IgM expression on mature recirculating B cells in the bone marrow (Fr.F), gated in (A), B220^{+} cells in the spleen and LN. H. Surface IgM on B cell populations in the peritoneum gated as in (E). I. Quantified altered surface CD21 and (J) IgD expression of splenic B cell populations. K. representative flow cytometry plots of IgA staining on B220^{+} gated cells across lymphoid organs, quantified by gating of IgA^{+} B220^{+} cells in L. Columns represent means with 95% CI error bars and are representative of at least three independent experiments, each with 3-6 mice per group. Statistical significance was determined by students t test, adjusting for multiple comparisons using the Holm Sidak method. * p = <0.05, ** p = <0.01.*

by elevated IgM expression and reduced CD21 and IgD expression (Figure 5.6G-J). Despite significantly increased IgA serum titres and associated renal deposition, there was no significant differences in IgA^{+} B cell populations in the spleen, MLN, BM, or Peyer's patches (PP) (Figure 5.6K,L).

5.2.2.2 The IgM phenotype associated with prolidase deficiency is BCR-independent, though B cell anergy is intact with loss of Pepd

Though *Pepd* deficiency resulted in impaired maintenance of tolerance in unchallenged mice, accompanied by an altered B cell phenotype and dysregulated immunoglobulin production (Figures 5.2-5.6), the induction and maintenance of B cell anergy was not affected with loss of prolidase, as tested by reconstitution of lethally irradiated CD45.1^{+} non-tg and sHEL mice with WT or *Pepd*$^{-/-}$ CD45.2^{+} Ig^{HEL} BM (Fig. 5.7A). Though *Pepd*$^{-/-}$ splenic B cells demonstrated significantly raised surface IgM as seen previously in non-tg mice (Fig. 5.7E), demonstrating that this phenotype is independent of BCR specificity, self-antigen induced down-modulation of surface IgM^{a} on mature recirculating cells in the BM and splenic B cells was equivalent in sHEL recipients of both WT and *Pepd*$^{-/-}$ Ig^{HEL} BM, indicating anergy induction was comparable (Figure 5.7C-E). Furthermore, proximal BCR signalling on *ex vivo* stimulation was blocked to the same level in the spleens of sHEL recipients, irrespective of donor *Pepd* expression (Figure 5.7F), demonstrating this aspect of anergy maintenance is also unaffected by prolidase loss.

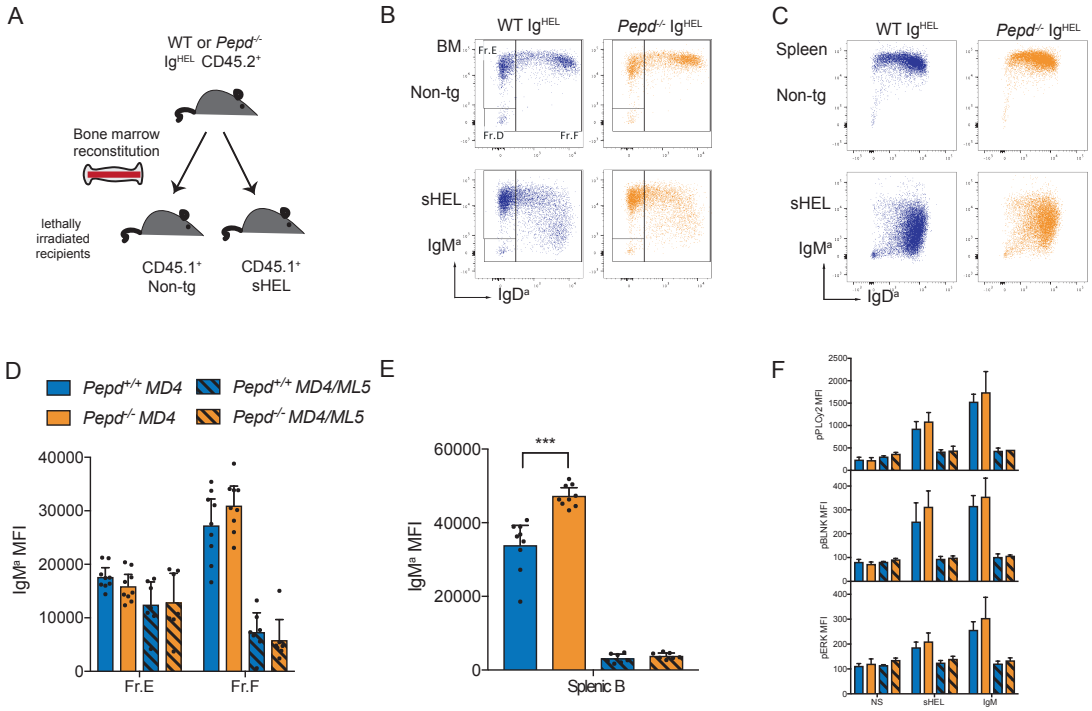


Figure 5.7 B cell anergy is intact in the absence of prolidase expression

*A. Lethally irradiated CD45.1^{+} sHEL or non-tg recipient mice were reconstituted with CD45.2^{+} WT or Pepd$^{-/-}$ Ig^{HEL} BM for 8 weeks. Representative flow cytometry plots of (B) CD45.2^{+}B220^{+}CD43^{-} BM cells and (C) splenic CD45.2^{+}B220^{+} B cells from mice reconstituted in (A). D. IgM^{a} surface expression quantified on mature recirculating B cells (CD45.2^{+}B220^{+}CD43-IgD^{+}) in the BM, and on (E) splenic CD45.2^{+}B220^{+}CD19^{+} cells, quantified by flow cytometry as MFI. F. MFIs of phospho-flow intracellular staining of pPLCy2, pBLNK and pERK in WT and Pepd$^{-/-}$ splenic CD45.2^{+}B220^{+}CD19^{+} B cells from (A), after stimulation ex vivo with media alone, 1μg/ml sHEL or 10μg/ml IgM. Results are representative (B,C,F) or pooled (D-E) from two independent experiments (3-5 mice per group) and bars show means with 95% CI error bars. Statistical significance was determined by students t test, adjusting for multiple comparisons using the Holm Sidak method, *** p = <0.001.*

5.2.2.3 Pepd$^{-/-}$ mice have a peripheral activated T cell phenotype

Prolidase loss is associated with a peripheral activated T cell phenotype; *Pepd$^{-/-}$* mice had significantly increased percentages and numbers of CD8^{+} CD44^{hi} CD62L^{-} effector T populations and reduced percentages and numbers of resting CD8^{+} subsets (Figure 5.8). The proportions of splenic CD4^{+} effector (CD44^{+} CD62L^{-}) and FoxP3^{+} CD4^{+} T regulatory populations were also significantly increased in *Pepd$^{-/-}$* mice (Figure 5.8A-C). ANOVA was used to determine significance across experimental datasets as data could not be pooled due to high variability across experiments, likely due to differences in fixation across panels and consequential alterations in gates, and biological factors such as ages and gender of the mice (Figure 5.8D).

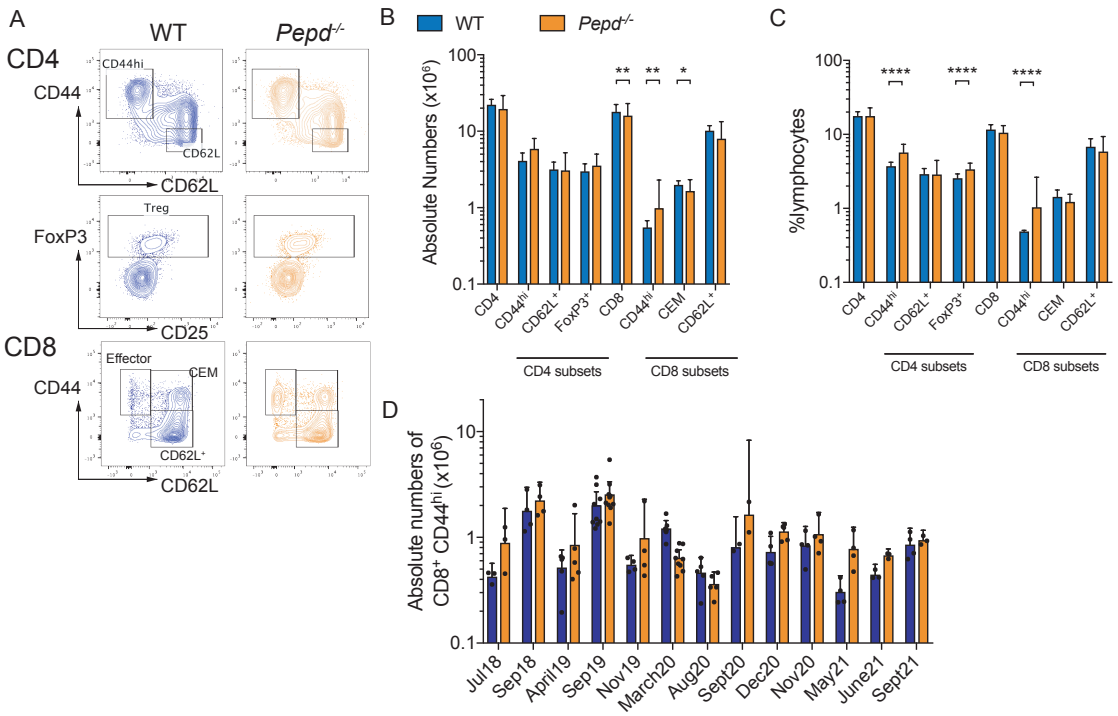


Figure 5.8 Pepd$^{-/-}$ mice have a peripherally activated T cell phenotype

*A. Representative flow cytometry plots of splenic CD4^{+} and CD8^{+} T cell subsets of WT and Pepd$^{-/-}$ mice. B. Representative quantification of splenic T cell numbers as gated in (A). ANOVA significance was determined across experiments; CD8^{+}CD44^{hi} (** p = 0.0075), CD8^{+}CEM (** p = 0.0014), CD8^{+}CD62L^{+} (* p = 0.0105). C. Quantification of T cell subsets gated in (A) as proportion of splenic lymphocytes. ANOVA significance; CD4^{+}CD44^{hi} (**** p = <0.0001), CD4^{+}FoxP3^{+} (**** p = <0.0001), CD8^{+}CD44^{hi} (**** p = <0.0001). D. Significance by ANOVA was determined across each T cell subset across experiments to account for variance. Columns represent means with 95% CI error bars and are representative of nine to twelve independent experiments, each with 3-10 mice per group.*

T cell development in the thymus of *Pepd*$^{-/-}$ mice appeared normal (Figure 5.9A,C), with the exception of significantly increased proportions of CD44^{hi} and FoxP3^{+} CD4^{+} thymocytes (Figure 5.9B,D).

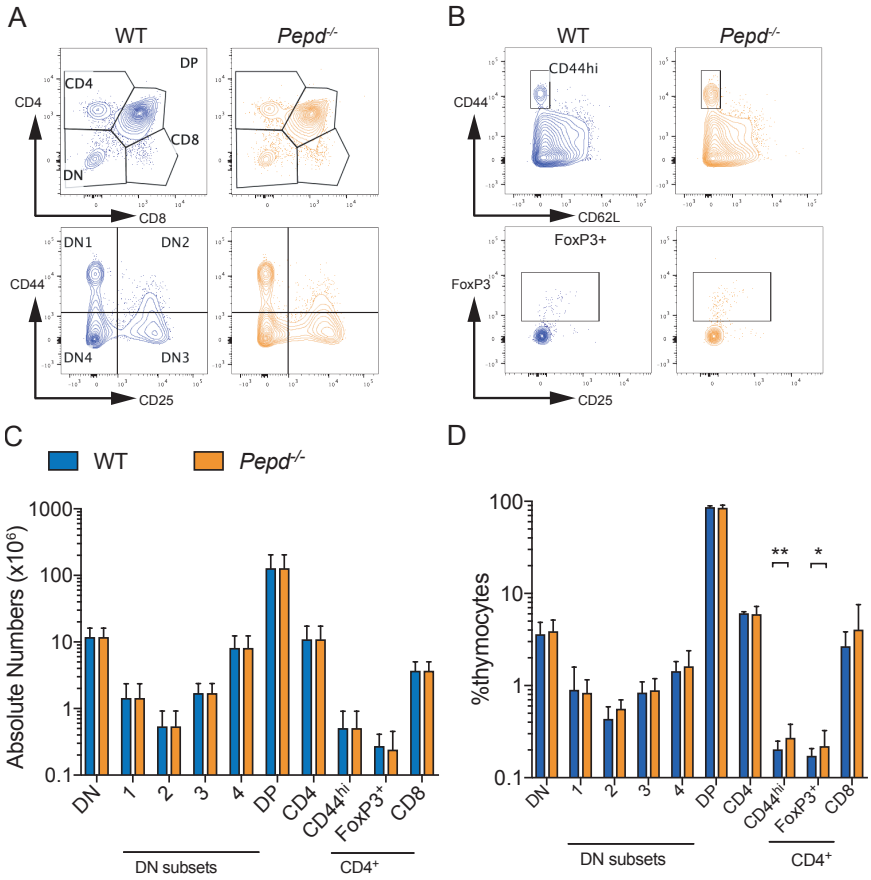


Figure 5.9 Pepd$^{-/-}$ mice have an activated T cell phenotype through development

A. Representative flow cytometry plots of T cell development in the thymus of WT and Pepd$^{-/-}$ mice. Top plot shows live thymocytes and gating of double positive (DP), double negative (DN) and single positive (SP) populations. Bottom plot shows gating of DN subsets. B. of CD4^{+} SP populations in the thymus. C. Quantification of thymus T cell numbers as gated in (A) and (B). D. Quantification of populations gating in (A) and (B) as proportion of thymocytes. ANOVA significance was determined across experiments; FoxP3^{+} (p = 0.039), CD44hi^{+} (** p = 0.0014). Columns represent means with 95% CI error bars and are representative of two to four independent experiments, each with 3-10 mice per group.*

5.2.3 Multimodal scRNA-Seq analysis shows that loss of prolidase is associated with an accumulation of exhausted effector CD8^{+} T cells and loss of *Ly6c2^{+}* memory precursor effector cell (MPEC)-like populations

5.2.3.1 Oligo-tagged antibody labelling clustering of single cells confirms the altered CD8^{+} phenotype

To comprehensively phenotype and explore how T cell populations are affected by prolidase loss, we subjected WT and *Pepd$^{-/-}$* total T cells to single cell 3' RNA-Seq, in combination with oligo-tagged antibody labelling (ADT) of T cell markers to aid characterisation (Figure 5.10A). Splenic T cells from 3 CD45.2^{+} WT and 3 *Pepd$^{-/-}$* samples were sorted and multiplexed using cell hashing oligo-tagged

antibodies, labelled with 15 oligo-tagged antibody-derived (ADT) T cell markers listed in the methods, then sequenced together using droplet-based scRNA-Seq. 4/6 samples contained 10% spiked WT CD45.1^{+} or WT CD45.1^{+}CD45.2^{+} cells in order to test whether populations could be separated by CD45.1 or CD45.2 ADT staining, as routinely performed with flow cytometry (Figure 5.10A), this latter step was to explore the scope for sequencing pooled mixed chimeric populations. While the majority of ADT labels worked well, reads of ADT markers, anti-CD45.1 and anti-CD45.2 were not detected, which may be due to a technical failure or incompatibility of the antibodies within this protocol. Therefore, they could not be used to separate congenically labelled samples in this experiment, leading to the conclusion that ADTs cannot be used to determine CD45 antigen

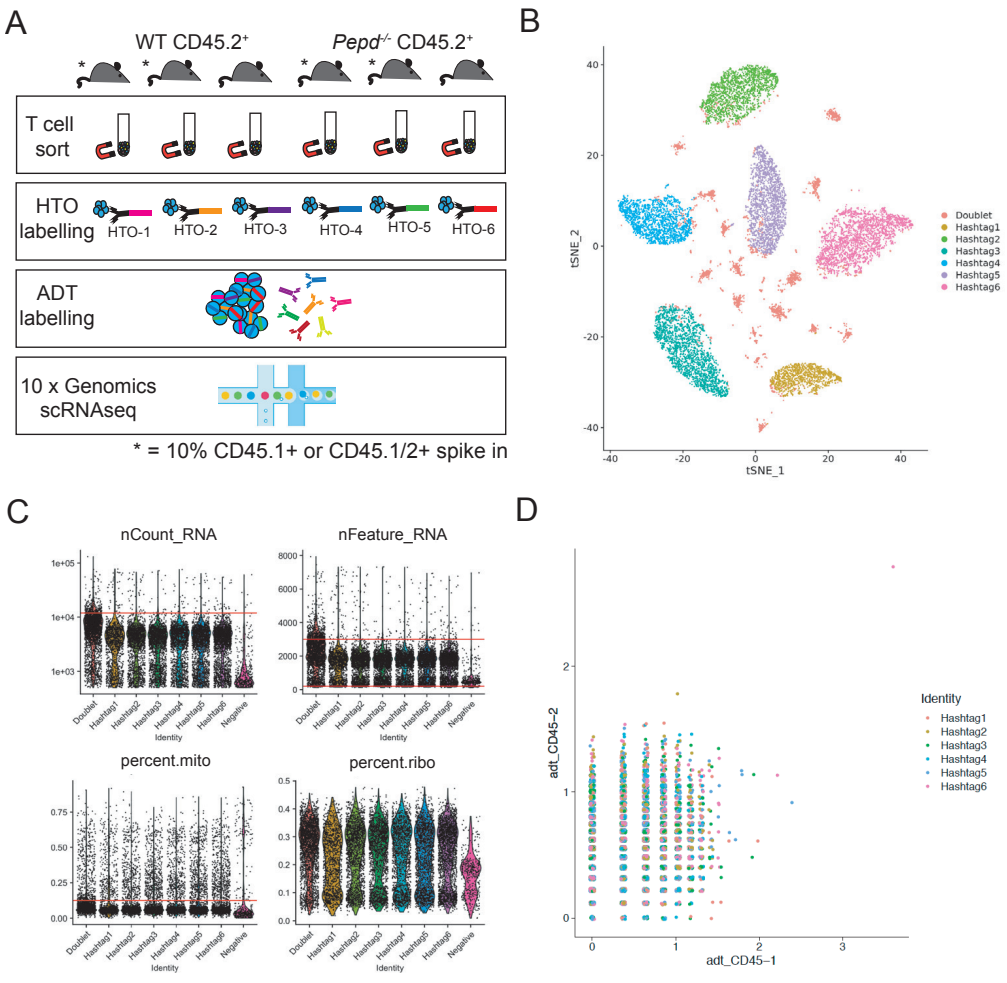


Figure 5.10 Multimodal proteomic and transcriptomic sequencing of WT and Pepd$^{-/-}$ splenic T cell populations; quality control and filtering

A. Schematic of experiment; T cells were sorted using negative enrichment from WT and Pepd$^{-/-}$ CD45.2^{+} mice, spiked with CD45.1^{+} or CD45.1^{+}/CD45.2^{+} cells. T cells were labelled with hashtag antibodies, pooled together then labelled with key ADT T cell markers before submission as one sample for 3' single cell

transcriptomic sequencing. B. Hashtag-labelled samples were demultiplexed for downstream analysis alongside heterogenous doublet removal. C. Singlets were filtered based on total RNA count library and feature (gene) counts per cell, and on mitochondrial gene expression. D. Expression of CD45.1 and CD45.2 ADT markers coloured by sample (hashtag).

specificity in subsequent chimeric experiments (Figure 5.10D). 14,568 cells were captured and sequenced in total with 8,449 mean reads per cell (number of unique molecular identifiers; nCount_RNA), with post-filtering and demultiplexing steps leaving 8220 singlets across the 6 samples, and an average of 1,783 genes detected per cell (Figure 5.10B,C).

Unsupervised clustering and visualisation on two-dimensional uniform manifold approximation and projection (UMAP) using solely the ADT assay information, identified 12 distinct clusters (Figure 5.11A). The cluster resolution of 0.7 was chosen based on the associated clustering tree and biological knowledge of T cell populations (Figure 5.11A,B). Cluster cell type identities were inferred based on protein expression, enabling identification of naïve, regulatory, effector and memory $CD4^+$ and $CD8^+$ T cell populations corresponding to those previously well characterised by flow cytometry (Figure 5.11C-E, appendix C). Naïve $CD4^+$ populations expressing *Satb1* and CD62L make up cluster 0, whereas clusters 1 and 3 represented naïve $CD8^+$ populations expressing high *Ccr9*, differing by expression of CD62L at the proteomic level (Figure 5.11C-E, appendix C). $CD4^+$ T regulatory populations contributed to clusters 6 and 11, both characterised by Foxp3 RNA and CD25 mRNA (*Il2ra*) and proteomic expression, although distinguished by the increased expression of effector-like markers such as KLRG1, PD1, CD44, and *S100a4* in cluster 11, suggesting this population represents effector T regulatory populations (Figure 5.11C-E, appendix C).

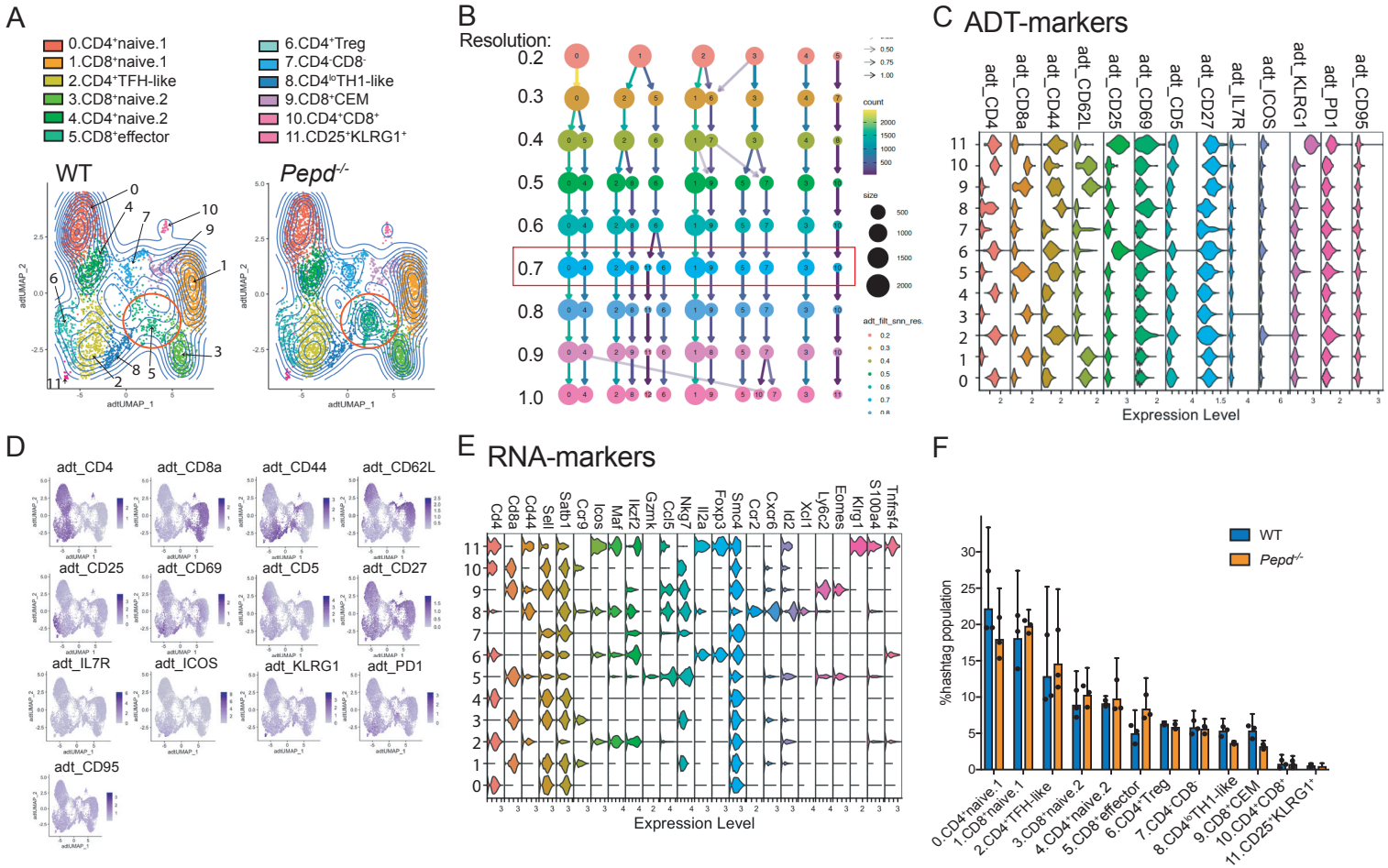


Figure 5.11 ADT clustering identifies enrichment of Pepd$^{-/-}$ CD8^{+} effector cells

A. ADT-marker driven UMAP dimensionality reduction visualisation of clusters derived from ADT-markers at a resolution of 0.7, visualised by WT or Pepd$^{-/-}$ identities. B. Clustering tree of ADT-determined clusters at different resolutions. C. Expression of ADT protein markers on T cell populations clustered by ADT information in (A) by VlnPlot. D. FeaturePlot of ADT markers overlaid onto ADT-derived UMAP dimensionality reduction from (A). E. Visualisation of RNA marker expression on ADT-marker clustered T cell populations from (A). F. Quantification of representation of WT or Pepd$^{-/-}$ samples within ADT-derived clusters.

Activated $CD4^+$ populations are represented in clusters 2 and 8; cluster 2 may characterise effector $CD4^+$ T cell populations skewed to a T_{FH}-like cell fate due to expression of markers including ICOS, PD1, *Maf* and *Ikzf2* (Andris *et al.*, 2017), whereas *Ccr2, Cxcr6*, *Id2* and CD69 expression differentiated cluster 8 suggesting a resident T_{H1}-like phenotype (Shaw *et al.*, 2016). $CD8^+$ effector cells are characterised in cluster 5, which expresses PD1, KLRG1, *Gzmk, Ccl5* and *Nkg7* amongst other effector molecules, whereas resting memory $CD8^+$ populations were represented by population 9, expressing *Ly6c2, Eomes, Ccl5* and CD44 (Martin and Badovinac, 2018; Chen *et al.*, 2019)(Figure 5.11C-E, appendix C). WT and *Pepd*$^{-/-}$ derived T cells contributed to all 12 clusters, however $CD8^+CD44^{hi}CD62L^{lo}$ areas of the UMAP appeared to be particularly enriched for *Pepd*$^{-/-}$ T cells (Figure 5.11A), as quantified in Figure 5.11F.

Differential gene expression analysis identified significant alterations in phenotype between WT and *Pepd* cluster 5.$CD8^+$effector T cells in an intrinsic manner; *Pepd* deficiency was associated with significant upregulation of both inflammatory and exhausted markers, such as *Gzmk, Nkg7, Maf, Ctla2a* and the S100 family of molecules (Figure 5.12). Conversely, regulatory molecules inversely correlated with activation were significantly reduced in *Pepd*$^{-/-}$ effector populations, including *Satb1, Sell, Myb,* and *Ly6c2*, suggesting an altered functional phenotype of $CD8^+$ effector populations (Figure 5.12).

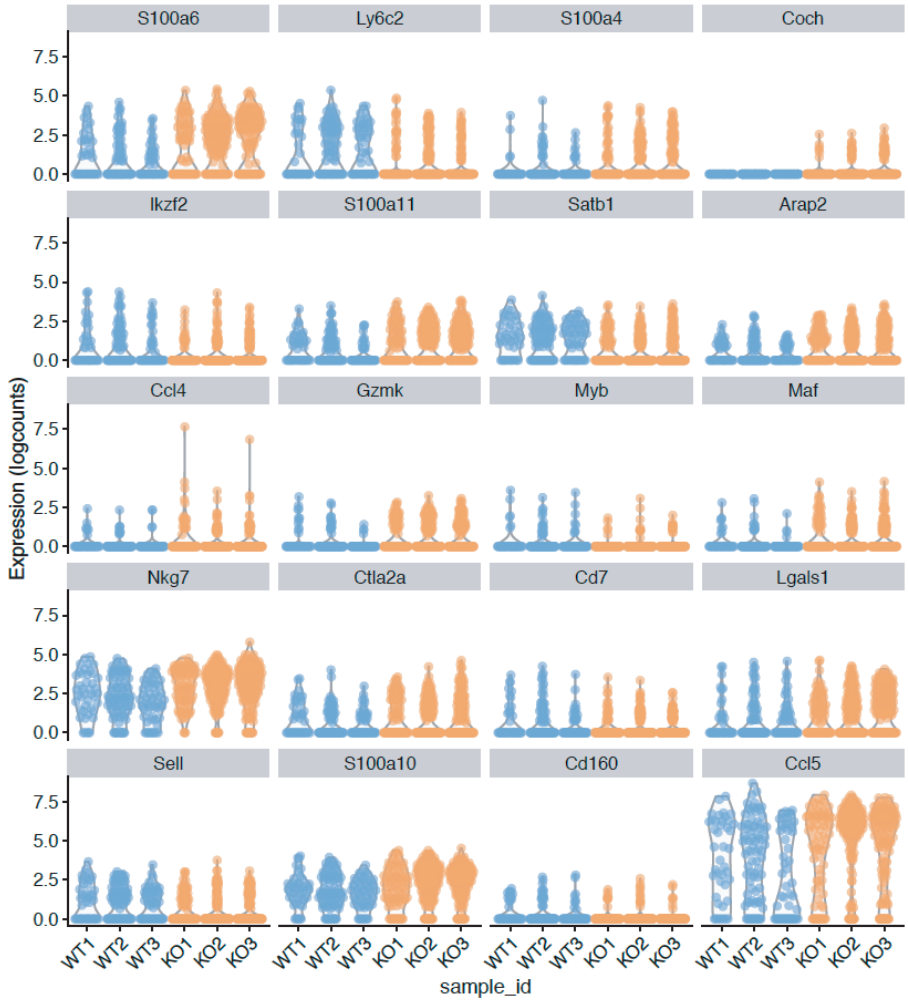


Figure 5.12 Pepd$^{-/-}$ CD8^{+} effector cells have an altered transcriptional phenotype

Top 20 differentially expressed genes between WT or Pepd$^{-/-}$ CD8^{+} effector populations (cluster 5) as determined by Pseudobulk (muscat) subpopulation differential state analysis at a threshold of logFC change 0.7 and adjusted p value 0.01.

5.2.3.2 Multimodal scRNA-Seq and ADT analysis demonstrates expansion of CD8^{+} effector population expressing an inflammatory exhaustion signature and loss of Ly6c-expressing non-effector populations

To take full advantage of the multi-modal dataset, CD8-expressing clusters were subsetted based on ADT and RNA CD8 expression and re-clustered by a Weighted Nearest Neighbour (WNN)-analysis, which integrates the proteomic and transcriptional information together (Figure 5.13A). Unsupervised clustering and subsequent clustering tree analysis identified eight distinct CD8^{+} populations at a clustering resolution of 0.5 (Figure 5.13B), characterised by naïve, activated, localisation and memory markers (Figure 5.13C-D, appendix D).

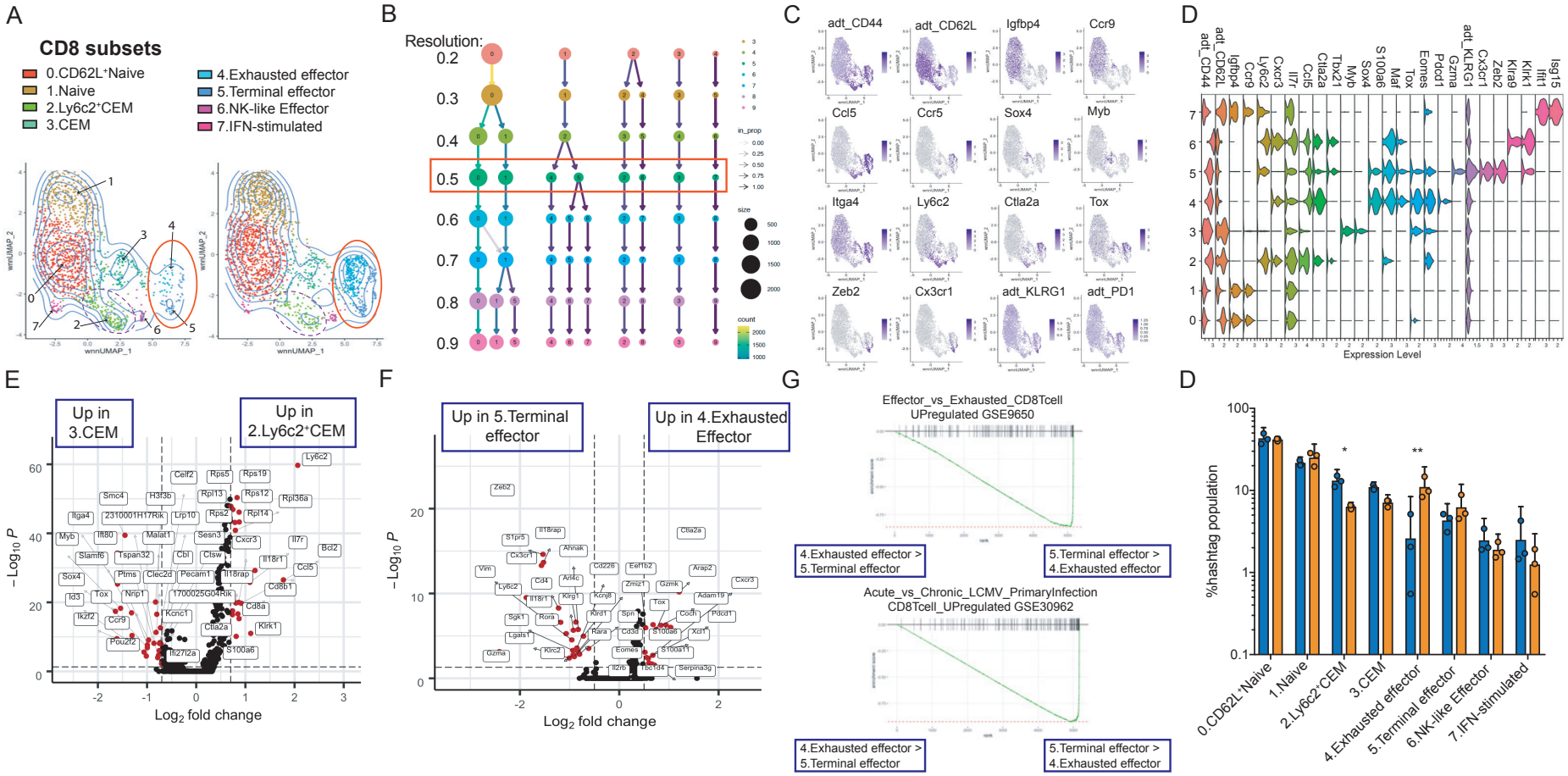


Figure 5.13 WNN-mediated analysis of CD8⁺ populations identifies enrichment of exhausted CD8⁺ effectors and loss of resting populations with Pepd deficiency

A. WNN-derived UMAP dimensionality reduction visualisation of WT and Pepd$^{-/-}$ WNN-determined CD8⁺ clusters by dual modality weighting of protein and RNA markers of T cell populations. B. Clustering tree analysis of resolutions of WNN-clusters of CD8⁺ populations. C. FeaturePlot overlays of key RNA and protein markers contributing to WNN-clustering of CD8⁺ T cell populations on WNN-mediated UMAP projections. D. VlnPlot of expression of RNA and protein markers of WNN-mediated CD8⁺ clusters. E.

VolcanoPlot visualisation of Seurat FindMarkers-defined differential expression of genes between 2.Ly6c2^{+}CEM and 3.CEM populations. DE genes are labelled and in red when they meet the threshold of a log2FC of 0.7 and local p-adjusted value of 0.05. F. VolcanoPlot visualisation of differential expression between effector populations (cluster 4.Exhausted effector versus cluster 5.Terminal effector) as determined by Seurat FindMarkers. DE genes are labelled and in red at a log2FC threshold of 0.5 and adjusted p value of 0.05. Total 5165 variables tested. G. FGSEA analysis of gene sets enriched in differential gene signatures between effector populations, cluster 4.Exhausted effector and cluster 5.Terminal effector. Genes are ranked from highest expressed (left) to lowest expressed (right) in cluster 4.Exhausted effector, negative enrichment of genes associated with effector (vs.exhausted) and acute (vs.chronic) conditions from published gene sets. Genes sets are considered enriched at an adjusted p value of 0.05. H. Quantification of contribution from WT or Pepd$^{-/-}$ cells of WNN-clustered populations as proportion of hashtagged CD8^{+} cells per sample and (I) further visualization of quantification from (H). Statistics in (H) and (I) were determined by two-way ANOVA, with significance adjusted by Sidak, p=<0.05, ** p=<0.01. Graphical data represents means with 95% CI error bars of one experiment.*

Naïve populations resided in clusters 0.CD62L+Naive and 1.Naive and could be separated by differential expression of CD62L at the protein level (Figure 5.13C,D). Central effector memory (CEM) clusters, 2.Ly6c2+CEM and 3.CEM both expressed high levels of CD44 and CD62L at the protein level, though were transcriptionally distinct; cluster 3.CEM could be characterised by higher expression of *Myb, Ikzf2* and *Sox4,* whereas *Ly6c2, Il7r* and *Cxcr3* were highly differentially expressed in 2.Ly6c2+CEM as well as effector molecules, *Ccl5* and *Ctla2a* (Figure 5.13E, appendix E). This expression profile suggests the 2.Ly6c2^{+}CEM cluster may contain heterogeneous, possibly dynamic naïve and memory populations such as memory cells differentiating from naïve populations, effectors surviving recent contraction and memory formation or those with a memory precursor effector cell (MPEC)-like signature, primed to respond and become effectors on new challenges (Joshi *et al.*, 2007; Martin and Badovinac, 2018; Diao and Pipkin, 2019).

Three clusters expressed effector-associated gene signatures; cluster 6.NK-like effector expressed high Ly6c2 along with cytotoxic genes encoding natural killer receptors, suggesting these cells are highly similar to CD8^{+}NKT-like populations (Figure 5.13,C,D, appendix D)(Harsha Krovi *et al.*, 2020). Both cluster 4.Exhausted effector and 5.Terminal effector expressed low *Il7r* and high amounts of effector molecules including *S100a4* and *S100a6, Ccl5* and *Nkg7*. However, differential expression analysis identified that cluster 5.Terminal effector was characterised by expression of markers downstream of *Tbet*, including *Zeb2, Cx3cr1* and KLRG1, which alongside low *Il7r* expression indicates a profile typical of terminally (T)-differentiated effectors, comparable to the transcriptional profile described as short-lived effector cells (SLEC) during early stages of viral infection or inflammation (Figure 5.13C,F, appendix F)(Joshi *et al.*, 2007; Omilusik *et al.*, 2015). On the other hand, cluster 4.Exhausted effectors, expressed relatively higher amounts of molecules characteristic for inflammation, *Gzmk*, *S100a6* and *S100a11*, and exhaustion, *Ctla2a, Pdcd1, Tox* and *Eomes* (Figure 5.13C,F, appendix F). This signature was comparable to transcriptional exhaustion patterns reported in other models of autoimmune disease (McKinney *et al.*, 2015;

Zakharov *et al.*, 2020; Dudek *et al.*, 2021). Gene set enrichment analysis of the genes significantly altered in 4.Exhausted effector in contrast to 5.Terminal effector identified negative enrichment of published gene sets enriched in effector states compared to exhausted, and acute infection versus chronic infection states, confirming that 4.Exhausted effector accurately reflects exhausted effectors, whereas 5.Terminal effector presents a terminally differentiated SLEC-like transcriptional signature similar to that reported in other mouse models (Figure 5.13G)(Joshi *et al.*, 2007; Omilusik *et al.*, 2015).

Population analyses identified significant over-representation of *Pepd*$^{-/-}$ derived cells specifically within the 4.Exhausted effector cluster, whereas cluster 2.Ly6c2^{+}CEM cells was predominantly composed of WT cells, suggesting altered CD8^{+} T cell subset differentiation or maintenance on loss of *Pepd* (Figure 5.13G,H).

5.2.3.3 Pepd deficiency drives altered differentiation of CD8⁺ populations

T cell development is complex and can often follow multiple bidirectional lineages between naïve, effector and central memory populations (Martin and Badovinac, 2018; Diao and Pipkin, 2019). Trajectory inference can indicate how inter-population relationships and differentiation pathways are affected by conditions in a reduced, more interpretable dimension (Trapnell *et al.*, 2014; Bézieux *et al.*, 2021). Inferred trajectory analysis of WT CD8^{+} T cells demonstrated lineages from naïve populations to 2.Ly6c2^{+}CEM and 3.CEM, and to effector populations via 5.Terminal effector (Figure 5.14A). In *Pepd* deficiency, the analysis suggested earlier lineage separation between CEM populations and effector populations, including earlier divergence to the 4.Exhausted effector population in contrast to the WT condition (Figure 5.14A), suggesting prolidase loss may disrupt developmental processes driving T cell differentiation and fate. However, while trajectory interference analyses can provide biological insight into continuous cellular differentiation in reduced dimensions, interpretations of directionality, in addition to the effects of conditions such

as genetic knockout are often limited; differential abundance between conditions can ultimately force differential lineage interference and skew results, whilst comparison of trajectories inferred independently across conditions are difficult to interpret (Roux De Bézieux *et al.*, 2021).

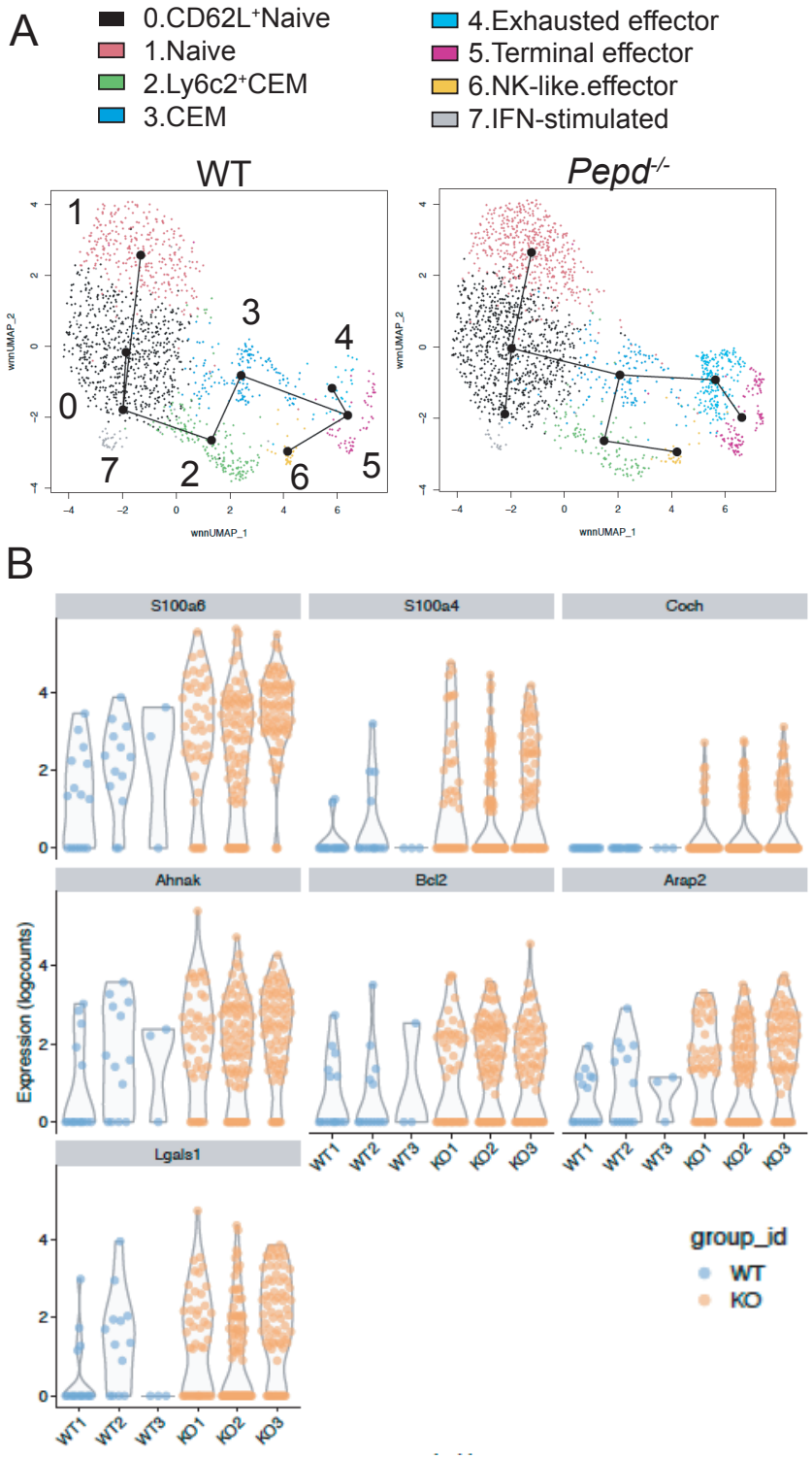


Figure 5.14 Trajectory analysis and differential gene expression demonstrate Pepd loss drives altered differentiation

A. Inferred trajectory analysis of differentiation states coloured and visualised by WNN-determined WT and Pepd$^{-/-}$ CD8^{+} clusters. B. Differential expression between WT and Pepd$^{-/-}$ cluster 4.Ex.effector.1 populations as determined by pseudobulk analysis, filtered at a locally adjusted p value threshold of 0.05 and logFC threshold of 0.5.

To determine transcriptional changes driving altered subset differentiation, differential gene expression analysis between WT and *Pepd*$^{-/-}$ cells was performed at a cluster level. Concurrent with population losses within cluster 2.Ly6c2^{+}CEM, *Pepd*$^{-/-}$ populations across multiple clusters demonstrated significantly reduced *Ly6c2* expression (*Ly6c2* logFC values; 0.CD62L^{+}Naive -1.168, 1.Naive -1.047, 5.Terminal effector -1.286). Additionally, several *Pepd*$^{-/-}$ populations showed significant reduction in expression of interferon-induced gene, Ifi27l2a (Ifi27l2a logFC values; 0.CD62L^{+}Naive -0.692, 1.Naive -0.650, 6.NK-like effector -2.495), knockdown of which has been shown to be associated with increased susceptibility to bacterial, and specific viral infections (Uhrin *et al.*, 2013; Lucas, Richner and Diamond, 2016). As well as increased expression of inflammatory and effector molecules *S100a4, S100a6, Lgals1*, *Arap2* and *Ahnak,* (Matza *et al.*, 2009; Jung *et al.*, 2016; Clemente *et al.*, 2017), survival marker *Bcl2* was significantly upregulated in *Pepd*$^{-/-}$ 4.Exhausted effector cells, suggesting loss of prolidase may be associated with both altered differentiation of T cell subsets and increased survival of T cells that carry an inflammatory, exhausted phenotype (Figure 5.14B).

5.2.4 Cytometric approaches confirm splenic CD8^{+} T cell phenotype associated with prolidase deficiency

Flow cytometric analysis using PD1 as a marker of both chronic inflammation and potential exhaustion confirmed the altered CD8^{+} populations identified by scRNA-Seq in *Pepd*$^{-/-}$ mice, demonstrating a significant increase in effector cells expressing PD1 as a percentage of total CD8^{+} populations, and significant reductions in proportions and numbers of Ly6c-expressing CD62L^{+} populations in *Pepd*$^{-/-}$ splenic samples. (Figure 5.15).

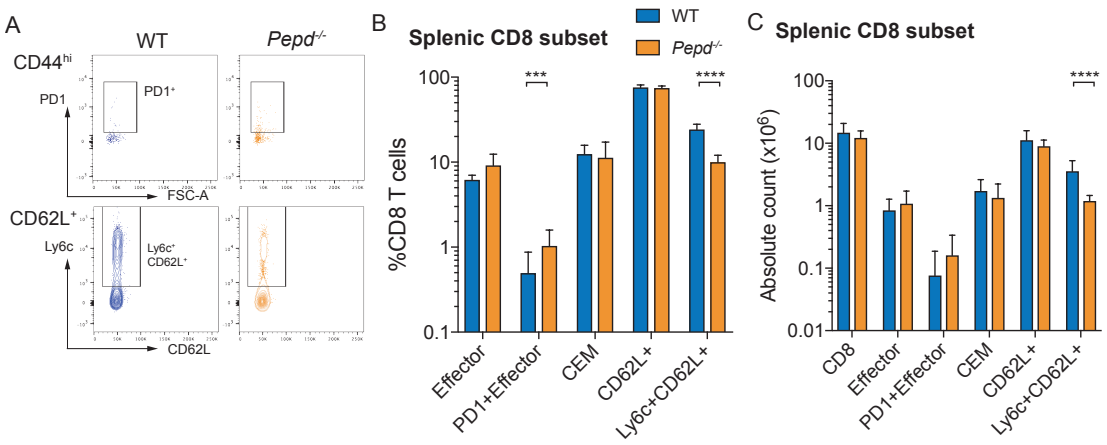


Figure 5.15 Confirmation of the CD8⁺ phenotype associated with Pepd deficiency

*A. Representative flow cytometry plots of gating of CD8⁺ splenic T cell populations in WT and Pepd$^{-/-}$ mice. B. Quantification of populations gated in (A) as a percentage of CD8⁺ T cells in WT and Pepd$^{-/-}$ mice. ANOVA significance; PD1⁺effector *** p=0.0001, Ly6c⁺CD62L⁺ **** p = <0.0001. C. Quantification of T cell numbers gated in (A). ANOVA significance was determined across experiments; PD1⁺effector (p = 0.0006, though interaction detected so cannot quote significance), Ly6c⁺CD62L⁺ **** <0.0001. Data presented are representative of seven independent experiments with 2 to 5 mice per group.*

These signatures were also mirrored in deeper immunophenotyping of splenic *Pepd*$^{-/-}$ and WT samples using a wide panel of metal isotope-tagged immunological markers to detect discrete lymphocyte populations by time of flight mass cytometry (CyTOF) and unsupervised clustering analyses tools and visualisation (Cytofkit) (Figure 5.15A-C)(Chen *et al.*, 2016). tSNE visualisation identified clear differences in immune populations with *Pepd* deficiency (Figure 5.16C), and further interrogation of subsetted CD8⁺ T cell populations confirmed the activated signature associated with *Pepd* loss as seen previously by other immunophenotyping methods (Figure 5.16D). Cluster analysis identified trend increases in effector clusters, 7 and 12, which represent PD1⁺CD69⁺ effectors and Ki-67⁺ PD1⁺ effectors, suggesting increases in proliferation of these populations (Figure 5.16E,F). Additionally, there were significant losses of Ly6c⁺ CXCR4⁺ CEM populations, and non-significant reductions of Ly6c⁺Bcl2⁺ naïve populations in *Pepd*$^{-/-}$ CD8⁺ samples (Figure 5.16E,F).

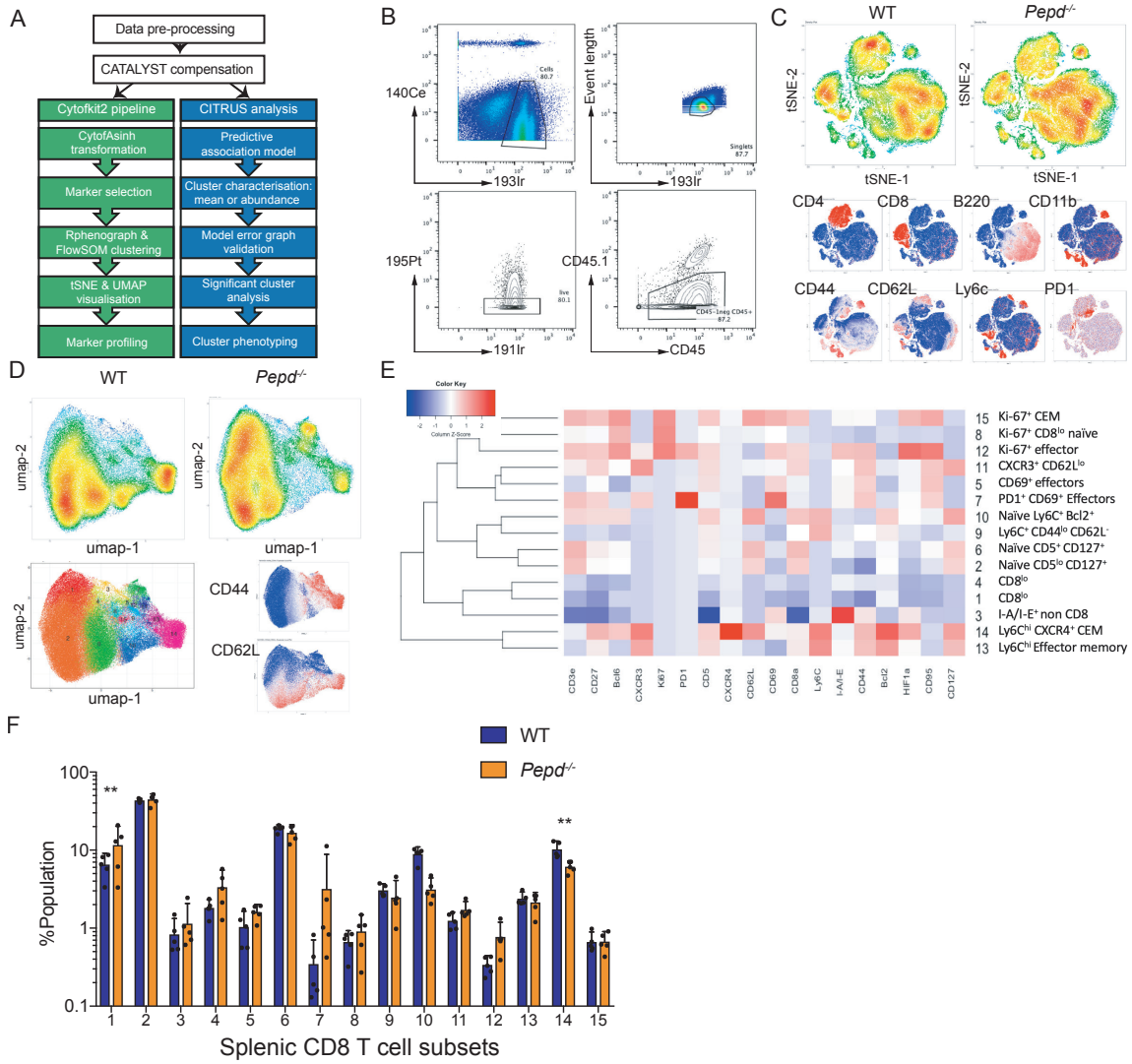


Figure 5.16 Cytofkit profiling of splenic T cells confirms loss of Ly6c-expressing CD8⁺ T cells and trend increases in activated CD8⁺ populations in Pepd$^{-/-}$ mice compared to WT populations

*A. Analysis pipeline for CyTOF, including downstream stages split into the cytofkit or citrus pipelines. B. Data pre-processing stage from (A) with initial manual gating of CD45.1^{-} live immune cells using FlowJo. C. tSNE visualisation of total CD45^{+} populations using the cytofkit analysis pipeline, split by genotype and coloured by density (upper panel), lower panel shows expression of markers on the above tSNE plots, blue to red represents low to high expression of each marker. D. UMAP visualisation of CD8^{+} subsetted cells clustered using the cytofkit pipeline, split by genotype (upper panel). Lower panel shows UMAP visualisation of the flowSOM clusters (left) and overlays of CD44 and CD62L expression (right). E. Heatmap of the expression of markers used to define the flowSOM clustering from (D), each column is scaled to that marker expression. F. Quantification of representation of WT or Pepd$^{-/-}$ cells to the FlowSOM clusters defined in (D,E). Significance was determined using two-way ANOVA, ** p= <0.01. Bars are means and error bars represent 95% CI. Data are from one experiment with 5 mice per group.*

To explore this dataset further, the citrus algorithm was employed, which is an alternative, data-driven analysis method used to stratifying populations and highlighting significant differences in high dimensional data between conditions (Bruggner *et al.*, 2014). The analysis run with the lowest

cross validation error rate and feature false discovery rate was chosen as the most appropriate model for data analysis in this instance (Figure 5.17A)(Kimball *et al.*, 2018). This algorithm clusters populations in a hierarchical parent and child tree then tests for differences in expression across groups (Figure 5.17B). Citrus clustering analysis identified that multiple cluster types expressed reduced CD62L amounts in the absence of *Pepd* (Figure 5.17C,D, appendix G), and *Pepd*$^{-/-}$ effector subset populations expressing PD1, CXCR3 and CD95 had an altered surface phenotype, characterised by increased PD1 expression, but lower Ly6c^{+} expression (Figure 5.17C,D, appendix G).

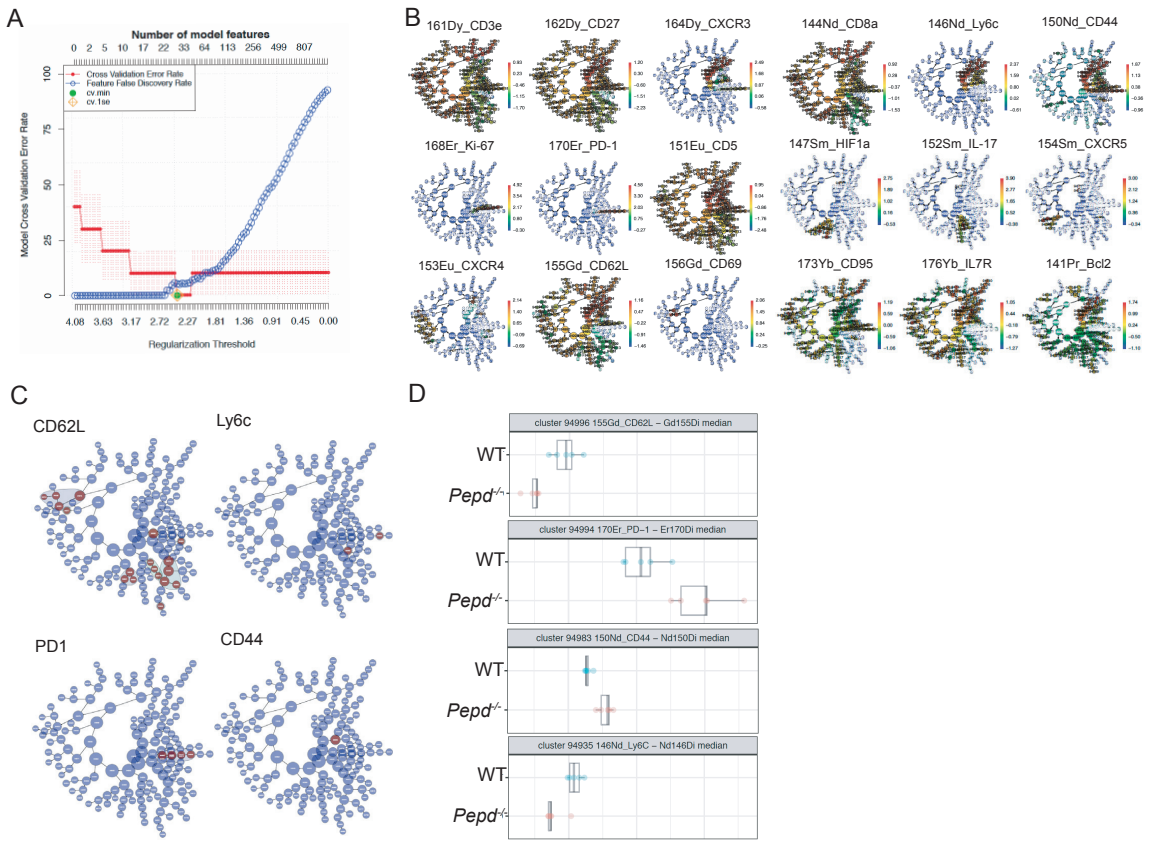


Figure 5.17 Citrus CyTOF analysis highlights altered surface phenotype of CD8^{+} Pepd$^{-/-}$ populations

A. Visualisation of the model error rate using the PAMR predictive association model to find significant differences between WT and Pepd$^{-/-}$ CD8^{+} populations with the lowest possible error rate. B. Hierarchical clustering tree of CD8^{+} populations, coloured by different channels used for analysis. C. Visualisation of the clusters within the tree by channel that have statistically significant differences in that channel between WT and Pepd$^{-/-}$cells. D. Quantification of differences of markers between WT and Pepd$^{-/-}$ cells in specific clusters. Data are from one experiment with 5 mice per group.

5.3 Summary of chapter

The role of the metallopeptidase, prolidase in regulating immune tolerance has previously been suggested by the syndrome seen in prolidase-deficient human patients, who present with a multi-organ disorder characterised by problems with wound healing, respiratory infections and hypergammaglobulinemia, often accompanied by clinical features consistent with loss of self-tolerance (Shrinath *et al.*, 1997; Kurien *et al.*, 2013). Prolidase-deficient mice demonstrate increased incidence of serum ANAs accompanied by an activated T cell phenotype and elevated serum IgA, with glomerular immune complex deposition consistent with SLE-like disease, confirming for the first time the direct association of autoimmunity and prolidase deficiency. Studying the *Pepd*$^{-/-}$ mouse offers a model system to delineate the roles of prolidase in regulating immune responses, without the possible confounding effects of chronic antigen exposure or inflammatory environment associated with recurrent infections in patients, as well as human genetic heterogeneity (A. Lupi *et al.*, 2006; Butbul Aviel *et al.*, 2012).

This chapter describes the deep immunophenotyping of *Pepd*$^{-/-}$ lymphocyte populations using cytometry combined with multimodal sequencing techniques. B cell development is normal in *Pepd*-deficient mice, though mature *Pepd*$^{-/-}$ B cell populations express higher IgM, but lower CD21 and IgD surface amounts. B cell anergy and self-antigen induced proximal signalling were not affected by prolidase loss, indicating B cell tolerance is likely to be intact in the absence of *Pepd,* at least in the context of restrained BCR specificity through tg expression.

In addition to the altered humoral and B cell phenotypes, loss of prolidase is associated with an activated T cell phenotype, characterised by increased CD4^{+} and CD8^{+} effector populations and loss of Ly6c-expressing non-effector CD8^{+} populations. Insights from transcriptional analysis demonstrate that *Pepd* deficiency is associated with a specific increase in CD8^{+} effectors with an inflammatory, exhausted effector phenotype, raising questions about how these cells respond to

antigen or differences in TCR specificity. Trajectory analysis suggested that this phenotype could be driven by altered differentiation, however the mechanisms directing such changes remain to be established.

Prolidase acts within multiple biological pathways which can be separated into both enzymatic-dependent and independent functions(Figure 5.1). Transcriptional analysis of differentially expressed genes between clusters failed to identify specific differences in HIF1α- or angiogenic-regulated factors, or indeed downstream of p53, Src or apoptotic pathways, potentially this could hint at a novel functional role for *PEPD* that leads to the accumulation of exhausted $CD8^+$ effectors.

6. Drivers of CD8$^+$ exhausted effector T cell accumulation with *Pepd* loss

6.1 Introduction to chapter

The importance of CD8$^+$ T cells within adaptive immunity is highlighted by the tight regulation of homeostatic proliferation during lymphopenia and contraction post-viral infection (Freitas and Rocha, 1993; Bell and Sparshott, 1997), as well as the immunodeficiency syndromes identified in humans deficient for CD8a$^+$ populations (De la Calle-Martin *et al.*, 2001; Mancebo *et al.*, 2008; Bernardo *et al.*, 2011; Dumontet *et al.*, 2015), highlighting the importance of exploring how novel genes regulate this fine balance. In chapter 5, initial immunophenotyping of prolidase-deficient mice demonstrated an altered splenic T cell phenotype characterised by accumulation of CD8$^+$ PD1$^+$ effectors with an inflammatory, exhausted profile, in addition to loss of resting Ly6c$^+$ populations, implicating the *Pepd* gene in the maintenance of T cell homeostasis.

T cell exhaustion is characteristically associated with chronic viral infection or cancer, however transcriptional signatures of exhaustion have been recorded in autoimmunity, across multiple autoimmune diseases including SLE and T1DM as well as in patients with inborn errors of immunity such as in primary immunodeficiency, activated PI3Kδ syndrome (McKinney *et al.*, 2015; Wherry and Kurachi, 2015; Wentink *et al.*, 2018; Delmonte *et al.*, 2019; Zakharov *et al.*, 2020; Collier *et al.*, 2021). The exhausted phenotypic signature is classically induced in the context of persistent antigen exposure, whether specifically in response to cognate antigen or due to unresolved inflammation, and is characteristically accompanied by the loss of effector functions, proliferative potential and altered response to cytokines (Wherry and Kurachi, 2015; McLane, Abdel-Hakeem and Wherry, 2019). Although exhausted, dysfunctional effector T cells can limit effective clearance of infection and cancer cells, the exhaustion signature can be positively associated with prognosis in autoimmune conditions, by intrinsically restraining the action of self-reactive lymphocytes from inappropriately damaging tissue (Collier *et al.*, 2021). Further research into the shared and distinct

pathways regulating the induction, maintenance and clearance of these cells, across these distinct biological states may provide novel therapeutic opportunities across disease boundaries, as seen by the promise of teplizumab in regulating T cell exhaustion in T1DM (Long *et al.*, 2016).

This chapter explores the effects of prolidase loss on T cell differentiation, fate and effector functions leading to accumulation of effector $CD8^+$ populations expressing an inflammatory, exhausted signature. As prolidase is ubiquitously expressed, possessing the unique role of breaking down dipeptides containing proline or hydroxyproline in the C-terminal position, a key question is whether the phenotypes seen in prolidase-deficient mice are driven by the cell-intrinsic loss of *Pepd* expression, or by cell-extrinsic factors such as altered peptide processing or trans effects from other cell populations affected by prolidase loss. Furthermore, as T cell exhaustion states are generally characterised by chronic exposure to antigen or chronic inflammation, the role of TCR specificity and response to antigen requires exploration, and the effects of prolidase on survival and proliferation are relevant to explain the altered abundance of T cell subsets.

6.2 Results

6.2.1 Cell intrinsic prolidase loss drives the activated T cell phenotype

Reconstitution of irradiated, congenically labelled $CD45.1^+$ recipients with 50:50 mixtures of $CD45.1^+$ $CD45.2^+$WT and $CD45.2^+$*Pepd*$^{-/-}$ (or $CD45.2^+$WT control; Figure 6.1A) bone marrow demonstrated increased representation of $CD45.2^+$ *Pepd*$^{-/-}$ cells within thymic $CD4^+CD44^{hi}$ populations in recipients of WT:*Pepd*$^{-/-}$ bone marrow (Figure 6.1B,C), and $CD4^+$CD44hi effector and

FoxP3$^+$ regulatory T cell populations in the spleen as ratio to CD4$^+$CD45.2$^+$ total reconstituted populations (Figure 6.1B,D). CD45.2$^+$ PD1$^+$ effector CD8$^+$ T cell populations were enriched for *Pepd*$^{-/-}$ cells, whereas CD45.2$^+$Ly6c-expressing non-effector populations were significantly reduced in WT:*Pepd*$^{-/-}$ BM recipients (Figure 6.1E) as previously identified in non-chimeric mice. The

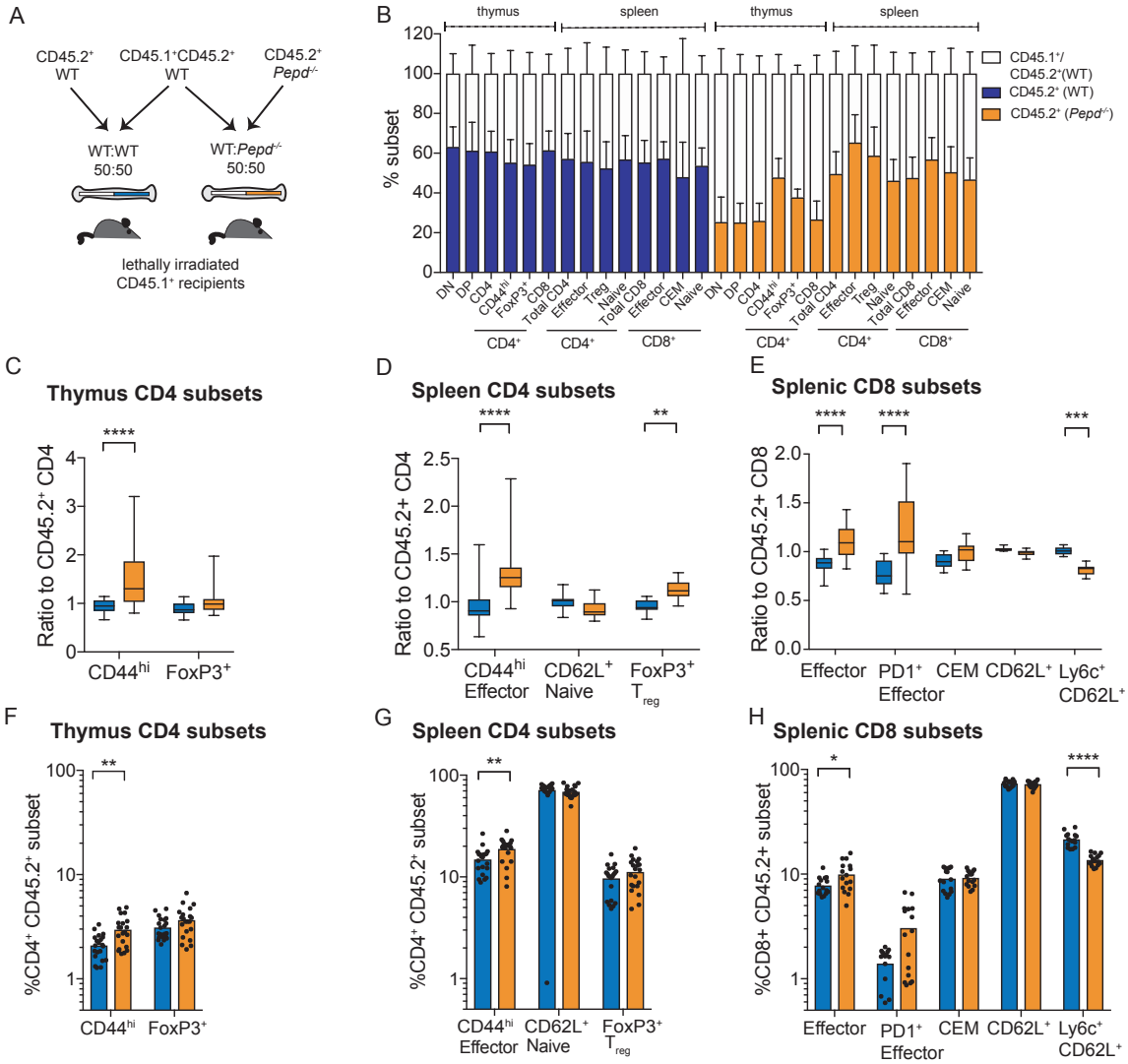


Figure 6.1 The T lymphocyte phenotype is driven by intrinsic loss of Pepd expression in mixed BM chimeras

*A. Schematic of experiment; congenically labelled CD45.1$^+$ recipients were lethally irradiated and reconstituted for 8 weeks with equal amounts of CD45.1$^+$CD45.2$^+$WT and either CD45.2$^+$ WT or CD45.2$^+$ Pepd$^{-/-}$ BM. B. Relative proportions of reconstituted thymic and splenic T cell populations from BM chimeras in (A), gated based on CD45.1 and CD45.2 expression. C. Reconstitution of WT and Pepd$^{-/-}$ thymic CD4$^+$ subsets as ratios to thymic CD45.2$^+$ CD4$^+$ SP proportions. D. Reconstitution of WT and Pepd$^{-/-}$ splenic CD4$^+$ subsets as ratios to splenic CD45.2$^+$ CD4$^+$ proportions. E. Reconstitution of WT and Pepd$^{-/-}$ splenic CD8$^+$ subsets as ratios to splenic CD45.2$^+$ CD8$^+$ proportions. F. Gated WT or Pepd$^{-/-}$ thymic CD4$^+$ subsets of CD45.2$^+$ populations from chimeras in (A) or G. of CD45.2$^+$ splenic CD4 subsets or H. CD45.2$^+$ splenic CD8+ subsets. Data are representative (B) or pooled from at least 3 (C-H) independent experiments. Significance was determined using two-way ANOVA or unpaired t test, adjusting for multiple comparisons. * P = <0.05, ** p = <0.01, *** p = <0.001, **** p = <0.0001.*

recapitulation of the activated T cell phenotype in the mixed chimera demonstrates that the activated T cell phenotype is caused by cell-intrinsic loss of *Pepd*.

Additionally, analysis of chimeric B cell populations demonstrated that the altered B cell phenotype is also driven by intrinsic loss of prolidase, as surface IgM, CD21 and IgD were affected in WT:*Pepd*$^{-/-}$ central and peripheral B cells (Figure 6.2B-D). The reconstitution and development of *Pepd*$^{-/-}$ B cell subsets were not affected by competition (Figure 6.2A). In contrast, serum IgA titres were equivalent in WT:*Pepd*$^{-/-}$ chimeras (Figure 6.2E) and serum ANA positivity was not enhanced (WT:WT 0 in 16 positive, WT:*Pepd*$^{-/-}$ 1 in 16, fisher's exact p = 0.99), indicating that elevated IgA amounts and ANA development may depend on trans effects of loss of prolidase, suggesting that the increase in exhausted T cells is not on its own sufficient to drive the excess secretion of IgA or production of ANA. On the other hand, the presence of WT regulatory T cell populations could rescue these phenomena in the chimeric system.

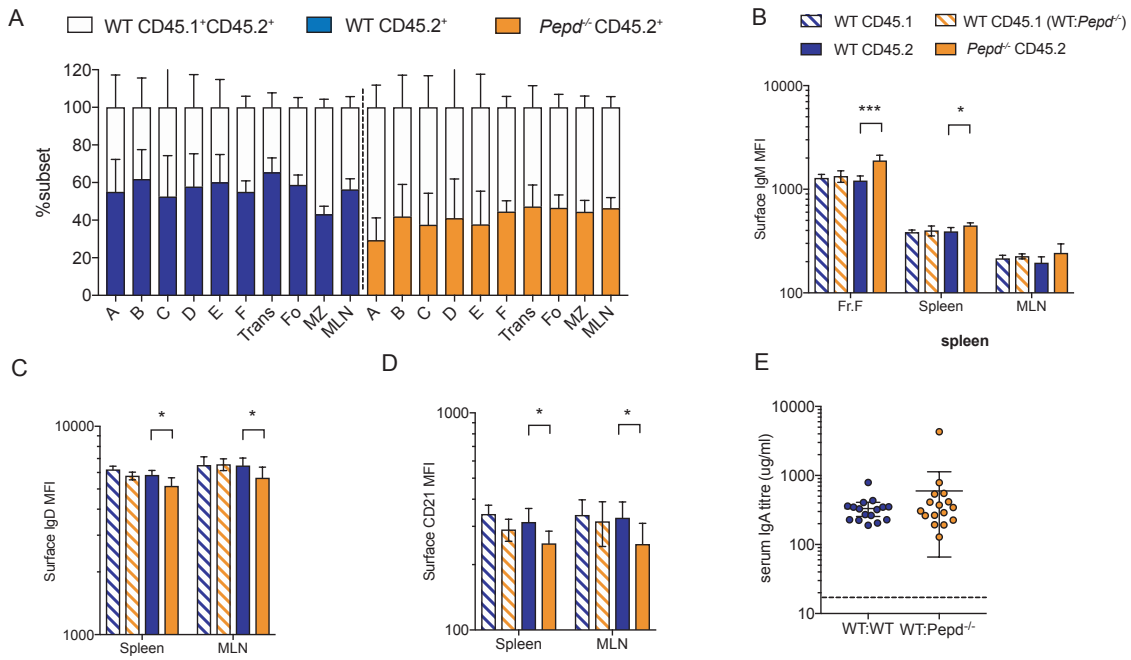


Figure 6.2 The B lymphocyte phenotype is driven by intrinsic loss of Pepd expression in mixed BM chimeras

A. Relative proportions of reconstituted BM populations and splenic B cell subsets from BM chimeras reconstituted with CD45.1^{+}CD45.2^{+}WT and either CD45.2^{+} WT or CD45.2^{+} Pepd$^{-/-}$ BM, end-gated based on CD45.1 and CD45.2 expression. B. Quantification of IgM surface marker expression on WT CD45.1^{+}CD45.2^{+} or WT or Pepd$^{-/-}$ CD45.2^{+} chimeric total B cell populations in the indicated peripheral lymphoid organ as MFI. C. Quantification of surface IgD expression as in (B). D. Quantification of CD21 surface expression as

*in (B). E. Serum IgA levels from WT:WT and WT: Pepd$^{-/-}$ mixed chimeras from (A) as determined by ELISA. Points represent individual mice, columns and lines represent means with 95% CI error bars. Data are representative (A-D) or pooled (E) of 3-5 independent experiments with 4-6 mice per group. Significance was determined using an unpaired t test, adjusting for multiple testing by the Holm-Sidak method. * P = <0.05, ** p = <0.01, *** p = <0.001*

6.2.2 Exhausted CD8^{+} effector transcriptional profile is consistent with intrinsic prolidase deficiency

In order to understand whether the transcriptional exhaustion signature associated with prolidase loss is fully intrinsic, we submitted sorted CD45.2^{+} T cells from 4 CD45.1^{+} CD45.2^{+}WT: CD45.2^{+}WT and 4 CD45.1^{+}CD45.2^{+}WT:CD45.2^{+}*Pepd*$^{-/-}$ mixed chimeras for 3' scRNA-Seq in combination with ADT T cell marker characterisation. 24981 cells were captured and sequenced in total with a mean 6,987 molecule reads per cell (number of unique molecular identifiers; nCount_RNA), with post-filtering and demultiplexing steps leaving 12275 singlets across the 8 samples, with an average of 1945 individual genes (nFeature_RNA) detected per cell (Figure 6.3A,B).

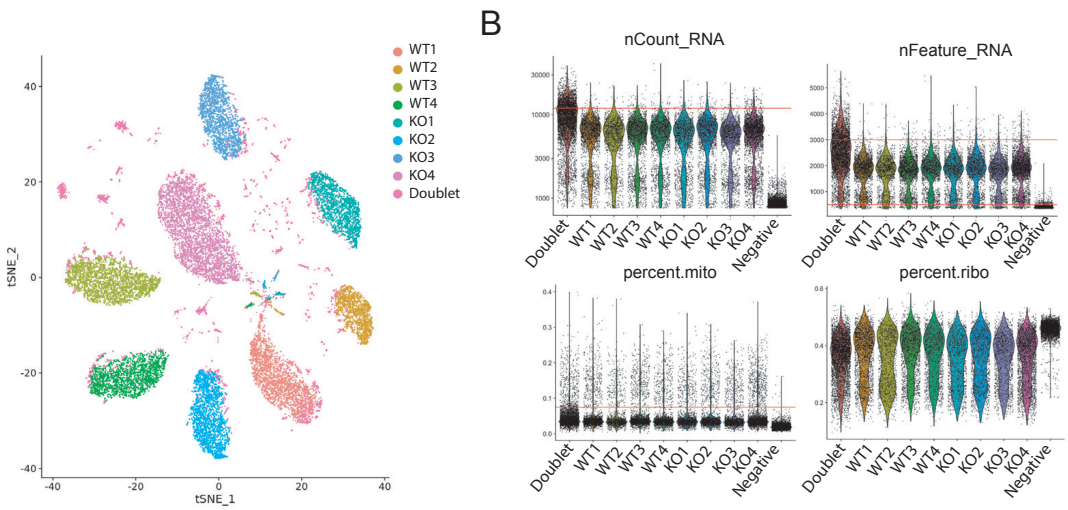


Figure 6.3 Quality control of multimodal scRNAseq of chimeric CD45.2^{+} WT and Pepd$^{-/-}$ T cells

A. Hashtag-labelled CD45.2^{+} WT or Pepd$^{-/-}$ samples were demultiplexed for downstream analysis alongside heterogenous doublet removal. B. Singlets were filtered based on RNA and gene (feature) counts per cell, and on mitochondrial gene expression.

Subsetting of populations expressing CD8 and subsequent WNN-clustering analysis demonstrated populations consistent with those seen in non-chimeric mice (Figure 6.4A-C, appendix H). CD8^{+} effector populations clustered into 3 concise populations, and as in straight mice were

characterised by expression of exhaustion, effector and localisation markers (Figure 6.4A-C, appendix H). Comparison of differential expression between the two effector clusters distinct from other populations by UMAP visualisation demonstrated 4.Exhausted effector and 6.Terminal effector share the same differential patterns of gene signatures as identified in non-chimeric mice (Figure 6.3D, appendix I), confirming their respective likely identities as exhausted and terminal effector, SLEC-like populations. Additionally, there was a non-significant trend towards increased representation of *Pepd*$^{-/-}$ cells within cluster, 4.Exhausted effector (Figure 6.4A,E), consistent with the hypothesis that the maintenance or induction of exhausted CD8^{+} effector T cells is dependent on cell-intrinsic prolidase loss, as indicated previously by flow cytometry (Figure 6.1E).

Again, inferred trajectory analysis demonstrated earlier lineage divergence between CD8^{+} naïve, CEM and effector populations in the absence of *Pepd*, suggesting prolidase deficiency may disrupt differentiation between CEM and effector populations, affecting CD8^{+} terminal fate (Figure 6.4F). As this result is consistent in mixed chimeras, this effect cannot be driven by trans effects of prolidase loss, such as altered extrinsic processing of ligands for T cell antigen presentation, and hence is likely to be downstream of cell-intrinsic loss of prolidase expression.

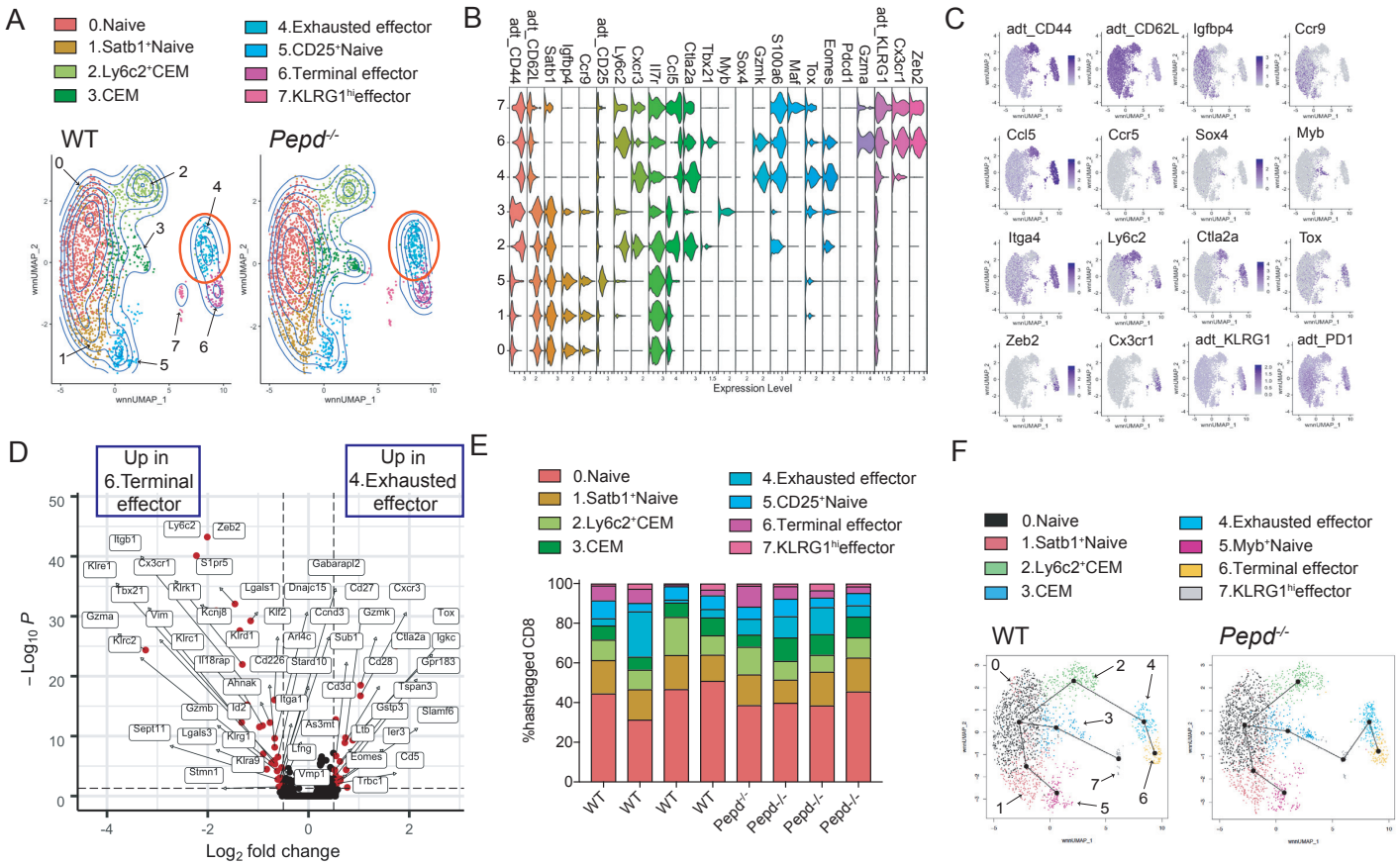


Figure 6.4 scRNAseq demonstrates exhausted CD8⁺ T cell phenotype is intrinsically driven by prolidase deficiency

A. WNN-analysis of WT and Pepd$^{-/-}$ CD8⁺ populations by WNN-UMAP dimensionality reduction and clustering from scRNAseq analysis of CD45.2⁺ samples from mixed BM chimeras. B. VlnPlot of expression of RNA and protein markers of CD8⁺ WNN-mediated clusters from (A). C. Feature plot visualisation of RNA and protein marker expression over WNN-mediated UMAPs of CD8⁺ populations. D. Volcano plot depicting differential gene expression between cluster 4.Exhausted effector and cluster 6.Terminal effector of WNN-clustered CD8⁺ populations. Differentially expressed genes are coloured in red at a threshold of log2FC = 0.5 and adjusted p value <0.05. Total 5626 variables tested. E. Quantification of populations as % hashtagged CD8⁺ per sample of WT and Pepd$^{-/-}$ T cell populations. F. Inferred trajectory analysis of WT and Pepd$^{-/-}$CD8⁺ T cell populations identified in (A).

6.2.3 The T cell phenotype associated with prolidase loss is driven by increased differentiation of proliferating cells into exhausted effectors

6.2.3.1 Survival markers of Pepd$^{-/-}$ CD8^{+} populations are equivalent

The effect of prolidase deficiency on CD8^{+} T cell lineage differentiation is causal in an intrinsic manner, rather than due to extrinsic effects from other cell types or by altered antigen processing and presentation by other cells. Recent literature reports that *Pepd* has a role in regulating cell survival via modulating p53-mediated apoptosis (Yang *et al.*, 2017), in addition to interacting within growth receptor and pro-survival signalling pathways mediated by TGF-β, HIF-1α and EGFR receptor modulation (Yang *et al.*, 2015; Misiura and Miltyk, 2020), therefore it was logical to ask whether enhanced survival in the absence of prolidase can explain the phenomenon of accumulating T cell populations, resulting in inflammation and exhaustion.

Despite increased *Bcl2* at the transcriptomic level (Figure 5.14), only a very modest increase in Bcl2 at the protein level was detected in *Pepd*$^{-/-}$ CD8^{+} effector T cells across experiments in non-chimeric mice (Figure 6.5A), and only a trend increase was detected in chimeric CD8^{+} effectors (Figure 6.5B), together suggesting the altered T cell phenotype is unlikely to be driven by modulated Bcl2-dependent survival.

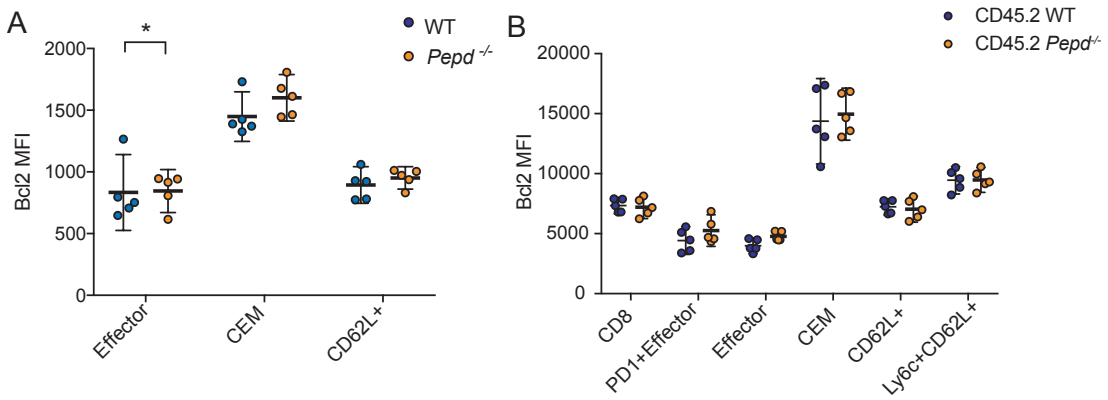


Figure 6.5 Bcl2 expression at the protein level is not affected by prolidase loss

*A. Quantification of Bcl2 expression of non-chimeric WT or Pepd$^{-/-}$ CD8^{+} populations determined by intracellular staining as MFI. ANOVA significance was determined across experiments; Effector * p = 0.034. B. Bcl2 expression quantified as (A) for chimeric CD8^{+} populations. Lines are at means with 95% CI error bars and each represents one mouse, data are representative of 5 (A) or 2 (B) independent experiments with 3-6 mice per group.*

6.2.3.2 Proliferating populations have an increased propensity to differentiate into exhausted effectors in the absence of prolidase

Expansion of CD8$^+$ effector populations could be explained by a number of possibilities; loss of prolidase could extend the survival of effector populations, or enhance their intrinsic ability to differentiate of proliferate, spontaneously or in response to self or foreign antigen. Assuming that the survival rate is equivalent between WT and *Pepd*$^{-/-}$ T cell populations as explored in the section above, I next hypothesised that increased populations of effectors on loss of *Pepd* may result from two scenarios; either phenotypic PD1$^+$ effector cells have a higher proliferative capacity with prolidase loss, which would result in an increased percentage of labelling of this population, or

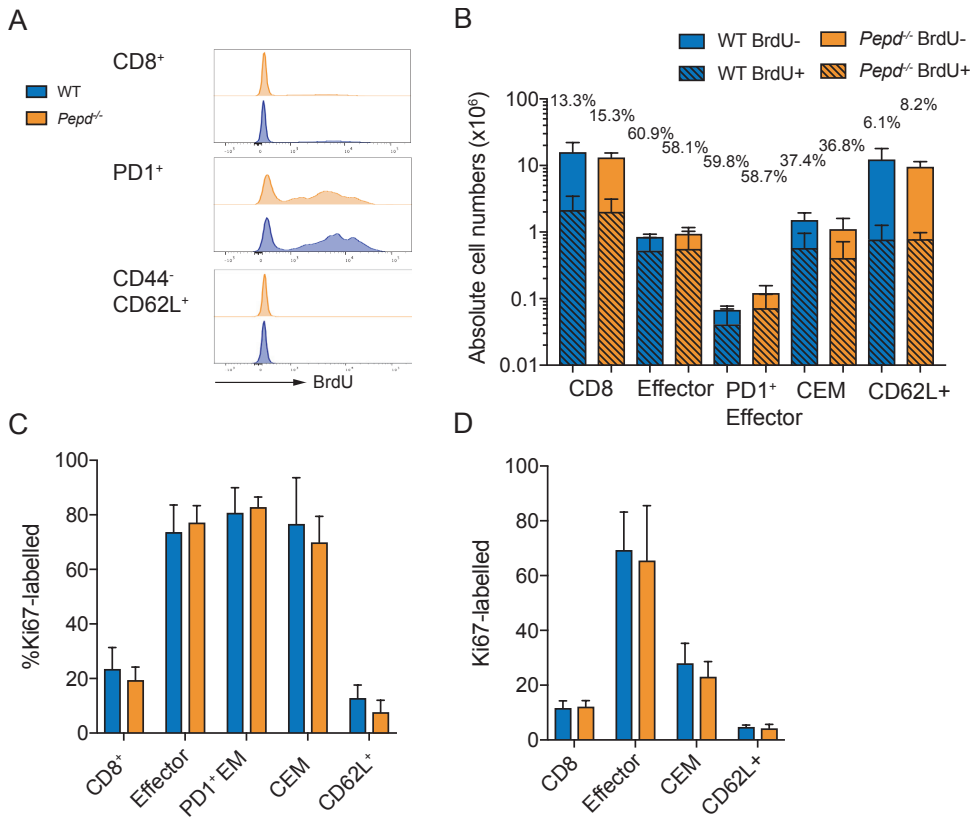


Figure 6.6 Proliferating pepd-deficient T cell populations are more likely to adopt an exhausted phenotype

A. Representative flow cytometry histogram plots of BrdU labelling of splenic WT or Pepd$^{-/-}$ T cell populations after 7 days exposure in the drinking water. B. Quantification of BrdU-labelled and unlabelled numbers of WT or Pepd$^{-/-}$ populations gated in (A). C. Intranuclear staining of Ki-67 antigen of WT or Pepd$^{-/-}$ CD8$^+$ subsets from non-chimeric or D. chimeric CD45.2$^+$ CD8$^+$ populations. Columns and lines represent means with 95% CI error bars. Data are representative of 2 (A-B, D) or 3 (C) independent experiments with 3-6 mice per group.

alternatively there is a higher rate of differentiation into this effector population, which would be detected as equivalent labelling percentages, in the context of a larger total cell population.

I sought to investigate this by administering BrdU orally for one week to WT or *Pepd*$^{-/-}$ mice. Although the *Pepd*$^{-/-}$ CD8 PD1^{+} effector T cell population was expanded as before, the percentage of BrdU-labelled cells was the same as in WT (Figure 6.6A-B). Since this equates to more cells being labelled, this indicates there is likely to be an increase in the number of *Pepd*-deficient CD8^{+} T cells that upon proliferating, subsequently adopt an exhausted inflammatory phenotype.

This hypothesis was supported by comparable *ex vivo* labelling with the proliferation marker Ki-67, between WT and *Pepd*$^{-/-}$ mice across CD8^{+} populations in non-chimeric and chimeric mice (Figure 6.6C,D). Together these findings indicate equivalent proliferation rate within the effector population. In the absence of evidence for altered survival, these observations suggest that expansion of the PD1^{+} effector pool is most likely due to increased differentiation into the subset. We can conclude that prolidase deficiency results in an intrinsic increase in the number of cells adopting an inflammatory effector CD8 T cell phenotype.

6.2.4 *Pepd*$^{-/-}$ exhausted populations accumulate in the liver in an intrinsic manner

Experiments so far indicate that the intrinsic increase in CD8^{+} PD1^{+} effectors in the absence of *Pepd* is dependent on increased differentiation of proliferating cells towards an inflammatory, exhausted fate. However, altered clearance or apoptosis could also affect the rate of turnover detected by BrdU labelling. Activated lymphocytes are actively removed at many important sites of peripheral tolerance; the liver represents a key immunological organ that acts to prevent autoimmunity by silencing and removing T cells by Bim-mediated apoptosis, among other mechanisms including CD8-driven pathways (Holz *et al.*, 2008; Wong *et al.*, 2016; Dudek *et al.*, 2021).

Flow cytometric analysis of *Pepd*$^{-/-}$ liver lymphocyte populations identified significant accumulation of CD8^{+} PD1^{+} effectors (Figure 6.7), indicating that the rate of apoptosis and clearance is likely to be equivalent to WT or sufficiently rate-limiting to result in accumulation of these exhausted, inflammatory populations accumulate in sites of likely breakdown.

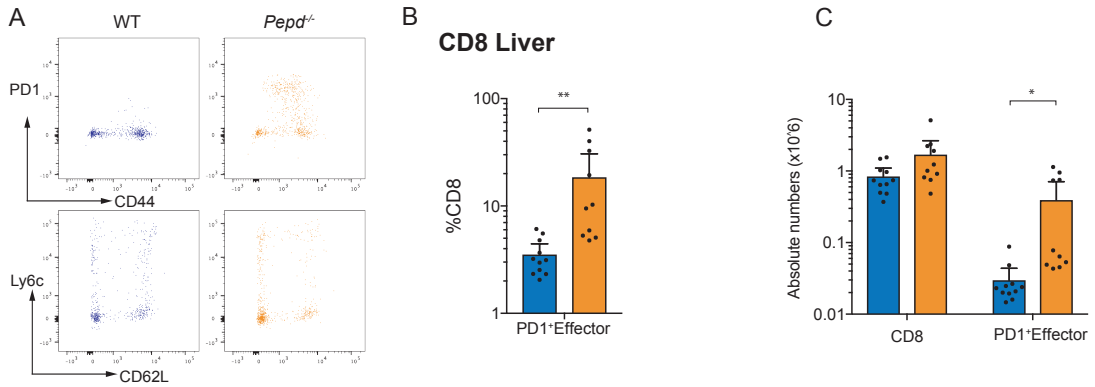


Figure 6.7 Exhausted CD8^{+} effectors accumulate in the liver on prolidase loss

A. Representative flow cytometric plots of WT or Pepd$^{-/-}$ liver CD8^{+} populations. B. Quantification of hepatic CD8^{+} populations as gated in (A) as a percentage of total CD8^{+} cells or as absolute cell numbers (C) in the livers of WT or Pepd$^{-/-}$ mice. Significance measured by multiple t test, %CD8 p = 0.009, absolute cell numbers p = 0.029. Bars represent means with 95%CI error bars and each point represents one mouse, data are pooled from 3 independent experiments with 3-4 mice per group.

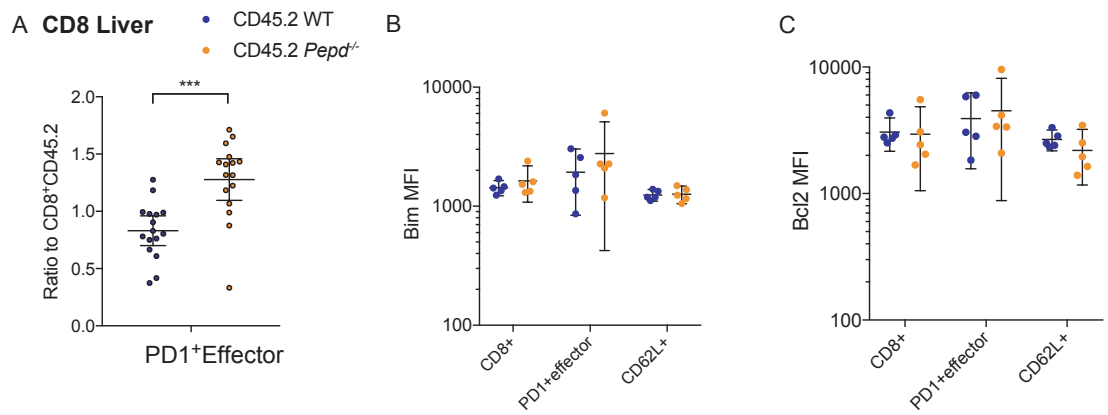


Figure 6.8 Cell-intrinsic loss of Pepd leads to hepatic accumulation of CD8^{+} PD1^{+} effectors with equivalent survival and apoptosis markers

*A. Quantification of reconstituted WT or Pepd$^{-/-}$ CD8^{+} PD1^{+} effector cells in ratio to CD45.2^{+} CD8^{+} proportions in the livers of mixed BM chimeras reconstituted with congenically labelled WT:WT BM or WT:Pepd$^{-/-}$ BM. Significance was determined by an unpaired t test, *** p = 0.000187. B. Quantification of intracellular Bim expression as MFI of WT and Pepd$^{-/-}$ CD45.2^{+} hepatic CD8^{+} populations from mice described in (A). C. Quantification of intracellular Bcl2 expression as in (B). Points represent individual mice, with lines at the mean and 95% CI as error bars. Data are pooled from 3 independent experiments (A) or are representative 2 (B,C) experiments with 5-6 mice per group.*

Furthermore, this result was also true in mixed BM chimeras reconstituted with WT:*Pepd*$^{-/-}$ BM compared to WT:WT, indicating accumulation in the liver is driven by intrinsic loss of *Pepd* (Figure

6.8A). Additionally, expression of Bcl2 and apoptotic protein, Bim were equivalent across hepatic WT and *Pepd*$^{-/-}$ CD45.2^{+} CD8^{+} chimeric populations (Figure 6.8B,C), indicating that neither Bim-mediated apoptosis or Bcl2-dependent survival appear affected by loss of *Pepd*, again indicating clearance of these cells is not sufficiently modulated to prevent the intrinsic persistence of these inflammatory CD8^{+} populations.

6.2.4 The accumulation of exhausted CD8^{+} T cells associated with prolidase loss is antigen-independent

6.2.4.1 T cell phenotype is partially rescued by TCR specificity

To explore the possible role of response to self and foreign antigen in driving the increased propensity of prolidase-deficient CD8^{+} effectors to differentiate into inflammatory, exhausted-like populations on proliferation, *Pepd*$^{-/-}$ mice were crossed to the TCR transgenic strain, OT-I, where all CD8^{+} T cells express a restricted TCR made up of Vα2 and Vβ5 chains that bind the SIINFEKL epitope of ovalbumin (Hogquist *et al.*, 1994; Clarke *et al.*, 2000).

Phenotyping of peripheral *Pepd*$^{-/-}$ OT-I^{+} CD8^{+} T cells demonstrated that exhausted CD8^{+} T cells still accumulated in the presence of the OT-I transgene in both the spleen and the liver, consistent with non-tg mice, indicating that this phenomenon is independent of TCR specificity and unlikely to be downstream of antigenic TCR signalling (Figure 6.9). However, complete rescue of *Pepd*$^{-/-}$ Ly6c^{+} CD62L-expressing cells was observed with significantly increased numbers and proportions in the spleen. One explanation for this dichotomous result is that reduction in these populations in non-TCR tg *Pepd*$^{-/-}$ may be TCR-dependent, with this phenomenon at least partially independent of the accumulation of PD1^{+}effectors (Figure 6.9A-C).

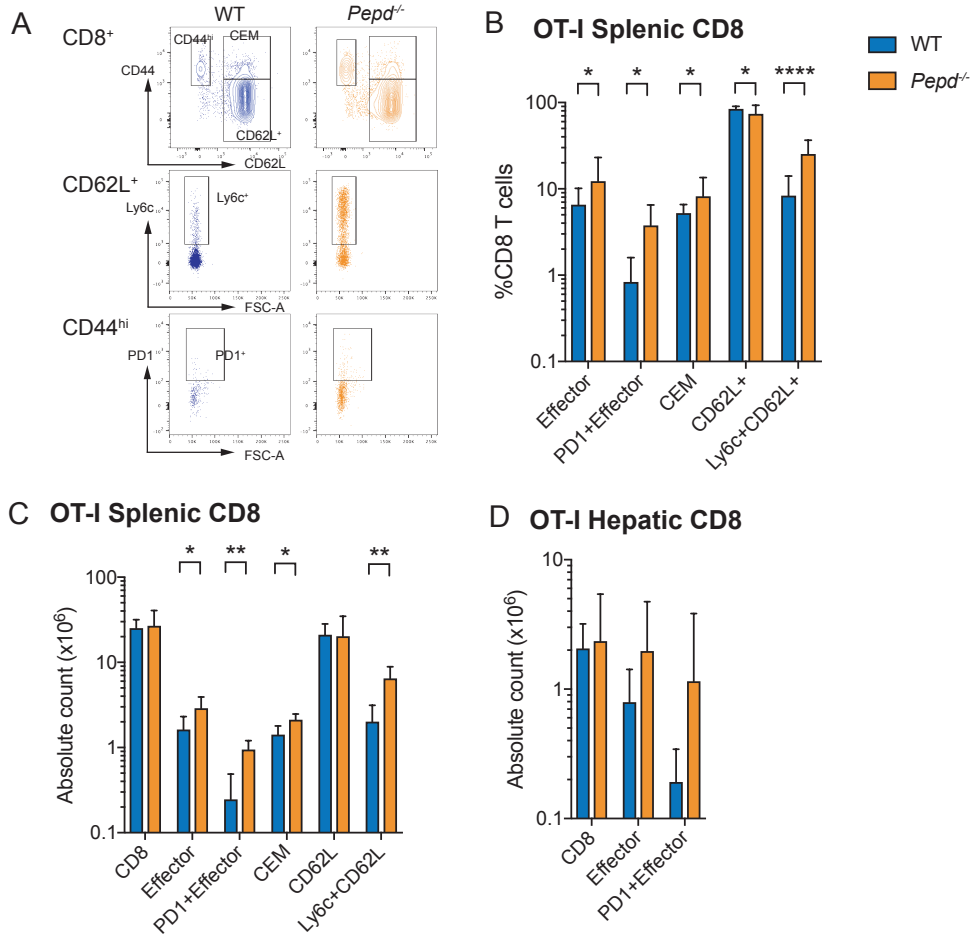


Figure 6.9 The T cell phenotype partially rescued by transgenic TCR expression

*A. Representative flow cytometry plots of splenic CD8⁺ T cell subsets of WT and Pepd$^{-/-}$ OT-I tg mice. B. Quantification of CD8⁺ T cell subsets of WT and Pepd$^{-/-}$ OT-I tg mice gated in (A) as % of CD8⁺ populations. ANOVA significance was determined across experiments for (B); Effector; * p =0.0209, PD1⁺effector; * p = 0.029, CEM * p = 0.0146, CD62L+; * 0.0163, Ly6c⁺CD62L⁺ **** p = <0.0001. C. Quantification of CD8⁺ T cell subsets of WT and Pepd$^{-/-}$ OT-I tg mice gated in (A) as absolute numbers. ANOVA significance; Effector; * p = 0.0146, PD1+effector; ** p = 0.0035, CEM * p = 0.0242, Ly6c+CD62L ** p = <0.0012. D. Quantification of hepatic CD8⁺ cell numbers as gated in (A) in the livers of WT or Pepd$^{-/-}$ OT-I⁺ mice. Graphical data show mean and 95% CI error bars and is representative of 1 (D) or 3 (A-C) experiments with 3-4 mice per group.*

6.2.3.2 Accumulation of CD8⁺ PD1⁺ effectors phenotype is antigen-independent

To confirm whether altered antigenic-signalling downstream of the TCR plays a role in the accumulation of exhausted, inflammatory effectors in the absence of *Pepd*, we immunised and boosted mixed chimeras with modified vaccinia virus Ankara (MVA)-encoding ovalbumin (MVA-OVA) (Figure 6.10A). Prime-boost antigenic exposure replicated the baseline CD8⁺ non-tg *Pepd*-deficient phenotype, with significantly enrichment of *Pepd*$^{-/-}$ CD45.2⁺ PD1⁺ effector populations and reduction in Ly6c⁺CD62L⁻expressing populations (Figure 6.10B). To explore the functional capacity

of these cells to respond to stimulation, we measured IFNγ across CD8$^+$ populations, and found that despite increased phenotypically exhausted *Pepd*$^{-/-}$ cells compared to WT CD45.2$^+$ CD8$^+$ populations (Figure 6.10B), *Pepd*$^{-/-}$ CD8$^+$ cellular populations produced equivalent amounts of IFNγ indicating no intrinsic change in the functional response to T_H1-associated foreign antigen with loss of prolidase expression despite altered T cell populations (Figure 6.10C).

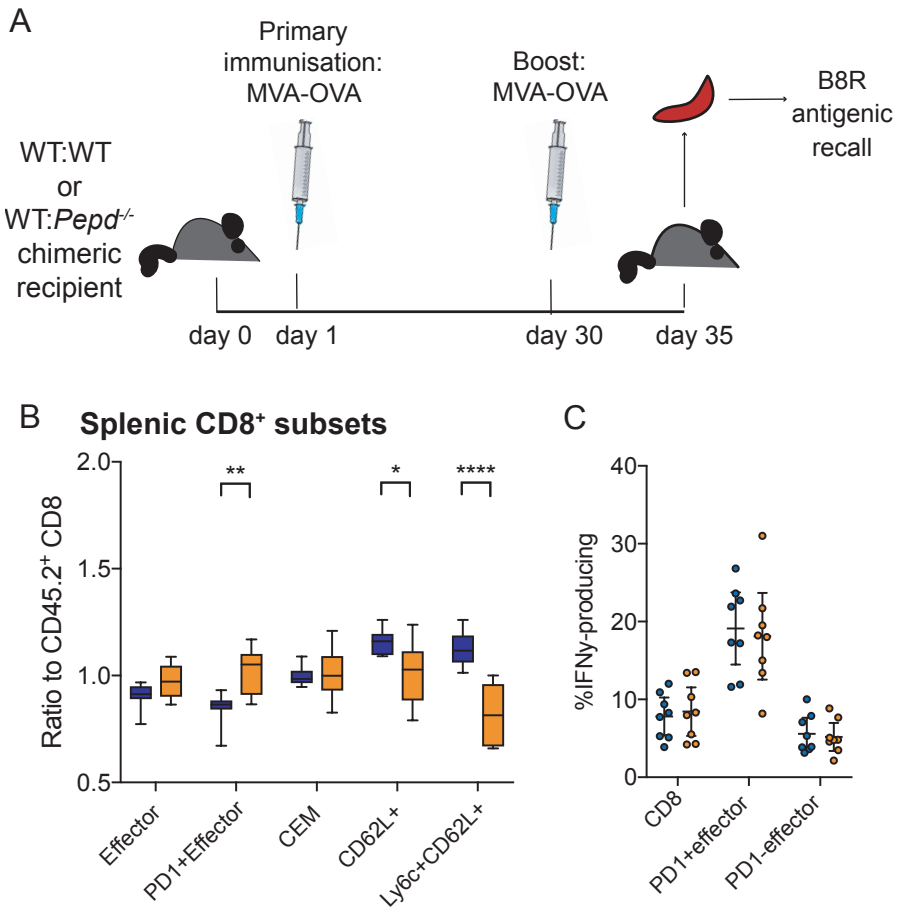


Figure 6.10 The Pepd$^{-/-}$ CD8$^+$ phenotype is antigen-independent

A. Schematic of immunisation programme of mixed WT:WT or WT:Pepd$^{-/-}$ BM chimeric mice with MVA-OVA. B. Quantification of WT and Pepd$^{-/-}$ CD8$^+$ subsets as ratios to CD45.2$^+$ CD8$^+$ proportions in the spleen of mixed BM chimeras immunised as in (A). C. Functional IFNγ production on B8R-peptide stimulated recall of WT or Pepd$^{-/-}$ CD45.2$^+$ CD8$^+$ splenocyte populations isolated from WT:WT and WT:Pepd$^{-/-}$ chimeras immunised as in (A), measured by intracellular cytokine staining. Data are pooled from 2 experiments with 4 mice per group. Two-way ANOVA was used to determine significance and adjusted with Sidak for multiple testing, p=<0.05, ** p=<0.01, *** p=<0.001,**** p=<0.0001. Graphical data shows mean and 95% confidence intervals.*

This conclusion is further supported by *in vitro* experiments demonstrating equivalent proliferative response of splenic non-tg CD8$^+$ T cells to anti-CD3 stimulation in absence of *Pepd* (Figure 6.11), as

well as *in vivo* transfer experiments of mixed 50:50 ratios of OT-I tg WT and *Pepd*$^{-/-}$ cells (Figure 6.12A). Seven days after immunisation, ratios of WT:WT and WT:*Pepd*$^{-/-}$ OT-I antigen-specific cells were unaltered from baseline (Figure 6.12B), and also showed equivalent IFNγ production post-immunisation with self-antigen, suggesting these cells mount a normal functional response to antigen (Figure 6.12C). Together these data suggest that intrinsic prolidase loss appears to drive a non-specific increase in proliferating cells that differentiate into effectors with an inflammatory, exhausted phenotype, which is independent of exposure to either self or foreign antigen.

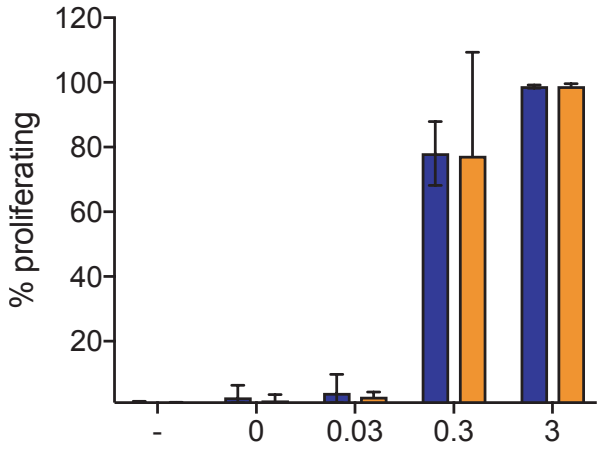


Figure 6.11 TCR-mediated proliferation is unaffected by Pepd deficiency

Proliferation of WT or Pepd-/- CD8+ populations stimulated with the specified concentrations of anti-CD3 or anti-CD28 in vitro for 72 hours, quantified by flow cytometric detection of CTV dilution. Data are representative of 3 independent experiments, with the addition of CD45.1^{+} control cells in some experiments.

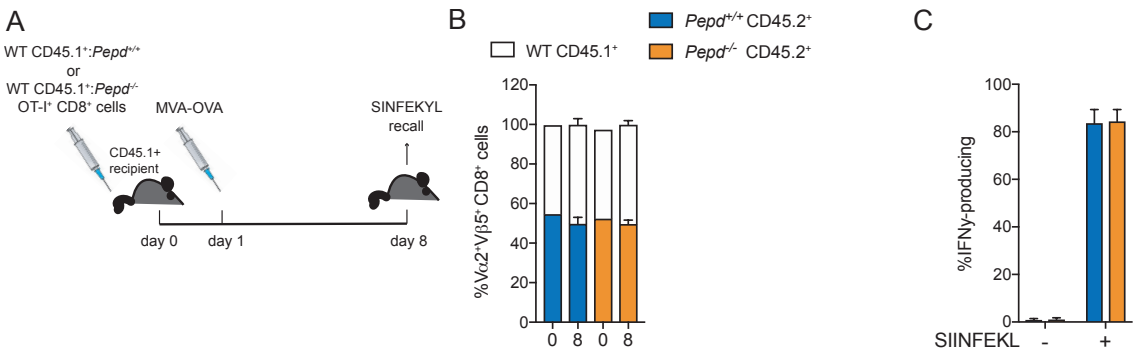


Figure 6.12 Pepd$^{-/-}$ CD8^{+} OT-I cells compete and produce comparable cytokine amounts in response to antigenic stimulation

A. Schematic of experiment; 50:50 ratios of WT:WT or WT: Pepd$^{-/-}$ OT-I cells were injected into recipient mice, then immunised with MVA-OVA. B. Resulting ratios of WT:WT or WT: Pepd$^{-/-}$ cells of Vα2^{+}Vβ5^{+}CD8^{+}

T cells from mice culled on day 8 from (A). C. Intracellular IFNγ production on recall of WT or Pepd$^{-/-}$ splenocytes isolated from (A) with SIINFEKL peptide. Data are representative of 3 or 2 (C) independent experiments. Graphical data shows mean and 95% confidence intervals.

6.3 Summary of chapter

Our studies identify that loss of prolidase drives an intrinsically activated T cell phenotype in a *Pepd*$^{-/-}$ mouse model, characterised by peripheral accumulation of effectors transcriptionally defined by a set of genes enriched with inflammatory and chronically-exhausted signatures, and negatively associated with SLEC-like acute functional effector molecules. *In vivo* labelling experiments demonstrate that the increase in this *Pepd*$^{-/-}$ effector population is likely to be driven by an increase in proliferating cells adopting this phenotype, which appears to be independent of TCR specificity or self or foreign antigenic stimulation. These exhausted cells appear to accumulate in sites of likely breakdown, such as the liver, suggesting that cell-extrinsic removal of these cells is likely to be rate limiting and not sufficiently modulated to compensate for increased populations in the absence of prolidase expression. This could result in autoimmunity indirectly via poor cellular clearance and associated inflammation. Hence, study of *Pepd* in immunological tolerance potentially may provide more generalised insight into how self-tolerance is normally maintained.

Reduced populations of CD8^{+}Ly6c^{+}CD62L-expressing populations were also associated with prolidase deficiency in a cell-intrinsic manner, though this phenomenon appeared to be at least partially independent of the accumulation of exhausted effectors as it could be rescued by expression of a tg TCR. Despite this, foreign antigen exposure did not rescue the development of this phenotype, suggesting that differences in TCR expression or non-antigen-dependent homeostatic TCR signalling may influence the differentiation of these populations in the absence of *Pepd*. How prolidase regulates T cell differentiation is still unclear and further research to explore how prolidase loss affects the inter-relationships between these non-linear subsets will help to understand T cell differentiation states and the impact of autoimmune disease on these lineages.

Also noteworthy is the B cell phenotype associated with intrinsic loss of prolidase expression; in mixed BM chimeras, *Pepd*$^{-/-}$ mature B cells demonstrated the same altered surface phenotype as seen in non-chimeric mice, though neither serum IgA or ANA production was raised in WT: *Pepd*$^{-/-}$ BM recipients, potentially indicating that elevated IgA amounts and ANA positivity may be driven in response to differential antigen presentation or availability to B cells, rather than intrinsically increased production by *Pepd*$^{-/-}$ B cells. This result indicates that excess *Pepd*$^{-/-}$ T cells with an inflammatory, exhausted phenotype are not sufficient to induce these humoral phenomena, or that the presence of competing WT T cells or other immune cells may rescue these phenotypes in a trans regulatory manner. Furthermore, how immunoglobulin levels relate to immune complex deposition in these mice, as well as the relationships between the SLE-like renal deposition with both B and T lymphocyte phenotypes require further elucidation.

7. Discussion

This thesis aimed to explore the genetic basis of autoimmune disease to advance our knowledge of the immunoregulatory pathways that function to maintain immune tolerance. Better understanding of the hereditary component immune tolerance loss is critical to the development of more targeted therapies for immune diseases as well as across other disease boundaries.

Specifically, this thesis describes the characterisation of two mouse models of genetic deficiency in order to understand the roles of previously immune-associated genes, *Ndrg1* and *Pepd*, in autoimmune disease. In the following chapter, I will discuss the significance of the results presented in this thesis and comment on future directions for this work.

7.1 The role of *Ndrg1* in tolerance is relevant for the development of anti-cancer therapies.

The development of more effective and better tolerated treatments for cancers, autoimmune and immunodeficiency diseases relies on defining the key molecular mechanisms that distinguish productive from tolerogenic lymphocyte responses (Yarkoni, Getahun and Cambier, 2010; Elizabeth Franks and Cambier, 2018). Despite the success of many monoclonal therapies targeting immune checkpoints, they are associated with an increased risk of autoimmune adverse events (Young, Quandt and Bluestone, 2018; Killestein and van Oosten, 2019; Ramos-Casals *et al.*, 2020). Pre-clinical investigation into the immune consequences of modulation of novel anti-cancer targets is therefore vital to prevent serious immunopathology.

NDRG1 is a stress- and hypoxia-inducible regulator of cell growth and differentiation (Piquemal *et al.*, 1999; Ellen *et al.*, 2008; Sahni *et al.*, 2014), implicated in some contexts as a metastasis inhibitor due to involvement within multiple signalling pathways (Hosoi *et al.*, 2009; Chen *et al.*, 2012;

Kovacevic *et al.*, 2013; Sun *et al.*, 2013). Consistent with this, anti-cancer iron chelators, Dp44mT and DFO may act via NDRG1-upregulation (Chen *et al.*, 2012, 2018). More pertinently for the significance of the results presented in this thesis, in multiple human cancers, increased tissue expression of NDRG1 is associated with poor outcomes (Ring *et al.*, 2006; Lu, Chua and So, 2014), with *in vitro* evidence for suppression of NDRG1 as a novel anti-cancer agent (Luo *et al.*, 2021; Zhao *et al.*, 2021). The therapeutic targeting of NDRG1 presents a promising treatment opportunity for multiple human cancers, but requires clarification of the immune effects of inhibition of NDRG1 (Sun *et al.*, 2013; Chen *et al.*, 2018; Sevinsky *et al.*, 2018).

7.1.1 NDRG1 represents a redundant biomarker of chronically stimulated lymphocytes

The work within chapter 3 demonstrates conclusively that although *Ndrg1* transcriptional regulation is anergy-dependent in B lymphocytes, there is no non-redundant functional role for NDRG1 within B cell tolerance during development or in the periphery. Additionally, in chapter 4, I show that experiments used to support published work proposing NDRG1 as a T cell anergy factor, were not reproducible and in fact generate T cell recall-like responses, rather than anergy, and are intact in the absence of NDRG1 expression. This finding raises questions about the previously proposed role of NDRG1 in T cells and highlights that better models of *in vivo* peptide-induced T cell anergy are required to better characterise the molecular mechanisms of this phenomenon.

Clinical investigations of other CMTD types have identified a potential immune component, as demonstrated by the increased presence of autoantibodies recognising peripheral myelin protein 22 (PMP22) in both CMTD1A and CMTD2, though whether these autoantibodies result from disease or actively play a role in disease pathogenesis has not been determined (Ritz *et al.*, 2000; Gabriel *et al.*, 2002). However, alongside the evidence from murine immunophenotyping, it is notable that immune disease is not described in patients with CMTD4d due to mutations in *Ndrg1* (Kalaydjieva *et al.*, 2000; Parman *et al.*, 2004; Echaniz-Laguna *et al.*, 2007; Okamoto *et al.*, 2014). On the other

hand, no studies have explicitly reported normal immune functioning in CMTD4d patients, hence subtle alterations could have been missed. Nevertheless, this lack of immune phenotype in either patients or mouse models of CMTD4d positions NDRG1 as a redundant bystander, which may solely represent a biomarker of chronically stimulated lymphocytes, presenting promise for the development of NDRG1 modulators for the treatment of multiple human cancers.

Chapters 3 and 4 demonstrate that not only is NDRG1 expression dispensable for the induction or maintenance of B cell anergy, and other processes downstream of chronic BCR stimulation, but also find humoral responses are equivalent on loss of NDRG1 at baseline and on challenge. Together, these findings are encouraging results for the safety profile of therapeutic agents that knockdown the expression of NDRG1, and enhance the potential for silencing NDRG1 for human anti-cancer treatment in some contexts (Luo *et al.*, 2021; Zhao *et al.*, 2021). Despite this, further experiments using an inducible knockout *Ndrg1*$^{-/-}$ mouse or NDRG1 modulators *in vivo* could be envisaged to specifically investigate of the effect of inhibiting NDRG1 on tolerance during immunological maturity, in order to provide more clinically relatable information for therapeutic interventions downregulating NDRG1. Furthermore, the findings of these chapters are limited to characterising the effects of downregulation of NDRG1 on tolerance, and hence cannot be generalised to assess the immunological safety of modulators that increase the expression of NDRG1, which may be desirable in some cancers given the proposed role of NDRG1 in suppression of metastasis (Chen *et al.*, 2012, 2018).

7.1.2 Understanding the association of NDRG1 expression in lymphocyte anergic responses

Elucidating the shared and specific molecular mechanisms that block early BCR and TCR signalling during the induction of *in vivo* lymphocyte tolerance may unlock new treatments for autoimmune and immunodeficient diseases. In both B and peptide-induced T cell anergy, low avidity chronic antigen stimulation drives impaired proximal antigen receptor signalling resulting in selective ERK

activation and chronically low oscillations of calcium, yielding low levels of transcription factor NFAT sufficient to activate key anergy factors (Dolmetsch *et al.*, 1997; Kimura *et al.*, 2000; Macián *et al.*, 2002; Jeon *et al.*, 2004a; Safford *et al.*, 2005; Barrington *et al.*, 2006; Borde *et al.*, 2006; Chiodetti *et al.*, 2006; Baine, Abe and Macian, 2009). NF-κB signalling and JNK-MAPK pathways are also selectively blocked, preventing antigen-induced proliferation and effector functions in both cases, which can be reversed by the removal of chronic *in vivo* lymphocyte antigen stimulation (Beverly *et al.*, 1992; Healy *et al.*, 1997; Chiodetti *et al.*, 2006). On the other hand, clonal anergy shares limited similarity in regards to signalling alterations, and is likely to represent a distinct phenomenon potentially limited to reactivation of *in vitro* activated $CD4^+$ T cell clones (Chiodetti *et al.*, 2006; Fathman and Lineberry, 2007). Thus, the significance and physiological relevance of studying the genetic drivers of clonal anergy as a model of peripheral T cell tolerance is limited.

Despite these differences, some molecules including the early growth response (*Egr*) gene family, downstream of NFAT activation have been actively implicated in both *in vitro* $CD4^+$ and *in vivo* forms of T and B lymphocyte anergy, suggesting some shared molecular control of the inactivated lymphocyte states (Safford *et al.*, 2005; Merrell *et al.*, 2006; Baine, Abe and Macian, 2009; Sabouri *et al.*, 2016). Other proximal signalling molecules such as the E3 ubiquitin ligases, Cbl-b, which regulate calcium mobilisation, have been associated with maintaining both B and T cell tolerance mechanisms (Jeon *et al.*, 2004b; Kitaura *et al.*, 2007), though such molecules may not be specific to the anergy response and act as general regulators of antigen receptor signalling (Bachmaier *et al.*, 2000).

One hypothesis that remains untested in this thesis is the possibility that whilst NDRG1 may not be essential for tolerogenic lymphocyte responses *in vivo*, NDRG1 may act redundantly in B cell anergy and adaptive T cell tolerance. The alternate pathways that drive *in vitro* clonal anergy could by contrast rely on NDRG1, as this phenomenon, not known to be physiologically significant, may not have been subject to the same evolutionary pressures that could drive redundancy of pathways

within *in vivo* peripheral tolerance mechanisms to prevent autoimmunity. Of note, there are three other members of the NDRG family, which share 53-65% homology and transcriptional repression via Myc. However, their expression is limited to a few tissues; brain, heart, testis and skeletal muscle, indicating they are unlikely players within lymphocyte tolerance (Qu *et al.*, 2002; Zhang *et al.*, 2006; Ellen *et al.*, 2008). Nevertheless, other independent compensatory pathways cannot be discounted. This hypothesis could be tested for by transcriptional analysis; specific upregulation of genes within *Ndrg1*$^{-/-}$ anergic cells in comparison to WT anergic, but not in *Ndrg1*$^{-/-}$ naïve might detect whether compensatory pathways are in play to induce anergy. Such pathways identified could then be targeted by siRNA interference or CRISPR/Cas9 to assess whether combinational knockdown with NDRG1 is sufficient to disrupt B cell tolerance.

NDRG1 may thus highlight the challenges of modelling human disease in the context of a high level of redundancy within the human genome; genes that have evolved redundant functions are likely to represent the most essential pathways in human homeostasis, and require multiple genes to be edited to observe a phenotype. Disease-linked genes have been demonstrated to be significantly enriched in functional duplicates, which may differ between organisms again increasing the complexity of modelling human disease (Gregersen and Olsson, 2009; Chen *et al.*, 2013). Furthermore, a key problem for identifying the role of a gene within biological pathways is testing for the right phenotype. For example, an orthogonal function for solute channel, *Slc15a4* as a regulator of TLR signalling in plasmacytoid dendritic cells was identified using an *in vivo* mutagenesis screen, leading to subsequent identification of a novel regulatory pathway of pDC endosomal TLR7 and TL9 signalling that is not required in conventional DC populations (Blasius *et al.*, 2010). Thus, it is possible that an untested contextual role for NDRG1 in untested areas of B cell tolerance may be uncovered by further experimenters who ask the correct questions.

7.1.3 Limitations of the gene-editing approaches used to model the role of NDRG1 in lymphocyte anergy

Amongst the common limitations of modelling human disease using mouse models, there are additional problems associated with some of the gene editing approaches utilised within these chapters. Despite clear loss of protein in the kidney, where NDRG1 is highly expressed, in *Ndrg1*$^{-/-}$ CRISPR/Cas9-generated mice, knockdown could not be assessed in immune tissues or lymphocytes specifically, due to the very low levels of protein expression undetectable by western blotting in WT cells. However, mRNA analysis demonstrated that the same transcript could be detected within *Ndrg1*$^{-/-}$ lymphocyte populations that carried the 11bp deletion as in kidney lysates, indicating that nonsense mediated decay would follow and no protein would be produced in this population. Though unlikely given the method of mutagenesis and features of peripheral neuropathy in these mice, it is possible that leaky NDRG1 expression in lymphocytes could have masked an immune phenotype. Non-constitutive knockdown in B and T cells such as CD21-Cre, as well as overexpression experiments would help to confirm a lack of role for NDRG1 within lymphocyte tolerance, and also provide further information for the safety of anti-NDRG1 modulators for cancer therapy.

Another potential limitation of this work is the reliance on the Ig^{HEL} mouse model of peripheral B cell tolerance. No single model can accurately capture all of the aspects of B cell anergy, and the relevance of such experimental systems to natural tolerance in humans is often questioned (Cambier *et al.*, 2007). The Ig^{HEL}/sHEL model is well established, and central to the field. It clearly recapitulates many of the phenotypical and functional characteristics of human B cell anergy including the role of the PTEN phosphatase (Browne *et al.*, 2009; Smith *et al.*, 2019), however it fails to address the role of responses to lower affinity antigen, hence a role for NDRG1 in this regard cannot yet be discounted. Other tg systems, including the azophenyl-arsonate (Ars)/A1 model, address anergy in the context of moderate affinity for antigen, which has been useful for

understanding the phenomenon of pathogen mimicry in addition to the affinity-modulated recovery of anergic cells (Benschop *et al.*, 2001; Gauld *et al.*, 2005). Despite this limitations, naturally anergic B cells identified in non-transgenic wildtype mice are reminiscent of the transitional T3 anergic phenotype described in both the Ars/A1 and Ig^{HEL}/sHEL models (Merrell *et al.*, 2006). Hence, tg models can provide relevant insights into B cell anergy, a true peripheral tolerance mechanism, as evidenced by human studies demonstrating 2.5% to 30% of the naïve B cell repertoire present as characteristically anergised cells (Wardemann *et al.*, 2003; Duty *et al.*, 2009; Quách *et al.*, 2011).

7.1.4 Modelling adaptive tolerance requires appropriate models and controls

The findings in chapter 4 highlight the importance of developing assays that better model adaptive T cell tolerance. On repeat of experiments by Oh *et al* to model the effect of NDRG1 loss on peptide-induced T cell anergy, reduced IL-2 production was apparent in wells containing antigen-experienced T cells as reported previously (Oh *et al.*, 2015), though we could not replicate the suppression of proliferation on restimulation, and instead detected enhanced proliferation. Experimental differences between assay setup across laboratories included the detection of proliferation by flow cytometry of antigen-specific cells in our experiments, versus total thymidine incorporation in the published data, though this is unlikely to explain the contrasting results reported here as explored by BrdU pulsing. Additionally, WT OT-II and *Ndrg1*$^{-/-}$ OT-II tg mice were crossed to *Rag1*$^{-/-}$ strains previously, where experiments described here used immunocompetent mice throughout. This would not normally be expected to alter the behaviour of the OT-II cells, but an effect due to background strain cannot be excluded. The proliferative and functional responses of T cells isolated from immunodeficient donor mice exposed to altered homeostatic conditions in absence of other lymphocyte populations may not be comparable to populations derived from immunocompetent mice (Moses *et al.*, 2003; J. Kim *et al.*, 2018). Furthermore, populations from non-*Rag1*$^{-/-}$ donors used here may contain a small contamination (<5%) of non-tg polyclonal $CD4^+$

T cells, though as antigen-specific cell numbers were determined prior to *in vitro* assay setup in both cases, this should not have affected the subsequent readout across experiments.

This assay relies on the low immunogenicity of injected soluble peptide intravenously to provide signal one to injected Ag-specific T cells, in the absence of co-stimulation (Oh *et al.*, 2015). Soluble peptide-induced anergy has been modelled previously using this assay in multiple publications, however these responses were typically compared to alternative, more immunogenic peptide delivery methods with adjuvant rather than naïve un-injected $CD4^+$ T cells (Kearney *et al.*, 1994; Perez *et al.*, 1997; Pape *et al.*, 1998; Safford *et al.*, 2005). The trans effect of bystander naïve recipient cells *in vivo* in a system where large numbers of antigen-specific T cells and cognate peptide have been introduced has not been considered; peripheral inflammation and activation could provide co-stimulation leading to productive T cell activation instead of suboptimal priming, which could theoretically lead to the recall-like response reported here. Contrasting results have been recorded using this experimental system to model the effect of CTLA-4 on T cell tolerance (Perez *et al.*, 1997; Inobe and Schwartz, 2004). Thus, peptide-induced anergy has been considered a distinct phenomenon from adaptive tolerance (Choi and Schwartz, 2007). Alternative models of adaptive tolerance are likely to bear more physiological relevance to peripheral T cell tolerance as self-peptide is expressed as a neo-antigen throughout development. These models employ double tg strains that mimic the BCR IgHEL/sHEL B cell anergy system, where peptide-specific TCR-tg cells are injected into antigen-expressing recipients (Tanchot *et al.*, 2001; Huang *et al.*, 2003; Safford *et al.*, 2005).

Hyporesponsive states observed in T cells are by no means limited to adaptive tolerance, and there is controversy and crossover between the fields of T cell exhaustion, the induction of regulatory $CD4^+$ T cells and adaptive tolerance (Schwartz, 2003; Kalekar and Mueller, 2017; Trefzer *et al.*, 2021). Thymically-derived $CD25^+CD4^+$ T cells that bear self-reactive TCRs can mirror the suppressive

state of anergy as characterised by reduced proliferation and impaired IL-2 production, though also possess non-cell autonomous suppressive functions (Itoh *et al.*, 1999). Several reports describe anergy as a precursor, intermediate state for the induction of the regulatory T cell lineage, which may then depend on additional external cues such as TGF-B and IL-10 for further differentiation (Chappert and Schwartz, 2010; Kalekar *et al.*, 2016; Kalekar and Mueller, 2017). It is hypothesised that these two mechanisms act both independently and in concert by regulating peripheral immune responses in order to prevent autoimmunity, whilst complete suppression of foreign immune responses is prevented by cell-autonomous anergy of regulatory T cells (Schwartz, 2003; Kalekar and Mueller, 2017).

Historically, anergy and exhaustion were also thought to represent independent mechanisms dependent on strength of antigen signalling and incomplete activation in the former, versus loss of functionality post successful activation in the latter, such as with chronic viral infection (Rocha, Grandien and Freitas, 1995; Liu *et al.*, 2018). However, transcriptional similarities have recently been characterised between *in vivo* anergic and exhausted $CD4^+$ T cells, with the roles of molecular regulators, *NFAT, NR4A1,* and *Egr2* implicated across both states (Martinez *et al.*, 2015; Trefzer *et al.*, 2021; Wagle *et al.*, 2021). It is clear suppressive states within T cell biology rely on complex overlapping pathways, and further work is required to understand specific and shared mechanisms of tolerogenic states in order to maximise therapeutic efficacy for both autoimmune and immunodeficient diseases, as also exemplified by study of the role of prolidase in $CD8^+$ T cell differentiation in this thesis.

7.2 Prolidase deficiency drives autoimmunity

Chapters 5 and 6 demonstrate for the first time, the explicit contribution of prolidase in regulating immune tolerance, by characterisation and phenotyping of a mouse model of PD that replicates the SLE-like renal phenotype seen in a subset of human PD patients. I demonstrate that prolidase

regulates T cell differentiation and fate in an intrinsic manner, characterised by two *Pepd*-dependent T cell phenotypes that appear to carry differential dependence on TCR specificity. The peripheral accumulation of chronic inflammatory $CD8^+$ effectors appears to be driven by an increased propensity of $Pepd^{-/-}$ cells to adopt this phenotype on proliferation, though this is likely to be independent of altered T cell survival or self or foreign antigenic response. Together, results from these chapters characterise a model for monogenic autoimmune human disease, and provide new clues as to how loss of prolidase drives the association between PD and autoimmunity.

7.2.1 The role of prolidase in T cell differentiation and associated disease relevance

T cell differentiation and fate is closely regulated by central and peripheral mechanisms in order to prevent immunodeficiency or autoimmunity. Prolidase loss drives the accumulation of $CD8^+$ effectors with a transcriptional profile characteristic of exhaustion in an intrinsic manner. *In vivo* labelling identified that, in the absence of prolidase, there is an increased rate of proliferation into this chronically exhausted, inflammatory population. This change in T cell fate was non-specific, not driven by either foreign or self-antigen stimulation. Additionally, as there was no obvious defect in Bim-induced apoptosis or Bcl2-mediated survival of these populations, these cells appear to accumulate in tissues where they would normally be removed, such as the liver in this instance. Though non-antigen driven, the dysregulated build-up of these cells could lead to non-specific inflammation, initiating autoimmunity, as clearance appears to be rate-limiting. However, further experiments are required to confirm that clearance of these cells is not functionally altered in a T cell intrinsic manner.

Such dysregulation of hepatic peripheral tolerance mechanisms that usually remove exhausted $CD8^+$ T cells has been described in in autoimmune diseases such as NASH (Wong *et al.*, 2016; Dudek *et al.*, 2021). Such mechanisms include Bim-mediated apoptosis and suicidal emperipolesis (SE), the latter of which is an intrinsic CD8-driven phenomenon where *in situ* activated T cells invade

hepatocytes and are lysosomally destroyed (Benseler *et al.*, 2011). Bim expression was equivalent in *Pepd*$^{-/-}$ CD8^{+} effectors, though a role for *Pepd* in regulating SE requires further experiments to eliminate. Notably this mechanism is driven by actin rearrangement downstream of TCR engagement (Benseler *et al.*, 2011), and many proline-rich proteins are involved in actin-dependent membrane motility (Holt and Koffer, 2001). Since this rearrangement is post-translational, such actin skeletal changes could have been missed by RNA assays used in this thesis.

The expansion of the effector pool in prolidase-deficient mice was independent of self or foreign antigen stimuli and was present in a CD8-intrinsic manner; however, it is possible that altered intrinsic response to other stimulators such as inflammatory cytokines could still play a role in a mixed chimeric system. Altered IFN-β signalling in prolidase-deficient patient fibroblasts has been attributed to enzymatic-independent prolidase regulation of IFNAR1 subunit cell surface expression (Lubick *et al.*, 2015). An inflammatory environment leading to T cell exhaustion might contribute to the primary immunodeficiency seen in PD patients with recurrent respiratory infections. The interferon-induced gene, *Ifi27l2a* was significantly reduced in multiple *Pepd*$^{-/-}$ CD8^{+} T cell subsets as identified by transcriptomic analysis in this thesis, though this finding was not reproducible in chimeric *Pepd*$^{-/-}$ T cells. This suggests that any effect on *Ifi27l2a* cannot account for the intrinsic expansion of effectors with an exhaustion profile in chimeric recipients of WT:*Pepd*$^{-/-}$ BM, though additional experiments are required to understand whether intrinsic IFN-signalling in CD8^{+} populations is altered and any subsequent effect on T cell subset differentiation. The role of prolidase within IFN-signalling and downstream effects could also be further explored by application of viral IFN-antagonist molecule, NS5 which has been demonstrated to bind *Pepd* and thus reduce IFN-receptor trafficking to the cell surface (Lubick *et al.*, 2015).

The cellular metabolic consequences of prolidase deficiency could also theoretically drive altered T cell populations and result in autoimmunity. Upon activation, CD8^{+} T cells exhibit a significant

increase in aerobic glycolysis via AKT-mediated GLUT1 upregulation, enabling T cells to use more energy to proliferate, amongst other effector functions (Frauwirth *et al.*, 2002; Wieman, Wofford and Rathmell, 2007; MacIver, Michalek and Rathmell, 2013). Other peptidases have been implicated in the regulation of lymphocyte glycolysis, such as identification of the mechanism of the proteolytic complex, tripeptidyl peptidase II (TPPII) in balancing glycolytic flux, cellular amino acid levels and lysosomal abundance. Patients with mutations in *TPP2* demonstrate primary immunodeficiency combined with autoimmunity and neurodevelopmental delay; metabolic analyses have demonstrated loss of TPPII enzymatic deficiency leads to increased lysosomal degradation of glycolytic enzyme, hexokinase-2, which results in decreased glycolysis, impairing T cell effector functions on stimulation (Lu *et al.*, 2014). Recapitulation of such experiments in prolidase-deficient T cells, or complementation experiments by enzymatic-inactive *Pepd* mutants as well as mass spectrometric metabolomic analyses would shed light on whether loss of prolidase alters the balance of T cell metabolism in a mechanism sufficient to affect T cell development and tolerance breakdown.

Furthermore, the disease relevance of the build-up of these $CD8^+$ effectors also requires further analysis; though $CD8^+$ populations with an exhausted signature have been described in human autoimmune diseases and patients with inborn errors of immunodeficiency with autoimmune features, this is typically driven by chronic antigen exposure or unresolved infection and inflammation and correlates with better prognosis (McKinney *et al.*, 2015; Wherry and Kurachi, 2015; Delmonte *et al.*, 2019; Zakharov *et al.*, 2020; Collier *et al.*, 2021). It is however conceivable that the impaired removal of these cells could lead to augmented non-specific inflammation through dysregulated apoptosis and thus, increased availability of cell debris for autoantigen sampling, which could enhance the potential for loss of immune tolerance.

In this work, a definitive link between the exhausted T effector accumulation and autoimmunity is unclear. In the WT:*Pepd*$^{-/-}$ chimeric mice, serum IgA and ANA production was normal, despite the continued presence of the excess CD8^{+} exhausted like effectors. This suggests that the T cell phenotype may not be sufficient to induce clinical autoimmunity, and that the latter may depend on extrinsic actions of prolidase, or be inhibited or rescued by the presence of WT cells in a mixed chimeric system. Further experiments by transfer or depletion of WT regulatory T cell populations, or reconstitution of irradiated *Pepd*$^{-/-}$ recipients with WT BM may help to shed light on this rescue. Thus, how and if the increased presence of *Pepd*$^{-/-}$ activated CD8^{+} cells independent of TCR specificity or antigenic exposure, relates to both the autoimmune renal deposition and altered humoral phenotype observed requires further exploration. Such experiments will require development of novel T cell-specific conditional *Pepd*$^{-/-}$ knockout mouse lines.

T cell exhaustion has been characterised by suppression of effector function (Wherry and Kurachi, 2015), yet despite the increase in representation of *Pepd*$^{-/-}$ CD8^{+} effectors expressing a chronic exhaustion transcriptional signature, *Pepd*$^{-/-}$ CD8^{+} T cells overall demonstrate equivalent IFNγ production as a proportion, suggesting these cells continue to function as effectors, in contrast to the functional suppression typically associated with exhaustion. Further analyses of the functional capacities of *Pepd*$^{-/-}$ exhausted effectors are required in comparison to non-exhausted effectors; these experiments could include *in vitro* polarisation assays with cytokine combinations in order to assess further differentiation capacity and cytokine production, as well as experiments to assess cytolytic capacity for targeted cell killing (Cerwenka *et al.*, 1998; Nguyen *et al.*, 2016). Such analyses may shed light on the potential relationship between the expanded population of inflammatory effectors and clinical autoimmunity. However, limitations of these functional analyses include over-dependence on FACS proteomic surface profiling of these populations for sorting, whereas the signature is transcriptionally defined. The difficulty hence lies in the clean isolation of exhausted effector populations, exemplified here by the imperfect use of PD1 as a non-specific surface maker

of exhaustion. Though expressed highly on exhausted populations, PD1 is induced on TCR activation and is a key marker of antigen-specific $CD8^+$ T cells in both viral and anti-tumour immunity (Chikuma *et al.*, 2009; Inozume *et al.*, 2010; Youngblood *et al.*, 2011).

7.2.2 *Pepd* deficiency in the regulation of humoral immunity and renal immune complex deposition

Prolidase-deficient patients have hypergammaglobulinemia, typically with increased levels of IgG, IgA and IgE, though raised levels of IgM have also been reported (Shrinath *et al.*, 1997; Kurien *et al.*, 2013; Ferreira and Wang, 2015; Rossignol *et al.*, 2021). Though prolidase-deficient mice show enhanced glomerular deposition of immune complexes, indicating a renal phenotype consistent with SLE, and demonstrate increased serum IgA, they have normal levels of IgG and IgM. Additional experiments are required to test whether IgE levels are also dysregulated in the sera of *Pepd*$^{-/-}$ mice as reported in some PD patients (Lopes *et al.*, 2002; Spodenkiewicz *et al.*, 2020; Rossignol *et al.*, 2021).

The differences between immunoglobulin levels in *Pepd*$^{-/-}$ mice and prolidase-deficient patients may reflect the effects of recurrent respiratory infections, or other genetic, epigenetic or environmental confounders, though species differences in humoral immunity also cannot be ignored. Increased serum immunoglobulin levels are characteristic of connective tissue diseases and positively correlate with disease activity (Levinsky, Cameron and Soothill, 1977; Hassan *et al.*, 1998; Kudose *et al.*, 2019). However, patients with lupus nephritis have lower serum C1q levels than normal controls, which negatively correlates with immune complex deposition (Tan *et al.*, 2013), highlighting an example of significant dichotomy between clinical relevance of concentrations of immunoglobulin in the periphery versus tissue activity. Hence, understanding how specific elevation of serum IgA levels relates to glomerular immune complex deposition in this mouse model is complex.

Of specific note, are the limitations of murine models that reproduce IgA renal deposition both in the context of modelling SLE and IgA nephropathy (IgAN), the most common form of human glomerulonephritis (Tashakkorinia and Tudor, 2020). Species differences in IgA subtype and glycosylation of the IgA hinge region, the target for self-reactive IgG, a key driver of self-aggregation, and mesangial binding leading to renal injury, limit the translational power of murine modelling of IgAN (Wehbi *et al.*, 2021). Existing models lack this feature, and often have a variable or late onset phenotype (Suzuki et al Seminars in Nephrology 2018). However, there is value to murine models that mimic shared aspects of such diseases. For example tg mice over-expressing BAFF present with raised hypo-glycosylated serum IgA levels and accompanying renal deposition of varying amounts of IgA, IgM and IgG, modelling several aspects of SLE and IgAN (McCarthy *et al.*, 2006, 2011). In the context of the clinical success of BAFF-blocking immunotherapy, belimumab, in treating autoimmune disease (Shin *et al.*, 2018; Arvaniti *et al.*, 2020), this highlights the importance such models to enrich understanding of common disease pathogenesis mechanisms and for the design of novel therapies. Current treatments for IgAN are non-specific and of very limited efficacy, with around 30% of patients progressing to end stage renal failure (Paolo Schena, 1990). The development of novel treatment approaches including monoclonals and cell therapies requires better *in vivo* models of glomerular IgA deposition, thus *Pepd*$^{-/-}$ has potential as a tool for model system testing for IgAN therapeutics.

This renal immunofluorescence pattern in *Pepd*$^{-/-}$ mice, taken in the context of enhanced ANA positivity and a peripheral activated T cell phenotype, is characteristic of mild SLE-like renal disease. Insights from studying the *Pepd*-deficient mouse model may provide valuable information on the pathways driving SLE and other systemic complex autoimmune disorders. This is exemplified by other mouse models of monogenic autoimmune disease; characterisation of *Trex1*$^{-/-}$mice unexpectedly revealed an inflammatory myocarditis phenotype (Morita *et al.*, 2004), while further studies demonstrate that TREX1 is essential for the breakdown of dsDNA, hence preventing

exposure to autoantigens (Stetson *et al.*, 2008; Grieves *et al.*, 2015). 25% of patients diagnosed with Aicardi-Goutieres disease have mutations in the *TREX1* gene and present with autoimmune features, though *TREX1* mutations are also reported to be associated across a spectrum of autoimmune diseases including vasculitis and SLE, exemplifying phenotypic variability and how monogenic immune-associated genes can give pathway insight across complex disease (Rice, Rodero and Crow, 2015).

7.2.3 Future insights into modelling prolidase deficiency

Insights from human PD patients are complicated by the phenotypic variability of PD, as exemplified by report of heterogenous clinical symptoms in carriers of the same mutation (A. Lupi *et al.*, 2006; Ferreira and Cusmano-Ozog, 2017; Spodenkiewicz *et al.*, 2020). Similarly, the phenotype seen in *Pepd*-deficient mice is moderately variable, potentially suggesting extrinsic modifiers may also be at play in the mice. For example, age, commensal microorganisms and viral infections within the natural oscillations of immune homeostasis may contribute to the scale of the phenotype, as exemplified by analyses of homeostatic immune variation (Abeler-Dörner *et al.*, 2020).

PD genotype does not necessarily reflect phenotype, However, a recent forward genetics driven systematic review found significant differences in ulcer-free survival and other clinical manifestations by Kaplan-Meier analyses by variant consequence type (loss of function, missense and splicing) (Rossignol *et al.*, 2021), highlighting the importance of genetic testing to help classify and stratify these patients. This review also finds average residual activity of prolidase across cellular subsets varies from 0% of normal activity in plasma, to 13.5% in WBC or lymphoblastoid cells, which may also contribute to phenotypic variability. In relation to this, as prolidase is uniquely required for the hydrolysis of peptides containing C-terminal proline or hydroxyproline, it is unclear how much other peptidases, including the N-terminal cleaving prolinase, can compensate for loss

of prolidase activity, and how much this contributes to variability in syndrome by patient (Miech *et al.*, 1988).

PD is a rare, but likely under-diagnosed disorder, which has historically relied on biochemical detection of massive imidodipeptiduria, in addition to >90% reduction of normal prolidase activity as tested in patient samples. The more recent identification of the enzymatic-independent roles of prolidase within multiple biological pathways (Misiura and Miltyk, 2020) suggests that imidodipeptiduria may not be a broad enough readout for PD as it fails to capture non-enzymatic function alterations. The intrinsic nature of the T cell phenotype in *Pepd*$^{-/-}$ mice could be consistent with such functions; further work, using enzymatically-dead *Pepd*, and linking alternative prolidase mechanisms to immune dysregulation is needed, and may eventually lead to more precise and clinically relevant assays for prolidase function and more broadly, to new therapeutic targets of relevance to autoimmune disease.

To progress this work, CRISPR-Cas9 mutagenesis can be harnessed for development of strains expressing hypomorphic variants or gain-of-function mutations. Cell type-specific and -inducible knockout models will provide useful tools to complement those experiments in chapter 6, to delineate which altered immunophenotypes can be attributed to intrinsic cellular deficiency of enzymatic activity, and which to physical loss of the expressed protein (Misiura and Miltyk, 2020).

Currently, treatment is restricted to managing the symptoms of PD, with reported limited success in treating chronic leg ulcers with topically applied proline or orally given supplements, though gene therapy, through liposomal or adenovirus gene delivery for replacement enzyme therapy has also shown some success in improving wound healing (Karthikeyan *et al.*, 2019; Spodenkiewicz *et al.*, 2020; Rossignol *et al.*, 2021). The autoimmune manifestations in PD patients are managed by strategies used in SLE including steroid treatments, transplantation and splenectomy, which have

limited efficacy and a heavy side effect burden (Shrinath *et al.*, 1997; Butbul Aviel *et al.*, 2012; Spodenkiewicz *et al.*, 2020). Better models of the disease will advance our understanding of the pathogenic mechanisms, enabling the development of more efficacious therapies.

7.3 The future of human autoimmune disease models

Better medicines rely on advancements to our mechanistic understanding of disease pathogenesis, necessitating suitable experimental models of autoimmunity. Traditionally, the identification of new immune genes contributing to autoimmunity uses two strategies; forward and reverse genetics. Forward genetics screens traditionally relied on laborious, expensive and challenging linkage to go from phenotype to genotype, typified by phenotype-driven mouse mutagenesis screens, or large systematic family studies, whereas reverse genetics starts from mutations of a candidate gene to test for a resultant phenotype (Moresco, Li and Beutler, 2013). Limitations of the latter include minimal prior evidence to support disease association, which is associated with a high risk of finding no phenotype or embryonic lethality. Furthermore, it is both costly and time-consuming to invest in a novel mutant without promise of a direct phenotype (Dawes and Uren, 2021).

This thesis exemplifies how newer methodologies can allow a more targeted and informed approach to the generation of autoimmune genetic models with forward and reverse genetics approaches, which can provide complementary recognition and validation of the effects of novel genes on human disease.

Advances in transcriptomic profiling permit identification of strongly linked candidate genes in an agnostic manner, as shown by the association of NDRG1 upregulation with anergy in B cells. Furthermore, improvements to gene editing strategies such as CRISPR/Cas9 mutagenesis enable generation of strong autoimmune candidate models in an accelerated time frame. In fact,

CRISPR/Cas9 can produce first generation homozygote mutant mice that can be phenotypically screened for phenotype, as well as simultaneous introduction of mutations to multiple genes, therefore fast-tracking the study of pathways containing functionally redundant genes (Wang *et al.*, 2013). This genetic engineering technology also presents huge promise for forward genetic approaches by the large-scale creation of CRISPR/Cas9 knockout libraries targeting thousands of genes in human cell lines (Shalem *et al.*, 2014; Gurumurthy *et al.*, 2016). Such wide-ranging gene-targeting approaches are key to generation of libraries of specific knockout mouse models, facilitating phenotypic screens such as the 3i's immunophenotyping pipeline in order to identify whether loss of genes can affects immune homeostasis (Abeler-Dörner *et al.*, 2020).

7.3.1 Modelling human genetics; limitations of genetic targeting approaches

Close recapitulation of disease both in terms of phenotype and genotype is of essential importance in relating the findings from mouse models to human studies. Studying monogenic variants with large phenotypic effects in mouse models can provide valuable insight into the molecular basis of both rare and common human autoimmune disease (Cirulli and Goldstein, 2010; Brown, 2021). However, this information has to be interpreted with caution as the genetic basis of most human autoimmune disease is complex, and as exemplified by GWAS studies, many SNPs of multiple genes together contribute individual modest risk (Manolio *et al.*, 2009). Murine genetic approaches targeting individual genes thus oversimplify the basis of most human disease, and these models do not capture epistatic genetic interactions, the effect of environmental factors or epigenetic effects.

Prior to the development of CRISPR/Cas9-mutagenesis, gene targeting led to removal of whole genes and associated proteins, or total disruption of protein function (Bedell, Jenkins and Copeland, 1997; Beutler, Du and Xia, 2007). Yet, classical *null* allele ES cell-generated murine models do not accurately recapitulate the single bp changes or hypomorphic mutations that cause the majority of monogenic human disease. Human pathogenic variation can include hypomorphs,

gain of function and dominant negative variants, for example collagen type X in mutant mice; where strains carrying a homozygous null mutation in the *Col10a1* gene had no phenotype (Rosati *et al.*, 1994), mice carrying a dominant negative tg mutation recapitulated the chondrodysplasia phenotype observed in human patients with *COL10A1* mutations (Jacenko, Luvalle and Olsen, 1993).

Classical forward murine genetic mutagenesis screens employing agents such as ENU had the advantage of replicating many of the point mutations seen in human patients, creating allelic series of mild to moderate phenotypic variants based on different point mutations in the same gene, thus allowing fine exploration of function of the gene within biological pathways (Quwailid *et al.*, 2004; Vinuesa and Goodnow, 2004; Cordes, 2005). More recently, the development of CRISPR/Cas9 technologies has allowed the direct reverse generation of single bp mutants, such as an allelic series of mice carrying mutations in *Zip7* orthologous to those detected in patients with immunodeficiency (Anzilotti *et al.*, 2019).The use of a *null* mutant in this thesis is a thus a potential limitation of characterising immunophenotypes of PD; although the majority of patients with PD do present with absent or severely reduced levels of prolidase. Likewise the full knockout does not permit delineation of the enzymatic from the enzymatically-independent functions of prolidase.

Murine phenotypes can be strain dependant, with unknown modifiers masking phenotypes. For example, many ES cell-derived mutant models studying loss of immune tolerance were based on homologous recombination between the 129 and B6 strain; on backcrossing to the B6 strain, autoimmune phenotypes were diminished due to the loss of the additional 129 alleles that were initially transferred alongside the mutant gene (Bygrave *et al.*, 2004; Morel, 2004). It is therefore conceivable that NDRG1 might have some role in tolerance that was not detectable in mice, either as a species or strain difference.

7.3.2 Validating and translating findings from mouse models of human autoimmune disease to the clinic

Mouse models present potential to directly aid clinical diagnosis, provide a therapeutic screening platform, and advance clinical research of the pathogenesis of disease (Lee *et al.*, 2012; Richard and Gilkeson, 2018). Though 99% of mouse genes have an identified human homolog, and 80% represent 1:1 orthologues, as defined by match to the same conserved syntenic intervals in humans (Gibbs *et al.*, 2002), there are clear biological differences between mice and humans that can limit clinical relevance of mouse model data. Immunological interspecies differences between mice and humans include but are not limited to Ig and FcR isotypes, activity and expression, meaning the screening of novel compounds in disease models can have limited clinic relevance (Pierre Bruhns and Friederike Jönsson, 2015). To combat this, development of humanised mice, such as those expressing humanised or chimeric forms of receptors that then link up with mouse signalling machinery have provided key resources for screening of therapeutic interventions (Brown, 2021). Furthermore, mice with humanised immune systems created by engraftment of human immune systems into immunodeficient mice are becoming increasingly popular in biomedical research and are likely to represent an invaluable resource for personalised medicine (Walsh *et al.*, 2017; Zhu *et al.*, 2019; Adigbli *et al.*, 2021).

Murine models also fail to recapitulate the heterogeneous presentation of human autoimmunity associated with complex environmental and genetic variation (Richard and Gilkeson, 2018). This is partially exemplified in the *Pepd*$^{-/-}$ model of PD used here, which develops autoimmunity as seen in human patients, though does not demonstrate gross dermatological manifestations including skin ulcerations, as seen in the majority of PD patients (Rossignol *et al.*, 2021), which may reflect differences in environmental pathogen exposure. Other examples of partial phenotype and intrinsic differences between human and mice disease mechanism included global knockout mouse models of human dedicator of cytokinesis 8 (*Dock8*) immunodeficiency, which recapitulated the

immunodeficiency seen in human *DOCK8*-deficient patients (Randall *et al.*, 2009; Zhang *et al.*, 2009), but hyper-IgE syndrome was only detected in mice when *Dock8* was specifically mutated in T cells (Gowthaman *et al.*, 2019).

Additionally, valid clinical translation of experimental murine models that do identify a novel phenotype to genotype correlation may require multiple observations of the same phenotype associated with alternative models carrying variants of the same gene, and additional experimentation demonstrating phenotypic rescue, complementation and further mechanistic insights to support a molecular basis for phenotype (Hmeljak and Justice, 2019).

For example, the role of BAFF in immunity has been explored by complementary *null* mutants and overexpression of the gene, *Tnfrsf13b*, which results in immunodeficiency or autoimmunity respectively (Schiemann *et al.*, 2001; Groom *et al.*, 2002). Further experimentation within this pathway included the *Act1*-deficient mouse, which helped to identify the importance of BAFF regulation within B cell immunity (Qian *et al.*, 2004). Such models have advanced our understanding of the disease pathogenesis of Sjogren's Syndrome, and SLE (McCarthy *et al.*, 2011; Lee *et al.*, 2012). Therapeutic intervention within the BAFF system thus represents a promising area (Nakayamada and Tanaka, 2016); BAFF-antagonist, belimumab demonstrated significant reduction of disease activity in SLE patients (Navarra *et al.*, 2011) and novel reagents such as BAFF-Trap have shown promise in mouse models of collagen-induced arthritis (Zhou *et al.*, 2019).

Together this exemplifies the role of mouse models of autoimmunity in identifying causal genetic variants, defining disease mechanisms, and as pre-clinical therapeutic efficacy screening systems for testing novel interventions.

7.4 Conclusions

Studying monogenic mouse models can offer novel insights into the hereditary basis of human autoimmune disease. Experiments in this thesis exemplify this by demonstrating the significant discovery that NDRG1 is not required for the induction or maintenance of B cell tolerance, despite a clear transcriptional association with lymphocyte anergy. This is significant as modulation of NDRG1 presents a promising therapeutic strategy across multiple human cancers, though further work is required to address the immunological effects of upregulation of NDRG1. Furthermore, the relevance of these findings extends to an important rebuttal of the previous T cell data published in Nature Communications by Oh *et al,* and thus, rejection of the general perception that NDRG1 is a primary anergy factor.

Further work in this thesis clearly identifies the direct relationship of prolidase loss with autoimmunity, a key conclusion as the autoimmune phenotype in patients with PD is not fully penetrant. Experiments demonstrate that loss of prolidase drives a renal phenotype with features of early SLE nephritis or IgA nephropathy, accompanied by elevated serum IgA and altered lymphocyte phenotypes. The relationship of the intrinsic chronic inflammatory, exhausted T cell phenotype identified here, to the renal deposition and immunoglobulin changes in the *Pepd*$^{-/-}$ mouse is unclear, and further experiments with tools such as T cell specific *Pepd*$^{-/-}$ knockout mice are required to understand the relevance of this phenotype to clinical disease. Such studies will help to further our knowledge about how the immunophenotypes observed in *Pepd*-deficient mice contribute to disease pathogenesis, and may advance understanding of the genetic regulatory pathways in play in more complex genetic human disease.

References

Aaltonen, J. *et al.* (1997) 'An autoimmune disease, APECED, caused by mutations in a novel gene featuring two PHD-type zinc-finger domains', *Nature Genetics*, 17(december), pp. 399–403.

Abeler-Dörner, L. *et al.* (2020) 'High-throughput phenotyping reveals expansive genetic and structural underpinnings of immune variation', *Nature Immunology*. Nature Research, 21(1), pp. 86–100. doi: 10.1038/s41590-019-0549-0.

Acuto, O. and Michel, F. (2003) 'CD28-mediated co-stimulation: A quantitative support for TCR signalling', *Nature Reviews Immunology*, 3(12), pp. 939–951. doi: 10.1038/nri1248.

Adigbli, G. *et al.* (2021) 'Development of LT-HSC-Reconstituted Non-Irradiated NBSGW Mice for the Study of Human Hematopoiesis In Vivo', *Frontiers in Immunology*, 12. doi: 10.3389/fimmu.2021.642198.

Aggarwal, R. *et al.* (2009) 'Anti-citrullinated peptide antibody assays and their role in the diagnosis of rheumatoid arthritis', *Arthritis Care and Research*. Arthritis Rheum, 61(11), pp. 1472–1483. doi: 10.1002/art.24827.

Allen, C. D. C. *et al.* (2004) 'Germinal center dark and light zone organization is mediated by CXCR4 and CXCR5', *Nature Immunology 2004 5:9*. Nature Publishing Group, 5(9), pp. 943–952. doi: 10.1038/ni1100.

Allman, D. *et al.* (2001) 'Resolution of Three Nonproliferative Immature Splenic B Cell Subsets Reveals Multiple Selection Points During Peripheral B Cell Maturation', *The Journal of Immunology*. J Immunol, 167(12), pp. 6834–6840. doi: 10.4049/jimmunol.167.12.6834.

Alt, F. W. *et al.* (1984) 'Ordered rearrangement of immunoglobulin heavy chain variable region segments.', *The EMBO journal*, 3(6), pp. 1209–1219. doi: 10.1002/j.1460-2075.1984.tb01955.x.

Amaya-Uribe, L. *et al.* (2019) 'Primary immunodeficiency and autoimmunity: A comprehensive review', *Journal of Autoimmunity*, 99, pp. 52–72. doi: 10.1016/j.jaut.2019.01.011.

Anderson, M. S. *et al.* (2005) 'The cellular mechanism of Aire control of T cell tolerance', *Immunity*, 23(2), pp. 227–239. doi: 10.1016/j.immuni.2005.07.005.

Anderson, M. S. and Su, M. A. (2011) 'Aire and T cell development', *Current Opinion in Immunology*. NIH Public Access, pp. 198–206. doi: 10.1016/j.coi.2010.11.007.

Andris, F. *et al.* (2017) 'The Transcription Factor c-Maf Promotes the Differentiation of Follicular Helper T Cells', *Frontiers in Immunology*. Frontiers, 0(APR), p. 480. doi: 10.3389/FIMMU.2017.00480.

Angst, E. *et al.* (2011) 'N-myc downstream regulated gene-1 expression correlates with reduced pancreatic cancer growth and increased apoptosis in vitro and in vivo', *Surgery*. Mosby, 149(5), pp. 614–624. doi: 10.1016/j.surg.2010.11.002.

Annacker, O. *et al.* (2003) 'Interleukin-10 in the regulation of T cell-induced colitis', *Journal of Autoimmunity*. Academic Press, pp. 277–279. doi: 10.1016/S0896-8411(03)00045-3.

Anzilotti, C. *et al.* (2019) 'An essential role for the Zn 2+ transporter ZIP7 in B cell development', *Nature Immunology*. NIH Public Access, 20(3), pp. 350–361. doi: 10.1038/s41590-018-0295-8.

Arbuckle, M. R. *et al.* (2003) 'Development of Autoantibodies before the Clinical Onset of Systemic Lupus Erythematosus', *New England Journal of Medicine*. Massachusetts Medical Society , 349(16), pp. 1526–1533. doi: 10.1056/nejmoa021933.

Arnett, F. C. and Reveille, J. D. (1992) 'Genetics of systemic lupus erythematosus', *Rheumatic Disease Clinics of North America*, 18(4), pp. 865–892. doi: 10.1016/s0889-857x(21)00155-1.

Arruvito, L. *et al.* (2007) ' Expansion of CD4 + CD25 + and FOXP3 + Regulatory T Cells during the Follicular Phase of the Menstrual Cycle: Implications for Human Reproduction ', *The Journal of Immunology*. The American Association of Immunologists, 178(4), pp. 2572–2578. doi: 10.4049/jimmunol.178.4.2572.

Arvaniti, P. *et al.* (2020) 'Belimumab is a promising third-line treatment option for refractory autoimmune hepatitis', *JHEP Reports*, 2(4). doi: 10.1016/j.jhepr.2020.100123.

Austin, C. P. *et al.* (2004) 'The Knockout Mouse Project', *Nature Genetics*. Nature Publishing Group, 36(9), pp. 921–924. doi: 10.1038/ng0904-921.

Bachmaier, K. *et al.* (2000) 'Negative regulation of lymphocyte activation and autoimmunity by the molecular adaptor Cbl-b', *Nature*. Nature Publishing Group, 403(6766), pp. 211–216. doi: 10.1038/35003228.

Baine, I., Abe, B. T. and Macian, F. (2009) 'Regulation of T-cell tolerance by calcium/NFAT signaling', *Immunological Reviews*, 231(1), pp. 225–240. doi: 10.1111/j.1600-065X.2009.00817.x.

Bandyopadhyay, S. *et al.* (2003) *The Drg-1 gene suppresses tumor metastasis in prostate*

cancer, *Cancer Research*. Available at: https://pubmed.ncbi.nlm.nih.gov/12702552/ (Accessed: 2 February 2021).

Bandyopadhyay, S. *et al.* (2004) 'Role of the putative tumor metastasis suppressor gene Drg-1 in breast cancer progression', *Oncogene*. Oncogene, 23(33), pp. 5675–5681. doi: 10.1038/sj.onc.1207734.

Barnden, M. J. *et al.* (1998) 'Defective TCR expression in transgenic mice constructed using cDNA- based α- and β-chain genes under the control of heterologous regulatory elements', *Immunology and Cell Biology*, 76(1), pp. 34–40. doi: 10.1046/j.1440-1711.1998.00709.x.

Barrington, R. A. *et al.* (2006) 'Involvement of NFAT1 in B Cell Self-Tolerance', *The Journal of Immunology*. American Association of Immunologists, 177(3), pp. 1510–1515. doi: 10.4049/jimmunol.177.3.1510.

Barthlott, T., Kassiotis, G. and Stockinger, B. (2003) 'T cell regulation as a side effect of homeostasis and competition', *Journal of Experimental Medicine*. J Exp Med, 197(4), pp. 451–460. doi: 10.1084/jem.20021387.

Baxter, A. G. and Hodgkin, P. D. (2002) 'Activation rules: The two-signal theories of immune activation', *Nature Reviews Immunology*, pp. 439–446. doi: 10.1038/nri823.

Bedell, M. A., Jenkins, N. A. and Copeland, N. G. (1997) 'Mouse models of human disease. Part I: Techniques and resources for genetic analysis in mice', *Genes and Development*, 11(1), pp. 1–10. doi: 10.1101/gad.11.1.1.

Belkaid, Y. and Hand, T. W. (2014) 'Role of the microbiota in immunity and inflammation', *Cell*. Cell Press, pp. 121–141. doi: 10.1016/j.cell.2014.03.011.

Bell, E. B. and Sparshott, S. M. (1997) 'The peripheral T-cell pool: regulation by non-antigen induced proliferation?'

Bengtsson, A. A. *et al.* (2000) 'Activation of type I interferon system in systemic lupus erythematosus correlates with disease activity but not with antiretroviral antibodies', *Lupus*, 9(9), pp. 664–671. doi: 10.1191/096120300674499064.

Bennett, C. L. *et al.* (2001) 'The immune dysregulation, polyendocrinopathy, enteropathy, X-linked syndrome (IPEX) is caused by mutations of FOXP3', *Nature Genetics*, 27(1), pp. 20–21. doi: 10.1038/83713.

Benschop, R. J. *et al.* (2001) 'Activation and anergy in bone marrow B cells of a novel immunoglobulin transgenic mouse that is both hapten specific and autoreactive', *Immunity*, 14(1), pp. 33–43. doi: 10.1016/S1074-7613(01)00087-5.

Benseler, V. *et al.* (2011) 'Hepatocyte entry leads to degradation of autoreactive CD8 T cells', *Proceedings of the National Academy of Sciences of the United States of America*. National Academy of Sciences, 108(40), pp. 16735–16740. doi: 10.1073/pnas.1112251108.

Bernardo, I. *et al.* (2011) 'Phenotypic and functional evaluation of CD3 +CD4 -CD8 -T cells in human cd8 immunodeficiency', *Haematologica*, 96(8), pp. 1195–1203. doi: 10.3324/haematol.2011.041301.

Besio, R. *et al.* (2015) 'Lack of prolidase causes a bone phenotype both in human and in mouse', *Bone*. Elsevier, 72, pp. 53–64. doi: 10.1016/j.bone.2014.11.009.

Beutler, B., Du, X. and Xia, Y. (2007) 'Precis on forward genetics in mice', *Nature Immunology*, 8(7), pp. 659–664. doi: 10.1038/ni0707-659.

Beverly, B. *et al.* (1992) 'Reversal of in vitro T cell clonal anergy by IL-2 stimulation', *International Immunology*, 4(6), pp. 661–671. doi: 10.1093/intimm/4.6.661.

Bézieux, H. R. de *et al.* (2021) 'Trajectory inference across multiple conditions with condiments: differential topology, progression, differentiation, and expression', *bioRxiv*. Cold Spring Harbor Laboratory, p. 2021.03.09.433671. doi: 10.1101/2021.03.09.433671.

Blasius, A. L. *et al.* (2010) 'Slc15a4, AP-3, and Hermansky-Pudlak syndrome proteins are required for Toll-like receptor signaling in plasmacytoid dendritic cells', *Proceedings of the National Academy of Sciences of the United States of America*, 107(46), pp. 19973–19978. doi: 10.1073/pnas.1014051107.

Blighe, K., Rana, S. and Lewis, M. (2019) 'EnhancedVolcano: Publication-ready volcano plots with enhanced colouring and labelin', *R-Package*, pp. 1–8.

Boekel, E. Ten, Melchers, F. and Rolink, A. (1995) 'The status of Ig loci rearrangements in single cells from different stages of B cell development', *International Immunology*, 7(6), pp. 1013–1019. doi: 10.1093/intimm/7.6.1013.

Borde, M. *et al.* (2006) 'Transcriptional basis of lymphocyte tolerance', *Immunological Reviews*. John Wiley & Sons, Ltd, 210(1), pp. 105–119. doi: 10.1111/j.0105-2896.2006.00370.x.

Boyman, O. (2010) 'Bystander activation of CD4+ T cells', *European Journal of Immunology*, 40(4), pp. 936–939. doi: 10.1002/eji.201040466.

Boyton, R. J. and Altmann, D. M. (2002) 'Transgenic models of autoimmune disease', *Clinical and Experimental Immunology*. Wiley-Blackwell, pp. 4–11. doi: 10.1046/j.1365-2249.2002.01771.x.

Brand, D. D., Latham, K. A. and Rosloniec, E. F. (2007) 'Collagen-induced arthritis', *Nature Protocols*. Nature Publishing Group, 2(5), pp. 1269–1275. doi: 10.1038/nprot.2007.173.

Breed, E. R., Lee, S. T. and Hogquist, K. A. (2018) 'Directing T cell Fate: How Thymic Antigen Presenting Cells Coordinate Thymocyte Selection', *Seminars in cell & developmental biology*. NIH Public Access, 84, p. 2. doi: 10.1016/J.SEMCDB.2017.07.045.

Bretscher, P. A. (1999) *A two-step, two-signal model for the primary activation of precursor helper T cells*, *Proceedings of the National Academy of Sciences of the United States of America*. doi: 10.1073/pnas.96.1.185.

Bretscher, P. and Cohn, M. (1970) 'A theory of self-nonself discrimination', *Science*, 169(3950), pp. 1042–1049. doi: 10.1126/science.169.3950.1042.

Briney, B. S. and Crowe, J. E. J. (2013) 'Secondary mechanisms of diversification in the human antibody repertoire', *Frontiers in Immunology*. Frontiers, 0(MAR), p. 42. doi: 10.3389/FIMMU.2013.00042.

Brink, R. and Phan, T. G. (2018) 'Self-Reactive B Cells in the Germinal Center Reaction', *Annual Review of Immunology*, 36, pp. 339–357. doi: 10.1146/annurev-immunol-051116-052510.

Brown, S. D. M. (2021) 'Advances in mouse genetics for the study of human disease', *Human Molecular Genetics*. doi: 10.1093/hmg/ddab153.

Browne, C. D. *et al.* (2009) 'Suppression of PI(3,4,5)P3 production is a key determinant of B cell anergy', *Immunity*, 31(5), pp. 749–760.

Bruggner, R. V. *et al.* (2014) 'Automated identification of stratifying signatures in cellular subpopulations', *Proceedings of the National Academy of Sciences of the United States of America*. Proc Natl Acad Sci U S A, 111(26). doi: 10.1073/pnas.1408792111.

Brunkow, M. E. *et al.* (2001) 'Disruption of a new forkhead/winged-helix protein, scurfin, results in the fatal lymphoproliferative disorder of the scurfy mouse', *Nature Genetics*. Nature Publishing Group, 27(1), pp. 68–73. doi: 10.1038/83784.

Brunstein, C. G. *et al.* (2011) 'Infusion of ex vivo expanded T regulatory cells in adults transplanted with umbilical cord blood: Safety profile and detection kinetics', *Blood*. Blood, 117(3), pp. 1061–1070. doi: 10.1182/blood-2010-07-293795.

Bull, K. R. *et al.* (2013) 'Unlocking the Bottleneck in Forward Genetics Using Whole-Genome Sequencing and Identity by Descent to Isolate Causative Mutations', *PLoS Genetics*. PLoS Genet, 9(1). doi: 10.1371/journal.pgen.1003219.

Burkly, L. C. *et al.* (1993) 'Clonal deletion of Vβ5+ T cells by transgenic I-E restricted to thymic medullary epithelium', *The Journal of Immunology*, 151(8), pp. 3954–3960.

Butbul Aviel, Y. *et al.* (2012) 'Prolidase deficiency associated with systemic lupus erythematosus (SLE): Single site experience and literature review', *Pediatric Rheumatology*. BioMed Central, 10(1), p. 18. doi: 10.1186/1546-0096-10-18.

Bygrave, A. E. *et al.* (2004) 'Spontaneous autoimmunity in 129 and C57BL/6 mice-implications for autoimmunity described in gene-targeted mice', *PLoS Biology*, 2(8). doi: 10.1371/journal.pbio.0020243.

Cambier, J. C. *et al.* (2007) 'B-cell anergy: From transgenic models to naturally occurring anergic B cells?', *Nature Reviews Immunology*, 7(8), pp. 633–643. doi: 10.1038/nri2133.

Cao, X. *et al.* (2007) 'Granzyme B and Perforin Are Important for Regulatory T Cell-Mediated Suppression of Tumor Clearance', *Immunity*. Immunity, 27(4), pp. 635–646. doi: 10.1016/j.immuni.2007.08.014.

Carlson, M. (2019) 'org.Mm.eg.db: Genome wide annotation for Mouse. R package version 3.8.2.', *Bioconductor*.

Caulfield, M. *et al.* (2017) 'The 100,000 Genomes Project Protocol', *The Genomics England Protocol*, (January), pp. 1–112.

Caza, T. and Landas, S. (2015) 'Functional and Phenotypic Plasticity of CD4+ T Cell Subsets', *BioMed Research International*, 2015, p. 10.1155/2015/521957. doi: 10.1155/2015/521957.

Cebrian-Serrano, A. *et al.* (2017) 'Maternal supply of cas9 to zygotes facilitates the efficient generation of site-specific mutant mouse models', *PLoS ONE*. Edited by H. Fujii. Public Library of Science, 12(1), p. e0169887. doi: 10.1371/journal.pone.0169887.

Cerwenka, A. *et al.* (1998) 'In vivo persistence of CD8 polarized T cell subsets producing type 1 or type 2 cytokines', *Journal of immunology (Baltimore, Md. : 1950)*, 161(1), pp. 97–105.

Chang, X. *et al.* (2016) 'NDRG1 Controls Gastric Cancer Migration and Invasion through Regulating MMP-9', *Pathology and Oncology Research*. Springer Netherlands, 22(4), pp. 789–796. doi: 10.1007/s12253-016-0071-8.

Chappert, P. and Schwartz, R. H. (2010) 'Induction of T cell anergy: Integration of environmental cues and infectious tolerance', *Current Opinion in Immunology*, 22(5), pp. 552–559. doi: 10.1016/j.coi.2010.08.005.

Chen, H. *et al.* (2016) 'Cytofkit: A Bioconductor Package for an Integrated Mass Cytometry Data Analysis Pipeline', *PLoS Computational Biology*. PLoS Comput Biol, 12(9). doi: 10.1371/journal.pcbi.1005112.

Chen, W. H. *et al.* (2013) 'Human Monogenic Disease Genes Have Frequently Functionally Redundant Paralogs', *PLoS Computational Biology*, 9(5). doi: 10.1371/journal.pcbi.1003073.

Chen, W. J. *et al.* (2003) 'Conversion of Peripheral CD4+CD25- Naive T Cells to CD4+CD25+ Regulatory T Cells by TGF-β Induction of Transcription Factor Foxp3', *Journal of Experimental Medicine*, 198(12), pp. 1875–1886. doi: 10.1084/jem.20030152.

Chen, Y. G., Mathews, C. E. and Driver, J. P. (2018) 'The role of NOD mice in type 1 diabetes research: Lessons from the past and recommendations for the future', *Frontiers in Endocrinology*. Frontiers Media S.A., 9(FEB), p. 51. doi: 10.3389/fendo.2018.00051.

Chen, Z. *et al.* (2012) 'The iron chelators Dp44mT and DFO inhibit TGF-β-induced epithelial-mesenchymal transition via up-regulation of N-Myc downstream-regulated gene 1 (NDRG1)', *Journal of Biological Chemistry*, 287(21), pp. 17016–17028. doi: 10.1074/jbc.M112.350470.

Chen, Z. *et al.* (2018) 'Iron chelator-induced up-regulation of Ndrg1 inhibits proliferation and EMT process by targeting Wnt/β-catenin pathway in colon cancer cells', *Biochemical and Biophysical Research Communications*. Elsevier B.V., 506(1), pp. 114–121. doi: 10.1016/j.bbrc.2018.10.054.

Chen, Z. *et al.* (2019) 'TCF-1-Centered Transcriptional Network Drives an Effector versus Exhausted CD8 T Cell-Fate Decision', *Immunity*. Cell Press, 51(5), pp. 840-855.e5. doi: 10.1016/J.IMMUNI.2019.09.013.

Chevrier, S. *et al.* (2018) 'Compensation of Signal Spillover in Suspension and Imaging Mass Cytometry', *Cell Systems*. Cell Syst, 6(5), pp. 612-620.e5. doi: 10.1016/j.cels.2018.02.010.

Chikuma, S. *et al.* (2009) ' PD-1-Mediated Suppression of IL-2 Production Induces CD8 + T Cell Anergy In Vivo ', *The Journal of Immunology*, 182(11), pp. 6682–6689. doi: 10.4049/jimmunol.0900080.

Chiodetti, L. *et al.* (2006) 'Adaptive Tolerance and Clonal Anergy Are Distinct Biochemical States', *The Journal of Immunology*. American Association of Immunologists, 176(4), pp. 2279–2291. doi: 10.4049/jimmunol.176.4.2279.

Choi, S. and Schwartz, R. H. (2007) 'Molecular mechanisms for adaptive tolerance and

other T cell anergy models', *Seminars in Immunology*, 19(3), pp. 140–152. doi: 10.1016/j.smim.2007.02.005.

Chua, M. S. *et al.* (2007) 'Overexpression of NDRG1 is an indicator of poor prognosis in hepatocellular carcinoma', *Modern Pathology*. Nature Publishing Group, 20(1), pp. 76–83. doi: 10.1038/modpathol.3800711.

Chung, S. A. and Shum, A. K. (2016) 'Rare variants, autoimmune disease, and arthritis', *Current Opinion in Rheumatology*, 28(4), pp. 346–351. doi: 10.1097/BOR.0000000000000298.

Chung, Y. *et al.* (2011) 'Follicular regulatory T cells expressing Foxp3 and Bcl-6 suppress germinal center reactions', *Nature Medicine*. Nat Med, 17(8), pp. 983–988. doi: 10.1038/nm.2426.

Cinamon, G. *et al.* (2004) 'Sphingosine 1-phosphate receptor 1 promotes B cell localization in the splenic marginal zone', *Nature Immunology*. Nat Immunol, 5(7), pp. 713–720. doi: 10.1038/ni1083.

Cirulli, E. T. and Goldstein, D. B. (2010) 'Uncovering the roles of rare variants in common disease through whole-genome sequencing', *Nature Reviews Genetics*, 11(6), pp. 415–425. doi: 10.1038/nrg2779.

Clarke, S. Rm. K. *et al.* (2000) 'Characterization of the ovalbumin-specific TCR transgenic line OT-I: MHC elements for positive and negative selection', *Immunology and Cell Biology*, 78(2), pp. 110–117. doi: 10.1046/j.1440-1711.2000.00889.x.

Cleary, M. A. *et al.* (1994) 'Immune function in prolidase deficiency', *Journal of Inherited Metabolic Disease*. Kluwer Academic Publishers, 17(3), pp. 345–348. doi: 10.1007/BF00711826.

Clemente, T. *et al.* (2017) 'Proteomic and functional analysis identifies galectin-1 as a novel regulatory component of the cytotoxic granule machinery', *Cell death & disease*. Nature Publishing Group, 8(12), p. e3176. doi: 10.1038/cddis.2017.506.

Collier, J. L. *et al.* (2021) 'Not-so-opposite ends of the spectrum: CD8+ T cell dysfunction across chronic infection, cancer and autoimmunity', *Nature Immunology 2021 22:7*. Nature Publishing Group, 22(7), pp. 809–819. doi: 10.1038/s41590-021-00949-7.

Collins, S. *et al.* (2008) 'Opposing regulation of T cell function by Egr-1/NAB 2 and Egr-2/Egr-3', *European Journal of Immunology*. Eur J Immunol, 38(2), pp. 528–536. doi: 10.1002/eji.200737157.

Consortium, I. M. K. *et al.* (2007) 'A Mouse for All Reasons', *Cell*. Cell Press, pp. 9–13. doi: 10.1016/j.cell.2006.12.018.

Cook, M. C., Basten, A. and Fazekas De St. Groth, B. (1998) 'Rescue of self-reactive B cells by provision of T cell help in vivo', *European Journal of Immunology*, 28(8), pp. 2549–2558. doi: 10.1002/(SICI)1521-4141(199808)28:08<2549::AID-IMMU2549>3.0.CO;2-O.

Cooke, M. P. *et al.* (1994) 'Immunoglobulin signal transduction guides the specificity of B cell-T cell interactions and is blocked in tolerant self-reactive B cells', *Journal of Experimental Medicine*. Rockefeller University Press, 179(2), pp. 425–438. doi: 10.1084/jem.179.2.425.

Cordes, S. P. (2005) ' N -Ethyl- N -Nitrosourea Mutagenesis: Boarding the Mouse Mutant Express ', *Microbiology and Molecular Biology Reviews*. American Society for Microbiology, 69(3), pp. 426–439. doi: 10.1128/mmbr.69.3.426-439.2005.

Cotsapas, C. *et al.* (2011) 'Pervasive sharing of genetic effects in autoimmune disease', *PLoS Genetics*. Public Library of Science, 7(8). doi: 10.1371/journal.pgen.1002254.

Craxton, A. *et al.* (2005) 'BAFF regulates B cell survival by downregulating the BH3-only family member Bim via the ERK pathway', *Journal of Experimental Medicine*. The Rockefeller University Press, 202(10), pp. 1363–1374. doi: 10.1084/jem.20051283.

Criswell, L. A. *et al.* (2005) *Analysis of families in the multiple autoimmune disease genetics consortium (MADGC) collection: The PTPN22 620W allele associates with multiple autoimmune phenotypes*, *American Journal of Human Genetics*. doi: 10.1086/429096.

Crotty, S. (2014) 'T Follicular Helper Cell Differentiation, Function, and Roles in Disease', *Immunity*. Cell Press, pp. 529–542. doi: 10.1016/j.immuni.2014.10.004.

Crow, Y. J. *et al.* (2006) 'Mutations in the gene encoding the 3'-5' DNA exonuclease TREX1 cause Aicardi-Goutières syndrome at the AGS1 locus', *Nature Genetics*, 38(8), pp. 917–920. doi: 10.1038/ng1845.

Crowell, H. L. *et al.* (2020) 'Muscat Detects Subpopulation-Specific State Transitions From Multi-Sample Multi-Condition Single-Cell Transcriptomics Data', *Nature Communications*, 11(1). doi: 10.1038/s41467-020-19894-4.

Cunningham, A. F. *et al.* (2014) 'B1b cells recognize protective antigens after natural infection and vaccination', *Frontiers in Immunology*. Frontiers Media S.A. doi: 10.3389/fimmu.2014.00535.

Cusick, M. F., Libbey, J. E. and Fujinami, R. S. (2012) 'Molecular mimicry as a mechanism of

autoimmune disease', *Clinical Reviews in Allergy and Immunology*. Nature Publishing Group, 42(1), pp. 102–111. doi: 10.1007/s12016-011-8294-7.

Cyster, J. G. and Goodnow, C. C. (1995) 'Antigen-induced exclusion from follicles and anergy are separate and complementary processes that influence peripheral B cell fate', *Immunity*, 3(6), pp. 691–701. doi: 10.1016/1074-7613(95)90059-4.

Cyster, J. G., Hartley, S. B. and Goodnow, C. C. (1994) 'Competition for follicular niches excludes self-reactive cells from the recirculating B-cell repertoire', *Nature*, 371(6496), pp. 389–395. doi: 10.1038/371389a0.

Dawes, J. C. and Uren, A. G. (2021) 'Forward and Reverse Genetics of B Cell Malignancies: From Insertional Mutagenesis to CRISPR-Cas', *Frontiers in Immunology*, 12. doi: 10.3389/fimmu.2021.670280.

De la Calle-Martin, O. *et al.* (2001) 'Familial CD8 deficiency due to a mutation in the CD8α gene', *Journal of Clinical Investigation*. American Society for Clinical Investigation, 108(1), pp. 117–123. doi: 10.1172/JCI10993.

Delmonte, O. M. *et al.* (2019) 'Inborn Errors of Immunity With Immune Dysregulation: From Bench to Bedside', *Frontiers in Pediatrics*, 7. doi: 10.3389/fped.2019.00353.

Diao, H. and Pipkin, M. (2019) 'Stability and flexibility in chromatin structure and transcription underlies memory CD8 T-cell differentiation [version 1; peer review: 2 approved]', *F1000Research*. F1000Res, 8. doi: 10.12688/f1000research.18211.1.

Dolmetsch, R. E. *et al.* (1997) 'Differential activation of transcription factors induced by Ca2+ response amplitude and duration', *Nature*. Nature Publishing Group, 386(6627), pp. 855–858. doi: 10.1038/386855a0.

Dudek, M. *et al.* (2021) 'Auto-aggressive CXCR6+ CD8 T cells cause liver immune pathology in NASH', *Nature*. Nature Publishing Group, 592(7854), pp. 444–449. doi: 10.1038/s41586-021-03233-8.

Dumontet, E. *et al.* (2015) 'Recurrent Respiratory Infections Revealing CD8α Deficiency', *Journal of Clinical Immunology*, 35(8), pp. 692–695. doi: 10.1007/s10875-015-0213-x.

Duty, J. A. *et al.* (2009) 'Functional anergy in a subpopulation of naive B cells from healthy humans that express autoreactive immunoglobulin receptors', *Journal of Experimental Medicine*, 206(1), pp. 139–151. doi: 10.1084/jem.20080611.

Echaniz-Laguna, A. *et al.* (2007) 'NDRG1-linked Charcot-Marie-Tooth disease (CMT4D) with central nervous system involvement', *Neuromuscular Disorders*. Elsevier Ltd, 17(2), pp.

163–168. doi: 10.1016/j.nmd.2006.10.002.

Elhanati, Y. *et al.* (2015) 'Inferring processes underlying B-cell repertoire diversity', *Philosophical Transactions of the Royal Society B: Biological Sciences*. Royal Society of London, 370(1676). doi: 10.1098/rstb.2014.0243.

Elizabeth Franks, S. and Cambier, J. C. (2018) 'Putting on the brakes: Regulatory kinases and phosphatases maintaining B cell anergy', *Frontiers in Immunology*. Frontiers, 9(APR), p. 665. doi: 10.3389/fimmu.2018.00665.

Ellen, T. P. *et al.* (2008) 'NDRG1, a growth and cancer related gene: Regulation of gene expression andfunction in normal and disease states', *Carcinogenesis*. Oxford Academic, 29(1), pp. 2–8. doi: 10.1093/carcin/bgm200.

Enders, A. *et al.* (2003) 'Loss of the pro-apoptotic BH3-only Bcl-2 family member Bim inhibits BCR stimulation-induced apoptosis and deletion of autoreactive B cells', *Journal of Experimental Medicine*. J Exp Med, 198(7), pp. 1119–1126. doi: 10.1084/jem.20030411.

Ermann, J. and Glimcher, L. H. (2012) 'After GWAS: Mice to the rescue?', *Current Opinion in Immunology*. NIH Public Access, 24(5), pp. 564–570. doi: 10.1016/j.coi.2012.09.005.

Falik-Zaccai, T. C. *et al.* (2010) 'A broad spectrum of developmental delay in a large cohort of prolidase deficiency patients demonstrates marked interfamilial and intrafamilial phenotypic variability', *American Journal of Medical Genetics Part B: Neuropsychiatric Genetics*. John Wiley & Sons, Ltd, 153B(1), pp. 46–56. doi: 10.1002/AJMG.B.30945.

Fang, B. A. *et al.* (2014) 'Molecular functions of the iron-regulated metastasis suppressor, NDRG1, and its potential as a molecular target for cancer therapy', *Biochimica et Biophysica Acta - Reviews on Cancer*. Biochim Biophys Acta, 1845(1), pp. 1–19. doi: 10.1016/j.bbcan.2013.11.002.

Farid, N. R. *et al.* (1980) 'Polyglandular Autoimmune Disease and HLA', *Tissue Antigens*, 16(1), pp. 23–29. doi: 10.1111/j.1399-0039.1980.tb00284.x.

Fathman, C. G. and Lineberry, N. B. (2007) 'Molecular mechanisms of CD4+ T-cell anergy', *Nature Reviews Immunology*. Nature Publishing Group, 7(8), pp. 599–609. doi: 10.1038/nri2131.

Ferreira, C. R. and Cusmano-Ozog, K. (2017) 'Spurious elevation of multiple urine amino acids by ion-exchange chromatography in patients with prolidase deficiency', *JIMD Reports*, 31, pp. 45–49. doi: 10.1007/8904_2016_552.

Ferreira, C. and Wang, H. (2015) 'Prolidase Deficiency', *Skin research*. University of

Washington, Seattle, 30(6), pp. 734–740.

Ferry, H. *et al.* (2003) 'The Cellular Location of Self-antigen Determines the Positive and Negative Selection of Autoreactive B Cells', *Journal of Experimental Medicine*. J Exp Med, 198(9), pp. 1415–1425. doi: 10.1084/jem.20030279.

Ferry, H. *et al.* (2006) 'B-cell tolerance', *Transplantation*, 81(3), pp. 308–315. doi: 10.1097/01.tp.0000203830.79357.39.

Fields, M. L. and Erikson, J. (2003) 'The regulation of lupus-associated autoantibodies: Immunoglobulin transgenic models', *Current Opinion in Immunology*. Elsevier Current Trends, pp. 709–717. doi: 10.1016/j.coi.2003.09.016.

Fischer, A. *et al.* (2017) 'Autoimmune and inflammatory manifestations occur frequently in patients with primary immunodeficiencies', *Journal of Allergy and Clinical Immunology*, 140(5), pp. 1388-1393.e8. doi: 10.1016/j.jaci.2016.12.978.

Flajnik, M. F. and Kasahara, M. (2010) 'Origin and evolution of the adaptive immune system: Genetic events and selective pressures', *Nature Reviews Genetics*. NIH Public Access, pp. 47–59. doi: 10.1038/nrg2703.

Frauwirth, K. A. *et al.* (2002) 'The CD28 Signaling Pathway Regulates Glucose Metabolism', *Immunity*, 16, pp. 769–777.

Freitas, A. A. and Rocha, B. B. (1993) 'Lymphocyte lifespans: homeostasis, selection and competition', *Immunology Today*. Immunol Today, 14(1), pp. 25–29. doi: 10.1016/0167-5699(93)90320-K.

Friedline, R. H. *et al.* (2009) 'CD4+ regulatory T cells require CTLA-4 for the maintenance of systemic tolerance', *Journal of Experimental Medicine*, 206(3), pp. 721–721. doi: 10.1084/jem.2008181120409c.

Fulcher, D. A. *et al.* (1996) 'The fate of self-reactive B cells depends primarily on the degree of antigen receptor engagement and availability of T cell help', *Journal of Experimental Medicine*, 183(5), pp. 2313–2328. doi: 10.1084/jem.183.5.2313.

Gabriel, C. M. *et al.* (2002) 'Immunological study of hereditary motor and sensory neuropathy type 1 a (HMSN 1 a)', *Journal of Neurology Neurosurgery and Psychiatry*, 72(2), pp. 230–235. doi: 10.1136/jnnp.72.2.230.

Gaffney, P. M. *et al.* (1998) *A genome-wide search for susceptibility genes in human systemic lupus erythematosus sib-pair families*, *Proceedings of the National Academy of Sciences of the United States of America*. doi: 10.1073/pnas.95.25.14875.

Gauld, S. B. *et al.* (2005) 'Maintenance of B cell anergy requires constant antigen receptor occupancy and signaling', *Nature Immunology*, 6(11), pp. 1160–1167. doi: 10.1038/ni1256.

Gibbs, R. A. *et al.* (2002) 'Initial sequencing and comparative analysis of the mouse genome', *Nature*, 420(6915), pp. 520–62.

Godfrey, V. L., Wilkinson, J. E. and Russell, L. B. (1991) 'X-linked lymphoreticular disease in the scurfy (sf) mutant mouse', *American Journal of Pathology*, 138(6), pp. 1379–1387.

Golubovskaya, V. and Wu, L. (2016) 'Different subsets of T cells, memory, effector functions, and CAR-T immunotherapy', *Cancers*. Multidisciplinary Digital Publishing Institute (MDPI), 8(3). doi: 10.3390/cancers8030036.

Goodnow, C. C. *et al.* (1988) 'Altered immunoglobulin expression and functional silencing of self-reactive B lymphocytes in transgenic mice', *Nature*. Nature Publishing Group, 334(6184), pp. 676–682. doi: 10.1038/334676a0.

Goodnow, C. C. *et al.* (2005) 'Cellular and genetic mechanisms of self tolerance and autoimmunity', *Nature*. Nature Publishing Group, pp. 590–597. doi: 10.1038/nature03724.

Gourraud, P. A. *et al.* (2012) 'The genetics of multiple sclerosis: An up-to-date review', *Immunological Reviews*. NIH Public Access, 248(1), pp. 87–103. doi: 10.1111/j.1600-065X.2012.01134.x.

Gowthaman, U. *et al.* (2019) 'Identification of a T follicular helper cell subset that drives anaphylactic IgE', *Science*, 365(6456). doi: 10.1126/science.aaw6433.

Graham, R. R. *et al.* (2008) 'Genetic variants near TNFAIP3 on 6q23 are associated with systemic lupus erythematosus', *Nature Genetics*, 40(9), pp. 1059–1061. doi: 10.1038/ng.200.

Gregersen, P. K. and Olsson, L. M. (2009) 'Recent advances in the genetics of autoimmune disease', *Annual Review of Immunology*, 27, pp. 363–391. doi: 10.1146/annurev.immunol.021908.132653.

Grieves, J. L. *et al.* (2015) 'Exonuclease TREX1 degrades double-stranded DNA to prevent spontaneous lupus-like inflammatory disease', *Proceedings of the National Academy of Sciences of the United States of America*, 112(16), pp. 5117–5122. doi: 10.1073/pnas.1423804112.

Groom, J. *et al.* (2002) 'Association of BAFF/BLyS overexpression and altered B cell differentiation with Sjögren's syndrome', *Journal of Clinical Investigation*, 109(1), pp. 59–68. doi: 10.1172/JCI0214121.

Gurumurthy, C. B. *et al.* (2016) 'CRISPR: a versatile tool for both forward and reverse genetics research', *Human Genetics*, 135(9), pp. 971–976. doi: 10.1007/s00439-016-1704-4.

Gutierrez-Arcelus, M., Rich, S. S. and Raychaudhuri, S. (2016) 'Autoimmune diseases-connecting risk alleles with molecular traits of the immune system', *Nature Reviews Genetics*. Nature Publishing Group, pp. 160–174. doi: 10.1038/nrg.2015.33.

Hadaschik, E. N. *et al.* (2015) 'Regulatory T cell-deficient scurfy mice develop systemic autoimmune features resembling lupus-like disease', *Arthritis Research and Therapy*. BioMed Central Ltd., 17(1). doi: 10.1186/s13075-015-0538-0.

Hao, Y. *et al.* (2021) 'Integrated analysis of multimodal single-cell data', *Cell*, 184(13), pp. 3573-3587.e29. doi: 10.1016/j.cell.2021.04.048.

Hardtke, S., Ohl, L. and Förster, R. (2005) 'Balanced expression of CXCR5 and CCR7 on follicular T helper cells determines their transient positioning to lymph node follicles and is essential for efficient B-cell help', *Blood*. American Society of Hematology, 106(6), pp. 1924–1931. doi: 10.1182/BLOOD-2004-11-4494.

Hardy, R. R. *et al.* (1982) 'B-cell subpopulations identified by two-colour fluorescence analysis', *Nature*. Nature Publishing Group, 297(5867), pp. 589–591. doi: 10.1038/297589a0.

Hardy, R. R. *et al.* (1994) 'Distinctive Developmental Origins and Specificities of Murine CD5+ B Cells', *Immunological Reviews*. Immunol Rev, 137(1), pp. 91–118. doi: 10.1111/j.1600-065X.1994.tb00660.x.

Harsha Krovi, S. *et al.* (2020) 'Thymic iNKT single cell analyses unmask the common developmental program of mouse innate T cells', *Nature Communications 2020 11:1*. Nature Publishing Group, 11(1), pp. 1–15. doi: 10.1038/s41467-020-20073-8.

Hassan, A. B. *et al.* (1998) 'Increased serum levels of immunoglobulins, C-reactive protein, type 1 and type 2 cytokines in patients with mixed connective tissue disease', *Journal of Autoimmunity*, 11(5), pp. 503–508. doi: 10.1006/jaut.1998.0236.

Healy, J. I. *et al.* (1997) 'Different nuclear signals are activated by the B cell receptor during positive versus negative signaling', *Immunity*, 6(4), pp. 419–428. doi: 10.1016/S1074-7613(00)80285-X.

Healy, J. I. and Goodnow, C. C. (1998) 'Positive versus negative signaling by lymphocyte antigen receptors', *Annual Review of Immunology*, 16(1), pp. 645–670. doi:

10.1146/annurev.immunol.16.1.645.

Hiam-Galvez, K. J., Allen, B. M. and Spitzer, M. H. (2021) 'Systemic immunity in cancer', *Nature Reviews Cancer*. Nature Publishing Group, 21(6), pp. 345–359. doi: 10.1038/s41568-021-00347-z.

Hippen, K. L., Tze, L. E. and Behrens, T. W. (2000) 'CD5 maintains tolerance in anergic B cells', *Journal of Experimental Medicine*. J Exp Med, 191(5), pp. 883–889. doi: 10.1084/jem.191.5.883.

Hmeljak, J. and Justice, M. J. (2019) 'From gene to treatment: Supporting rare disease translational research through model systems', *DMM Disease Models and Mechanisms*, 12(2). doi: 10.1242/DMM.039271.

Hogquist, K. A. *et al.* (1994) 'T cell receptor antagonist peptides induce positive selection', *Cell*. Cell Press, 76(1), pp. 17–27. doi: 10.1016/0092-8674(94)90169-4.

Holt, M. R. and Koffer, A. (2001) 'Cell motility: Proline-rich proteins promote protrusions', *Trends in Cell Biology*, 11(1), pp. 38–46. doi: 10.1016/S0962-8924(00)01876-6.

Holz, L. E. *et al.* (2008) 'Intrahepatic Murine CD8 T-Cell Activation Associates With a Distinct Phenotype Leading to Bim-Dependent Death', *Gastroenterology*, 135(3), pp. 989–997.

Hosoi, F. *et al.* (2009) 'N-myc downstream regulated gene 1/Cap43 suppresses tumor growth and angiogenesis of pancreatic cancer through attenuation of inhibitor of κB kinase β expression', *Cancer Research*, 69(12), pp. 4983–4991. doi: 10.1158/0008-5472.CAN-08-4882.

Hozumi, K. *et al.* (2004) 'Delta-like 1 is necessary for the generation of marginal zone B cells but not T cells in vivo', *Nature Immunology*. Nat Immunol, 5(6), pp. 638–644. doi: 10.1038/ni1075.

Hsu, P. D., Lander, E. S. and Zhang, F. (2014) 'Development and applications of CRISPR-Cas9 for genome engineering', *Cell*. Cell Press, pp. 1262–1278. doi: 10.1016/j.cell.2014.05.010.

Huang, C.-T. *et al.* (2003) ' CD4 + T Cells Pass Through an Effector Phase During the Process of In Vivo Tolerance Induction ', *The Journal of Immunology*, 170(8), pp. 3945–3953. doi: 10.4049/jimmunol.170.8.3945.

Inobe, M. and Schwartz, R. H. (2004) ' CTLA-4 Engagement Acts as a Brake on CD4 + T Cell Proliferation and Cytokine Production but Is Not Required for Tuning T Cell Reactivity in Adaptive Tolerance ', *The Journal of Immunology*, 173(12), pp. 7239–7248. doi: 10.4049/jimmunol.173.12.7239.

Inozume, T. *et al.* (2010) 'Selection of CD8++PD-1+ lymphocytes in fresh human melanomas enriches for tumor-reactive T cells', *Journal of Immunotherapy*, 33(9), pp. 956–964. doi: 10.1097/CJI.0b013e3181fad2b0.

Ise, W. *et al.* (2010) 'CTLA-4 suppresses the pathogenicity of self antigen-specific T cells by cell-intrinsic and cell-extrinsic mechanisms', *Nature Immunology*, 11(2), pp. 129–135. doi: 10.1038/ni.1835.

Itoh, M. *et al.* (1999) 'Thymus and autoimmunity: production of CD25+CD4+ naturally anergic and suppressive T cells as a key function of the thymus in maintaining immunologic self-tolerance.', *Journal of immunology (Baltimore, Md. : 1950)*, 162(9), pp. 5317–26.

Ivanov, I. I. *et al.* (2006) 'The Orphan Nuclear Receptor RORγt Directs the Differentiation Program of Proinflammatory IL-17+ T Helper Cells', *Cell*, 126(6), pp. 1121–1133. doi: 10.1016/j.cell.2006.07.035.

Jacenko, O., Luvalle, P. A. and Olsen, B. R. (1993) 'Spondylometaphyseal dysplasia in mice carrying a dominant negative mutation in a matrix protein specific for cartilage-to-bone transition', *Nature*, 365(6441), pp. 56–61. doi: 10.1038/365056a0.

Jeon, M. S. *et al.* (2004a) 'Essential role of the E3 ubiquitin ligase Cbl-b in T cell anergy induction', *Immunity*, 21(2), pp. 167–177. doi: 10.1016/j.immuni.2004.07.013.

Jeon, M. S. *et al.* (2004b) 'Essential role of the E3 ubiquitin ligase Cbl-b in T cell anergy induction', *Immunity*. Immunity, 21(2), pp. 167–177. doi: 10.1016/j.immuni.2004.07.013.

Jiang, S. H., Stanley, M. and Vinuesa, C. G. (2020) 'Rare genetic variants in systemic autoimmunity', *Immunology and Cell Biology*. John Wiley and Sons Inc., 98(6), pp. 490–499. doi: 10.1111/imcb.12339.

Johnson, J. G. and Jenkins, M. K. (1994) 'Minireview The role of anergy in peripheral T cell unresponsiveness', *Life Sciences*. Pergamon, 55(23), pp. 1767–1780. doi: 10.1016/0024-3205(94)90087-6.

Jones, S. C., Murphy, G. F. and Korngold, R. (2003) 'Post-hematopoietic cell transplantation control of graft-versus-host disease by donor CD4+25+ T cells to allow an effective graft-versus-leukemia response', *Biology of Blood and Marrow Transplantation*. Biol Blood Marrow Transplant, 9(4), pp. 243–256. doi: 10.1053/bbmt.2003.50027.

Joshi, N. S. *et al.* (2007) 'Inflammation Directs Memory Precursor and Short-Lived Effector CD8(+) T Cell Fates via the Graded Expression of T-bet Transcription Factor', *Immunity*. NIH Public Access, 27(2), p. 281. doi: 10.1016/J.IMMUNI.2007.07.010.

Jung, S. H. *et al.* (2016) 'ARAP, a Novel Adaptor Protein, Is Required for TCR Signaling and Integrin-Mediated Adhesion', *The Journal of Immunology*, 197(3), pp. 942–952. doi: 10.4049/jimmunol.1501913.

Kalaydjieva, L. *et al.* (2000) 'N-myc downstream-regulated gene 1 is mutated in hereditary motor and sensory neuropathy-Lom', *American Journal of Human Genetics*. Am J Hum Genet, 67(1), pp. 47–58. doi: 10.1086/302978.

Kalekar, L. A. *et al.* (2016) 'CD4+ T cell anergy prevents autoimmunity and generates regulatory T cell precursors', *Nature Immunology*, 17(3), pp. 304–314. doi: 10.1038/ni.3331.

Kalekar, L. A. and Mueller, D. L. (2017) 'Relationship between CD4 Regulatory T Cells and Anergy In Vivo', *The Journal of Immunology*, 198(7), pp. 2527–2533. doi: 10.4049/jimmunol.1602031.

Kantor, A. B. *et al.* (1997) *An unbiased analysis of V(H)-D-J(H) sequences from B-1a, B-1b, and conventional B cells.*, *Journal of immunology (Baltimore, Md. : 1950)*.

Karasuyama, H., Kudo, A. and Melchers, F. (1990) 'The proteins encoded by the VpreB and λ5 Pre-B cell-specific genes can associate with each other and with μ heavy chain', *Journal of Experimental Medicine*, 172(3), pp. 969–972. doi: 10.1084/jem.172.3.969.

Karthikeyan, K. *et al.* (2019) 'Topical proline therapy in prolidase deficiency', *Clinical and Experimental Dermatology*. John Wiley & Sons, Ltd, 44(3), pp. 344–346. doi: 10.1111/ced.13702.

Kearney, E. R. *et al.* (1994) 'Visualization of peptide-specific T cell immunity and peripheral tolerance induction in vivo', *Immunity*, 1(4), pp. 327–339. doi: 10.1016/1074-7613(94)90084-1.

Kendal, A. R. *et al.* (2020) 'Multi-omic single cell analysis resolves novel stromal cell populations in healthy and diseased human tendon', *Scientific Reports 2020 10:1*. Nature Publishing Group, 10(1), pp. 1–14. doi: 10.1038/s41598-020-70786-5.

Khattri, R. *et al.* (2017) 'An essential role for Scurfin in CD4+CD25+T regulatory cells', *Journal of Immunology*. Nature Publishing Group, 198(3), pp. 993–998. doi: 10.1038/ni909.

Killestein, J. and van Oosten, B. (2019) 'Emerging safety issues in alemtuzumab-treated MS patients', *Multiple Sclerosis Journal*, 25(9), pp. 1206–1208. doi: 10.1177/1352458519851219.

Kim, D. *et al.* (2019) 'Graph-based genome alignment and genotyping with HISAT2 and

HISAT-genotype', *Nature Biotechnology*, 37(8), pp. 907–915. doi: 10.1038/s41587-019-0201-4.

Kim, H. *et al.* (2018) 'Mouse Cre-LoxP system: general principles to determine tissue-specific roles of target genes', *Laboratory Animal Research*. Springer Science and Business Media LLC, 34(4), p. 147. doi: 10.5625/lar.2018.34.4.147.

Kim, J. *et al.* (2018) 'Spontaneous Proliferation of CD4+ T Cells in RAG-Deficient Hosts Promotes Antigen-Independent but IL-2-Dependent Strong Proliferative Response of Naïve CD8+ T Cells', *Frontiers in Immunology*, 9. doi: 10.3389/fimmu.2018.01907.

Kimball, A. K. *et al.* (2018) 'A Beginner's Guide To Analyzing and Visualizing Mass Cytometry Data', *Journal of immunology (Baltimore, Md. : 1950)*. NIH Public Access, 200(1), p. 3. doi: 10.4049/JIMMUNOL.1701494.

Kimura, M. *et al.* (2000) 'Impaired Ca/calcineurin pathway in in vivo energized CD4 T cells', *International Immunology*, 12(6), pp. 817–824. doi: 10.1093/intimm/12.6.817.

King, R. H. M. *et al.* (2011) 'Ndrg1 in development and maintenance of the myelin sheath', *Neurobiology of Disease*. Academic Press, 42(3), pp. 368–380. doi: 10.1016/j.nbd.2011.01.030.

Kitaura, Y. *et al.* (2007) 'Control of the B Cell-Intrinsic Tolerance Programs by Ubiquitin Ligases Cbl and Cbl-b', *Immunity*. NIH Public Access, 26(5), pp. 567–578. doi: 10.1016/j.immuni.2007.03.015.

Klarquist, J. and Janssen, E. M. (2015) 'The bm12 inducible model of systemic lupus erythematosus (SLE) in C57BL/6 mice', *Journal of Visualized Experiments*. Journal of Visualized Experiments, 2015(105), p. 53319. doi: 10.3791/53319.

Klein, L. *et al.* (2014) 'Positive and negative selection of the T cell repertoire: What thymocytes see (and don't see)', *Nature Reviews Immunology*, 14(6), pp. 377–391. doi: 10.1038/nri3667.

Korotkevich, G. *et al.* (2016) 'Fast gene set enrichment analysis'. doi: 10.1101/060012.

Kotzin, B. L. (1996) 'Systemic lupus erythematosus', *Cell*. Cell Press, pp. 303–306. doi: 10.1016/S0092-8674(00)81108-3.

Kovacevic, Z. *et al.* (2013) 'The iron-regulated metastasis suppressor NDRG1 targets NEDD4L, PTEN, and SMAD4 and inhibits the PI3K and ras signaling pathways', *Antioxidants and Redox Signaling*, 18(8), pp. 874–887. doi: 10.1089/ars.2011.4273.

Kraus, M. *et al.* (2004) 'Survival of resting mature B lymphocytes depends on BCR signaling

via the Igα/β heterodimer', *Cell*. Cell Press, 117(6), pp. 787–800. doi: 10.1016/j.cell.2004.05.014.

Kronenberg, M. and Rudensky, A. (2005) 'Regulation of immunity by self-reactive T cells', *Nature*. Nature Publishing Group, pp. 598–604. doi: 10.1038/nature03725.

Kudose, S. *et al.* (2019) 'Sensitivity and specificity of pathologic findings to diagnose lupus nephritis', *Clinical Journal of the American Society of Nephrology*, 14(11), pp. 1605–1615. doi: 10.2215/CJN.01570219.

Kuhn, K. A. and Stappenbeck, T. S. (2013) 'Peripheral education of the immune system by the colonic microbiota', *Seminars in Immunology*, 25(5), pp. 364–369. doi: 10.1016/j.smim.2013.10.002.

Kurdistani, S. K. *et al.* (1998) 'Inhibition of tumor cell growth by RTP/rit42 and its responsiveness to p53 and DNA damage', *Cancer Research*, 58(19), pp. 4439–4444.

Kurien, B. T. *et al.* (2013) 'Prolidase deficiency breaks tolerance to lupus-associated antigens', *International Journal of Rheumatic Diseases*. NIH Public Access, 16(6), pp. 674–680. doi: 10.1111/1756-185X.12254.

Laxminarayana, D. (2017) 'Is Tolerance Broken in Autoimmunity?', *Clinical Medicine Insights: Pathology*, 10, pp. 1–5. doi: 10.1177/1179555717712716.

Lee, B. H. *et al.* (2012) 'Animal models in autoimmune diseases: Lessons learned from mouse models for Sjögren's Syndrome', *Clinical Reviews in Allergy and Immunology*, 42(1), pp. 35–44. doi: 10.1007/s12016-011-8288-5.

Lehmann, P. V. *et al.* (1992) 'Spreading of T-cell autoimmunity to cryptic determinants of an autoantigen', *Nature*. Nature, 358(6382), pp. 155–157. doi: 10.1038/358155a0.

Lenschow, D. J. *et al.* (1992) 'Long-term survival of xenogeneic pancreatic islet grafts induced by CTLA4Ig', *Science*. Wiley, 257(5071), pp. 789–792. doi: 10.1126/science.1323143.

Lesley, R. *et al.* (2004) 'Reduced competitiveness of autoantigen-engaged B cells due to increased dependence on BAFF', *Immunity*, 20(4), pp. 441–453. doi: 10.1016/S1074-7613(04)00079-2.

Levinsky, R. J., Cameron, J. S. and Soothill, J. F. (1977) 'Serum Immune Complexes and Disease Activity in Lupus Nephritis', *The Lancet*, 309(8011), pp. 564–567. doi: 10.1016/S0140-6736(77)91998-5.

Li, A. *et al.* (2019) 'Upregulation of NDRG1 predicts poor outcome and facilitates disease

progression by influencing the EMT process in bladder cancer', *Scientific Reports*. Nature Publishing Group, 9(1), pp. 1–12. doi: 10.1038/s41598-019-41660-w.

Li, B. *et al.* (2007) 'FOXP3 is a homo-oligomer and a component of a supramolecular regulatory complex disabled in the human XLAAD/IPEX autoimmune disease', *International Immunology*. Oxford Academic, 19(7), pp. 825–835. doi: 10.1093/intimm/dxm043.

Li, H. *et al.* (2020) 'Applications of genome editing technology in the targeted therapy of human diseases: mechanisms, advances and prospects', *Signal Transduction and Targeted Therapy*, 5(1). doi: 10.1038/s41392-019-0089-y.

Li, L. X. *et al.* (2017) 'Identification and functional characterization of two missense mutations in NDRG1 associated with Charcot-Marie-Tooth disease type 4D', *Human Mutation*. John Wiley and Sons Inc., 38(11), pp. 1569–1578. doi: 10.1002/humu.23309.

Li, M. O., Wan, Y. Y. and Flavell, R. A. (2007) 'T Cell-Produced Transforming Growth Factor-β1 Controls T Cell Tolerance and Regulates Th1- and Th17-Cell Differentiation', *Immunity*. Elsevier, 26(5), pp. 579–591. doi: 10.1016/j.immuni.2007.03.014.

Liao, Y., Smyth, G. K. and Shi, W. (2014) 'FeatureCounts: An efficient general purpose program for assigning sequence reads to genomic features', *Bioinformatics*. Oxford University Press, 30(7), pp. 923–930. doi: 10.1093/bioinformatics/btt656.

Linterman, M. A. *et al.* (2011) 'Foxp3+ follicular regulatory T cells control the germinal center response', *Nature Medicine*, 17(8), pp. 975–982. doi: 10.1038/nm.2425.

Liu, X. *et al.* (2018) 'Regulatory T cells trigger effector T cell DNA damage and senescence caused by metabolic competition', *Nature Communications*, 9(1). doi: 10.1038/s41467-017-02689-5.

Liu, Y. *et al.* (2008) 'A critical function for TGF-β signaling in the development of natural CD4+CD25+Foxp3+ regulatory T cells', *Nature Immunology*. Nature Publishing Group, 9(6), pp. 632–640. doi: 10.1038/ni.1607.

Liu, Z. *et al.* (2011) 'The kinase LRRK2 is a regulator of the transcription factor NFAT that modulates the severity of inflammatory bowel disease', *Nature Immunology*. NIH Public Access, 12(11), pp. 1063–1070. doi: 10.1038/ni.2113.

Loder, F. *et al.* (1999) 'B cell development in the spleen takes place in discrete steps and is determined by the quality of B cell receptor-derived signals', *Journal of Experimental Medicine*. J Exp Med, 190(1), pp. 75–89. doi: 10.1084/jem.190.1.75.

Long, S. A. *et al.* (2016) 'Partial exhaustion of CD8 T cells and clinical response to teplizumab

in new-onset type 1 diabetes', *Science Immunology*. NIH Public Access, 1(5). doi: 10.1126/sciimmunol.aai7793.

Lopes, I. *et al.* (2002) 'Prolidase deficiency with hyperimmunoglobulin E: A case report', *Pediatric Allergy and Immunology*. Pediatr Allergy Immunol, 13(2), pp. 140–142. doi: 10.1034/j.1399-3038.2002.00075.x.

Love, M. I., Huber, W. and Anders, S. (2014) 'Moderated estimation of fold change and dispersion for RNA-seq data with DESeq2', *Genome Biology*. BioMed Central Ltd., 15(12), p. 550. doi: 10.1186/s13059-014-0550-8.

Lu, T. T. and Cyster, J. G. (2002) 'Integrin-mediated long-term B cell retention in the splenic marginal zone', *Science*, 297(5580), pp. 409–412. doi: 10.1126/science.1071632.

Lu, W.-J. J., Chua, M.-S. S. and So, S. K. (2014) 'Suppressing N-Myc downstream regulated gene 1 reactivates senescence signaling and inhibits tumor growth in hepatocellular carcinoma', *Carcinogenesis*. Oxford University Press, 35(4), pp. 915–922. doi: 10.1093/carcin/bgt401.

Lu, W. *et al.* (2014) 'Dual proteolytic pathways govern glycolysis and immune competence', *Cell*, 159(7), pp. 1578–1590. doi: 10.1016/j.cell.2014.12.001.

Lubick, K. J. *et al.* (2015) 'Flavivirus antagonism of type i interferon signaling reveals prolidase as a regulator of IFNAR1 surface expression', *Cell Host and Microbe*, 18(1), pp. 61–74. doi: 10.1016/j.chom.2015.06.007.

Lucas, T. M., Richner, J. M. and Diamond, M. S. (2016) ' The Interferon-Stimulated Gene Ifi27l2a Restricts West Nile Virus Infection and Pathogenesis in a Cell-Type- and Region-Specific Manner ', *Journal of Virology*, 90(5), pp. 2600–2615. doi: 10.1128/jvi.02463-15.

Luo, Z. *et al.* (2021) 'MiR-188-3p and miR-133b Suppress Cell Proliferation in Human Hepatocellular Carcinoma via Post-Transcriptional Suppression of NDRG1', *Technology in Cancer Research & Treatment*, 20, p. 153303382110330. doi: 10.1177/15330338211033074.

Lupi, Anna *et al.* (2006) 'Human recombinant prolidase from eukaryotic and prokaryotic sources: Expression, purification, characterization and long-term stability studies', *FEBS Journal*, 273(23), pp. 5466–5478. doi: 10.1111/j.1742-4658.2006.05538.x.

Lupi, A. *et al.* (2006) 'Molecular characterisation of six patients with prolidase deficiency: identification of the first small duplication in the prolidase gene and of a mutation generating symptomatic and asymptomatic outcomes within the same family.', *Journal of*

medical genetics. BMJ Publishing Group, 43(12), p. e58. doi: 10.1136/jmg.2006.043315.

Lupi, A. *et al.* (2008) 'Human prolidase and prolidase deficiency: An overview on the characterization of the enzyme involved in proline recycling and on the effects of its mutations', *Amino Acids*. Springer, pp. 739–752. doi: 10.1007/s00726-008-0055-4.

Macián, F. *et al.* (2002) 'Transcriptional mechanisms underlying lymphocyte tolerance', *Cell*. Cell, 109(6), pp. 719–731. doi: 10.1016/S0092-8674(02)00767-5.

MacIver, N. J., Michalek, R. D. and Rathmell, J. C. (2013) 'Metabolic regulation of T lymphocytes', *Annual Review of Immunology*, pp. 259–283.

Makino, S. *et al.* (1980) 'Breeding of a non-obese, diabetic strain of mice', *Experimental Animals*. Jikken Dobutsu, 29(1), pp. 1–13. doi: 10.1538/expanim1978.29.1_1.

Mancebo, E. *et al.* (2008) 'Gly111Ser mutation in CD8A gene causing CD8 immunodeficiency is found in Spanish Gypsies', *Molecular Immunology*, 45(2), pp. 479–484. doi: 10.1016/j.molimm.2007.05.022.

Manolio, T. A. *et al.* (2009) 'Finding the missing heritability of complex diseases', *Nature*, 461(7265), pp. 747–753. doi: 10.1038/nature08494.

Marson, A., Housley, W. J. and Hafler, D. A. (2015) 'Genetic basis of autoimmunity', *Journal of Clinical Investigation*. American Society for Clinical Investigation, 125(6), pp. 2234–2241. doi: 10.1172/JCI78086.

Mårtensson, I.-L. and Ceredig, R. (2000) 'Role of the surrogate light chain and the pre-B-cell receptor in mouse B-cell development', *Immunology*. Wiley-Blackwell, 101(4), p. 435. doi: 10.1046/J.1365-2567.2000.00151.X.

Martin, M. D. and Badovinac, V. P. (2018) 'Defining memory CD8 T cell', *Frontiers in Immunology*. Frontiers, 9(NOV), p. 2692. doi: 10.3389/fimmu.2018.02692.

Martinez, G. J. *et al.* (2015) 'The Transcription Factor NFAT Promotes Exhaustion of Activated CD8+ T Cells', *Immunity*, 42(2), pp. 265–278. doi: 10.1016/j.immuni.2015.01.006.

Matza, D. *et al.* (2009) 'Requirement for AHNAK1-mediated calcium signaling during T lymphocyte cytolysis', *Proceedings of the National Academy of Sciences of the United States of America*, 106(24), pp. 9785–9790. doi: 10.1073/pnas.0902844106.

McCarthy, D. *et al.* (2016) 'scater: pre-processing, quality control, normalisation and visualisation of single-cell RNA-seq data in R', *Scater: Pre-processing, quality control, normalization and visualization of single-cell RNA-seq data in R*, p. 069633. doi: 10.1101/069633.

McCarthy, D. D. *et al.* (2006) 'BAFF induces a hyper-IgA syndrome in the intestinal lamina propria concomitant with IgA deposition in the kidney independent of LIGHT', *Cellular Immunology*, 241(2), pp. 85–94. doi: 10.1016/j.cellimm.2006.08.002.

McCarthy, D. D. *et al.* (2011) 'Mice overexpressing BAFF develop a commensal flora-dependent, IgA-associated nephropathy', *Journal of Clinical Investigation*, 121(10), pp. 3991–4002. doi: 10.1172/JCI45563.

McKinney, E. F. *et al.* (2015) 'T-cell exhaustion, co-stimulation and clinical outcome in autoimmunity and infection', *Nature*, 523(7562), pp. 612–616. doi: 10.1038/nature14468.

McLane, L. M., Abdel-Hakeem, M. S. and Wherry, E. J. (2019) 'CD8 T Cell Exhaustion During Chronic Viral Infection and Cancer', *Annual Review of Immunology*. Annu Rev Immunol, 37, pp. 457–495. doi: 10.1146/annurev-immunol-041015-055318.

Merlot, A. M. *et al.* (2019) 'The metastasis suppressor, NDRG1, differentially modulates the endoplasmic reticulum stress response', *Biochimica et Biophysica Acta - Molecular Basis of Disease*. Elsevier B.V., 1865(9), pp. 2094–2110. doi: 10.1016/j.bbadis.2019.04.007.

Merrell, K. T. *et al.* (2006) 'Identification of Anergic B Cells within a Wild-Type Repertoire', *Immunity*. Cell Press, 25(6), pp. 953–962. doi: 10.1016/j.immuni.2006.10.017.

Van Der Merwe, P. A. *et al.* (1997) 'CD80 (B7-1) binds both CD28 and CTLA-4 with a low affinity and very fast kinetics', *Journal of Experimental Medicine*, 185(3), pp. 393–403. doi: 10.1084/jem.185.3.393.

Mescher, M. F. *et al.* (2006) 'Signals required for programming effector and memory development by CD8+ T cells', *Immunological Reviews*, 211(1), pp. 81–92. doi: 10.1111/j.0105-2896.2006.00382.x.

Miech, G. *et al.* (1988) 'Prolinase activity in prolidase-deficient fibroblasts', *Journal of Inherited Metabolic Disease*. J Inherit Metab Dis, 11(3), pp. 266–269. doi: 10.1007/BF01800368.

Misiura, M. and Miltyk, W. (2020) 'Current understanding of the emerging role of prolidase in cellular metabolism', *International Journal of Molecular Sciences*. MDPI AG, 21(16), pp. 1–20. doi: 10.3390/ijms21165906.

Miyagawa, F. *et al.* (2010) 'The use of mouse models to better understand mechanisms of autoimmunity and tolerance', *Journal of Autoimmunity*. NIH Public Access, 35(3), pp. 192–198. doi: 10.1016/j.jaut.2010.06.007.

Mok, C. C. and Lau, C. S. (2003) 'Pathogenesis of systemic lupus erythematosus', *Journal of*

Clinical Pathology. BMJ Publishing Group, pp. 481–490. doi: 10.1136/jcp.56.7.481.

Monroe, J. G. (2006) 'ITAM-mediated tonic signalling through pre-BCR and BCR complexes', *Nature Reviews Immunology*. Nature Publishing Group, pp. 283–294. doi: 10.1038/nri1808.

Morel, L. (2004) 'Mouse models of human autoimmune diseases: Essential tools that require the proper controls', *PLoS Biology*. Public Library of Science. doi: 10.1371/journal.pbio.0020241.

Moresco, E. M. Y., Li, X. and Beutler, B. (2013) 'Going Forward with Genetics', *The American Journal of Pathology*, 182(5), pp. 1462–1473. doi: 10.1016/j.ajpath.2013.02.002.

Morita, M. *et al.* (2004) 'Gene-Targeted Mice Lacking the Trex1 (DNase III) 3'→5' DNA Exonuclease Develop Inflammatory Myocarditis', *Molecular and Cellular Biology*, 24(15), pp. 6719–6727. doi: 10.1128/mcb.24.15.6719-6727.2004.

Moses, C. T. *et al.* (2003) 'Competition for self ligands restrains homeostatic proliferation of naive CD4 T cells', *Proceedings of the National Academy of Sciences of the United States of America*, 100(3), pp. 1185–1190. doi: 10.1073/pnas.0334572100.

Muñoz-Fuentes, V. *et al.* (2018) 'The International Mouse Phenotyping Consortium (IMPC): a functional catalogue of the mammalian genome that informs conservation', *Conservation Genetics*. Springer Netherlands, 19(4), pp. 995–1005. doi: 10.1007/s10592-018-1072-9.

Murphy, Kenneth; Travers, Paul; Walport, M. (2008) 'Janeway's Immunobiology1. Murphy, Kenneth; Travers, Paul; Walport, M. Janeway's Immunobiology. chapter 7 7th editio, (2008).', *Chapter 7*, 7th editio.

Nagamine, K. *et al.* (1997) 'Positional cloning of the APECED gene', *Nature Genetics*. Nature Publishing Group, 17(4), pp. 393–398. doi: 10.1038/ng1297-393.

Nagaoka, H. *et al.* (2000) 'Immunization and Infection Change the Number of Recombination Activating Gene (Rag)-Expressing B Cells in the Periphery by Altering Immature Lymphocyte Production', *The Journal of Experimental Medicine*. The Rockefeller University Press, 191(12), p. 2113. doi: 10.1084/JEM.191.12.2113.

Nair, R. P. *et al.* (2009) 'Genome-wide scan reveals association of psoriasis with IL-23 and NF-κB pathways', *Nature Genetics*. Nature Publishing Group, 41(2), pp. 199–204. doi: 10.1038/ng.311.

Nakayamada, S. and Tanaka, Y. (2016) 'BAFF- and APRIL-targeted therapy in systemic autoimmune diseases', *Inflammation and Regeneration*, 36(1). doi: 10.1186/s41232-016-0015-4.

Navarra, S. V. *et al.* (2011) 'Efficacy and safety of belimumab in patients with active systemic lupus erythematosus: A randomised, placebo-controlled, phase 3 trial', *The Lancet*, 377(9767), pp. 721–731. doi: 10.1016/S0140-6736(10)61354-2.

Nelms, K. A. and Goodnow, C. C. (2001) 'Genome-wide ENU mutagenesis to reveal immune regulators', *Immunity*. Cell Press, pp. 409–418. doi: 10.1016/S1074-7613(01)00199-6.

Nemazee, D. (2017) 'Mechanisms of central tolerance for B cells', *Nature Reviews Immunology*. Nature Publishing Group, pp. 281–294. doi: 10.1038/nri.2017.19.

Nguyen, H. H. *et al.* (2016) 'Naïve CD8 + T cell derived tumor-specific cytotoxic effectors as a potential remedy for overcoming TGF-β immunosuppression in the tumor microenvironment', *Scientific Reports*, 6. doi: 10.1038/srep28208.

Nguyen, N. *et al.* (2011) 'Random mutagenesis of the mouse genome: A strategy for discovering gene function and the molecular basis of disease', *American Journal of Physiology - Gastrointestinal and Liver Physiology*, 300(1), pp. 1–11. doi: 10.1152/ajpgi.00343.2010.

Nguyen, V. H. *et al.* (2007) 'In vivo dynamics of regulatory T-cell trafficking and survival predict effective strategies to control graft-versus-host disease following allogeneic transplantation', *Blood*. American Society of Hematology, 109(6), pp. 2649–2656. doi: 10.1182/blood-2006-08-044529.

Niewold, T. B. *et al.* (2008) 'Age- and sex-related patterns of serum interferon-α activity in lupus families', *Arthritis and Rheumatism*. Arthritis Rheum, 58(7), pp. 2113–2119. doi: 10.1002/art.23619.

Nishino, H. *et al.* (1981) 'Lupus erythematosus-like syndrome with selective complete deficiency of C1q', *Annals of Internal Medicine*, 95(3), pp. 322–324. doi: 10.7326/0003-4819-95-3-322.

O'Neill, S. K. *et al.* (2011) 'Monophosphorylation of CD79a and CD79b ITAM motifs initiates a SHIP-1 phosphatase-mediated inhibitory signaling cascade required for B cell anergy', *Immunity*, 35(5), pp. 746–756. doi: 10.1016/j.immuni.2011.10.011.

Oh, Y. M. *et al.* (2015) 'Ndrg1 is a T-cell clonal anergy factor negatively regulated by CD28 costimulation and interleukin-2', *Nature Communications*, 6(May), p. 8698. doi: 10.1038/ncomms9698.

Okada, T. *et al.* (2005) 'Antigen-Engaged B Cells Undergo Chemotaxis toward the T Zone and Form Motile Conjugates with Helper T Cells', *PLOS Biology*. Public Library of Science,

3(6), p. e150. doi: 10.1371/JOURNAL.PBIO.0030150.

Okamoto, Y. *et al.* (2014) 'Exonic duplication CNV of NDRG1 associated with autosomal-recessive HMSN-Lom/CMT4D', *Genetics in Medicine*, 16(5), pp. 386–394. doi: 10.1038/gim.2013.155.

Okuda, T. *et al.* (2004) 'Ndrg1-Deficient Mice Exhibit a Progressive Demyelinating Disorder of Peripheral Nerves', *Molecular and Cellular Biology*, 24(9), pp. 3949–3956. doi: 10.1128/mcb.24.9.3949-3956.2004.

Oliver, A. M. *et al.* (1997) 'Marginal zone B cells exhibit unique activation, proliferative and immunoglobulin secretory responses', *European Journal of Immunology*. Eur J Immunol, 27(9), pp. 2366–2374. doi: 10.1002/eji.1830270935.

Omilusik, K. D. *et al.* (2015) 'Transcriptional repressor ZEB2 promotes terminal differentiation of CD8+ effector and memory T cell populations during infection', *Journal of Experimental Medicine*. The Rockefeller University Press, 212(12), pp. 2027–2039. doi: 10.1084/JEM.20150194.

Onengut-Gumuscu, S. *et al.* (2015) 'Fine mapping of type 1 diabetes susceptibility loci and evidence for colocalization of causal variants with lymphoid gene enhancers', *Nature Genetics*. Nature Research, 47(4), pp. 381–386. doi: 10.1038/ng.3245.

Pandiyan, P. *et al.* (2007) 'CD4+CD25+Foxp3+ regulatory T cells induce cytokine deprivation-mediated apoptosis of effector CD4+ T cells', *Nature Immunology*. Nat Immunol, 8(12), pp. 1353–1362. doi: 10.1038/ni1536.

Paolo Schena, F. (1990) 'A retrospective analysis of the natural history of primary IgA nephropathy worldwide', *The American Journal of Medicine*, 89(2), pp. 209–215. doi: 10.1016/0002-9343(90)90300-3.

Pape, K. A. *et al.* (1998) 'Direct evidence that functionally impaired CD4+ T cells persist in vivo following induction of peripheral tolerance', *The Journal of Immunology*, 160(10), pp. 4719–4729.

Parman, Y. *et al.* (2004) 'Clinicopathological and genetic study of early-onset demyelinating neuropathy', *Brain*, 127(11), pp. 2540–2550.

Pascale Lachat, Philip Shaw, Sandra Gebhard, Nico van Belzen, P. C. & F. T. B. (2002) 'Expression of NDRG1, a differentiation-related gene, in human tissues', *Histochemistry and Cell Biology*, 118, pp. 399–408.

Perez, V. L. *et al.* (1997) 'Induction of peripheral T cell tolerance in vivo requires CTLA-4

engagement', *Immunity*. Cell Press, 6(4), pp. 411–417. doi: 10.1016/S1074-7613(00)80284-8.

Pernis, B. *et al.* (1965) 'Cellular localization of immunoglobulins with different allotypic specificities in rabbit lymphoid tissues.', *The Journal of experimental medicine*, 122(5), pp. 853–876. doi: 10.1084/jem.122.5.853.

Pierre Bruhns and Friederike Jönsson (2015) 'Mouse and human FcR effector functions', *Immunological Reviews*, 268(1), pp. 25–51.

Pietiäinen, V. *et al.* (2013) 'NDRG1 functions in LDL receptor trafficking by regulating endosomal recycling and degradation', *Journal of Cell Science*. The Company of Biologists Ltd, 126(17), pp. 3961–3971. doi: 10.1242/jcs.128132.

Pillai, S. and Cariappa, A. (2009) 'The follicular versus marginal zone B lymphocyte cell fate decision', *Nature Reviews Immunology*. Nat Rev Immunol, pp. 767–777. doi: 10.1038/nri2656.

Piquemal, D. *et al.* (1999) 'Differential expression of the RTP/Drg1/Ndr1 gene product in proliferating and growth arrested cells', *Biochimica et Biophysica Acta - Molecular Cell Research*. Biochim Biophys Acta, 1450(3), pp. 364–373. doi: 10.1016/S0167-4889(99)00056-7.

Powell, J. D. *et al.* (1998) 'Molecular regulation of interleukin-2 expression by CD28 co-stimulation and anergy', *Immunological Reviews*, 165, pp. 287–300. doi: 10.1111/j.1600-065X.1998.tb01246.x.

Qi, H. *et al.* (2008) 'SAP-controlled T-B cell interactions underlie germinal centre formation', *Nature*. Nature Publishing Group, 455(7214), pp. 764–769. doi: 10.1038/nature07345.

Qian, Y. *et al.* (2004) 'Act1, a negative regulator in CD40- and BAFF-mediated B cell survival', *Immunity*, 21(4), pp. 575–587. doi: 10.1016/j.immuni.2004.09.001.

Qu, X. *et al.* (2002) 'Characterization and expression of three novel differentiation-related genes belong to the human NDRG gene family', *Molecular and Cellular Biochemistry*, 229(1–2), pp. 35–44. doi: 10.1023/A:1017934810825.

Quách, T. D. *et al.* (2011) 'Anergic Responses Characterize a Large Fraction of Human Autoreactive Naive B Cells Expressing Low Levels of Surface IgM', *The Journal of Immunology*, 186(8), pp. 4640–4648. doi: 10.4049/jimmunol.1001946.

Quwailid, M. M. *et al.* (2004) 'A gene-driven ENU-based approach to generating an allelic

series in any gene', *Mammalian Genome*, 15(8), pp. 585–591. doi: 10.1007/s00335-004-2379-z.

Ramos-Casals, M. *et al.* (2020) 'Immune-related adverse events of checkpoint inhibitors', *Nature Reviews Disease Primers*, 6(1). doi: 10.1038/s41572-020-0160-6.

Randall, K. L. *et al.* (2009) 'Dock8 mutations cripple B cell immunological synapses, germinal centers and long-lived antibody production', *Nature Immunology*, 10(12), pp. 1283–1291. doi: 10.1038/ni.1820.

Rathmell, J. C. *et al.* (1995) 'CD95 (Fas)-dependent elimination of self-reactive B cells upon interaction with CD4+T cells', *Nature*. Nature Publishing Group, 376(6536), pp. 181–184. doi: 10.1038/376181a0.

Raychaudhuri, S. *et al.* (2012) 'Five amino acids in three HLA proteins explain most of the association between MHC and seropositive rheumatoid arthritis', *Nature Genetics*. NIH Public Access, 44(3), pp. 291–296. doi: 10.1038/ng.1076.

Reed, J. H. *et al.* (2016) 'Clonal redemption of autoantibodies by somatic hypermutation away from self-reactivity during human immunization', *Journal of Experimental Medicine*, 213(7), pp. 1255–1265. doi: 10.1084/jem.20151978.

Reid, S. *et al.* (2020) 'High genetic risk score is associated with early disease onset, damage accrual and decreased survival in systemic lupus erythematosus', *Annals of the Rheumatic Diseases*. BMJ Publishing Group Ltd, 79(3), pp. 363–369. doi: 10.1136/ANNRHEUMDIS-2019-216227.

Reif, K. *et al.* (2002) 'Balanced responsiveness to chemoattractants from adjacent zones determines B-cell position', *Nature*, 416(6876), pp. 94–99. doi: 10.1038/416094a.

Renaud, J. & Dagenais, P. (2009) 'Agence d'évaluation des technologies et des modes d'intervention en santé (AETMIS). La pertinence du dépistage néonatal urinaire des erreurs innées du métabolisme réalisé au Québec.', *ETMIS, Montreal, Quebec*.

Rice, G. I., Rodero, M. P. and Crow, Y. J. (2015) 'Human Disease Phenotypes Associated With Mutations in TREX1', *Journal of Clinical Immunology*, 35(3), pp. 235–243. doi: 10.1007/s10875-015-0147-3.

Rich, S. S., Weitkamp, L. R. and Barbosa, J. (1984) *Genetic heterogeneity of insulin-dependent (type I) diabetes mellitus: Evidence from a study of extended haplotypes*, *American Journal of Human Genetics*. Elsevier.

Richard, M. L. and Gilkeson, G. (2018) 'Mouse models of lupus: What they tell us and what

they don't', *Lupus Science and Medicine*, 5(1). doi: 10.1136/lupus-2016-000199.

Ring, B. Z. *et al.* (2006) 'Novel prognostic immunohistochemical biomarker panel for estrogen receptor-positive breast cancer', *Journal of Clinical Oncology*, 24(19), pp. 3039–3047. doi: 10.1200/JCO.2006.05.6564.

Rioux, J. D. and Abbas, A. K. (2005) 'Paths to understanding the genetic basis of autoimmune disease', *Nature*. Nature Publishing Group, 435(7042), pp. 584–589. doi: 10.1038/nature03723.

Ritz, M. *et al.* (2000) 'Characterisation of Autoantibodies To Peripheral Myelin Protein 22 in Patients With Hereditary and Acquired Neuropathies', *Journal of the Peripheral Nervous System*, 5(4), pp. 239–239. doi: 10.1046/j.1529-8027.2000.00022-13.x.

Rocha, B., Grandien, A. and Freitas, A. A. (1995) 'Anergy and exhaustion are independent mechanisms of peripheral T cell tolerance', *Journal of Experimental Medicine*, 181(3), pp. 993–1003. doi: 10.1084/jem.181.3.993.

Rodig, S. J. *et al.* (2005) 'BAFF-R, the major B cell-activating factor receptor, is expressed on most mature B cells and B-cell lymphoproliferative disorders', *Human Pathology*. Hum Pathol, 36(10), pp. 1113–1119. doi: 10.1016/j.humpath.2005.08.005.

Root-Bernstein, R. and Fairweather, D. (2014) 'Complexities in the relationship between infection and autoimmunity', *Current Allergy and Asthma Reports*. NIH Public Access, 14(1), p. 407. doi: 10.1007/s11882-013-0407-3.

Rosati, R. *et al.* (1994) 'Normal long bone growth and development in type X collagen-null mice', *Nature Genetics*, 8(2), pp. 129–135. doi: 10.1038/ng1094-129.

Rossignol, F. *et al.* (2021) 'Quantitative analysis of the natural history of prolidase deficiency: description of 17 families and systematic review of published cases', *Genetics in Medicine 2021*. Nature Publishing Group, 15, pp. 1–12. doi: 10.1038/s41436-021-01200-2.

Rothenberg, E. V. (2014) 'Transcriptional control of early T and B cell developmental choices', *Annual Review of Immunology*. Annual Reviews, 32(1), pp. 283–321. doi: 10.1146/annurev-immunol-032712-100024.

Roux De Bézieux, H. *et al.* (2021) 'Trajectory inference across multiple conditions with condiments: 1 differential topology, progression, differentiation, and expression', *bioRxiv*, p. 2021.03.09.433671.

Rozzo, S. J. *et al.* (1996) *Effect of genetic background on the contribution of New Zealand*

Black loci to autoimmune lupus nephritis, *Proceedings of the National Academy of Sciences of the United States of America*. doi: 10.1073/pnas.93.26.15164.

Rui, L. *et al.* (2003) 'Resistance to CpG DNA-induced autoimmunity through tolerogenic B cell antigen receptor ERK signaling', *Nature Immunology*, 4(6), pp. 594–600. doi: 10.1038/ni924.

Rui, L. *et al.* (2006) 'ERK Signaling Is a Molecular Switch Integrating Opposing Inputs from B Cell Receptor and T Cell Cytokines to Control TLR4-Driven Plasma Cell Differentiation', *The Journal of Immunology*, 177(8), pp. 5337–5346. doi: 10.4049/jimmunol.177.8.5337.

Russell, W. L. *et al.* (1979) 'Specific-locus test shows ethylnitrosourea to the the most potent mutagen in the mouse', *Proceedings of the National Academy of Sciences of the United States of America*, 76(11), pp. 5818–5819. doi: 10.1073/pnas.76.11.5818.

Sabouri, Z. *et al.* (2016) 'IgD attenuates the IgM-induced anergy response in transitional and mature B cells', *Nature Communications*, 7, p. 13381. doi: 10.1038/ncomms13381.

Sadovnick, A. D. *et al.* (1993) 'A population-based study of multiple sclerosis in twins: Update', *Annals of Neurology*, 33(3), pp. 281–285. doi: 10.1002/ana.410330309.

Sadovnick, A. D., Baird, P. A. and Ward, R. H. (1988) 'Multiple sclerosis: Updated risks for relatives', *American Journal of Medical Genetics*. John Wiley & Sons, Ltd, 29(3), pp. 533–541. doi: 10.1002/ajmg.1320290310.

Safford, M. *et al.* (2005) 'Egr-2 and Egr-3 are negative regulators of T cell activation', *Nature Immunology*. Nature Publishing Group, 6(5), pp. 472–480. doi: 10.1038/ni1193.

Sahni, S. *et al.* (2014) 'The metastasis suppressor, N-myc Downstream-regulated gene 1 (NDRG1), inhibits stress-induced autophagy in cancer cells', *Journal of Biological Chemistry*. American Society for Biochemistry and Molecular Biology Inc., 289(14), pp. 9692–9709. doi: 10.1074/jbc.M113.529511.

Saito, T. *et al.* (2003) 'Notch2 is preferentially expressed in mature B cells and indispensable for marginal zone B lineage development', *Immunity*, 18(5), pp. 675–685. doi: 10.1016/S1074-7613(03)00111-0.

Sakaguchi, S. *et al.* (1995) 'Immunologic self-tolerance maintained by activated T cells expressing IL-2 receptor alpha-chains (CD25). Breakdown of a single mechanism of self-tolerance causes various autoimmune diseases.', *Journal of immunology (Baltimore, Md. : 1950)*, 155(3), pp. 1151–64.

Sander, J. D. and Joung, J. K. (2014) 'CRISPR-Cas systems for editing, regulating and

targeting genomes', *Nature Biotechnology*. Nature Publishing Group, pp. 347–350. doi: 10.1038/nbt.2842.

Sawitzki, B. *et al.* (2020) 'Regulatory cell therapy in kidney transplantation (The ONE Study): a harmonised design and analysis of seven non-randomised, single-arm, phase 1/2A trials', *The Lancet*. Elsevier, 395(10237), pp. 1627–1639. doi: 10.1016/S0140-6736(20)30167-7.

Schiemann, B. *et al.* (2001) 'An essential role for BAFF in the normal development of B cells through a BCMA-independent pathway', *Science*, 293(5537), pp. 2111–2114. doi: 10.1126/science.1061964.

Schmidt, E. M. *et al.* (2009) 'CTLA-4 Controls Regulatory T Cell Peripheral Homeostasis and Is Required for Suppression of Pancreatic Islet Autoimmunity', *The Journal of Immunology*, 182(1), pp. 274–282. doi: 10.4049/jimmunol.182.1.274.

Schroeder, M. A. and DiPersio, J. F. (2011) 'Mouse models of graft-versus-host disease: Advances and limitations', *DMM Disease Models and Mechanisms*. Company of Biologists, pp. 318–333. doi: 10.1242/dmm.006668.

Schubert, D. *et al.* (2014) 'Autosomal dominant immune dysregulation syndrome in humans with CTLA4 mutations', *Nature Medicine*. Nature Publishing Group, 20(12), pp. 1410–1416. doi: 10.1038/nm.3746.

Schwartz, R. H. *et al.* (1989) 'T-cell clonal anergy', *Cold Spring Harbor Symposia on Quantitative Biology*. Cold Spring Harb Symp Quant Biol, 54(2), pp. 605–610. doi: 10.1101/sqb.1989.054.01.072.

Schwartz, R. H. (2003) 'T cell anergy', *Annual Review of Immunology*, 21, pp. 305–334. doi: 10.1146/annurev.immunol.21.120601.141110.

Sebbag, M. *et al.* (1995) 'The antiperinuclear factor and the so-called antikeratin antibodies are the same rheumatoid arthritis-specific autoantibodies', *Journal of Clinical Investigation*, 95(6), pp. 2672–2679. doi: 10.1172/JCI117969.

Seder, R. A. and Ahmed, R. (2003) 'Similarities and differences in CD4+ and CD8+ effector and memory T cell generation', *Nature Immunology*. Nature Publishing Group, 4(9), pp. 835–842. doi: 10.1038/ni969.

Sevinsky, C. J. *et al.* (2018) 'NDRG1 regulates neutral lipid metabolism in breast cancer cells', *Breast Cancer Research*. BioMed Central Ltd., 20(1), p. 55. doi: 10.1186/s13058-018-0980-4.

Shalem, O. *et al.* (2014) 'Genome-scale CRISPR-Cas9 knockout screening in human cells',

Science, 343(6166), pp. 84–87. doi: 10.1126/science.1247005.

Shaw, L. A. *et al.* (2016) 'Id2 reinforces TH1 cell differentiation and inhibits E2A to repress TFH cell differentiation', *Nature immunology*. NIH Public Access, 17(7), p. 834. doi: 10.1038/NI.3461.

Shevach, E. M. and Thornton, A. M. (2014) 'tTregs, pTregs, and iTregs: Similarities and differences', *Immunological Reviews*. Blackwell Publishing Ltd, 259(1), pp. 88–102. doi: 10.1111/imr.12160.

Shin, W. *et al.* (2018) 'BAFF-neutralizing interaction of belimumab related to its therapeutic efficacy for treating systemic lupus erythematosus', *Nature Communications*, 9(1). doi: 10.1038/s41467-018-03620-2.

Shrinath, M. *et al.* (1997) *Prolidase deficiency and systemic lupus erythematosus*, *Archives of Disease in Childhood*. doi: 10.1136/adc.76.5.441.

Singer, A., Adoro, S. and Park, J.-H. (2008) 'Lineage fate and intense debate: myths, models and mechanisms of CD4/CD8 lineage choice', *Nature reviews. Immunology*. NIH Public Access, 8(10), p. 788. doi: 10.1038/NRI2416.

Skarnes, W. C. *et al.* (2011) 'A conditional knockout resource for the genome-wide study of mouse gene function', *Nature*. Europe PMC Funders, 474(7351), pp. 337–344. doi: 10.1038/nature10163.

Smith, M. J. *et al.* (2019) 'Elevated PTEN expression maintains anergy in human B cells and reveals unexpectedly high repertoire autoreactivity', *JCI Insight*, 4(3). doi: 10.1172/jci.insight.123384.

Spencer-Green, G., Alter, D. and Welch, H. G. (1997) 'Test performance in systemic sclerosis: Anti-centromere and anti-Scl-70 antibodies', *American Journal of Medicine*. Am J Med, 103(3), pp. 242–248. doi: 10.1016/S0002-9343(97)00023-5.

Spodenkiewicz, Marta *et al.* (2020) 'Clinical genetics of prolidase deficiency: An updated review', *Biology*. MDPI AG. doi: 10.3390/biology9050108.

Stanford, W. L., Cohn, J. B. and Cordes, S. P. (2001) 'Gene-trap mutagenesis: Past, present and beyond', *Nature Reviews Genetics*. Nat Rev Genet, pp. 756–768. doi: 10.1038/35093548.

Stebegg, M. *et al.* (2018) 'Regulation of the germinal center response', *Frontiers in Immunology*. Frontiers Media S.A., p. 2469. doi: 10.3389/fimmu.2018.02469.

Stein, J. V and Nombela-Arrieta, C. (2005) 'Chemokine control of lymphocyte trafficking: a

general overview', *Immunology*. Wiley-Blackwell, 116(1), p. 1. doi: 10.1111/J.1365-2567.2005.02183.X.

Stein, S. *et al.* (2004) 'NDRG1 is necessary for p53-dependent apoptosis', *Journal of Biological Chemistry*. American Society for Biochemistry and Molecular Biology, 279(47), pp. 48930–48940. doi: 10.1074/jbc.M400386200.

Stetson, D. B. *et al.* (2008) 'Trex1 Prevents Cell-Intrinsic Initiation of Autoimmunity', *Cell*, 134(4), pp. 587–598. doi: 10.1016/j.cell.2008.06.032.

Stottmann, R. and Beier, D. (2014) 'ENU mutagenesis in the mouse', *Current Protocols in Human Genetics*. Blackwell Publishing Inc., 2014, pp. 15.4.1-15.4.10. doi: 10.1002/0471142905.hg1504s82.

Strasser, A., Harris, A. W., Corcoran, L. M., *et al.* (1994) 'Bcl-2 expression promotes B- but not T-lymphoid development in scid mice', *Nature*. Nature, 368(6470), pp. 457–460. doi: 10.1038/368457a0.

Strasser, A., Harris, A. W., Von Boehmer, H., *et al.* (1994) 'Positive and negative selection of T cells in T-cell receptor transgenic mice expressing a bcl-2 transgene', *Proceedings of the National Academy of Sciences of the United States of America*. National Academy of Sciences, 91(4), pp. 1376–1380. doi: 10.1073/pnas.91.4.1376.

Strasser, A., Harris, A. W. and Cory, S. (1991) 'bcl-2 transgene inhibits T cell death and perturbs thymic self-censorship', *Cell*. Cell, 67(5), pp. 889–899. doi: 10.1016/0092-8674(91)90362-3.

Street, K. *et al.* (2018) 'Slingshot: Cell lineage and pseudotime inference for single-cell transcriptomics', *BMC Genomics*, 19(1). doi: 10.1186/s12864-018-4772-0.

Stritesky, G. L. *et al.* (2013) 'Murine thymic selection quantified using a unique method to capture deleted T cells', *Proceedings of the National Academy of Sciences of the United States of America*. Proc Natl Acad Sci U S A, 110(12), pp. 4679–4684. doi: 10.1073/pnas.1217532110.

Stuart, T. *et al.* (2019) 'Comprehensive Integration of Single-Cell Data', *Cell*, 177(7), pp. 1888-1902.e21. doi: 10.1016/j.cell.2019.05.031.

Sun, J. *et al.* (2013) 'Metastasis suppressor, NDRG1, mediates its activity through signaling pathways and molecular motors', *Carcinogenesis*, 34(9), pp. 1943–1954. doi: 10.1093/carcin/bgt163.

Surazynski, A. *et al.* (2008) 'Extracellular matrix and HIF-1 signaling: The role of prolidase',

International Journal of Cancer. Int J Cancer, 122(6), pp. 1435–1440. doi: 10.1002/ijc.23263.

Szabo, S. J. *et al.* (2000) 'A novel transcription factor, T-bet, directs TH1 lineage commitment', *Cell*, 100, pp. 655–669.

Tadokoro, C. E. *et al.* (2006) 'Regulatory T cells inhibit stable contacts between CD4+ T cells and dendritic cells in vivo', *Journal of Experimental Medicine*. The Rockefeller University Press, 203(3), pp. 505–511. doi: 10.1084/jem.20050783.

Takaba, H. and Takayanagi, H. (2017) *The Mechanisms of T Cell Selection in the Thymus*, *Trends in Immunology*. doi: 10.1016/j.it.2017.07.010.

Takagawa, T. *et al.* (2018) 'An increase in LRRK2 suppresses autophagy and enhances dectin-1–induced immunity in a mouse model of colitis', *Science Translational Medicine*. NIH Public Access, 10(444), p. 8162. doi: 10.1126/scitranslmed.aan8162.

Taketomi, Y. *et al.* (2007) ' Impaired Mast Cell Maturation and Degranulation and Attenuated Allergic Responses in Ndrg1 -Deficient Mice ', *The Journal of Immunology*, 178(11), pp. 7042–7053. doi: 10.4049/jimmunol.178.11.7042.

Tam, V. *et al.* (2019) 'Benefits and limitations of genome-wide association studies', *Nature Reviews Genetics 2019 20:8*. Nature Publishing Group, 20(8), pp. 467–484. doi: 10.1038/s41576-019-0127-1.

Tan, J. T. *et al.* (2001) 'IL-7 is critical for homeostatic proliferation and survival of naïve T cells', *Proceedings of the National Academy of Sciences*. National Academy of Sciences, 98(15), pp. 8732–8737. doi: 10.1073/PNAS.161126098.

Tan, Y. *et al.* (2013) 'Serum levels and renal deposition of C1q complement component and its antibodies reflect disease activity of lupus nephritis', *BMC Nephrology*, 14(1). doi: 10.1186/1471-2369-14-63.

Tanchot, C. *et al.* (2001) ' Adaptive Tolerance of CD4 + T Cells In Vivo: Multiple Thresholds in Response to a Constant Level of Antigen Presentation ', *The Journal of Immunology*, 167(4), pp. 2030–2039. doi: 10.4049/jimmunol.167.4.2030.

Tashakkorinia, N. and Tudor, M. E. (2020) 'Berger Disease', *StatPearls*.

Taylor, J. C. *et al.* (2015) 'Factors influencing success of clinical genome sequencing across a broad spectrum of disorders', *Nature Genetics*, 47(7), pp. 717–726. doi: 10.1038/ng.3304.

Teare, M. D. and Barrett, J. H. (2011) 'Genetic linkage studies', *An Introduction to Genetic Epidemiology*, pp. 39–59. doi: 10.2307/j.ctt1t895v2.8.

Testa, G. *et al.* (2004) 'A Reliable lacZ Expression Reporter Cassette for Multipurpose, Knockout-First Alleles', *Genesis*. John Wiley & Sons, Ltd, 38(3), pp. 151–158. doi: 10.1002/gene.20012.

Tivol, E. A. *et al.* (1995) 'Loss of CTLA-4 leads to massive lymphoproliferation and fatal multiorgan tissue destruction, revealing a critical negative regulatory role of CTLA-4', *Immunity*. Immunity, 3(5), pp. 541–547. doi: 10.1016/1074-7613(95)90125-6.

Todd, J. A., Bell, J. I. and McDevitt, H. O. (1987) 'HLA-DQβ gene contributes to susceptibility and resistance to insulin-dependent diabetes mellitus', *Nature*. Nature, 329(6140), pp. 599–604. doi: 10.1038/329599a0.

Trapnell, C. *et al.* (2014) 'The dynamics and regulators of cell fate decisions are revealed by pseudotemporal ordering of single cells', *Nature Biotechnology*. Nature Publishing Group, 32(4), pp. 381–386. doi: 10.1038/nbt.2859.

Trefzer, A. *et al.* (2021) 'Dynamic adoption of anergy by antigen-exhausted CD4+ T cells', *Cell Reports*, 34(6). doi: 10.1016/j.celrep.2021.108748.

Tsokos, G. C. *et al.* (2016) 'New insights into the immunopathogenesis of systemic lupus erythematosus', *Nature Reviews Rheumatology*. Nat Rev Rheumatol, 12(12), pp. 716–730. doi: 10.1038/nrrheum.2016.186.

Tsubata, T. and Reth, M. (1990) 'The products of pre-B cell-specific genes (λ5 and VpreB) and the immunoglobulin μ chain form a complex that is transported onto the cell surface', *Journal of Experimental Medicine*, 172(3), pp. 973–976. doi: 10.1084/jem.172.3.973.

Uhrin, P. *et al.* (2013) 'ISG12 is a critical modulator of innate immune responses in murine models of sepsis', *Immunobiology*. Elsevier, 218(9), pp. 1207–1216. doi: 10.1016/j.imbio.2013.04.009.

Van Belzen, N. *et al.* (1997) 'A novel gene which is up-regulated during colon epithelial cell differentiation and down-regulated in colorectal neoplasms', *Laboratory Investigation*, 77(1), pp. 85–92.

Vanderlugt, C. L. and Miller, S. D. (2002) 'Epitope spreading in immune-mediated diseases: Implications for immunotherapy', *Nature Reviews Immunology*. Nature Publishing Group, 2(2), pp. 85–95. doi: 10.1038/nri724.

Vettermann, C. and Schlissel, M. S. (2010) 'Allelic exclusion of immunoglobulin genes: Models and mechanisms', *Immunological Reviews*, 237(1), pp. 22–42. doi: 10.1111/j.1600-065X.2010.00935.x.

Victora, G. D. *et al.* (2010) 'Germinal Center Dynamics Revealed by Multiphoton Microscopy Using a Photoactivatable Fluorescent Reporter', *Cell*. NIH Public Access, 143(4), p. 592. doi: 10.1016/J.CELL.2010.10.032.

Vignali, D. A. A., Collison, L. W. and Workman, C. J. (2008) 'How regulatory T cells work', *Nature Reviews Immunology*. Nature Publishing Group, pp. 523–532. doi: 10.1038/nri2343.

Vinuesa, C. G. *et al.* (2005) 'A RING-type ubiquitin ligase family member required to repress follicular helper T cells and autoimmunity', *Nature*. Nature, 435(7041), pp. 452–458. doi: 10.1038/nature03555.

Vinuesa, C. G. and Goodnow, C. C. (2004) 'Illuminating autoimmune regulators through controlled variation of the mouse genome sequence', *Immunity*. Immunity, 20(6), pp. 669–679. doi: 10.1016/j.immuni.2004.05.012.

Van Der Vliet, H. J. J. and Nieuwenhuis, E. E. (2007) 'IPEX as a result of mutations in FOXP3', *Clinical and Developmental Immunology*. Hindawi Limited, 2007. doi: 10.1155/2007/89017.

Vojdani, A., Pollard, K. M. and Campbell, A. W. (2014) 'Environmental triggers and autoimmunity', *Autoimmune Diseases*. Hindawi Limited, 2014. doi: 10.1155/2014/798029.

Vyse, T. J. and Todd, J. A. (1996) 'Genetic analysis of autoimmune disease', *Cell*. Cell Press, pp. 311–318. doi: 10.1016/S0092-8674(00)81110-1.

Wagle, M. V. *et al.* (2021) 'Antigen-driven EGR2 expression is required for exhausted CD8+ T cell stability and maintenance', *Nature Communications*, 12(1). doi: 10.1038/s41467-021-23044-9.

Walsh, N. C. *et al.* (2017) 'Humanized Mouse Models of Clinical Disease', *Annual Review of Pathology: Mechanisms of Disease*, 12, pp. 187–215. doi: 10.1146/annurev-pathol-052016-100332.

Wandstrat, A. E. *et al.* (2006) 'Autoantibody profiling to identify individuals at risk for systemic lupus erythematosus', *Journal of Autoimmunity*, 27(3), pp. 153–160. doi: 10.1016/j.jaut.2006.09.001.

Wang, H. *et al.* (2006) 'A nonsense mutation of PEPD in four amish children with prolidase deficiency', *American Journal of Medical Genetics*, 140 A(6), pp. 580–585. doi: 10.1002/ajmg.a.31134.

Wang, H. *et al.* (2013) 'One-step generation of mice carrying mutations in multiple genes by CRISPR/cas-mediated genome engineering', *Cell*, 153(4), pp. 910–918. doi:

10.1016/j.cell.2013.04.025.

Wang, Y.-F. *et al.* (2021) 'Identification of 38 novel loci for systemic lupus erythematosus and genetic heterogeneity between ancestral groups', *Nature Communications 2021 12:1*. Nature Publishing Group, 12(1), pp. 1–13. doi: 10.1038/s41467-021-21049-y.

Wardemann, H. *et al.* (2003) 'Predominant autoantibody production by early human B cell precursors', *Science*, 301(5638), pp. 1374–1377. doi: 10.1126/science.1086907.

Watari, K. *et al.* (2016) 'Impaired differentiation of macrophage lineage cells attenuates bone remodeling and inflammatory angiogenesis in Ndrg1 deficient mice', *Scientific Reports*, 6(19470). doi: 10.1038/srep19470.

Waterston, R. H. *et al.* (2002) 'Initial sequencing and comparative analysis of the mouse genome', *Nature*. Nature Publishing Group, 420(6915), pp. 520–562. doi: 10.1038/nature01262.

Wehbi, B. *et al.* (2021) 'History of IgA Nephropathy Mouse Models', *Journal of Clinical Medicine*, 10(14), p. 3142. doi: 10.3390/jcm10143142.

Wei, S. C. *et al.* (2019) 'Combination anti–CTLA-4 plus anti–PD-1 checkpoint blockade utilizes cellular mechanisms partially distinct from monotherapies', *Proceedings of the National Academy of Sciences of the United States of America*, 116(45), pp. 22699–22709. doi: 10.1073/pnas.1821218116.

Weintraub, B. C. *et al.* (2000) 'Entry of B cell receptor into signaling domains is inhibited in tolerant B cells', *Journal of Experimental Medicine*, 191(8), pp. 1443–1448. doi: 10.1084/jem.191.8.1443.

Wentink, M. W. J. *et al.* (2018) 'Exhaustion of the CD8+ T cell compartment in patients with mutations in phosphoinositide 3-kinase delta', *Frontiers in Immunology*, 9(MAR). doi: 10.3389/fimmu.2018.00446.

Wherry, E. J. and Kurachi, M. (2015) 'Molecular and cellular insights into T cell exhaustion', *Nature reviews. Immunology*. NIH Public Access, 15(8), p. 486. doi: 10.1038/NRI3862.

Wieman, H. L., Wofford, J. A. and Rathmell, J. C. (2007) 'Cytokine stimulation promotes glucose uptake via phosphatidylinositol-3 kinase/Akt regulation of Glut1 activity and trafficking', *Molecular Biology of the Cell*, 18(4), pp. 1437–1446. doi: 10.1091/mbc.E06-07-0593.

Wilcock, M. (2018) *Characterisation of the mechanism of B-cell receptor triggering*.

Wim Ang, C., Jacobs, B. C. and Laman, J. D. (2004) 'The Guillain-Barré syndrome: A true

case of molecular mimicry', *Trends in Immunology*. Elsevier Ltd, 25(2), pp. 61–66. doi: 10.1016/j.it.2003.12.004.

Wing, J. B. *et al.* (2014) *Regulatory T cells control antigen-specific expansion of Tfh cell number and humoral immune responses via the coreceptor CTLA-4*, *Immunity*. Cell Press. doi: 10.1016/j.immuni.2014.12.006.

Wirnsberger, G., Hinterberger, M. and Klein, L. (2011) 'Regulatory T-cell differentiation versus clonal deletion of autoreactive thymocytes', *Immunology and Cell Biology*. John Wiley & Sons, Ltd, 89(1), pp. 45–53. doi: 10.1038/icb.2010.123.

Wirth, J. R. *et al.* (2020) 'TLR7 Agonism Accelerates Disease and Causes a Fatal Myeloproliferative Disorder in NZM 2410 Lupus Mice', *Frontiers in Immunology*. Frontiers Media S.A., 10, p. 3054. doi: 10.3389/fimmu.2019.03054.

Wollenberg, I. *et al.* (2011) ' Regulation of the Germinal Center Reaction by Foxp3 + Follicular Regulatory T Cells ', *The Journal of Immunology*. J Immunol, 187(9), pp. 4553–4560. doi: 10.4049/jimmunol.1101328.

Wong, P. *et al.* (2001) 'Dynamic tuning of T cell reactivity by self-peptide-major histocompatibility complex ligands', *Journal of Experimental Medicine*. The Rockefeller University Press, 193(10), pp. 1179–1187. doi: 10.1084/jem.193.10.1179.

Wong, Y. C. *et al.* (2016) 'The CD8 T-cell response during tolerance induction in liver transplantation', *Clinical & Translational Immunology*. Wiley-Blackwell, 5(10), p. e102. doi: 10.1038/CTI.2016.53.

Xing, Y. and Hogquist, K. A. (2012) 'T-Cell tolerance: Central and peripheral', *Cold Spring Harbor Perspectives in Biology*. Cold Spring Harbor Laboratory Press, 4(6), pp. 1–15. doi: 10.1101/cshperspect.a006957.

Xu, X. (2018) *Investigating the positive and negative selection of B cell development*.

Xu, X. *et al.* (2020) 'An ontogenetic switch drives the positive and negative selection of B cells', *Proceedings of the National Academy of Sciences of the United States of America*. National Academy of Sciences, 117(7), pp. 3718–3727. doi: 10.1073/pnas.1915247117.

Yadav, M., Stephan, S. and Bluestone, J. A. (2013) 'Peripherally induced Tregs-role in immune homeostasis and autoimmunity', *Frontiers in Immunology*, 4(AUG). doi: 10.3389/fimmu.2013.00232.

Yang, L. *et al.* (2015) 'Inhibition of ERBB2-overexpressing Tumors by Recombinant Human Prolidase and Its Enzymatically Inactive Mutant', *EBioMedicine*, 2(5), pp. 396–405. doi:

10.1016/j.ebiom.2015.03.016.

Yang, L. *et al.* (2016) 'Dual inhibition of ErbB1 and ErbB2 in cancer by recombinant human prolidase mutant hPEPD-G278D', *Oncotarget*, 7(27), pp. 42340–42352. doi: 10.18632/oncotarget.9851.

Yang, L. *et al.* (2017) 'PEPD is a pivotal regulator of p53 tumor suppressor', *Nature Communications*. Nature Publishing Group, 8(1), pp. 1–15. doi: 10.1038/s41467-017-02097-9.

Yang, L., Li, Y. and Zhang, Y. (2014) 'Identification of prolidase as a high affinity ligand of the ErbB2 receptor and its regulation of ErbB2 signaling and cell growth', *Cell Death and Disease*. Nature Publishing Group, 5(5). doi: 10.1038/cddis.2014.187.

Yarkoni, Y., Getahun, A. and Cambier, J. C. (2010) 'Molecular underpinning of B-cell anergy', *Immunological Reviews*, 237(1), pp. 249–263. doi: 10.1111/j.1600-065X.2010.00936.x.

Ye, B. H. *et al.* (1997) 'The BCL-6 proto-oncogene controls germinal-centre formation and Th2-type inflammation', *Nature Genetics 1997 16:2*. Nature Publishing Group, 16(2), pp. 161–170. doi: 10.1038/ng0697-161.

Yinshi Yue, Y. Y. (2013) 'Microbial Infection and Rheumatoid Arthritis', *Journal of Clinical & Cellular Immunology*. OMICS Publishing Group, 04(06), p. 174. doi: 10.4172/2155-9899.1000174.

Yokogawa, M. *et al.* (2014) 'Epicutaneous application of toll-like receptor 7 agonists leads to systemic autoimmunity in wild-type mice: A new model of systemic lupus erythematosus', *Arthritis and Rheumatology*. John Wiley and Sons Inc., 66(3), pp. 694–706. doi: 10.1002/art.38298.

Yosef, N. *et al.* (2013) 'Dynamic regulatory network controlling TH 17 cell differentiation', *Nature*. NIH Public Access, 496(7446), pp. 461–468. doi: 10.1038/nature11981.

Young, A., Quandt, Z. and Bluestone, J. A. (2018) 'The balancing act between cancer immunity and autoimmunity in response to immunotherapy', *Cancer Immunology Research*, 6(12), pp. 1445–1452. doi: 10.1158/2326-6066.CIR-18-0487.

Youngblood, B. *et al.* (2011) 'Chronic Virus Infection Enforces Demethylation of the Locus that Encodes PD-1 in Antigen-Specific CD8+ T Cells', *Immunity*, 35(3), pp. 400–412. doi: 10.1016/j.immuni.2011.06.015.

Yu, D. *et al.* (2009) 'The Transcriptional Repressor Bcl-6 Directs T Follicular Helper Cell Lineage Commitment', *Immunity*. Immunity, 31(3), pp. 457–468. doi:

10.1016/j.immuni.2009.07.002.

Di Yu *et al.* (2007) 'Roquin represses autoimmunity by limiting inducible T-cell co-stimulator messenger RNA', *Nature*. Nature Publishing Group, 450(7167), pp. 299–303. doi: 10.1038/nature06253.

Yu, G. *et al.* (2012) 'ClusterProfiler: An R package for comparing biological themes among gene clusters', *OMICS A Journal of Integrative Biology*. Mary Ann Liebert, Inc. 140 Huguenot Street, 3rd Floor New Rochelle, NY 10801 USA , 16(5), pp. 284–287. doi: 10.1089/omi.2011.0118.

Zakharov, P. N. *et al.* (2020) 'Single-cell RNA sequencing of murine islets shows high cellular complexity at all stages of autoimmune diabetes', *The Journal of Experimental Medicine*. The Rockefeller University Press, 217(6). doi: 10.1084/JEM.20192362.

Zhang, Jian *et al.* (2006) 'The repression of human differentiation-related gene NDRG2 expression by Myc via Miz-1-dependent interaction with the NDRG2 core promoter', *Journal of Biological Chemistry*, 281(51), pp. 39159–39168. doi: 10.1074/jbc.M605820200.

Zhang, Q. *et al.* (2009) ' Combined Immunodeficiency Associated with DOCK8 Mutations ', *New England Journal of Medicine*, 361(21), pp. 2046–2055. doi: 10.1056/nejmoa0905506.

Zhao, T. *et al.* (2021) 'NDRG1 regulates osteosarcoma cells via mediating the mitochondrial function and CSCs differentiation', *Journal of Orthopaedic Surgery and Research*, 16(1). doi: 10.1186/s13018-021-02503-5.

Zheng, W. P. and Flavell, R. A. (1997) 'The transcription factor GATA-3 is necessary and sufficient for Th2 cytokine gene expression in CD4 T cells', *Cell*, 89(4), pp. 587–596. doi: 10.1016/S0092-8674(00)80240-8.

Zhou, B. *et al.* (2019) 'Therapeutic effects of a novel BAFF blocker on arthritis', *Signal Transduction and Targeted Therapy*, 4(1). doi: 10.1038/s41392-019-0051-z.

Zhu, F. *et al.* (2019) 'Humanising the mouse genome piece by piece', *Nature Communications*, 10(1). doi: 10.1038/s41467-019-09716-7.

Zhu, J., Yamane, H. and Paul, W. E. (2010) 'Differentiation of effector CD4+ T cell populations', *Annual Review of Immunology*, 28, pp. 445–489. doi: 10.1146/annurev-immunol-030409-101212.

Appendix

Appendix A. Antibodies used for flow cytometry

Antigen	Clone	Fluorochrome	Company	Catalog	Titration
IgD	11-26c.2a	FITC	Biolegend	405704	400
		APC-Cy7	Biolegend	405716	300-400
		AlexaFluor647	Biolegend	405708	400
IgDa	AMS-9.1	FITC	Biolegend	406104	400
IgM	II/41	FITC	BD Pharmigen	553437	500
	RMM-1	PE	Biolegend	406508	500
		PerCP-Cy5.5	Biolegend	406512	400
		PE-Cy7	Biolegend	406514	200
	eB121-15F9	e450	eBioscience	48-5890-82	200
IgMa	MA-69	PE	Biolegend	408608	500
	DS-1	FITC	BD Pharmigen	553516	500
CD45.1	A20	PE	Biolegend	110708	200
		APC-Cy7	Biolegend	110716	200
		PE-Cy7	Biolegend	110730	200
		Pacific Blue	Biolegend	110722	200
CD45.2	104	BV605	Biolegend	109841	200
		APC-Cy7	Biolegend	109824	200
		AlexaFluor647	Biolegend	109818	200
		BV421	Biolegend	109832	200
CD43	S7	PerCP-Cy5.5	BD Pharmigen	562865	100
CD23	B3B4	PE-Cy7	Biolegend	101614	250
CD93	AA4.1	APC	Biolegend	136510	200
CD19	6D5	AF700	Biolegend	115528	400
		APC Cy7	Biolegend	115530	500
CD3	145-2C11	APC-Cy7	Biolegend	100330	100
		PerCP-Cy5.5	Biolegend	100328	100
	17A2	Pacific Blue	Biolegend	100214	100
CD5	53-7.3	BV421	Biolegend	100629	100
Zombie Aqua Live/Dead		BV510	Biolegend	423102	200-400
Near IR Live/Dead		APC-Cy7	Biolegend	423106	400
B220	RA3-6B2	PerCP-Cy5.5	Biolegend	103236	500
		AF700	Biolegend	103232	500
		APC	Biolegend	103212	400
		BV605	Biolegend	103243	400
HyHEL9	HyHEL10	FITC	N/A	N/A	400

		Pacific Blue	N/A	N/A	400
CD21	7G6	BV605	BD Pharmigen	563176	500
	7E9	APC-Cy7	Biolegend	123418	400
		APC	Biolegend	123412	400
BP-1	Lg-51	PE	BD Pharmigen	553735	100
CD24	M1/69	BV421	Biolegend	101820	400
		AF700	Biolegend	101836	400
IgG1	RMG1-1	PE-Cy7	Biolegend	406614	200
	A85-1	BV605	BD Bioscience	563285	500
IgA	C10-3	FITC	BD Pharmigen	559354	100
CD25	PC61	PE	Biolegend	102008	500-800
		Pacific Blue	Biolegend	102022	500-800
CD69	H1.2F3	BV605	Biolegend	104530	200
		PE-Cy7	Biolegend	104512	400
CD86	GL-1	APC	Biolegend	105046	400
		PerCP-Cy5.5	Biolegend	105028	400
CD44	IM7	FITC	Biolegend	103006	100
		PerCP-Cy5.5	Life Technologies	45-0441-82	100-200
		APC	Biolegend	103012	100
		Pacific Blue	Biolegend	103020	100
CD62L	MEL-14	FITC	Biolegend	104406	100-200
		PE	Biolegend	104408	100-200
		APC	Biolegend	104412	100-200
PD1	RMP1-30	FITC	eBioscience	11-9981-82	100
		PE-Cy7	Biolegend	109110	100
OX40	OX-86	PE-Cy7	Biolegend	119415	100
CD90.1/Thy1.2	53-2.1	FITC	BD Pharmigen	553003	1000
CD4	GK1.5	PE-Cy7	Biolegend	100528	400
			ThermoFisher	25-0041-82	400
		AF700	Biolegend	100430	400
		APC-Cy7	Biolegend	100414	400
CD8a	53-6.7	PerCP-Cy5.5	Biolegend	100734	400
		AF700	Biolegend	100730	400
		APC-Cy7	Biolegend	100714	400
Phospho-ERK pT202/4	MILAN8R	Alexafluor488	eBioscience	53-9109-42	50
Phospho-AKT pT308	J1-223.371	PE	BD Pharmigen	558275	25
Phospho-pPLCy2 pY759	L86-689.37	APC	BD Pharmigen	558498	25

Phospho-BLNK pY84	J117-1278	AlexaFluor647	BD pharmigen	558443	25
Phospho-Syk Y348	moch1ct	PE	eBioscience	12-9014-42	50
Bim	C34C5	AlexaFluor647	CST NEB	10408S	100
Bcl2	3F11	PE	BD Bioscience	556537	5
BAFF-R	7H22-E16	PE	Biolegend	134103	200
CD95	SA367H8	APC	Biolegend	152604	200
	Jo2	PE-Cy7	BD Bioscience	557653	200
TCR Vα2	B20.1	PE	Biolegend	127806	400
BrdU	3D4	AlexaFluor647	BD Pharmigen	364108	20
CXCR5	L138D7	BV605	Biolegend	145513	200
CellTraceViolet Kit	N/A	CellTrace Violet	ThermoFisher	C34557	NA
Ki-67	16A8	AlexaFluor647	Biolegend	652408	400
		Pacific Blue	Biolegend	652422	400
Ly6c	HK1.4	PerCP-Cy5.5	Biolegend	128012	400
KLRG1	MAFA	FITC	Biolegend	138410	100
		PE	Biolegend	138408	100
CD127/IL7R		PE-Cy7	Biolegend	135014	100
	A7R34	APC	Biolegend	135012	100
FoxP3	MF-14	PE	Biolegend	126404	100-200
IL-2	JES6-5H4	AF700	Biolegend	504818	50
IFNγ	XMG1.2	e450	Biolegend	505808	50-100
		PE-Cy7	eBioscience	48-7311-82	100-200
		PE	eBioscience	25-7311-82	100

Appendix B. Top differentially expressed genes between anergic and naïve follicular B cells

Genes differentially expressed over 1 log2FoldChange and below a significance threshold of adjusted p value 0.05 between splenic anergic and naïve follicular B cells isolated from Ig^{HEL}/sHEL double-tg or Ig^{HEL} tg mice respectively, as determined by DESeq2. Genes are sorted here by log2FoldChange. Top results are visualised in Figure 3.2.

baseMean	log2FoldChange	lfcSE	pvalue	padj	mgi_symbol
12.8190405	8.34334976	2.8299479	1.15E-08	1.91E-07	Gm8183
10.0100991	7.79585385	2.68561054	5.56E-08	8.35E-07	Fibcd1
481.377316	7.37848608	0.31606479	4.53E-120	7.41E-117	Ndrg1
26.8692833	7.33345468	1.30794554	5.81E-10	1.14E-08	Mcam
67.2129042	6.9664848	0.73596796	3.78E-21	2.02E-19	Fam20c
6.59378537	6.81513892	2.6291768	3.47E-06	3.92E-05	Gm15479
98.9693046	6.64968526	0.56539153	4.14E-32	4.58E-30	Gfi1
5.47058293	6.63071694	2.77268427	1.67E-05	0.00016266	Col5a3
150.901105	6.48698528	0.70362339	1.71E-21	9.45E-20	Col4a5
5.46648722	6.41963892	2.63851911	1.54E-05	0.00015153	Rbm24
24.3521698	6.35211321	1.02223252	1.78E-10	3.72E-09	Rasgef1a
136.542136	6.3215006	0.64485462	6.10E-24	4.04E-22	Rgs13
35.2097237	6.08639833	0.80479183	3.54E-14	1.08E-12	Wnt10a
127.331426	5.88047458	0.39077798	2.36E-51	5.30E-49	Kifc3
44.5691873	5.86228566	0.66566312	1.19E-18	5.40E-17	Bcl6b
134.199826	5.742926	0.36148664	3.14E-57	9.34E-55	Nrgn
4.74639575	5.68024119	2.66353808	0.00015553	0.00121477	Igkv1-115
48.8313697	5.54536622	0.5814372	4.98E-22	2.87E-20	Nyx
3.51385412	5.53638725	2.85169721	0.00036721	0.00262592	Ccl3
7.02968388	5.49882609	2.42194668	5.97E-05	0.00051555	Reln
86.6076486	5.48257703	0.73599356	2.59E-15	8.86E-14	Havcr1
8.43097691	5.46115628	1.4368041	8.98E-06	9.29E-05	Cecr6
8.81379681	5.39474074	1.47767906	1.05E-05	0.00010752	Lonrf3
3.51822105	5.3680109	2.74177365	0.00034619	0.00249572	Lgr6
77.8855796	5.35957886	1.24096013	1.38E-06	1.68E-05	Chst7
614.416382	5.2258721	0.3420596	3.88E-54	9.35E-52	Myb
3.31777555	5.16769319	2.77734787	0.00054395	0.00370142	Spp1
378.489926	5.09915799	0.22979445	5.97E-112	8.15E-109	Egr2
66.9916228	4.97620957	0.43298438	7.94E-31	8.03E-29	Nr4a3
26.5158235	4.96758588	0.71206232	2.99E-13	8.45E-12	Sv2b
66.8518165	4.956668	0.47867547	5.38E-26	4.06E-24	6330403A02Rik
10.9745319	4.95179069	1.13564711	2.28E-06	2.66E-05	Tnfsf4
20.0307069	4.89075618	0.81570772	6.06E-10	1.19E-08	Ankrd13b
9.59717379	4.8618188	1.4140313	4.13E-05	0.00037246	Tnip3
6.19363476	4.85106825	1.52007565	8.91E-05	0.00074036	Ifng
328.800002	4.82015075	0.2473318	7.59E-85	4.97E-82	Ahr
2.96846035	4.77993321	2.82849439	0.00102923	0.00639277	Gm5300
24.0323188	4.76176167	0.77757923	7.97E-11	1.75E-09	Fabp5
19.0844666	4.69263425	0.77410066	1.89E-10	3.93E-09	RP23-453G13.1
13.4573795	4.5645954	1.04543429	2.49E-06	2.89E-05	Kcnc1
5.28048162	4.54965402	1.60687202	0.00027394	0.00202022	Dlk1
5.22625405	4.5399864	1.60636767	0.00028169	0.00206899	A430072P03Rik
6.37174898	4.4958996	1.47644746	0.00015586	0.00121677	Igkv4-80
10.659063	4.46822132	1.0019868	1.31E-06	1.59E-05	Ccl4
2.69037007	4.4584917	3.07071479	0.00205806	0.01167612	Aebp1
948.231693	4.45439552	0.14710645	5.35E-202	2.92E-198	Egr3
53.7183829	4.44760465	0.46236868	2.43E-22	1.44E-20	Rragd
11.7639927	4.44233686	0.98889966	7.71E-07	9.87E-06	Spry2
15.3127334	4.42697602	0.85734195	4.40E-08	6.73E-07	Tmc3
2.65895199	4.4138968	3.09225667	0.00218204	0.01226482	Slc24a2
257.052862	4.41154662	0.24166686	1.68E-75	8.89E-73	Hpgds
16.6413988	4.39920357	0.87172877	5.08E-08	7.67E-07	Trpm5

80.3462871	4.36877767	0.82858076	9.43E-08	1.38E-06	Rhobtb1
133.995767	4.34669609	0.28174697	2.55E-54	6.24E-52	Sdc1
11.2154875	4.33831069	0.987539	1.80E-06	2.13E-05	Dnm3
240.292751	4.32697424	0.1998368	4.70E-105	4.53E-102	Mreg
651.097458	4.30888247	0.15436433	6.90E-174	2.26E-170	Nr4a1
26.3580056	4.27391309	0.63666107	7.31E-13	2.03E-11	Rgs1
75.0356809	4.20749138	0.37400347	1.27E-30	1.26E-28	Tbx21
17.7304299	4.1628464	1.30356457	0.0001347	0.00106635	Alpl
27.2128107	4.16188259	0.57219063	3.25E-14	9.99E-13	Tacc2
112.155042	4.11929853	0.35917156	3.48E-31	3.59E-29	Npr2
23.8787174	4.08669607	0.64392572	8.47E-12	2.06E-10	F2rl1
228.586997	4.08645301	0.2200084	1.63E-78	9.21E-76	Gad1
12.4429894	4.08079653	0.89686041	7.76E-07	9.93E-06	Hcrtr2
15.8485571	4.04190618	0.81485646	9.46E-08	1.38E-06	Nrxn1
37.0176177	3.98568701	0.48880958	3.85E-17	1.53E-15	Gpr56
4.13641085	3.84304372	1.6656306	0.00112239	0.00689816	Adamtsl2
115.455066	3.82673325	0.6906275	9.53E-10	1.82E-08	Endou
941.882954	3.82549452	0.10664711	6.82E-283	1.12E-278	Rgl1
42.5695847	3.82071474	0.55722096	1.63E-12	4.34E-11	Echdc3
573.156653	3.79001092	0.15141171	6.56E-141	1.34E-137	Lck
73.8226489	3.76828863	0.34296469	4.73E-29	4.23E-27	Axl
10.6207196	3.72648924	0.96130784	1.00E-05	0.00010292	Efhc2
64.2417033	3.70458913	0.38954933	1.37E-22	8.33E-21	Loxhd1
67.6952925	3.69795801	0.3918641	4.48E-22	2.60E-20	Ighg1
3.88139906	3.69568484	1.71062238	0.00150309	0.00886855	Nr4a2
8.62695939	3.65786826	1.02607669	2.93E-05	0.00027208	Gpr176
24.7879676	3.65180159	0.5658715	6.74E-12	1.67E-10	Tcf7l2
19.2853212	3.63799541	0.64623587	1.56E-09	2.90E-08	A430093F15Rik
45.3399281	3.59665669	0.63691627	3.08E-09	5.56E-08	Tmem151b
197.559794	3.58866028	0.30947101	1.19E-31	1.28E-29	Prdm1
37.696998	3.56866285	0.43473267	2.11E-17	8.54E-16	Zfp704
434.733063	3.53184984	0.16221815	7.90E-106	8.09E-103	Ets2
13.1912676	3.5082622	0.86818926	2.42E-06	2.82E-05	Gm11463
130.634482	3.46779338	0.26201557	4.31E-41	6.42E-39	Fosb
27.3750493	3.46592326	0.52555148	2.27E-12	5.86E-11	Folr4
5.77870187	3.44037675	1.5482013	0.00159706	0.00935892	Il1r1
250.940579	3.3913849	0.20933563	3.01E-60	1.07E-57	Faah
14.2584758	3.38936393	1.38398566	0.00114514	0.00702217	6030419C18Rik
16.5125169	3.36731719	0.64019008	1.02E-08	1.72E-07	Pcp4
7.74806627	3.32078446	1.08483919	0.00024309	0.00181341	Cd63
455.326549	3.27508238	0.18337848	1.09E-72	5.60E-70	Crisp3
33.8849774	3.2741407	0.61699519	1.67E-08	2.73E-07	Obscn
1686.84059	3.27040301	0.09378764	4.63E-268	3.79E-264	Ephx1
38.725893	3.24898361	1.58146684	0.00123585	0.00747651	Igkv1-117
11.5586003	3.23750419	0.84660229	7.44E-06	7.83E-05	Ppnr
198.113067	3.22453271	0.42673167	1.49E-15	5.17E-14	Lef1
819.048795	3.21463818	0.1187609	2.35E-162	6.42E-159	Rgs2
23.0733379	3.19703821	0.53986846	2.95E-10	5.97E-09	Cenpv
7.75398436	3.14828009	0.99598849	0.00010423	0.00085068	Slc9b2
67.8688069	3.13332361	0.32727808	4.84E-23	3.05E-21	Kcnh4
31.6257779	3.13121837	0.50838799	7.85E-11	1.72E-09	Ms4a4a
769.801343	3.12018	0.11639575	1.21E-159	2.84E-156	Nab2
39.4840796	3.09859894	0.42135836	1.53E-14	4.85E-13	Lzts2
10.4187885	3.09006433	1.0398133	0.00034324	0.00247774	Synpo
33.1691832	3.08456016	0.51267744	8.65E-11	1.88E-09	Il18r1
34.9070046	3.0452056	0.44105343	4.12E-13	1.15E-11	RP23-412L18.4
3.74394908	3.01529649	1.90361516	0.00426743	0.02190418	Gm11754
360.903297	3.00072197	0.15777064	3.44E-82	2.01E-79	Cers6
28.7899031	2.99843138	0.59176494	4.55E-08	6.93E-07	Fam160a1
16.5047867	2.9788904	0.64281605	2.98E-07	4.03E-06	Eno2

85.4869157	2.97854573	0.30722395	1.39E-23	9.05E-22	2900026A02Rik
7.48028037	2.96690652	1.2121245	0.00053096	0.00362356	Gm13348
155.993402	2.93189541	0.27348588	5.77E-28	4.82E-26	Derl3
333.675971	2.91500373	0.1687541	2.66E-68	1.24E-65	Sox4
717.157505	2.89782475	0.14011508	8.40E-96	6.55E-93	Rgs3
23.291285	2.86624577	2.31639042	0.00338155	0.01789545	Gm26984
29.1000728	2.85424081	0.47884018	1.17E-10	2.49E-09	Ccr9
5.34453969	2.82596641	1.27768146	0.00136139	0.00812915	Pald1
3.08618319	2.82474759	2.30732366	0.00590544	0.02877013	Gm20539
10.9941275	2.8149622	0.84484866	5.11E-05	0.00044957	Sall2
389.490564	2.80644028	0.17153472	1.86E-61	6.94E-59	Litaf
111.905874	2.78989802	0.33903391	2.13E-17	8.60E-16	Gp49a
333.228662	2.78279462	0.16362833	5.15E-66	2.16E-63	Cacna1h
82.31154	2.75465525	0.26728841	4.68E-26	3.57E-24	Gm19585
324.489607	2.73060434	0.19185956	1.10E-47	2.17E-45	Zfpm1
495.947422	2.72670895	0.1594062	1.25E-66	5.41E-64	Bhlhe40
192.540458	2.71954079	0.22127232	7.12E-36	8.70E-34	Akap5
5.42000514	2.68514532	1.41989198	0.00317099	0.01693978	C230035I16Rik
240.383856	2.68403971	0.18107622	1.20E-50	2.58E-48	Zfp948
58.2463094	2.67819299	0.32538581	8.90E-18	3.74E-16	Dll1
6.60430252	2.67759191	1.22766256	0.00100785	0.00629097	A430105I19Rik
998.132738	2.67441869	0.10824328	1.36E-135	2.47E-132	Fam167a
23.116544	2.66070542	0.5172665	1.74E-08	2.83E-07	Pgpep1l
25.8595654	2.6466868	0.55835269	1.17E-07	1.69E-06	RP23-412L18.2
181.190349	2.64058315	0.18348662	2.48E-48	5.14E-46	Plk2
8.24137354	2.63583909	1.06281465	0.00079574	0.0051353	Agbl1
96.3878168	2.62990687	0.26321585	1.19E-24	8.39E-23	Cdh24
23.2838836	2.62961727	0.56281551	2.44E-07	3.35E-06	Bcat1
51.2771503	2.62922238	0.42006518	1.24E-11	2.97E-10	Dcbld1
126.427798	2.62530391	0.22206992	3.13E-33	3.61E-31	Crip3
50.4874927	2.62312966	0.34949289	2.39E-15	8.18E-14	RP23-412L18.1
5.93817273	2.60899639	1.24754242	0.00182229	0.01049854	Lag3
24.2250361	2.60513045	0.48658808	6.53E-09	1.13E-07	Rgs7bp
14.0648366	2.57516679	1.00984795	0.00102223	0.00636534	Gm4956
9.00774979	2.56717141	0.93087928	0.00026846	0.00198426	Rimbp3
239.357503	2.55402953	0.18165441	3.14E-46	5.84E-44	Klf10
2178.58013	2.54903326	0.24458231	8.80E-27	7.03E-25	S1pr3
33.39802	2.51693626	0.480408	8.75E-09	1.49E-07	Akap1
12.9188894	2.51259301	0.76323942	6.42E-05	0.00054903	Rundc3a
239.976151	2.50484624	0.38805542	5.76E-12	1.43E-10	Abcb4
16.6686158	2.5028241	0.66888778	1.18E-05	0.00011938	Sema6d
6.40322763	2.49125419	1.36355867	0.00194484	0.01109915	Gab1
126.445218	2.48984604	0.26367506	3.17E-22	1.85E-20	Fam46c
29.1201793	2.48946996	0.46690913	6.16E-09	1.07E-07	Car2
122.621317	2.48842227	0.25831057	2.19E-23	1.41E-21	Rapgef3
18.6685403	2.48768801	0.5867268	1.34E-06	1.64E-05	Hbb-bt
1058.90973	2.47652532	0.19242718	3.93E-39	5.32E-37	Srgap3
26.3114577	2.46671035	0.47699264	1.45E-08	2.38E-07	Igf1r
5.42483484	2.45919481	2.88689417	0.00477334	0.02404875	Trav13n-4
129.525619	2.45062236	0.28292742	4.08E-19	1.93E-17	Dmd
511.34109	2.44185353	0.35102123	1.74E-13	5.02E-12	Egr1
657.026207	2.43006327	0.11085965	5.50E-108	6.43E-105	Shank1
15.0418687	2.41725029	0.64580189	1.14E-05	0.00011582	RP23-412L18.5
15.5905926	2.41462444	0.64520054	9.01E-06	9.32E-05	RP23-412L18.3
7.78933222	2.40445778	1.08618176	0.00143498	0.00852195	Tmem88
13.8487639	2.40424237	0.72771099	5.49E-05	0.00047877	Enthd1
19.1919832	2.39716846	0.58455274	2.70E-06	3.12E-05	Dhrs3
13.4978422	2.39056758	0.69394073	3.26E-05	0.00029972	Vasn
9.03167435	2.38763687	0.85533724	0.0002791	0.00205459	Gm13343
10.8348342	2.37821943	0.77834425	0.00013679	0.00108076	Nlgn2

365.251499	2.37671001	0.12877568	3.97E-77	2.17E-74	Dusp4
93.2813462	2.37220663	0.33925586	1.71E-13	4.95E-12	Cpd
345.661485	2.36638066	0.66725031	3.30E-05	0.00030285	Ackr3
137.877651	2.3487254	0.21696515	1.99E-28	1.70E-26	Phactr2
979.007532	2.34107992	0.11973759	3.45E-86	2.35E-83	Zfp52
10.4818938	2.33735948	1.02414492	0.00155899	0.00916206	Rims2
4.543179	2.32869253	1.67162264	0.00600512	0.02913443	Fzd6
254.786851	2.32552015	0.18476834	2.54E-37	3.25E-35	Abcb1b
23.777586	2.32523054	0.51722668	3.88E-07	5.18E-06	Klc3
24.2490345	2.31440421	0.58870873	6.82E-06	7.24E-05	Apba1
266.026883	2.30331141	0.20154033	2.30E-31	2.41E-29	Hmgn3
68.0644598	2.300464	0.30824312	5.26E-15	1.75E-13	Dnah1
820.459856	2.29598936	0.17132342	4.98E-42	7.77E-40	St8sia6
15.4525598	2.284718	0.77932317	0.00012113	0.00097258	Nrp1
5.73587711	2.2810273	1.1596995	0.00229989	0.01282164	Sptb
10.3606425	2.27364375	1.03090576	0.00116093	0.00709778	Igkv4-79
24.3075261	2.26755794	0.46620164	8.01E-08	1.18E-06	2900089D17Rik
295.485819	2.26432407	0.75928469	0.00022785	0.00171347	Lmo7
64.0622466	2.25860285	0.36115655	3.11E-11	7.12E-10	Gm26947
13.7640787	2.24937733	0.63677872	2.76E-05	0.00025764	RP23-412L18.6
15.9213808	2.24559672	0.63692931	2.27E-05	0.00021491	Arhgap32
28.076087	2.23984491	0.47772911	2.18E-07	3.02E-06	Hemgn
19.7198718	2.23404647	0.52222847	1.05E-06	1.31E-05	Gm12065
8.83442948	2.22898811	0.97074127	0.00138731	0.00826583	Gm10634
175.251652	2.22775948	0.22877152	1.32E-23	8.60E-22	Emr1
300.45864	2.22745974	0.26523511	4.20E-18	1.82E-16	Specc1
731.93828	2.21458591	0.1718851	2.01E-39	2.77E-37	Bhlhe41
45.9777919	2.21162812	0.34024456	6.92E-12	1.71E-10	Gm15880
10.8109868	2.19106347	0.95383245	0.00121436	0.00736396	Spire1
26.2522397	2.17929675	0.60480651	2.15E-05	0.00020468	Igkv10-96
424.26137	2.17692979	0.13883911	1.34E-56	3.78E-54	Pacsin1
32.1748527	2.17298846	0.4375999	3.93E-08	6.03E-07	RP23-453G13.2
1331.87395	2.16207329	0.25808897	3.20E-18	1.40E-16	Alcam
56.7780266	2.15719966	0.33209506	7.15E-12	1.76E-10	Ispd
21.9085486	2.14705259	0.61220143	1.87E-05	0.00018048	Mcf2l
17.9468238	2.1414438	0.5872033	1.79E-05	0.00017309	Tspan33
3440.13142	2.13860152	0.1242828	9.23E-68	4.20E-65	Ccnd2
11.3014661	2.12893248	0.7707629	0.00029181	0.00213522	Metrnl
8.88653075	2.12586714	0.87531406	0.00071901	0.0047144	Nat8l
150.527305	2.12576923	0.30278219	1.01E-13	2.99E-12	Sspn
365.610969	2.09657409	0.20862742	5.45E-25	3.90E-23	Pard3b
28.156913	2.09510518	0.5356944	5.22E-06	5.65E-05	Nol4l
47.6247159	2.09087706	0.4828877	1.01E-06	1.27E-05	RP23-327M13.2
16.3193085	2.08890861	0.58796287	1.95E-05	0.00018682	Kcnk3
111.674512	2.08818363	0.31479923	2.04E-12	5.36E-11	Sned1
1468.48277	2.08192204	0.15163105	6.11E-44	1.04E-41	Fcrl5
16.4598188	2.06318626	0.57565589	1.92E-05	0.00018408	Csdc2
8530.32411	2.0626629	0.09096854	3.51E-115	5.23E-112	Faim3
14.7687175	2.04303375	0.73376643	0.00024587	0.00182805	Sh2d5
107.971333	2.03215473	0.21980713	2.10E-21	1.14E-19	Rassf6
18.6631901	2.01366362	0.57991551	3.07E-05	0.00028389	Tcam1
12.1681053	2.00072416	0.74048539	0.00034129	0.00246583	A230005M16Rik
5.64208376	1.99578025	1.38957281	0.00475428	0.02397487	Klra1
155.580505	1.98328621	0.24483911	4.30E-17	1.70E-15	Bcl2a1b
259.984595	1.98148773	0.15217822	5.99E-40	8.45E-38	Renbp
84.8403647	1.98147221	0.30454111	4.60E-12	1.15E-10	Cldn10
216.704691	1.94618825	0.17545736	8.59E-30	8.14E-28	Shmt1
39.6834976	1.94587597	0.56370314	2.31E-05	0.00021812	Adamtsl4
838.749599	1.92930323	0.13025897	8.33E-51	1.82E-48	Nod1
21.2368018	1.92601963	0.50372079	6.38E-06	6.80E-05	2610307P16Rik

12.4866696	1.91979757	0.84910008	0.00116943	0.00714329	Cntnap1
10.2576762	1.91491485	1.02795692	0.00213015	0.01202677	Igkv1-88
28.6476448	1.90295426	0.45380203	1.30E-06	1.59E-05	6430571L13Rik
30.1154544	1.8941318	0.44796787	1.64E-06	1.97E-05	Lrp11
197.898928	1.89132674	0.19274027	8.26E-24	5.43E-22	Pogk
61.5951446	1.89074929	0.29891578	1.53E-11	3.62E-10	Slc4a11
6787.21847	1.88070573	0.11146713	5.31E-65	2.17E-62	Il4i1
4.79112019	1.87096906	1.51710112	0.00631978	0.03038205	Cfap70
6.78908333	1.8679204	1.01861705	0.00243793	0.01348103	A930024N18Rik
45.9749265	1.8664992	0.35535839	1.16E-08	1.93E-07	Actn1
24.4844081	1.86294367	1.0540111	0.00580137	0.02832208	Scamp1
125.663241	1.86192628	0.29657215	2.31E-11	5.35E-10	Bcl2a1d
96.1388438	1.86029541	0.28389088	3.01E-12	7.65E-11	Dtl
2236.2326	1.84582883	0.10380822	8.73E-72	4.33E-69	Cdk6
349.853864	1.83803375	0.14265446	5.24E-39	7.04E-37	Ehd3
47.0361726	1.82933118	0.44589206	1.89E-06	2.24E-05	Anln
20.603217	1.81035699	1.07012758	0.00593781	0.02888488	Timd2
88.4850615	1.80816408	0.26642936	8.46E-13	2.33E-11	Gpt2
166.744138	1.80417103	0.20697446	2.15E-19	1.03E-17	Slc43a3
36.0144191	1.80401032	0.49327029	1.25E-05	0.00012572	Rilpl1
96.700338	1.80342984	0.22877668	3.03E-16	1.11E-14	B3gnt7
16.3436617	1.78402824	0.79803617	0.00106781	0.00662011	Tnfsf18
147.184055	1.76801476	0.249244	1.28E-13	3.72E-12	Zfp827
12.2723851	1.76517471	0.720289	0.0007077	0.00464772	Tbkbp1
10.0132469	1.76247441	0.77963255	0.00095419	0.00600869	Serp2
147.789984	1.76093228	0.43421275	4.66E-06	5.12E-05	Rec8
264.481511	1.75697489	0.1400989	3.26E-37	4.11E-35	Mar-03
43.3477516	1.7559327	0.3892542	4.12E-07	5.46E-06	Camk2b
239.335097	1.75420276	0.15828934	1.08E-29	9.95E-28	Dgkh
141.685083	1.75372467	0.20831313	3.02E-18	1.32E-16	Ank
221.770905	1.75045076	0.30267267	7.99E-10	1.54E-08	Rgs10
63.8655945	1.7429284	0.29563824	2.64E-10	5.37E-09	Csrp2
21.3469495	1.73761217	0.51063564	4.02E-05	0.00036341	Frmd4b
202.293029	1.72932289	0.20049649	3.34E-19	1.58E-17	Gm26667
360.214055	1.7263133	0.24542692	1.21E-13	3.55E-12	Dnase1l3
25.8739671	1.72562716	0.54378662	8.23E-05	0.00068897	Klrd1
14.2659311	1.72472708	0.6074084	0.00024922	0.0018512	Foxj1
355.874525	1.72183561	0.13515204	2.47E-38	3.26E-36	Vat1
7.82814045	1.72173086	1.1682106	0.00480676	0.02417993	Pid1
89.8899864	1.71497751	0.29105658	2.51E-10	5.12E-09	Dos
27.9573689	1.70865268	0.49688856	3.57E-05	0.00032615	Gm16157
115.946637	1.69601819	0.46248115	1.84E-05	0.00017766	Sh2d1b1
18.9583929	1.68827322	0.62062692	0.00036266	0.00260297	Btn2a2
37.2479818	1.68489017	0.91195836	0.00490731	0.02459509	5033430I15Rik
1036.26369	1.67692844	0.10380996	6.93E-60	2.41E-57	Usp28
133.294723	1.67245433	0.25614006	4.47E-12	1.12E-10	Gm6264
11.5760376	1.67170119	0.82235627	0.00173	0.01002323	Nefh
13.0105784	1.67163519	0.90856057	0.00245965	0.01357366	Wnt10b
41.1741597	1.66680326	0.34369982	7.22E-08	1.07E-06	4933406C10Rik
25.4236395	1.66673414	0.5107921	5.73E-05	0.00049652	Fam83f
531.36255	1.65573843	0.28185562	2.53E-10	5.16E-09	Gm16026
82.4682705	1.65564142	0.51002379	8.71E-05	0.00072561	Aicda
34.0489345	1.65554304	0.38043783	9.44E-07	1.19E-05	Jup
300.708559	1.65368338	0.14720677	2.17E-30	2.12E-28	Plxna3
1200.05449	1.6511376	0.11504852	4.31E-48	8.72E-46	Mdfic
137.47494	1.6487251	0.2001922	1.52E-17	6.25E-16	Cenpe
1655.51718	1.63845173	0.07754631	2.60E-100	2.24E-97	Bcl2l11
53.9364639	1.63353886	0.33965468	1.06E-07	1.54E-06	Tns1
2952.94608	1.63346788	0.08456446	1.77E-84	1.07E-81	Rin3
17.6309051	1.63171259	0.69497054	0.00089566	0.00568162	Tbc1d30

22.247811	1.6265424	0.57956938	0.00024206	0.00180789	9330136K24Rik
334.560993	1.62359344	0.16512393	5.81E-24	3.87E-22	Ryr2
60.6259698	1.6185266	0.34586793	1.62E-07	2.28E-06	Spo11
1514.33801	1.61275362	0.10230728	3.95E-57	1.15E-54	Tagap
360.583362	1.61160967	0.13826762	1.19E-32	1.34E-30	Psat1
49.5230208	1.6100182	1.20402967	0.01154435	0.04969058	Cacnb4
67.7378212	1.60994133	0.30962818	1.52E-08	2.49E-07	Slc25a13
247.283621	1.59990069	0.15221926	7.01E-27	5.65E-25	Leprotl1
115.596256	1.599843	0.24101097	2.19E-12	5.67E-11	Tgfb3
113.955641	1.59950335	0.43204131	1.87E-05	0.00018048	Smyd2
296.069011	1.59178279	0.39576707	4.35E-06	4.81E-05	Plscr1
39.8278415	1.59013359	0.47139043	5.35E-05	0.00046801	Sema6b
9.26512041	1.5881159	0.83390013	0.00239698	0.01326804	1110018N20Rik
140.476142	1.5811788	0.22197739	7.58E-14	2.27E-12	Serpinb6b
708.674344	1.57976318	0.26749332	2.18E-10	4.50E-09	Gm10552
1658.59288	1.57921726	0.11499198	4.32E-44	7.52E-42	Cdyl2
651.993566	1.57251684	0.16508196	1.17E-22	7.16E-21	Scn4a
18.4832632	1.57243006	0.7060761	0.00139113	0.00828254	Mfsd2a
32.347198	1.56592502	0.44160584	2.18E-05	0.00020676	Fads1
7.69803615	1.56210764	1.23686987	0.00628285	0.03022225	Glt28d2
858.97986	1.56162662	0.28185724	2.00E-09	3.69E-08	Cd93
12.4532124	1.55251315	0.8830022	0.00364107	0.01911446	2810029C07Rik
15.9700833	1.55196841	0.63369904	0.00067308	0.0044669	Gm6020
30.8119111	1.55075306	0.44463962	2.58E-05	0.00024211	Gnb4
971.368523	1.55002088	0.12788653	6.77E-35	8.03E-33	Twsg1
33.4609863	1.54874634	0.4743216	5.09E-05	0.00044796	Egfl6
56.0605411	1.54525008	0.46986447	5.98E-05	0.00051614	Mgst1
45.497408	1.54036075	0.49921759	0.00010726	0.00087113	Snord118
211.22883	1.53653613	0.65054223	0.00075184	0.00489057	Igkv1-135
214.495159	1.51982626	0.18675203	2.83E-17	1.13E-15	Arhgap31
7.26801611	1.51757035	1.76024824	0.00712554	0.0334698	9630013D21Rik
119.931317	1.51177905	0.2661537	1.03E-09	1.95E-08	Hes5
71.5990314	1.50881975	0.31582536	1.46E-07	2.07E-06	Cntln
68.0486822	1.50392901	0.26789243	1.48E-09	2.76E-08	Mex3a
1223.31765	1.48534703	0.13229522	2.15E-30	2.11E-28	Tgif1
140.516432	1.48006653	0.29997264	6.83E-08	1.02E-06	Gm15472
62.0495544	1.4770378	0.35896206	3.19E-06	3.63E-05	Myo1h
45.9958815	1.47336313	0.36808706	4.01E-06	4.46E-05	9430020K01Rik
8.22520763	1.47268823	1.1555595	0.00590218	0.0287628	Sema4g
95.8000404	1.47260903	0.29083577	3.45E-08	5.32E-07	Ptov1
11.3506494	1.46965401	0.95631556	0.00397845	0.02061633	RP23-327M13.4
363.319472	1.4687538	0.20265804	3.40E-14	1.05E-12	Tmem26
311.290131	1.46824078	0.25484199	7.47E-10	1.45E-08	Ldlrad3
1147.30448	1.4619407	0.09078933	2.17E-59	7.41E-57	Vav3
20.4117198	1.46122147	0.50813261	0.00021645	0.0016376	Maff
617.246281	1.4510949	0.31484592	2.48E-07	3.40E-06	Ighg3
1101.31721	1.44862378	0.10925711	2.67E-41	4.05E-39	Irs2
37.0357454	1.44817036	0.42394531	3.43E-05	0.00031353	Hectd2
103.644046	1.44664504	0.22855489	2.08E-11	4.84E-10	Tmem86a
8.58385852	1.44632911	1.02586485	0.00626484	0.0301622	Neil3
306.047723	1.44614737	0.19366544	7.70E-15	2.51E-13	Slc16a1
27.350913	1.44460762	0.43951581	6.84E-05	0.00058224	Hap1
1095.91598	1.44078907	0.15308855	4.07E-22	2.38E-20	Lilrb4
22.609987	1.44011461	0.58940546	0.0008185	0.00525731	E130208F15Rik
150.117717	1.4365357	0.18488055	5.39E-16	1.93E-14	Abi2
90.5924475	1.43634083	0.38420339	1.27E-05	0.00012716	Igkv5-48
25.2036538	1.42955961	0.47325584	0.0001429	0.00112365	Mir6999
19.0375347	1.42829522	0.58128424	0.0006637	0.00441362	Lrrc32
923.304726	1.42818698	0.12542536	3.16E-31	3.27E-29	Gm6377
60.1217165	1.42473589	0.32434975	6.94E-07	8.93E-06	Sestd1

77.8629002	1.42233661	0.26445213	6.15E-09	1.07E-07	Dctd
14.2454091	1.42092721	0.74351852	0.00230076	0.01282211	Igkv12-89
87.5908013	1.41896875	0.2578812	2.79E-09	5.06E-08	Slc25a33
110.001305	1.41671716	0.23771405	1.98E-10	4.08E-09	Tle2
27.0902027	1.41553119	0.47009577	0.00015524	0.00121308	Car13
26.6846824	1.40987897	0.54741241	0.00049911	0.00343919	Cd28
17.5973555	1.40806164	0.66834468	0.00165682	0.00964651	Abca8b
21.6374012	1.40524655	0.53446675	0.00048938	0.00339068	Mar-08
9.13153258	1.40311861	0.94287961	0.00535963	0.02645283	Btbd11
41.914292	1.4005337	0.35477196	5.75E-06	6.18E-05	Gm28707
8.17838862	1.40037279	1.12054563	0.00599371	0.02910495	Pls1
4.96178624	1.4003127	2.60169343	0.00858009	0.0390262	Prlr
7200.24257	1.40015377	0.08300382	6.62E-65	2.64E-62	Cd72
1009.45778	1.39483148	0.252026	1.95E-09	3.60E-08	A530032D15Rik
138.390123	1.39262103	0.20513025	1.08E-12	2.93E-11	Gm23037
518.083786	1.39196775	0.1351191	5.35E-26	4.06E-24	Marcksl1
4277.84983	1.39002131	0.11034127	1.46E-37	1.89E-35	Marcks
43.5790219	1.3897082	0.35166201	5.14E-06	5.58E-05	Sepn1
556.38037	1.38906888	0.12108303	1.33E-31	1.42E-29	Zbtb10
28.5276817	1.38858869	0.48718072	0.00026036	0.00192703	RP23-327M13.3
15.8809739	1.38539784	0.81587657	0.00364481	0.01912794	Arhgap23
17.544815	1.38362049	0.58200769	0.00095966	0.00603851	Sgce
22.7486741	1.37030859	0.55197681	0.00079813	0.00514495	Adamts14
1019.74275	1.36977284	0.13151614	1.62E-26	1.26E-24	Tnik
476.935628	1.36472367	0.13637325	9.72E-25	6.86E-23	Timeless
53.9299763	1.35723802	0.36264823	1.29E-05	0.00012911	Ciart
755.696902	1.35719666	0.13603509	1.40E-24	9.76E-23	Akap12
706.685737	1.3553192	0.12496592	1.80E-28	1.56E-26	Casp4
21.6697928	1.35148336	0.60254283	0.00137184	0.00818258	Cdca5
1244.17594	1.34540622	0.14379455	6.35E-22	3.63E-20	Hdac9
1875.14892	1.34161262	0.10247238	3.18E-40	4.53E-38	Vmp1
6.9267023	1.34004427	1.43149861	0.00727705	0.03406424	Pgk2
7.11594144	1.33955282	1.13251433	0.00716312	0.03360776	Ephb6
16.831631	1.33650896	1.20542691	0.00650785	0.0311036	Iglv2
1519.04785	1.33621529	0.09206935	7.96E-49	1.67E-46	Slamf7
23.1051464	1.33300178	0.60168183	0.00145711	0.00863772	Ltbp4
27.6136711	1.33019707	0.44722186	0.00019527	0.00149317	Gm9320
273.198781	1.32995143	0.14902422	3.38E-20	1.69E-18	Hk2
140.68144	1.32975871	0.24996263	8.41E-09	1.43E-07	Tubg2
142.395285	1.32693093	0.27881379	1.47E-07	2.09E-06	Tjp2
150.158993	1.32412601	0.20956524	1.80E-11	4.24E-10	Gsto1
385.386122	1.32035585	0.15197496	2.46E-19	1.18E-17	Gm11998
102.944876	1.32005045	0.33833819	5.66E-06	6.09E-05	Cplx2
534.797999	1.31679985	0.12136201	1.95E-28	1.67E-26	Fam213a
317.729006	1.31307979	0.13845325	2.27E-22	1.35E-20	Gm15848
11.9201411	1.31281222	0.68441183	0.00271369	0.01478379	Gp5
469.806513	1.30767826	0.14165571	2.15E-21	1.17E-19	Snhg4
63.3659397	1.3055434	0.34006816	8.29E-06	8.63E-05	RP24-92E18.1
115.356061	1.30478562	0.28723478	4.75E-07	6.23E-06	Clstn1
13.5170919	1.30389695	0.75619503	0.00340369	0.01800681	Cysltr2
86.9217413	1.30094883	0.25977067	3.48E-08	5.35E-07	Hspa2
139.781182	1.30053726	0.25342708	2.17E-08	3.46E-07	Fos
222.395824	1.2951051	0.21456702	1.13E-10	2.42E-09	1110038B12Rik
17.596892	1.28490193	0.70483071	0.00351368	0.01852883	Kif4
14.1557956	1.28374489	0.72017282	0.00365843	0.01918099	Gm20449
419.797296	1.28093556	0.17307106	1.01E-14	3.26E-13	Inppl1
25.8420318	1.27888282	0.45348742	0.00030757	0.00224095	Reep2
1037.5783	1.27797597	0.09624698	3.14E-41	4.72E-39	Ppfibp2
41.4841381	1.27583922	0.37073683	3.64E-05	0.00033241	Maf
596.088602	1.2728358	0.12614078	4.51E-25	3.24E-23	Pdlim7

15.8896754	1.27088887	0.835454	0.00522475	0.02594004	Gm13245
404.826717	1.2704834	0.12861732	4.31E-24	2.88E-22	Spred1
741.994844	1.26688855	0.12561876	4.09E-25	2.96E-23	Xkrx
139.182688	1.26078624	0.2309109	3.65E-09	6.52E-08	Sla2
53.3102292	1.26063017	0.3791812	6.48E-05	0.00055337	Gm2427
36.1442101	1.26047294	0.41386208	0.00014763	0.00115919	Vegfa
700.230835	1.25587117	0.1091205	1.07E-31	1.16E-29	Dpp7
9890.36599	1.25486981	0.10066348	1.13E-36	1.40E-34	Zfp318
775.728161	1.25291375	0.0965139	1.50E-39	2.10E-37	Nsmf
43.6939013	1.25205313	0.3722527	5.54E-05	0.00048176	Alpk1
901.676692	1.24450416	0.13439813	1.44E-21	8.03E-20	Rilpl2
1294.31996	1.24137208	0.23183846	6.95E-09	1.20E-07	Arhgap24
51.1327547	1.23844076	0.37344369	6.33E-05	0.0005434	Zfp365
388.862918	1.2383298	0.13595683	7.13E-21	3.72E-19	Daam1
948.501552	1.23399201	0.15312555	7.90E-17	3.04E-15	Myc
30.1257271	1.23139578	0.44991763	0.00038038	0.00271114	Epb4.1l4b
64.3128157	1.22930977	0.2793512	9.06E-07	1.15E-05	Lrtm2
29.3987566	1.22681165	0.43976297	0.00031033	0.00225908	Lcat
31.8687036	1.21987337	0.85085572	0.00709884	0.03340187	2810417H13Rik
53419.1117	1.21223802	0.07742246	2.81E-56	7.54E-54	Ighd
282.708608	1.20612728	0.1484729	4.54E-17	1.78E-15	Uhrf1
424.68106	1.20589686	0.19787174	9.52E-11	2.06E-09	Top2a
501.227569	1.20419775	0.10537298	2.91E-31	3.03E-29	Ubash3b
4254.03287	1.20309507	0.12662931	1.82E-22	1.10E-20	Cd83
643.521881	1.19864067	0.10921029	5.09E-29	4.53E-27	Lpar2
25.113493	1.19300651	0.46617596	0.00069995	0.00460423	Tex14
24.9347723	1.18934116	0.59679289	0.00209662	0.01187434	Rapgefl1
131.490947	1.18719341	0.21506114	3.13E-09	5.64E-08	Sh2b2
4168.90163	1.18330792	0.10141513	1.38E-32	1.55E-30	Rftn1
40.7871607	1.18225377	0.42029162	0.00034607	0.00249572	Prodh
14.7021399	1.18195943	0.92230977	0.00765063	0.03547841	Ncs1
620.181465	1.17721772	0.28392958	2.50E-06	2.90E-05	Apoe
9.34896905	1.17712321	0.93471081	0.00689323	0.03259361	Spry1
28.562073	1.17638211	0.53038046	0.0017098	0.00991322	Dbn1
16.5512464	1.17527167	0.72539405	0.00460391	0.02334595	Apol7e
379.467742	1.17164491	0.20187151	7.27E-10	1.41E-08	Krt222
492.431558	1.17150688	0.12025475	1.84E-23	1.19E-21	Hspa4l
163.01793	1.16413251	0.22246299	1.52E-08	2.48E-07	Bicd1
174.703676	1.1605454	0.2392189	1.12E-07	1.62E-06	Kcnk13
26.7848792	1.16048778	0.45199262	0.00066899	0.00444338	Syde1
47.4388318	1.15986726	0.47858777	0.00086641	0.00552175	Il2ra
29.3802167	1.15963672	0.46305324	0.00081036	0.00521116	Ptchd1
554.104356	1.15943446	0.1269277	5.84E-21	3.08E-19	Otud1
41.7812362	1.15751103	0.32799978	3.28E-05	0.00030061	Neto2
1340.02583	1.15064655	0.0858942	7.45E-42	1.14E-39	Syne1
2650.06323	1.14123685	0.08000461	3.07E-47	5.98E-45	Grap2
418.552664	1.13855807	0.15028417	3.03E-15	1.03E-13	Spn
68.9460429	1.13362918	0.30153464	1.56E-05	0.00015293	Stmn1
490.689861	1.12943995	0.13530134	6.76E-18	2.86E-16	Capn5
47.0608736	1.12870642	0.35939951	0.0001396	0.00110156	Omp
34.7090157	1.12825801	0.58740072	0.00306155	0.01643025	Kntc1
928.910219	1.12758423	0.09260742	4.25E-35	5.09E-33	Prkab2
116.591344	1.12328984	0.3346975	6.00E-05	0.00051705	Astl
629.517671	1.12204919	0.09943554	1.34E-30	1.32E-28	Crat
557.553982	1.11936758	0.12996506	7.42E-19	3.41E-17	Synj2
253.457693	1.11719072	0.1683518	3.61E-12	9.13E-11	Rcn1
16.7901736	1.11409062	0.79303256	0.00643154	0.03083786	Il1rl2
7952.66725	1.11216632	0.07725239	4.22E-48	8.64E-46	Plek
57.3793525	1.11002276	0.33522337	7.50E-05	0.00063219	Galnt14
7513.53545	1.10571355	0.07254133	1.74E-53	4.08E-51	BE692007

436.604919	1.10397487	0.1619541	8.29E-13	2.29E-11	Tet1
101.121739	1.10036976	0.39967081	0.00049128	0.00340099	Sel1l3
24.1220332	1.09544539	0.45926752	0.0011765	0.00717955	Gm16353
45.3876122	1.09178667	0.36465011	0.00020359	0.00154954	Chek1
60.6523323	1.08216515	0.33140661	7.95E-05	0.00066763	Cd27
267.909038	1.08007383	0.2079996	1.99E-08	3.21E-07	Ccr1
177.025171	1.0777646	0.20927314	2.75E-08	4.32E-07	Il12rb1
17.4880159	1.07645574	0.76468425	0.00819048	0.03760914	Espl1
257.93535	1.07640778	0.17154626	3.17E-11	7.24E-10	Tubb2b
2463.60279	1.07560794	0.09652813	1.00E-29	9.27E-28	Ptpn22
9.94696986	1.0717366	1.15096565	0.00959639	0.04268857	Ano7
43.1727502	1.06914425	0.42357868	0.00074397	0.00485089	Spef2
952.311376	1.06838383	0.15328996	3.14E-13	8.85E-12	Il12a
239.657115	1.06444603	0.16887859	3.11E-11	7.12E-10	Wee1
21.7270784	1.06040056	0.50513187	0.00234563	0.01303667	Gm28285
74.0422029	1.05789827	0.28589553	2.11E-05	0.00020064	Jdp2
1425.25752	1.0544828	0.09491029	9.22E-30	8.63E-28	Bmf
729.815487	1.05309586	0.30419078	4.49E-05	0.00040098	Pdzd2
61.7429785	1.05204384	0.32142728	8.12E-05	0.00068073	Ly6c2
27.5790018	1.05152932	0.47741039	0.00187992	0.01077788	Tmem38b
86.3859501	1.04983813	0.2579244	4.39E-06	4.85E-05	Mis18bp1
54.4872379	1.04700584	0.34906323	0.00021715	0.00164207	Lgr5
119.92851	1.04670627	0.22847891	4.36E-07	5.76E-06	Slco4a1
374.710989	1.04470708	0.13760545	2.65E-15	9.04E-14	Ighd4-1
13.1364486	1.04044568	0.71501714	0.00706982	0.03329401	Gm15409
5272.12511	1.03791402	0.10431937	3.22E-24	2.18E-22	Bcl2
404.108652	1.03717043	0.15187951	9.48E-13	2.59E-11	Uck2
29.5520675	1.03692477	0.4637899	0.00181495	0.01046725	Magi2
17.5679446	1.03445412	0.58515918	0.00443672	0.02263126	Spag4
36.6395889	1.03036546	0.50157152	0.0027414	0.01489763	Gm12503
7.00475497	1.02960983	1.29898747	0.0115804	0.04982278	Spry4
16.931269	1.02851983	0.57729347	0.00438469	0.02240777	Arc
93.4530152	1.02554157	0.26296066	9.63E-06	9.93E-05	Zfp442
23.4577013	1.02362228	0.58818185	0.00470827	0.02380883	Cpq
672.473417	1.01903446	0.12950056	3.69E-16	1.34E-14	E330020D12Rik
45.9288314	1.01805469	0.35446842	0.0003569	0.00256388	Mtus2
55.7870852	1.01568112	0.39553547	0.00085111	0.00544119	Ncapg
83.6030986	1.01238606	0.29072454	5.20E-05	0.0004567	Fggy
33.0724126	1.011833	0.3855877	0.00067887	0.00449263	Gm25360
1961.74278	1.0110264	0.11285883	3.67E-20	1.83E-18	Gbp3
173.130492	1.01063276	0.18071641	2.65E-09	4.82E-08	Klf12
86.7622104	1.00927494	0.26320329	1.16E-05	0.000117	Pigr
29.3078266	1.00778876	0.4365655	0.00164314	0.00957759	Armcx4
6114.06125	1.00421617	0.07490273	7.37E-42	1.14E-39	Mxd4
1038.31366	1.0039655	0.12161564	1.86E-17	7.58E-16	Id3
317.121751	1.00219892	0.16717737	2.64E-10	5.37E-09	Serpina3f
189.574244	1.0009627	0.20692132	1.38E-07	1.97E-06	Sv2a
103.878091	-1.0000485	0.2268732	1.02E-06	1.28E-05	Cdc42ep4
3795.8059	-1.0009604	0.0891518	3.15E-30	3.03E-28	Gpr183
165.169653	-1.0030502	0.19414383	2.37E-08	3.77E-07	Pcbp4
471.771491	-1.0063886	0.12556668	1.11E-16	4.26E-15	Tenm4
94.9162306	-1.0067024	0.25200791	5.89E-06	6.32E-05	Cmtm4
14.9146631	-1.0079467	0.58282219	0.00466515	0.02362724	Ighv8-6
284.929613	-1.010576	0.1541044	5.72E-12	1.42E-10	Gm9581
1327.62797	-1.012813	0.09821824	6.89E-26	5.18E-24	Fxyd5
51.1575896	-1.0138946	0.33436265	0.00020795	0.0015798	Fsip1
183.245493	-1.0252036	0.21910356	2.89E-07	3.92E-06	Prkcg
183.86754	-1.0273988	0.17220556	2.57E-10	5.25E-09	Ctnnal1
15963.922	-1.0302544	0.06929165	6.20E-51	1.37E-48	Ptprj
1224.96769	-1.0313308	0.0922225	5.24E-30	5.02E-28	Entpd1

1228.11677	-1.0321474	0.10325178	1.90E-24	1.30E-22	Il6ra
128.674713	-1.0362324	0.22514155	3.85E-07	5.14E-06	Tanc1
136.266942	-1.0381812	0.1952124	1.09E-08	1.83E-07	Pfkm
6214.24711	-1.038924	0.06504877	1.49E-58	4.80E-56	Pld4
753.212722	-1.040416	0.09991722	9.67E-26	7.20E-24	Fam84b
7584.77586	-1.042435	0.09157736	5.64E-31	5.77E-29	Sla
149.343756	-1.0427945	0.211802	8.23E-08	1.21E-06	Rgag4
78.1146155	-1.0446181	0.25827255	5.02E-06	5.47E-05	Tmem17
735.179271	-1.0458498	0.11296299	2.08E-21	1.13E-19	Golm1
20.9642482	-1.0466738	0.48928726	0.00214623	0.01210924	Gm10045
1234.81569	-1.0475491	0.10706359	1.54E-23	9.96E-22	Nr1d2
882.903297	-1.0484308	0.10032142	1.47E-26	1.16E-24	Ddx60
502.210564	-1.0493634	0.12277632	1.44E-18	6.48E-17	Kcnn4
43.8076193	-1.0516994	0.35633037	0.00024555	0.00182647	Steap3
2550.14758	-1.0576295	0.08467533	1.20E-36	1.48E-34	Nbeal2
455.707381	-1.0616181	0.15740716	1.50E-12	4.03E-11	Crybg3
51.4245894	-1.0627905	0.31762953	7.07E-05	0.00059949	RP24-86O15.1
547.107236	-1.0700994	0.12109144	7.64E-20	3.74E-18	Ampd3
460.158245	-1.0727704	0.10345715	4.17E-26	3.19E-24	Rasa4
95.5126182	-1.0733534	0.29612199	2.43E-05	0.0002281	Smagp
25.7193876	-1.0748558	0.57376345	0.00366226	0.01919494	Snx21
12184.6286	-1.0752932	0.08107838	4.36E-41	6.43E-39	Cd97
30.1334563	-1.0779113	0.45460726	0.00118419	0.00721304	Tmem107
24.0263152	-1.0792676	0.47873941	0.00159793	0.00936071	Slc22a21
47.6957842	-1.0819159	0.46199414	0.00136923	0.0081702	Zfp612
1428.62639	-1.0825775	0.11227362	5.45E-23	3.42E-21	E330009J07Rik
259.257062	-1.0839569	0.15211988	1.00E-13	2.97E-12	Gm15448
42.7333858	-1.085163	0.39898583	0.00049883	0.00343869	1810006J02Rik
66.7841044	-1.0866611	0.36187497	0.00018741	0.00143773	Zfhx3
124.066182	-1.0971154	0.31152226	3.42E-05	0.0003133	RP23-380F8.1
32.9831528	-1.1038859	0.41929294	0.00063936	0.00426212	Tbc1d2
3853.84313	-1.1039959	0.10042915	5.47E-29	4.84E-27	Cd36
277.215813	-1.1065275	0.15306702	4.66E-14	1.41E-12	Oas3
6940.77129	-1.1066544	0.07933518	2.91E-45	5.24E-43	Plekhm3
661.777013	-1.1093948	0.12601488	1.28E-19	6.19E-18	Grk5
27.4137333	-1.1100984	0.41018309	0.00046278	0.00321889	Adcy6
85.6459966	-1.1134005	0.26076656	1.79E-06	2.12E-05	Endog
345.306043	-1.116662	0.39007928	0.00028089	0.00206491	Klf11
180.588545	-1.1178158	0.18074012	5.60E-11	1.25E-09	Dock6
610.430201	-1.1190688	0.14734251	3.08E-15	1.04E-13	Gm11346
24381.4598	-1.1216193	0.06905152	2.37E-60	8.63E-58	Notch2
11.7380471	-1.1226231	1.3153222	0.00847355	0.03865575	Trav13-2
437.935472	-1.1272591	0.12721572	7.34E-20	3.60E-18	Gm11690
20.7560487	-1.1273869	0.52335338	0.00189109	0.01082633	Ccdc158
208.531717	-1.1315124	0.20307622	2.37E-09	4.34E-08	Pik3cb
1011.49711	-1.1338135	0.08429291	2.84E-42	4.48E-40	Fes
3660.97025	-1.1363407	0.10829497	9.34E-27	7.39E-25	Zmiz1
518.142236	-1.1369175	0.13688598	9.47E-18	3.97E-16	Tyrobp
271.903474	-1.1376489	0.17023063	2.10E-12	5.48E-11	Abca5
273.117152	-1.1397214	0.22122901	2.13E-08	3.40E-07	Il5ra
299.072085	-1.1432804	0.1930297	3.02E-10	6.09E-09	Rnf43
1500.36344	-1.1455128	0.10372914	2.31E-29	2.09E-27	Nfam1
44.7331454	-1.1494349	0.36036752	0.00010135	0.00083046	Ift81
286.748508	-1.1498965	0.15170649	2.91E-15	9.87E-14	Lca5
984.411249	-1.1517449	0.11047645	1.44E-26	1.14E-24	Pou6f1
67.4498749	-1.1550544	0.29081833	5.93E-06	6.35E-05	Gm16046
796.954823	-1.1563757	0.10390062	9.83E-30	9.15E-28	Fcgrt
2014.769	-1.1655076	0.08223677	1.48E-46	2.79E-44	Cyfip1
1490.147	-1.1702444	0.10864532	3.16E-28	2.68E-26	Slfn5
123.432893	-1.1716788	0.19395789	1.34E-10	2.83E-09	9930012K11Rik

344.18243	-1.1726764	0.14762616	1.78E-16	6.62E-15	Cep170b
445.762983	-1.1744694	0.1225071	7.99E-23	4.98E-21	Trim36
1235.75163	-1.1767107	0.39939175	0.00020278	0.00154483	Ldlr
58.1888844	-1.1776182	0.3155231	1.47E-05	0.00014547	Mitf
33.3536073	-1.1785721	0.45651474	0.00062373	0.00417325	1700039E15Rik
20.1772387	-1.1819226	0.60010448	0.00270917	0.01476656	Ccdc92
33.2738947	-1.1833119	0.44825685	0.0004683	0.00325443	Avpi1
163.281974	-1.1865053	0.20967178	1.42E-09	2.66E-08	Zdhhc23
2905.16439	-1.1878757	0.19682758	1.54E-10	3.22E-09	Lrrc16a
115.229447	-1.1896567	0.23832752	4.89E-08	7.42E-07	Phf11d
35.1432309	-1.1942425	0.48332195	0.00085415	0.00545637	Tmc1
61.5185896	-1.1975238	0.37306587	9.10E-05	0.0007546	Fkbp11
61.3858505	-1.2002103	0.29652295	4.10E-06	4.56E-05	Mgmt
1217.6798	-1.2011912	0.12643008	1.90E-22	1.14E-20	Bbs9
156.178681	-1.2045242	0.22837219	1.10E-08	1.84E-07	Med12l
5853.18089	-1.2094527	0.08659876	2.33E-45	4.23E-43	Anxa6
1736.4719	-1.2105933	0.07937539	1.65E-53	3.92E-51	Gpr132
47.857304	-1.2114771	0.39037614	0.00013384	0.00106001	B230216N24Rik
11.9567987	-1.211497	0.74866241	0.00440746	0.02249604	Gzma
52.8772985	-1.2162252	0.32623841	1.41E-05	0.00013915	Fer
37.8036949	-1.2185061	0.4867827	0.00078705	0.0050913	Rgs11
370.369762	-1.2221357	0.13516892	1.46E-20	7.45E-19	Lilra6
89.7970212	-1.2259213	0.29141418	2.04E-06	2.41E-05	Itpripl2
434.01953	-1.2350399	0.12472987	3.76E-24	2.54E-22	B430306N03Rik
76.4581628	-1.2424465	0.34796483	2.22E-05	0.00021073	Rab20
40.6858843	-1.2499949	0.34458415	2.10E-05	0.00020027	Fgfrl1
4064.85942	-1.2502676	0.12642643	3.95E-24	2.65E-22	Tsc22d3
30.986723	-1.2511308	0.43056876	0.00021938	0.00165584	Gm568
31.5407769	-1.2513343	0.45373147	0.00037527	0.00267588	Fstl3
83.950154	-1.2535969	0.28584462	8.79E-07	1.11E-05	Wfdc17
541.074342	-1.2542302	0.11335802	1.73E-29	1.58E-27	Clec12a
85.0166828	-1.2572233	0.29438046	1.40E-06	1.70E-05	Dmwd
108.920038	-1.2584134	0.31254472	4.35E-06	4.81E-05	Fyb
500.263621	-1.2624144	0.14705331	7.86E-19	3.61E-17	Ptk2
3280.85998	-1.2635682	0.10346858	2.36E-35	2.84E-33	Tagln2
807.991997	-1.2651943	0.18544736	8.12E-13	2.24E-11	Ppl
398.310495	-1.2666109	0.35373546	2.28E-05	0.00021594	Hepacam2
54.8425487	-1.2668155	0.40856549	0.00012837	0.00102412	Capns2
1559.59793	-1.2702734	0.11224647	1.19E-30	1.19E-28	Zbtb7b
513.272403	-1.2712594	0.20258834	3.01E-11	6.92E-10	Cd300lf
964.303279	-1.2725688	0.1038135	1.24E-35	1.51E-33	Slc41a2
45.6960193	-1.2748973	0.31297323	3.20E-06	3.64E-05	Cpne5
1213.49253	-1.2757514	0.23694739	5.39E-09	9.41E-08	Ckap4
598.715737	-1.2808679	0.16181605	2.04E-16	7.55E-15	Dusp3
107.856172	-1.2813401	0.25860377	5.66E-08	8.48E-07	Thbs3
24.4047422	-1.2825451	0.51247872	0.00070042	0.00460544	Lcp2
81.591637	-1.2838299	0.37867383	5.49E-05	0.00047877	Dkkl1
265.521065	-1.2840795	0.15607034	1.74E-17	7.11E-16	Cltb
13.8310711	-1.2908836	1.01049649	0.0068461	0.03240816	Gm16069
1271.50503	-1.2909207	0.11564809	8.78E-30	8.26E-28	Lfng
3482.6795	-1.2925511	0.10734445	1.95E-34	2.29E-32	Hck
9.83776216	-1.3079831	0.97696996	0.00565925	0.02767775	Grin2d
16.2805812	-1.3105864	0.65252263	0.00218326	0.01226742	Rasl10a
81.8053008	-1.3144426	0.26251135	3.94E-08	6.05E-07	Akap2
169.06999	-1.3210776	0.19811311	2.21E-12	5.70E-11	Kcnk6
8.46268327	-1.3335445	1.59130669	0.01104737	0.04793242	Fscn1
422.288552	-1.3340547	0.12633608	3.84E-27	3.13E-25	Hsd11b1
462.617871	-1.3356081	0.4048684	5.83E-05	0.00050484	1700048O20Rik
7.9850601	-1.3358943	1.48320312	0.00843685	0.03851369	Cd3g
93.542222	-1.3359981	0.3339651	5.30E-06	5.73E-05	Tgm2

4988.54186	-1.3426068	0.09895814	4.80E-43	7.94E-41	5830416P10Rik
9.14257854	-1.3426482	0.89218886	0.00452363	0.02299722	Mir6538
189.766852	-1.3432529	0.19812416	9.77E-13	2.67E-11	Pam
240.59149	-1.3460421	0.15911724	2.29E-18	1.02E-16	Igsf9
427.229761	-1.3498494	0.15976434	2.25E-18	9.97E-17	Dhcr24
23.1018807	-1.3596694	0.95933247	0.00614077	0.02968701	Cd8b1
2097.48468	-1.3605976	0.21297679	1.25E-11	3.00E-10	Hip1
344.561646	-1.3638527	0.14958947	6.94E-21	3.63E-19	Gna15
114.488967	-1.3724428	0.24161515	1.03E-09	1.96E-08	RP23-81K14.2
50.6923981	-1.3764372	0.37638643	1.69E-05	0.00016457	Nek2
1489.58252	-1.3786475	0.09473183	5.18E-49	1.10E-46	Irak3
33.0309705	-1.3819515	0.43238946	8.52E-05	0.00071162	Gamt
569.552603	-1.3848702	0.14322442	3.09E-23	1.97E-21	Lacc1
16.8790416	-1.3940201	0.68680869	0.00197404	0.0112501	Grb7
134.166176	-1.4121021	0.3144543	4.78E-07	6.26E-06	Neb
1860.4187	-1.412138	0.08936376	2.34E-57	7.08E-55	B3gnt8
36.1596733	-1.4166874	0.86230019	0.00561342	0.02747826	Csf2rb2
1515.56966	-1.4198931	0.11099909	1.89E-38	2.51E-36	Irf2bpl
8.43196041	-1.4230266	1.0752145	0.00537917	0.02651382	Cfap45
30.420548	-1.424368	0.45103556	9.52E-05	0.00078539	Abhd15
694.474975	-1.425584	0.15418228	2.05E-21	1.12E-19	Alpk2
1678.83605	-1.4266979	0.10796952	5.23E-41	7.58E-39	Pim1
3012.53679	-1.4345904	0.19198091	7.68E-15	2.51E-13	I830077J02Rik
13.1620967	-1.4397095	0.67246639	0.00152199	0.00896713	Cpeb3
710.552241	-1.4413453	0.14112158	1.23E-25	9.04E-24	Pde8a
169.655581	-1.4450592	0.36227778	5.37E-06	5.81E-05	Tub
76.7281246	-1.4487174	0.29570423	6.58E-08	9.81E-07	Nek6
2684.88375	-1.4543175	0.20462497	8.66E-14	2.58E-12	Kbtbd11
6.31053598	-1.455109	1.90946664	0.00964531	0.04284797	Gm5424
80.9278946	-1.455904	0.27265323	6.05E-09	1.05E-07	Zbtb42
102.147086	-1.4596218	0.22638589	8.57E-12	2.08E-10	Sit1
33.1889548	-1.4596891	0.43452578	5.07E-05	0.00044623	Slc35e4
31.3336182	-1.4686574	0.59735971	0.00068263	0.004512	Slfn1
90.146888	-1.4698863	0.24782083	2.43E-10	4.98E-09	Nrarp
17.3237455	-1.4702087	0.65671916	0.00125023	0.00755351	Hdc
4965.22706	-1.4729127	0.0937405	8.44E-57	2.42E-54	Itgb7
78.8127178	-1.4731361	0.28959304	2.68E-08	4.22E-07	C130050O18Rik
3196.37258	-1.473763	0.09599205	2.34E-54	5.81E-52	Crip1
5179.76406	-1.4741062	0.38413361	6.85E-06	7.26E-05	Cacna1i
113.649529	-1.4754282	0.28916642	2.07E-08	3.32E-07	Vmn2r96
163.274678	-1.4829891	0.17634617	2.99E-18	1.31E-16	4833407H14Rik
1333.31566	-1.4908437	0.11070307	1.66E-42	2.67E-40	Nxpe2
149.109272	-1.4913968	0.19773682	3.34E-15	1.12E-13	Adam15
19.6001706	-1.4950072	0.6006482	0.00067538	0.00447495	Eya2
1332.27455	-1.4982125	0.16212546	2.18E-21	1.18E-19	Ackr2
2010.88816	-1.5045395	0.23096051	7.32E-12	1.80E-10	Asb2
37.2773062	-1.5134806	0.42029581	2.12E-05	0.00020133	AI427809
1301.49775	-1.5140834	0.12059946	2.04E-37	2.63E-35	Atrnl1
36.8722	-1.5164945	0.44253734	4.01E-05	0.0003629	Tcp11
212.182333	-1.5171459	0.61046254	0.00101158	0.0063087	Ptafr
29.8918953	-1.5290124	0.48780896	0.0001072	0.00087113	Eng
7.2535475	-1.5322812	0.97287371	0.00357046	0.01878593	Rsph9
372.852142	-1.5352025	0.19197681	7.77E-17	3.00E-15	Hspa12a
290.880952	-1.5362352	0.25772978	1.88E-10	3.92E-09	Mllt4
269.392175	-1.5461152	0.19435985	1.20E-16	4.57E-15	St6galnac3
49.5330975	-1.5469506	0.46034922	4.15E-05	0.00037354	Fam198a
176.740907	-1.5484039	0.19729105	3.01E-16	1.11E-14	RP23-59N15.2
181.717411	-1.5563251	0.20848946	5.94E-15	1.96E-13	Rfx2
6.45021579	-1.5726642	1.51089434	0.00794897	0.03668708	Klrk1
41.2376877	-1.5741041	0.42443775	1.34E-05	0.0001334	AU019990

276.267614	-1.58393	0.17520835	1.02E-20	5.31E-19	L1cam
23.3749444	-1.588928	0.66109251	0.0008671	0.00552399	Fam135a
53.5893152	-1.5911834	0.41710324	8.51E-06	8.84E-05	Gm9989
24.9990644	-1.5968263	0.60202333	0.00044345	0.00310659	Trim2
38.1709902	-1.5978687	0.41790752	8.09E-06	8.45E-05	Fbxl21
1701.18753	-1.5987097	0.0951522	2.71E-64	1.06E-61	Plbd1
8900.2455	-1.6071094	0.07589829	5.73E-101	5.22E-98	Fgd2
1423.99422	-1.6104364	0.09607442	4.64E-64	1.77E-61	Kcnk5
39.4867578	-1.6180073	0.48005635	3.95E-05	0.00035794	Gm9889
699.120067	-1.6263251	0.14511509	2.74E-30	2.65E-28	Itgam
10.5344076	-1.6462814	0.80092042	0.00154204	0.00907546	Gm12160
73.3646465	-1.652914	0.28290351	3.39E-10	6.79E-09	Bbs7
54.8698212	-1.6600928	0.33774398	5.51E-08	8.29E-07	Gm4540
24.790186	-1.6693186	0.48318643	3.22E-05	0.00029621	2310047D07Rik
831.687464	-1.6753347	0.10439617	3.63E-59	1.21E-56	4632428N05Rik
31.1126208	-1.6922949	0.46950452	1.98E-05	0.00018926	Pifo
231.558488	-1.6996317	0.19952466	9.57E-19	4.38E-17	Tbxa2r
45.4554314	-1.69979	0.34710089	6.08E-08	9.08E-07	Mapk12
961.272523	-1.711124	0.13631438	2.61E-37	3.32E-35	Arhgap5
414.533955	-1.7157594	0.21274303	6.48E-17	2.52E-15	Lmna
17.6268091	-1.7412605	0.59321	0.00015789	0.00123085	RP24-111C16.1
45.3272907	-1.7432941	0.41641856	1.64E-06	1.97E-05	Unc13b
67.8447404	-1.7472749	0.27695965	1.98E-11	4.64E-10	Gm10612
135.668539	-1.7479477	0.20667199	1.73E-18	7.74E-17	Zfp467
4326.488	-1.7642559	0.08091262	1.80E-106	1.97E-103	Cyp4f18
15.3930439	-1.7643254	0.70558166	0.00065331	0.00435157	Gm14199
2161.56897	-1.7661487	0.11634083	3.08E-53	7.11E-51	Myadm
193.140317	-1.7746238	0.19455437	5.46E-21	2.89E-19	Smpd3
37.2928712	-1.7746726	0.96536435	0.0041625	0.02140585	Tubb3
13.3541752	-1.7786914	0.82427156	0.00148842	0.00879784	Pls3
161.674649	-1.7865678	0.19275669	1.27E-21	7.12E-20	Ppfia4
543.680783	-1.8006765	0.11254358	7.95E-59	2.60E-56	Spns2
188.687724	-1.8027722	0.16775729	4.76E-28	4.00E-26	Cdkl1
325.241272	-1.8066428	0.15294835	2.71E-33	3.14E-31	Slc16a10
756.951221	-1.8067379	0.1052616	3.54E-67	1.57E-64	Lpcat2
378.441092	-1.811161	0.23520465	1.10E-15	3.86E-14	Emb
177.681851	-1.8173046	0.22990873	1.97E-16	7.32E-15	Fam212a
30.4892769	-1.8233015	0.46271973	5.16E-06	5.60E-05	Cebpb
43.4787716	-1.8295444	0.67864678	0.00050671	0.0034785	Gml
6.49399211	-1.8298021	1.22430341	0.00457268	0.02320917	Cd3e
4.25198629	-1.8321064	1.82168908	0.00737798	0.03447758	Cxcr2
231.316885	-1.8359572	0.19676341	6.77E-22	3.87E-20	Tha1
49.2919952	-1.8393296	0.31456862	3.14E-10	6.31E-09	Wscd2
46.3749239	-1.8502681	0.41076701	4.04E-07	5.37E-06	Tmem176a
95.1284119	-1.858474	0.24995966	6.79E-15	2.23E-13	Ggt5
33.7602571	-1.8784814	0.37094133	2.65E-08	4.18E-07	Tgfbi
183.532007	-1.890814	0.26442068	6.10E-14	1.83E-12	Id2
2776.2854	-1.8910191	0.22750655	6.01E-18	2.56E-16	Ptpn14
196.684371	-1.9005978	0.21546511	8.17E-20	3.98E-18	Rgmb
97.9951569	-1.9032087	0.23889813	9.66E-17	3.70E-15	Rbpms
11.2955502	-1.9061264	0.85308977	0.00098497	0.00617406	Cd8a
33.464778	-1.9075487	0.40631424	1.62E-07	2.29E-06	Olfr433
47.1488133	-1.9343942	0.37887141	2.05E-08	3.29E-07	A630081J09Rik
19.314452	-1.9401871	0.79756093	0.00089106	0.00566126	Cd59b
1200.4266	-1.9403476	0.12599144	1.92E-54	4.90E-52	Cdh17
15.4278716	-1.9408055	0.72439799	0.00036288	0.0026034	Cd4
108.542471	-1.9423179	0.2279263	1.22E-18	5.52E-17	Errfi1
1109.02006	-1.9498026	0.1269563	2.02E-54	5.09E-52	Sirpa
24.8744632	-1.95151	0.71859424	0.0003131	0.0022772	Il2rb
34.217018	-1.9547969	0.4011423	6.81E-08	1.02E-06	Zfp697

99.8643497	-1.9569485	0.25233749	5.31E-16	1.90E-14	Trim46
21.5174219	-1.9659531	0.68770959	0.00018166	0.00139689	Csf3r
4.12906282	-1.9678294	2.03880468	0.00885093	0.0400247	Gm13387
551.993501	-1.9783337	0.14406309	5.52E-44	9.51E-42	Rasgrp4
13.3262556	-1.9908256	0.61841683	6.28E-05	0.00053911	Scn4b
350.093865	-1.992237	0.1998367	1.65E-24	1.14E-22	Dse
841.357103	-1.9952949	0.12784298	7.06E-56	1.84E-53	Ttc28
433.824246	-1.9979717	0.1405564	4.45E-47	8.48E-45	Ppap2b
111.519352	-2.0010188	0.2493208	6.71E-17	2.60E-15	Pcx
16.1387702	-2.0089142	0.70361839	0.00021861	0.0016516	Gm13648
36852.4432	-2.0096353	0.18278058	2.45E-29	2.20E-27	Ahnak
6.92849019	-2.0131008	2.17433109	0.00826445	0.03783215	Dlc1
410.57624	-2.0172922	0.15276255	4.92E-41	7.20E-39	Prkcz
31.9145147	-2.0173868	1.05676453	0.00392117	0.02036946	Ttn
290.257718	-2.026184	0.21340969	1.35E-22	8.28E-21	Stac2
11.0512907	-2.0288947	1.08315918	0.00220008	0.01233654	Thy1
216.093444	-2.029334	0.19572769	2.15E-26	1.67E-24	Pygl
83.7880233	-2.0456216	0.32311702	1.90E-11	4.45E-10	Gm11707
37.3558907	-2.0591101	0.46157141	5.21E-07	6.80E-06	Enkur
55.9765858	-2.0603276	0.30594291	1.17E-12	3.17E-11	Acpp
16.3603575	-2.0704983	0.67786578	0.00011601	0.00093603	Trbc2
30.8835007	-2.0835766	0.54269216	6.55E-06	6.97E-05	Gm15608
771.747053	-2.114668	0.14211999	2.33E-51	5.30E-49	Gpr137b
62.9306021	-2.1242773	0.39595562	4.73E-09	8.33E-08	Tcp11l1
377.627925	-2.1291993	0.19502585	7.23E-29	6.37E-27	Socs3
38.7341516	-2.1373176	0.5543439	7.28E-06	7.69E-05	Osgin1
169.20517	-2.1383128	0.20720495	3.45E-26	2.66E-24	Extl1
411.939283	-2.1481915	0.33924438	2.26E-11	5.25E-10	Gm15228
103.569081	-2.1686453	0.39257242	2.72E-09	4.93E-08	Skap1
46.4684606	-2.1693446	0.4735857	2.54E-07	3.48E-06	1700028I16Rik
967.874313	-2.17334	0.30301078	4.24E-14	1.29E-12	Diras2
134.229428	-2.173882	1.10235675	0.00173849	0.01006531	Fn1
18.3431216	-2.177822	0.75862822	0.00021983	0.00165847	Gda
54.2538246	-2.1781646	0.85624596	0.0011073	0.00682078	Mocos
110.125814	-2.1925013	0.23554468	1.06E-21	5.96E-20	Tmprss13
5.27201016	-2.2116795	1.30835966	0.00311749	0.01669218	Clec7a
60.439227	-2.2210547	0.38437599	5.36E-10	1.06E-08	Sh2d6
4.81451753	-2.2255856	1.43049263	0.00379305	0.01979808	Ust
602.036431	-2.2309893	0.14016659	3.81E-58	1.20E-55	Ass1
92.175254	-2.27068	0.25204993	1.54E-20	7.85E-19	Tmem176b
588.359551	-2.2973015	0.1941689	1.74E-33	2.04E-31	Sorbs2
77.096881	-2.3372462	0.28040917	5.36E-18	2.30E-16	Dyrk3
939.371621	-2.4012903	0.15377826	6.62E-56	1.75E-53	Cdc42bpb
43.3476669	-2.4185161	0.43730352	2.51E-09	4.59E-08	Lrp8
42.033917	-2.4334462	0.3742037	3.98E-12	9.99E-11	Dmpk
10.1029716	-2.435773	0.8543712	0.00022451	0.00169069	Gm11725
685.721145	-2.4399185	0.15554922	1.60E-56	4.45E-54	Mical3
96.2192818	-2.4469921	0.29019643	2.56E-18	1.13E-16	Alox5ap
2889.77292	-2.4519201	0.21786872	1.05E-30	1.06E-28	Adrbk2
690.318632	-2.4625131	0.17708216	7.18E-45	1.28E-42	Flt3
1287.11509	-2.4764334	0.19465831	3.11E-38	4.08E-36	Trpm2
28.5171959	-2.4777771	0.58060546	1.15E-06	1.42E-05	Park2
21.8197502	-2.4912595	0.54029201	2.36E-07	3.25E-06	Dock4
118.033926	-2.5588617	0.79189264	0.0001781	0.00137214	S100a4
1544.28953	-2.5956351	0.19308844	2.59E-42	4.12E-40	S100a6
13.3889146	-2.6572544	0.93528173	0.00016702	0.0012922	S100a8
67.9093849	-2.6768673	0.38991233	3.20E-13	9.01E-12	RP23-118H3.3
5.48011602	-2.7306652	1.45579828	0.00360126	0.01892367	Gm14398
982.59761	-2.7385742	0.25706922	1.24E-27	1.02E-25	Rap1gap2
22.6639283	-2.7496096	0.88825038	0.00020094	0.00153148	Gcm2

10.3981957	-2.7770099	1.10537336	0.00088989	0.00565597	Osbpl3
480.628703	-2.7977518	0.19954338	8.54E-46	1.57E-43	Gpr34
22.8090841	-2.8386354	0.54512889	1.41E-08	2.32E-07	Pik3r6
30.0319216	-2.8536676	0.68737586	2.82E-06	3.23E-05	Clec4a3
51.7960235	-2.8637361	0.44889492	1.13E-11	2.74E-10	Lrrc23
686.939625	-2.8928799	0.14133734	3.39E-94	2.52E-91	Pltp
485.021612	-2.9194111	0.1478973	1.36E-87	9.72E-85	Amz1
30.9596074	-2.9375998	0.63976721	4.62E-07	6.07E-06	Lmntd1
21.1716194	-2.9449877	0.70561955	1.24E-06	1.52E-05	S100a9
353.093047	-2.9636418	0.18919558	1.96E-56	5.35E-54	Lrrc25
4.98178393	-2.9651588	1.54078726	0.00290977	0.01571352	RP23-145F12.1
16.5086592	-2.9742377	1.49081573	0.00219423	0.01230799	Klk8
721.718342	-2.980784	0.1338204	3.81E-111	4.80E-108	Cyp27a1
725.022621	-2.9989002	0.58465304	2.26E-08	3.60E-07	Tppp
8.49809807	-3.0665706	0.95616066	6.10E-05	0.00052514	Npr3
1249.92584	-3.109638	0.34185799	5.91E-21	3.10E-19	Tbc1d9
9.57780672	-3.1295702	1.20509302	0.00115361	0.00706352	Fzd10
145.881186	-3.1471881	0.25260803	1.00E-36	1.25E-34	Srms
103.593409	-3.1783065	0.48871287	7.68E-12	1.88E-10	Trabd2b
212.118848	-3.1802769	0.2337674	5.14E-43	8.42E-41	Rnd3
10.8873288	-3.1904296	0.97509641	6.91E-05	0.00058613	Trbc1
28.0046199	-3.2010042	0.50878302	2.28E-11	5.28E-10	C330046G13Rik
448.119893	-3.2435008	0.34139847	4.54E-22	2.62E-20	Ceacam2
56.9347622	-3.2498249	0.87521431	4.67E-05	0.00041609	Cd59a
166.85789	-3.273642	0.20690974	1.09E-57	3.35E-55	Col27a1
596.515946	-3.2845598	0.22983699	3.68E-47	7.09E-45	Lair1
1264.89524	-3.3115641	0.11663787	1.04E-178	4.25E-175	Lifr
234.158465	-3.3163521	0.19010531	3.03E-69	1.46E-66	F630028O10Rik
22.4746715	-3.3518845	0.5751055	4.69E-10	9.30E-09	Ptk6
16.7784061	-3.3888662	0.69399011	7.72E-08	1.14E-06	Gm26685
304.448468	-3.402991	0.31304967	3.42E-28	2.89E-26	Trem1
4.56035673	-3.4447077	1.64214837	0.00155303	0.00913689	RP23-353G11.4
9.76156484	-3.456572	1.03490743	0.00010024	0.00082297	Efna1
52.2477782	-4.0662147	0.54793701	2.06E-14	6.44E-13	Wbscr17
873.443951	-4.42078	0.21274219	7.59E-97	6.22E-94	Lurap1
4.90631312	-5.6628693	2.72709153	0.00012232	0.00098065	Axin2

Appendix C RNA cluster markers of ADT-marker defined splenic T cell clusters (Figure 5.11)

Top 10 differentially expressed markers for each ADT-defined splenic T cell cluster from WT and Pepd$^{-/-}$ mice as described in Figure 5.11 at a resolution of 0.7, filtered at a log2FC threshold of 0.25. pct represents the percentage of cells where the gene is detected in the first (pct.1 – named in cluster column) or second (pct.2 – rest of cells not in cluster) group.

	gene	avg_log2FC	pct.1	pct.2	p_val_adj	cluster
1	Cd4	0.73907723	0.739	0.315	2.42E-186	0.CD4+naïve.1
2	Satb1	0.7671427	0.97	0.748	3.01E-174	0.CD4+naïve.1
3	Igfbp4	1.24944402	0.662	0.386	6.45E-140	0.CD4+naïve.1
4	St8sia6	0.68326854	0.327	0.094	1.14E-126	0.CD4+naïve.1
5	Lef1	0.6184908	0.921	0.72	1.26E-114	0.CD4+naïve.1
6	Actn1	0.59529612	0.814	0.568	1.52E-92	0.CD4+naïve.1
7	Ccr7	0.53531641	0.694	0.502	4.73E-62	0.CD4+naïve.1
8	Atp1b1	0.5318063	0.391	0.203	2.26E-61	0.CD4+naïve.1
9	Gm12840	0.74223702	0.508	0.323	9.64E-57	0.CD4+naïve.1
10	Bach2	0.52097816	0.522	0.341	2.78E-49	0.CD4+naïve.1
11	Cd8b1	1.64605638	0.98	0.325	0	1.CD8+naïve.1
12	Cd8a	1.47250303	0.953	0.315	0	1.CD8+naïve.1
13	Ccr9	0.92068646	0.53	0.137	9.30E-239	1.CD8+naïve.1
14	Klrd1	0.61259936	0.591	0.225	1.58E-156	1.CD8+naïve.1
15	5730508B09Rik	0.54947455	0.373	0.142	3.13E-94	1.CD8+naïve.1
16	Plac8	0.53550629	0.314	0.106	8.84E-91	1.CD8+naïve.1
17	Rgcc	0.53571489	0.429	0.18	9.57E-91	1.CD8+naïve.1
18	Dapl1	0.68162604	0.409	0.172	3.69E-88	1.CD8+naïve.1
19	Epsti1	0.4839809	0.693	0.433	2.72E-65	1.CD8+naïve.1
20	Cmah	0.47904564	0.732	0.474	1.92E-64	1.CD8+naïve.1
21	Maf	2.08142544	0.675	0.133	0	2.CD4+TFH-like
22	Nrp1	1.68296662	0.434	0.069	2.08E-271	2.CD4+TFH-like
23	Tbc1d4	1.71440151	0.486	0.127	7.04E-214	2.CD4+TFH-like
24	Izumo1r	1.73397402	0.593	0.199	4.11E-210	2.CD4+TFH-like
25	Ikzf2	1.97447229	0.623	0.234	3.00E-194	2.CD4+TFH-like
26	Eea1	1.32826085	0.333	0.065	4.34E-170	2.CD4+TFH-like
27	S100a11	1.31094685	0.665	0.345	1.83E-155	2.CD4+TFH-like
28	Itgb1	1.65628716	0.562	0.239	6.41E-151	2.CD4+TFH-like
29	S100a6	1.40282745	0.49	0.162	4.60E-147	2.CD4+TFH-like
30	S100a4	1.51883841	0.287	0.07	9.47E-113	2.CD4+TFH-like
31	Cd8b1	1.36931981	0.973	0.396	4.57E-242	3.CD8+naïve.2
32	Cd8a	1.24777633	0.953	0.383	1.62E-222	3.CD8+naïve.2
33	Ccr9	1.05188015	0.575	0.174	2.11E-145	3.CD8+naïve.2
34	Adgrg5	0.44626128	0.325	0.117	1.05E-53	3.CD8+naïve.2
35	5730508B09Rik	0.54588664	0.392	0.165	1.10E-50	3.CD8+naïve.2
36	Itgae	0.46079849	0.296	0.106	2.81E-47	3.CD8+naïve.2
37	Tmem108	0.46517911	0.319	0.124	6.83E-46	3.CD8+naïve.2

38	Rgcc	0.55857424	0.435	0.206	1.41E-43	3.CD8+naïve.2
39	Runx3	0.49755019	0.715	0.45	7.26E-40	3.CD8+naïve.2
40	Dapl1	0.50917343	0.382	0.201	1.36E-26	3.CD8+naïve.2
41	Cd4	0.61211551	0.722	0.368	1.20E-69	4.CD4+naïve.2
42	Satb1	0.64838471	0.944	0.778	9.02E-59	4.CD4+naïve.2
43	St8sia6	0.62171844	0.332	0.121	2.41E-53	4.CD4+naïve.2
44	Igfbp4	0.80407541	0.612	0.424	3.67E-32	4.CD4+naïve.2
45	Lef1	0.47131344	0.889	0.748	2.29E-31	4.CD4+naïve.2
46	Actn1	0.50511552	0.77	0.602	6.40E-28	4.CD4+naïve.2
47	Ccr7	0.52117951	0.7	0.524	1.68E-23	4.CD4+naïve.2
48	Il6ra	0.46062853	0.615	0.472	7.94E-16	4.CD4+naïve.2
49	Gm12840	0.59287718	0.486	0.348	3.48E-15	4.CD4+naïve.2
50	Sepp1	0.49608557	0.421	0.297	2.15E-12	4.CD4+naïve.2
51	Gzmk	1.39349682	0.336	0.015	0	5.CD8+effector
52	Ccl5	4.15093432	0.826	0.252	8.96E-275	5.CD8+effector
53	Nkg7	2.39452746	0.903	0.411	9.30E-212	5.CD8+effector
54	Eomes	1.53650476	0.48	0.087	5.32E-185	5.CD8+effector
55	Ctla2a	1.79921422	0.468	0.083	1.24E-184	5.CD8+effector
56	S100a6	2.03819505	0.583	0.178	3.95E-135	5.CD8+effector
57	Ahnak	1.68280046	0.743	0.334	1.09E-117	5.CD8+effector
58	Lgals1	1.68509318	0.538	0.211	1.59E-85	5.CD8+effector
59	Itga4	1.33934929	0.797	0.595	2.60E-71	5.CD8+effector
60	Ly6c2	1.50247638	0.369	0.132	1.03E-54	5.CD8+effector
61	Il2ra	2.20306598	0.592	0.05	0	6.CD4+Treg
62	Foxp3	2.06683053	0.658	0.06	0	6.CD4+Treg
63	Ikzf2	2.09919374	0.825	0.252	6.13E-205	6.CD4+Treg
64	Izumo1r	1.62653207	0.708	0.223	6.00E-152	6.CD4+Treg
65	Ctla4	1.20308392	0.404	0.072	6.37E-137	6.CD4+Treg
66	Ikzf4	1.18210399	0.394	0.071	1.75E-133	6.CD4+Treg
67	Tnfrsf4	1.39745371	0.408	0.08	3.41E-125	6.CD4+Treg
68	Tiam1	1.16393199	0.427	0.087	9.36E-124	6.CD4+Treg
69	Nrp1	1.34209114	0.451	0.096	9.06E-122	6.CD4+Treg
70	Pim1	1.27562201	0.588	0.297	1.11E-57	6.CD4+Treg
71	Gm42418	0.34424	1	1	2.42E-14	7.CD4-CD8-
72	Ikzf2	0.77135633	0.445	0.277	1.32E-13	7.CD4-CD8-
73	Smc4	0.61701037	0.717	0.748	2.08E-05	7.CD4-CD8-
74	H2-Q7	0.27085576	0.901	0.968	0.0016286	7.CD4-CD8-
75	Ift80	0.57687262	0.388	0.332	0.05834668	7.CD4-CD8-
76	Malat1	0.32391587	1	1	0.07588207	7.CD4-CD8-
77	Rsrp1	0.3746946	0.822	0.901	0.17810505	7.CD4-CD8-
78	Cbl	0.3989097	0.605	0.687	1	7.CD4-CD8-
79	Vps54	0.43571767	0.25	0.221	1	7.CD4-CD8-
80	Celf2	0.32130183	0.697	0.796	1	7.CD4-CD8-
81	Ccr2	1.87524143	0.587	0.045	0	8.CD4+TH1-like

82	Xcl1	1.71221083	0.461	0.026	0	8.CD4+TH1-like
83	Mmp9	1.36774933	0.288	0.007	0	8.CD4+TH1-like
84	Cxcr6	2.90029496	0.844	0.176	1.41E-276	8.CD4+TH1-like
85	Ckb	1.49800388	0.489	0.048	4.57E-240	8.CD4+TH1-like
86	Id2	3.17981556	0.897	0.277	1.03E-230	8.CD4+TH1-like
87	Klrk1	1.51078134	0.388	0.04	5.49E-175	8.CD4+TH1-like
88	Rora	1.45014198	0.534	0.114	3.75E-120	8.CD4+TH1-like
89	Il2rb	1.37516085	0.774	0.274	1.21E-110	8.CD4+TH1-like
90	S100a6	1.46710433	0.514	0.191	1.07E-48	8.CD4+TH1-like
91	Ly6c2	2.36909242	0.727	0.123	1.31E-224	9.CD8+CEM
92	Eomes	1.32756717	0.596	0.093	1.07E-174	9.CD8+CEM
93	Ms4a4c	1.06229111	0.54	0.134	1.52E-92	9.CD8+CEM
94	Ctla2a	1.15318467	0.448	0.094	1.19E-89	9.CD8+CEM
95	Tm6sf1	0.89446668	0.549	0.159	1.24E-71	9.CD8+CEM
96	Nkg7	0.78171565	0.911	0.424	4.19E-68	9.CD8+CEM
97	Pde2a	0.92768776	0.626	0.233	2.17E-59	9.CD8+CEM
98	Sidt1	0.76929423	0.682	0.304	3.84E-45	9.CD8+CEM
99	Ccl5	0.78167114	0.602	0.277	5.24E-40	9.CD8+CEM
100	Myb	0.73384673	0.252	0.075	6.83E-27	9.CD8+CEM
101	Rplp1	0.37562119	1	0.998	1.14E-07	10.CD4+CD8+
102	Cd8b1	0.45494535	0.97	0.447	1.33E-05	10.CD4+CD8+
103	Rps3	0.35167199	1	0.986	2.33E-05	10.CD4+CD8+
104	Rps18	0.35305715	1	0.984	6.33E-05	10.CD4+CD8+
105	Rps20	0.38130788	1	0.992	9.17E-05	10.CD4+CD8+
106	Pde4b	0.40750988	0.53	0.229	0.00713815	10.CD4+CD8+
107	Zfos1	0.36344941	0.682	0.333	0.05761961	10.CD4+CD8+
108	Tsc22d3	0.38646095	0.682	0.358	0.07682926	10.CD4+CD8+
109	Sh3bp5	0.38713994	0.53	0.254	0.07738714	10.CD4+CD8+
110	Npc2	0.37427778	0.939	0.746	0.16495115	10.CD4+CD8+
111	Klrg1	2.14171986	0.634	0.011	1.42E-256	11.CD25+KLRG1+
112	Il1rl1	1.81040843	0.463	0.007	4.39E-203	11.CD25+KLRG1+
113	Foxp3	2.40585284	0.805	0.093	2.12E-52	11.CD25+KLRG1+
114	Tnfrsf4	2.1065833	0.78	0.097	1.59E-47	11.CD25+KLRG1+
115	Ikzf2	2.78560497	0.951	0.283	3.38E-27	11.CD25+KLRG1+
116	Cd81	1.65984742	0.512	0.069	2.80E-25	11.CD25+KLRG1+
117	Il2ra	1.882607	0.537	0.08	7.65E-23	11.CD25+KLRG1+
118	Maf	1.8817319	0.829	0.202	4.35E-22	11.CD25+KLRG1+
119	Serinc3	1.72143088	0.854	0.526	7.32E-09	11.CD25+KLRG1+
120	H2afz	1.69723196	0.854	0.727	0.00010467	11.CD25+KLRG1+

Appendix D RNA cluster markers of WNN-clustered splenic CD8^{+} populations (Figure 5.13)

Top 10 differentially expressed markers for each WNN-defined splenic CD8 cluster from WT and Pepd$^{-/-}$ T cell populations subjected to scRNA-Seq in combination with ADT-antibody labelling, as described in Figure 5.13 at a clustering resolution of 0.5, filtered at a log2FC threshold of 0.25. pct represents the percentage of cells where the gene is detected in the first (pct.1 – named in cluster column) or second (pct.2 – rest of cells not in cluster) group.

	gene	avg_log2FC	pct.1	pct.2	p_val_adj	cluster
1	Igfbp4	0.621804015	0.634	0.361	8.39E-48	0.CD62L+Naïve
2	Lef1	0.4200894	0.954	0.754	2.47E-44	0.CD62L+Naïve
3	Ccr9	0.444269906	0.543	0.292	6.64E-39	0.CD62L+Naïve
4	Cd8b1	0.371452313	0.981	0.783	1.86E-38	0.CD62L+Naïve
5	Ccr7	0.424025538	0.757	0.511	5.25E-37	0.CD62L+Naïve
6	Actn1	0.425864907	0.831	0.596	4.83E-36	0.CD62L+Naïve
7	Il6ra	0.409748753	0.589	0.372	2.26E-30	0.CD62L+Naïve
8	Rgcc	0.384939275	0.436	0.246	1.08E-25	0.CD62L+Naïve
9	Dapl1	0.365672328	0.418	0.286	6.24E-12	0.CD62L+Naïve
10	Gm12840	0.377857311	0.409	0.296	4.21E-09	0.CD62L+Naïve
11	Ccr9	0.496217719	0.566	0.347	1.52E-23	1.Naive
12	Lef1	0.342176697	0.931	0.811	1.85E-18	1.Naive
13	Igfbp4	0.451655541	0.616	0.434	5.36E-18	1.Naive
14	Ccr7	0.360324191	0.744	0.576	2.58E-15	1.Naive
15	Cd8b1	0.285815972	0.979	0.833	5.72E-12	1.Naive
16	Npc2	0.298519634	0.902	0.799	1.07E-11	1.Naive
17	Actn1	0.291916301	0.798	0.664	8.50E-10	1.Naive
18	Rgcc	0.341447928	0.432	0.294	8.99E-10	1.Naive
19	Fam101b	0.32665171	0.577	0.444	1.82E-08	1.Naive
20	Itgae	0.308895135	0.297	0.192	1.33E-06	1.Naive
21	Ly6c2	2.358849662	0.932	0.215	2.50E-193	2.Ly6c2+CEM
22	Klra7	0.739758795	0.201	0.006	1.73E-96	2.Ly6c2+CEM
23	Samd3	0.67985647	0.35	0.05	9.95E-73	2.Ly6c2+CEM
24	1700025G04Rik	0.724603761	0.375	0.059	1.56E-72	2.Ly6c2+CEM
25	Cxcr3	0.764795718	0.453	0.087	9.92E-72	2.Ly6c2+CEM
26	Cd44	0.70343285	0.453	0.112	4.75E-52	2.Ly6c2+CEM
27	Il2rb	0.971967413	0.731	0.313	1.95E-51	2.Ly6c2+CEM
28	Ctla2a	0.816261783	0.495	0.14	6.06E-50	2.Ly6c2+CEM
29	Il18r1	0.813175773	0.576	0.213	2.38E-40	2.Ly6c2+CEM
30	Ms4a4c	0.766820702	0.566	0.23	1.19E-34	2.Ly6c2+CEM
31	Myb	1.676823915	0.464	0.062	1.05E-114	3.CEM
32	Ikzf2	2.322760815	0.573	0.162	2.23E-77	3.CEM
33	Sox4	1.566516443	0.322	0.047	1.18E-70	3.CEM
34	Smc4	1.356146068	0.946	0.748	6.08E-69	3.CEM
35	Ift80	1.443284	0.715	0.302	3.39E-66	3.CEM
36	Id3	1.417431804	0.502	0.138	1.69E-61	3.CEM
37	Ptms	0.899390177	0.288	0.087	2.50E-25	3.CEM
38	Slamf6	1.071140011	0.695	0.478	1.62E-24	3.CEM
39	Vmp1	1.032082162	0.522	0.271	3.46E-23	3.CEM
40	Eomes	0.879675015	0.356	0.214	8.44E-06	3.CEM
41	Gzmk	2.156041452	0.703	0.027	0	4.Exhausted effector

42	S100a6	3.015410997	0.837	0.153	1.15E-174	4.Exhausted effector
43	Ccl5	3.568897579	0.984	0.309	5.60E-161	4.Exhausted effector
44	Ctla2a	2.420861301	0.744	0.128	5.51E-153	4.Exhausted effector
45	Maf	1.744475367	0.463	0.056	1.08E-109	4.Exhausted effector
46	Nkg7	2.167783725	0.98	0.793	1.11E-105	4.Exhausted effector
47	S100a4	2.05769021	0.431	0.057	4.45E-93	4.Exhausted effector
48	Ccl4	2.436775179	0.285	0.024	2.99E-82	4.Exhausted effector
49	Itga4	1.641024331	0.943	0.626	4.80E-77	4.Exhausted effector
50	S100a11	1.782786073	0.756	0.395	2.49E-60	4.Exhausted effector
51	Cx3cr1	2.538371237	0.582	0.02	7.05E-253	5.Terminal effector
52	Zeb2	3.119093984	0.61	0.026	9.38E-246	5.Terminal effector
53	Ccl5	3.017006811	0.984	0.323	2.16E-114	5.Terminal effector
54	Gzma	3.312759444	0.335	0.027	1.27E-86	5.Terminal effector
55	Ahnak	2.4674287	0.896	0.39	1.78E-79	5.Terminal effector
56	Lgals1	2.741774878	0.725	0.212	4.39E-76	5.Terminal effector
57	Il18rap	1.844352699	0.516	0.095	2.98E-73	5.Terminal effector
58	Nkg7	1.767318554	0.967	0.798	1.88E-67	5.Terminal effector
59	S100a4	1.750242882	0.39	0.067	4.71E-52	5.Terminal effector
60	Itgb1	1.94355316	0.654	0.256	1.80E-44	5.Terminal effector
61	Klra9	1.806105926	0.42	0.011	1.11E-131	6.NK-like effector
62	Klrc2	1.86700877	0.652	0.038	9.12E-115	6.NK-like effector
63	Klrk1	2.472219114	0.826	0.067	1.04E-113	6.NK-like effector
64	Fgl2	1.664135609	0.391	0.014	1.26E-98	6.NK-like effector
65	S100a6	2.639261664	0.884	0.188	7.09E-51	6.NK-like effector
66	Ly6c2	2.774589615	0.957	0.266	1.44E-49	6.NK-like effector
67	Ahnak	1.957250105	0.942	0.406	5.13E-31	6.NK-like effector
68	Id2	2.46323861	0.855	0.323	3.56E-30	6.NK-like effector
69	Il18r1	1.762811087	0.768	0.235	8.57E-29	6.NK-like effector
70	Itgb1	1.666415299	0.768	0.267	9.38E-23	6.NK-like effector
71	Ifit3	2.007612549	0.754	0.035	9.53E-158	7.IFN-stimulated
72	Rsad2	1.977713402	0.508	0.013	2.15E-155	7.IFN-stimulated
73	Ifit1	3.127315255	0.923	0.067	3.55E-144	7.IFN-stimulated
74	Isg15	2.306345219	0.815	0.07	1.18E-105	7.IFN-stimulated
75	Usp18	2.07372881	0.8	0.078	1.83E-93	7.IFN-stimulated
76	Slfn5	2.109440804	0.631	0.087	2.99E-50	7.IFN-stimulated
77	Iigp1	1.875594943	0.631	0.112	2.55E-37	7.IFN-stimulated
78	Bst2	1.725981697	0.831	0.328	4.75E-24	7.IFN-stimulated
79	Herc6	1.828372283	0.738	0.245	6.05E-23	7.IFN-stimulated
80	Rnf213	1.713507461	0.8	0.366	5.06E-19	7.IFN-stimulated

Appendix E Differential gene expression analysis between splenic CD8$^+$ CEM populations, 2.Ly6c2$^+$CEM and 3.CEM as visualised in Figure 5.13E

Seurat-defined differential expression of genes between 2.Ly6c2$^+$CEM and 3.CEM populations identified in Figure 5.13 by WNN-clustering at a resolution of 0.5 from WT and Pepd$^{-/-}$ T cell populations subjected to scRNA-Seq in combination with ADT-antibody labelling. Results were filtered at a threshold of a log2FC of 0.25 and p-adjusted value of 0.05. pct.1 represents 2.Ly6c2$^+$CEM and pct.2 represents 3.CEM.2.

	avg_log2FC	pct.1	pct.2	p_val_adj
Ly6c2	2.064456039	0.932	0.251	2.00E-60
Rps19	0.830955583	1	0.997	4.48E-51
Rpl23	0.686740948	1	0.993	1.35E-50
Rps21	0.629845945	1	0.993	9.50E-49
Rplp1	0.660241859	1	1	1.04E-48
Rpl13	0.705969898	1	0.99	1.51E-48
Rps5	0.746360211	1	0.99	1.25E-47
Rps12	0.8719792	1	0.993	7.39E-47
Rps24	0.546491817	1	1	3.62E-46
Rpsa	0.687838989	1	0.993	3.39E-45
Rpl5	0.696628711	1	0.986	2.59E-44
Rpl39	0.685385886	1	0.997	3.20E-44
Rpl14	0.875551928	1	0.942	5.26E-44
Rps16	0.596054859	1	0.997	5.86E-44
Rps2	0.787648117	1	0.986	7.17E-44
Rps23	0.577226513	1	0.997	3.77E-43
Rpl17	0.601694481	1	0.99	8.25E-42
Rpl36a	0.796330871	1	0.969	1.38E-41
Smc4	-1.449008746	0.757	0.946	3.68E-40
Rps6	0.68698445	1	0.99	1.44E-39
Tpt1	0.492247577	1	1	1.50E-39
Rpl12	0.62532125	1	0.997	1.27E-38
Rplp2	0.527047321	1	1	3.35E-38
Rps18	0.65957334	1	0.983	4.15E-38
Rpl18a	0.588826799	1	0.986	7.09E-38
Rps7	0.601755628	1	0.997	3.03E-37
Rps4x	0.626356315	1	0.997	1.39E-36
Rpl30	0.518582633	1	0.997	2.36E-36
Rpl27a	0.575580498	1	0.986	3.52E-36
Rps20	0.644381253	1	0.993	3.69E-36
Rps10	0.551279859	1	0.99	1.47E-35
Rpl3	0.658556348	0.997	0.966	1.70E-35
Ift80	-1.606205515	0.262	0.715	5.61E-35
Rps8	0.557873581	1	1	1.11E-33
Rpl38	0.53553139	1	0.997	1.58E-33
Rps14	0.452203722	1	0.997	7.66E-33
Rps28	0.559043094	1	0.993	2.70E-32
Rpl32	0.568745778	1	0.997	4.17E-32
Rplp0	0.64089681	1	0.969	2.12E-31
Rps27	0.50731388	1	0.997	3.91E-31

Rps29	0.469855517	1	0.997	1.86E-30
Il18r1	1.195323969	0.576	0.092	5.95E-30
Rpl6	0.562532784	1	0.973	1.69E-29
Rpl13a	0.435677818	1	0.99	1.95E-29
Rps27a	0.486959227	1	0.993	5.47E-29
Rpl8	0.509967188	1	0.993	2.91E-28
Rps15	0.47030678	1	1	4.27E-28
Eef1b2	0.628067076	1	0.963	6.15E-28
Rpl37a	0.434985256	1	1	7.05E-28
Rps9	0.447431361	1	0.997	2.24E-27
Ccl5	1.772876052	0.748	0.305	3.11E-27
Rps3	0.473976944	1	0.993	9.62E-27
Il7r	1.09099395	0.864	0.393	1.64E-26
Rps13	0.47201494	1	0.986	2.78E-26
Rps15a	0.451899561	1	0.997	3.01E-26
Itga4	-1.600264999	0.447	0.783	4.98E-26
Gnb2l1	0.509080055	1	0.99	1.03E-24
Rpl9	0.453715458	1	0.993	2.26E-24
Rpl23a	0.506627826	1	0.983	2.79E-22
Rpl34	0.44851524	1	0.993	6.78E-22
Eef1a1	0.356393442	1	0.997	4.25E-21
Malat1	-0.827486008	1	1	8.12E-21
Cxcr3	0.863294689	0.453	0.071	1.01E-20
Rpl22	0.466808033	1	0.98	1.41E-20
Il18rap	0.805723109	0.44	0.064	1.57E-20
Bcl2	0.915468027	0.851	0.536	1.86E-20
Rpl35a	0.392362173	1	1	2.33E-20
Rpl10a	0.490747809	1	0.969	3.35E-20
Rpl37	0.449617454	1	0.986	7.12E-20
Rps3a1	0.41037378	1	0.993	1.67E-19
Myb	-1.538308458	0.129	0.464	5.30E-19
Rpl4	0.519900443	0.997	0.963	6.90E-19
mt-Nd2	0.442443401	1	0.997	8.37E-19
Npm1	0.62462083	0.99	0.881	2.40E-18
Ctsw	0.739777604	0.793	0.349	3.00E-18
Rpl21	0.396686669	1	0.997	3.59E-18
Sox4	-1.642466743	0.029	0.322	4.09E-18
Rpl19	0.34733907	1	0.997	5.70E-18
Arl4c	0.649897303	0.955	0.742	8.92E-18
Slamf6	-1.316115467	0.437	0.695	1.10E-17
Cd8a	0.847642561	0.851	0.441	2.25E-17
H3f3b	-0.802080359	0.877	0.919	2.89E-17
1700025G04Rik	0.73647422	0.375	0.047	3.89E-17
Rpl7a	0.508318528	1	0.946	4.40E-17
Rpl18	0.387370394	1	0.997	5.42E-17
Rpl26	0.418184313	1	0.983	6.91E-17
Eef1g	0.531306611	0.994	0.925	1.12E-16
Cd8b1	0.870885143	0.816	0.441	5.39E-16

Rpl36	0.431083896	1	0.98	1.10E-15
Rpl41	0.341787668	1	0.997	5.87E-15
Rps25	0.398006529	1	0.969	5.89E-14
Ifitm10	0.617290227	0.333	0.051	1.31E-13
Rpl35	0.478296411	1	0.929	1.46E-13
Celf2	-0.729273993	0.883	0.898	2.35E-13
Rpl11	0.383286815	1	0.986	9.66E-13
Rpl10	0.430264377	1	0.946	1.03E-12
Shisa5	-0.495297616	0.997	0.973	1.85E-12
Rpl29	0.50422178	0.994	0.912	1.88E-12
Btg1	-0.583407507	0.971	0.976	2.24E-12
Thy1	0.521522137	0.99	0.702	5.03E-12
Clec2d	-0.816034956	0.783	0.82	5.04E-12
Klrk1	1.108005697	0.249	0.024	9.93E-12
Ahnak	0.667552369	0.748	0.4	1.20E-11
Ets1	-0.603626408	0.968	0.973	1.95E-11
Hcst	0.574027356	0.951	0.702	2.63E-11
Rps26	0.351477335	1	0.99	3.74E-11
Samd3	0.596931358	0.35	0.075	3.84E-11
Ccr9	-1.306423305	0.032	0.251	4.15E-11
Ctla2a	0.81247128	0.495	0.197	7.29E-11
Actb	-0.340339819	1	0.993	2.46E-10
F2r	0.485308879	0.307	0.058	3.15E-10
Ikzf2	-1.613041841	0.33	0.573	3.36E-10
Tcf7	-0.541484876	0.971	0.942	3.73E-10
Il2rb	0.560301272	0.731	0.383	4.17E-10
Gnai2	-0.583041251	0.854	0.898	6.04E-10
Aim1	0.526809905	0.333	0.075	7.81E-10
Nrip1	-0.967807271	0.324	0.553	7.97E-10
Rpl24	0.36352719	1	0.983	1.49E-09
Klra7	0.6661693	0.201	0.014	3.90E-09
Cbl	-0.739899091	0.735	0.817	4.67E-09
Hspe1	0.467516552	0.945	0.712	7.05E-09
Tspan32	-0.859979581	0.188	0.424	7.23E-09
Fgf13	0.504859319	0.369	0.105	7.54E-09
Lrp10	-0.74816764	0.379	0.583	8.01E-09
Rps11	0.327309472	1	0.986	9.00E-09
Sesn3	-0.713500783	0.583	0.722	1.18E-08
Rpl22l1	0.53617823	0.942	0.736	2.20E-08
Ptms	-0.993398515	0.078	0.288	2.31E-08
Fau	0.260595389	1	0.993	2.38E-08
Rps12-ps3	0.57370963	0.693	0.403	3.90E-08
St8sia6	-0.623673052	0.006	0.159	8.49E-08
Lbh	-0.631234146	0.706	0.783	1.06E-07
Tox	-0.994521486	0.243	0.454	1.38E-07
Ipcef1	-0.682439684	0.579	0.695	1.83E-07
Racgap1	0.42255928	0.356	0.112	2.52E-07
Sptbn1	-0.642872144	0.605	0.722	3.15E-07

mt-Nd5	0.467400646	0.968	0.841	5.85E-07
Prrc2c	-0.542129669	0.916	0.895	6.23E-07
Lat	-0.575934157	0.822	0.854	7.12E-07
Rhoh	-0.640075689	0.731	0.807	7.51E-07
Cd53	-0.520971739	0.89	0.908	8.24E-07
S100a6	0.903141938	0.414	0.163	8.80E-07
Kcnc1	-0.752697037	0.049	0.224	9.57E-07
Wdr89	0.435018802	0.816	0.549	9.93E-07
Tbx21	0.376101489	0.265	0.058	1.00E-06
Utrn	-0.608139209	0.644	0.736	1.03E-06
Gzmm	0.483571636	0.152	0.007	1.20E-06
Hopx	0.475211275	0.492	0.22	1.31E-06
Amica1	0.491234958	0.256	0.058	1.53E-06
Adrbk1	-0.562890378	0.738	0.817	1.77E-06
Wdr95	0.388576728	0.181	0.02	1.82E-06
Git2	-0.623859286	0.673	0.732	2.36E-06
Id3	-1.060763964	0.32	0.502	2.65E-06
Dmrta1	0.284946363	0.139	0.003	2.68E-06
Cd200	-0.401888852	0.003	0.132	2.84E-06
H3f3a	-0.458470494	0.932	0.942	3.02E-06
Plek	0.440274433	0.301	0.088	4.62E-06
Ptpn6	0.472736762	0.647	0.373	4.85E-06
Nkg7	0.423502774	0.955	0.769	5.11E-06
Cd27	-0.559275042	0.828	0.854	5.33E-06
St3gal6	0.432419371	0.427	0.18	5.37E-06
Dkc1	0.382130922	0.492	0.21	6.33E-06
Gimap6	-0.512620214	0.838	0.875	7.44E-06
Dennd2d	-0.69360351	0.353	0.525	7.62E-06
Cd44	0.439533588	0.453	0.197	1.08E-05
Ramp1	-0.537203338	0.055	0.22	1.21E-05
Rpl28	0.289138998	1	0.986	1.30E-05
Ypel3	-0.62957476	0.528	0.62	1.84E-05
Fcgrt	0.39625288	0.126	0.003	1.99E-05
Rpl7	0.25119596	1	0.993	2.11E-05
Lag3	-0.493079808	0.006	0.129	2.13E-05
Itgb1	0.423388484	0.505	0.244	2.26E-05
Pecam1	-0.767209845	0.317	0.502	2.36E-05
Pou2f2	-1.01558287	0.317	0.485	3.74E-05
Klrd1	0.33196598	0.706	0.386	4.16E-05
Mpp1	-0.607851324	0.159	0.349	4.22E-05
Xcl1	0.289304721	0.204	0.041	4.73E-05
H2-K1	-0.285780878	1	1	5.59E-05
Sidt1	0.435449305	0.761	0.481	5.77E-05
Ncor1	-0.532933853	0.828	0.858	6.09E-05
Eef2	0.279878324	0.994	0.946	8.99E-05
Sema4a	0.437786325	0.482	0.234	0.000105779
2310001H17Rik	-0.783303478	0.285	0.454	0.000106931
Izumo1r	-0.474941749	0.042	0.186	0.000135312

F2rl1	0.400956067	0.304	0.105	0.000154336
Foxp1	-0.504316681	0.871	0.902	0.000174605
Qrfp	0.321976047	0.152	0.02	0.000188425
Cd84	-0.547365125	0.534	0.675	0.000191085
Slfn5	-0.556249503	0.068	0.227	0.000196684
Gramd3	0.431051397	0.709	0.397	0.000199592
Adgrg5	0.336780323	0.285	0.092	0.000203128
Gm11808	0.452319768	0.618	0.366	0.000234481
Pde7a	-0.617638934	0.647	0.742	0.00028899
Rpl15	0.34498139	0.932	0.763	0.000345677
Rpl31	0.295453582	0.99	0.929	0.000441249
Il16	-0.546954009	0.515	0.654	0.000462689
Ephx1	-0.474798056	0.104	0.268	0.000572689
Hmha1	-0.468967756	0.913	0.922	0.000577926
Cst7	0.370243349	0.521	0.261	0.000611567
Son	-0.459921846	0.858	0.861	0.00071095
AW112010	0.298766361	0.951	0.746	0.0007652
Nhp2	0.292213522	0.434	0.2	0.000786823
Runx1	-0.634166275	0.265	0.42	0.000868222
Tcf4	-0.563018233	0.019	0.136	0.000879687
Trp53inp1	-0.663947226	0.531	0.634	0.000931995
Setd2	-0.59512951	0.479	0.603	0.001012389
Ankrd12	-0.693908449	0.657	0.742	0.001123893
Mcl1	-0.522806959	0.783	0.82	0.001255665
Gm8369	-0.697381285	0.382	0.519	0.001262256
Bbc3	0.275739048	0.162	0.031	0.001330466
Myc	0.33249976	0.294	0.108	0.00133891
Kdm5b	-0.596904682	0.262	0.42	0.001521312
Ablim1	-0.398793687	0.948	0.942	0.001540053
Bcl11b	-0.642114926	0.809	0.824	0.001695672
Zfpm1	-0.536920622	0.149	0.315	0.00170995
Tpm4	-0.65576601	0.472	0.576	0.001844633
Cd9	-0.549341743	0.084	0.231	0.002055335
Hid1	0.378321161	0.272	0.102	0.00207188
Elk3	-0.635929537	0.197	0.356	0.00214074
Lcp2	-0.578937033	0.521	0.62	0.0022083
Ccr2	0.369606056	0.129	0.017	0.00234512
Ptprc	-0.289228286	0.997	0.997	0.002408497
Basp1	-0.37472532	0.013	0.115	0.002825292
Gimap1	-0.550433163	0.699	0.729	0.002947175
Gm10073	0.40033155	0.45	0.244	0.002998626
Rpl27	0.253070998	1	0.963	0.003102388
Chsy1	0.319108045	0.395	0.186	0.00335608
Msi2	-0.533830831	0.43	0.559	0.003825356
Pfn1	-0.304487792	0.994	0.98	0.003842045
Myo1f	0.336865494	0.362	0.163	0.004079691
Ms4a4b	-0.290644241	1	0.986	0.004083709
Luc7l2	-0.50787592	0.848	0.868	0.004889625

Mettl1	0.28979627	0.204	0.058	0.005153986
D8Ertd82e	0.274796987	0.207	0.061	0.005181875
Akap13	-0.39949534	0.919	0.905	0.005299704
Ifi27l2a	-0.705502046	0.366	0.515	0.005794993
Ssbp3	-0.657800211	0.246	0.393	0.005856017
2010107E04Rik	0.348062569	0.816	0.617	0.006003563
Stk17b	-0.430327901	0.906	0.912	0.007053628
Cd2	0.3559159	0.764	0.478	0.00737237
Eif5a	0.359307668	0.78	0.569	0.007487484
Il6ra	0.373262561	0.463	0.244	0.00788431
Ptprcap	-0.375684924	0.903	0.878	0.008006503
Arl6ip1	-0.435821712	0.744	0.78	0.008538836
Malt1	0.318576175	0.414	0.19	0.008587877
Pyhin1	-0.547690646	0.537	0.61	0.008815704
Sla	0.361782563	0.547	0.319	0.009380494
Pnrc1	-0.5055419	0.634	0.681	0.009917896
Dpcd	0.309173285	0.379	0.183	0.010112652
Hsp90ab1	0.264488114	0.99	0.942	0.012542091
Mar-07	-0.568911286	0.456	0.59	0.012836164
Tnik	-0.632865318	0.385	0.508	0.013848389
Lta4h	-0.508512344	0.23	0.373	0.015049341
Stk4	-0.368317655	0.735	0.81	0.015279567
Ube2d2a	-0.457653818	0.573	0.658	0.015681662
Erbb2ip	-0.52377391	0.414	0.549	0.015806299
Fbl	0.297551954	0.544	0.298	0.016915178
Ltb	-0.36673023	0.955	0.925	0.018015128
Gm14085	-0.594489463	0.126	0.275	0.018524408
AI504432	-0.614204656	0.282	0.427	0.018734578
Il4ra	0.291312674	0.46	0.244	0.019185675
Laptm5	-0.296890405	0.997	0.99	0.019658709
Pou2af1	-0.420985526	0.026	0.129	0.020284639
Larp1	0.349705305	0.663	0.42	0.021495257
Nme1	0.335446702	0.66	0.414	0.02162849
Actg1	-0.359021656	0.987	0.976	0.021895918
Rbm39	-0.359604741	0.984	0.963	0.02204676
Dpp4	-0.568150262	0.285	0.437	0.022168894
Bmyc	0.272963207	0.201	0.064	0.025837208
Smek2	-0.467621357	0.479	0.58	0.027250058
Sp100	-0.370024747	0.961	0.919	0.028513675
H2-Q7	-0.339962697	0.997	0.983	0.032457184
Klhl24	-0.548079087	0.172	0.312	0.03262227
Fam63b	-0.603966354	0.317	0.431	0.033878509
Sntb2	0.26256635	0.256	0.102	0.035158619
Ran	0.307508932	0.793	0.536	0.035425721
St8sia1	-0.438337621	0.084	0.214	0.035826209
Prkch	-0.51120744	0.427	0.542	0.03836561
Pa2g4	0.309030713	0.437	0.231	0.03843624
Uba52	0.367968104	0.761	0.512	0.039132342

Klra6	0.253682915	0.113	0.017	0.041908033

Appendix F Differential gene expression analysis between splenic CD8^{+} effector populations, 4.Exhausted effector and 5.Terminal effector as visualised in Figure 5.13F

Seurat-defined differential expression of genes between effector populations, 4.Exhausted effector and 5.Terminal effector identified in Figure 5.13 by WNN-clustering at a resolution of 0.5 from WT and Pepd$^{-/-}$ T cell populations subjected to scRNA-Seq in combination with ADT-antibody labelling. Results were filtered at a threshold of a log2FC of 0.25 and p-adjusted value of 0.05. pct.1 represents 4.Exhausted Effector and pct.2 represents 5.Terminal Effector.

	avg_log2FC	pct.1	pct.2	p_val_adj
Zeb2	-2.352240857	0.15	0.61	4.54E-23
Ctla2a	1.446830656	0.744	0.269	5.40E-18
S1pr5	-1.534633788	0.033	0.363	2.42E-15
Il18rap	-1.525744348	0.154	0.516	2.18E-14
Cx3cr1	-1.566550878	0.207	0.582	5.01E-14
Arap2	1.205465662	0.663	0.302	6.54E-11
Ly6c2	-1.872479307	0.122	0.423	3.06E-10
Cd4	-1.222557315	0.045	0.291	5.22E-09
Rpl37a	0.377120926	1	0.989	1.20E-08
Rps18	0.476977984	0.988	0.973	2.66E-08
Rpl32	0.412234061	0.996	0.973	1.34E-07
Rpl27a	0.398424448	0.996	0.973	2.14E-07
Arl4c	-0.873920368	0.614	0.797	2.40E-07
Il18r1	-1.180848274	0.118	0.385	2.50E-07
Rpl12	0.466237809	0.992	0.956	4.56E-07
Tox	0.67999942	0.675	0.291	4.72E-07
S100a6	0.939164325	0.837	0.637	5.18E-07
Adam19	0.839745297	0.463	0.143	5.56E-07
Rps14	0.349815201	1	0.995	7.13E-07
Coch	1.03453872	0.244	0.016	9.66E-07
Eef1b2	0.530401293	0.963	0.868	1.10E-06
Gzmk	0.746073066	0.703	0.352	1.63E-06
Ahnak	-0.826917508	0.78	0.896	1.77E-06
Klrg1	-0.924032224	0.028	0.225	2.17E-06
Rora	-1.0696047	0.146	0.39	5.34E-06
Rps21	0.340967718	0.996	0.984	5.74E-06
Kcnj8	-0.721135437	0.008	0.17	1.09E-05
Eef1a1	0.32368476	0.996	0.984	1.36E-05

Rpl18a	0.371069796	0.996	0.984	1.55E-05
Rplp1	0.302256352	0.996	1	2.25E-05
Rps15a	0.382103643	0.992	0.989	2.75E-05
Vim	-0.955517386	0.354	0.593	2.95E-05
Rps24	0.286894888	1	0.989	5.50E-05
Rpl37	0.382473561	0.988	0.962	6.38E-05
Fau	0.314674919	0.996	0.973	6.88E-05
Rpl17	0.304238302	0.996	0.995	7.98E-05
Rps5	0.357392407	0.988	0.984	9.37E-05
Rpl36	0.421441979	0.984	0.945	0.000116891
Rpl22	0.351129766	0.996	0.967	0.000139092
Cd226	-0.853225325	0.061	0.247	0.000263911
Rpl38	0.317032827	0.992	0.973	0.000294921
Spn	-0.617422156	0.736	0.835	0.00030044
Rpl18	0.334015941	0.988	0.984	0.00037215
Rpl9	0.333543612	0.988	0.989	0.000398384
Xcl1	0.854481325	0.203	0.022	0.000453208
Sgk1	-0.933826407	0.089	0.28	0.000506619
Rps27	0.293427139	0.996	0.995	0.000533103
Rpl5	0.324383352	0.992	0.978	0.000570235
Zmiz1	-0.829893418	0.252	0.467	0.000712264
Gzma	-2.415372293	0.138	0.335	0.000719367
Cd3d	0.516900571	0.894	0.797	0.000844487
Rpl23	0.344610493	1	0.978	0.001283143
Rps28	0.361487936	0.988	0.918	0.001451654
Rara	-0.80048278	0.069	0.242	0.001465534
Klrc2	-0.925924657	0.041	0.198	0.00168756
Rpl30	0.287667718	0.988	0.995	0.001725441
Rps19	0.328040766	0.988	0.984	0.001813511
Rps9	0.310544388	1	0.984	0.001825384
Pdcd1	0.675013469	0.26	0.06	0.001942493
Rpl34	0.33079885	0.992	0.973	0.002002944
Klrd1	-0.9057302	0.354	0.566	0.002775014
Rps23	0.274207322	0.996	0.984	0.002781296
Eomes	0.553905693	0.687	0.412	0.003513394
Rpsa	0.32004728	0.996	0.989	0.003938616
Lgals1	-1.007894262	0.606	0.725	0.004121184
Cxcr3	0.583299889	0.407	0.165	0.00449347
Rps13	0.272528261	0.996	0.984	0.005803122
Rpl21	0.32457844	0.988	0.967	0.00791475
Rps10	0.265105994	1	0.995	0.011695807
Rps3	0.30851599	0.988	0.956	0.012054569

Rps27a	0.262871147	0.992	0.978	0.013394285
Ms4a4b	0.33267379	0.992	0.956	0.014028786
Iqgap1	-0.468788604	0.793	0.835	0.014054193
Tbc1d4	0.597152435	0.276	0.088	0.015565332
Rpl3	0.351937416	0.988	0.923	0.019865424
S100a11	0.65834221	0.756	0.571	0.020282778
Plscr1	0.475371827	0.171	0.022	0.020498132
Rpl13	0.315435241	0.988	0.967	0.023022118
Rps16	0.252565993	1	0.984	0.024190859
Rps20	0.317002853	0.984	0.984	0.025563343
Il2rb	0.629281619	0.703	0.478	0.026603912
Serpina3g	0.708355102	0.435	0.198	0.027340743
Shisa5	0.374367561	0.98	0.885	0.046541627

Appendix G Differential surface phenotype of CD8+ populations identified by Citrus clustering analysis

Citrus PAMR association model identified features in this table as differentially expressed between WT and Pepd-/- populations, clusters are specified by numbers in the clustering tree graphs in Figure 5.16.

	CD62L expression																	
	94932	94911	94948	94996	94873	94888	94973	94920	94865	94958	94814	94953	94944	94941	94866	94863	94834	94970
WT1	-0.61	-0.32	-0.41	-0.10	-0.50	-0.63	0.04	-0.38	-0.63	-0.54	-0.01	-0.65	-0.54	-0.63	-0.56	-0.26	0.01	-0.49
WT2	-0.56	-0.32	-0.15	0.42	-0.37	-0.46	0.15	-0.32	-0.51	-0.33	-0.08	-0.48	-0.41	-0.43	-0.83	-0.30	0.27	-0.34
WT3	-0.44	-0.03	-0.24	0.06	-0.24	-0.30	0.11	-0.28	-0.26	-0.31	0.08	-0.48	-0.43	-0.43	-0.80	-0.34	0.12	-0.29
WT4	-0.71	-0.22	-0.41	-0.61	-0.61	-0.70	-0.05	-0.34	-0.65	-0.52	-0.18	-0.57	-0.60	-0.52	-0.92	-0.43	-0.17	-0.57
WT5	-0.61	-0.07	-0.46	-0.37	-0.32	-0.53	-0.11	-0.35	-0.59	-0.50	0.07	-0.67	-0.70	-0.91	-0.85	-0.62	-0.14	-0.49
KO1	-0.98	-0.83	-0.81	-1.10	-0.83	-0.91	-0.29	-0.57	-1.02	-0.79	-0.57	-0.83	-0.83	-0.91	-1.27	-0.73	-0.33	-0.78
KO2	-1.08	-0.95	-0.91	-0.92	-1.06	-1.08	-0.55	-0.75	-1.00	-0.92	-0.56	-0.95	-0.96	-0.98	-1.18	-0.83	-0.57	-0.92
KO3	-1.07	-0.76	-0.68	-1.45	-0.75	-0.90	-0.43	-0.59	-0.85	-0.71	-0.47	-0.83	-0.84	-0.99	-1.03	-0.86	-0.23	-0.60
KO4	-1.26	-0.61	-0.83	-0.97	-1.00	-1.07	-0.53	-0.69	-0.92	-0.97	-0.20	-0.94	-1.08	-1.16	-1.13	-1.08	-0.45	-0.76
KO5	-1.10	-1.11	-0.92	-0.96	-0.99	-1.08	-0.29	-0.74	-1.07	-0.79	-0.71	-0.91	-0.85	-1.10	-1.20	-0.59	-0.39	-0.81

	Ly6c expression			PD1 expression					CD44 expression		CD27 expression
	94956	94935		94965	94982	94994	94978		94983		94873
WT1	0.21	0.31		3.28	3.42	1.68	3.32		0.49		-0.62
WT2	0.58	0.46		2.89	3.01	1.62	3.02		0.52		-0.62
WT3	0.34	-0.03		2.80	3.06	2.13	2.84		0.58		-0.35
WT4	-0.11	0.15		3.67	3.76	3.06	3.73		0.74		-0.78
WT5	0.77	0.02		2.90	3.32	2.41	3.32		0.52		-0.34
KO1	-0.56	-0.54		4.37	4.86	4.08	4.48		1.20		-0.99
KO2	-0.30	0.07		4.06	4.19	3.31	4.12		0.96		-1.12
KO3	-0.60	-0.60		4.98	5.24	5.18	5.14		0.81		-0.83
KO4	-0.40	-0.60		4.59	4.69	4.05	4.72		1.16		-0.81
KO5	-0.60	-0.52		3.61	3.72	3.02	3.63		1.32		-1.01

Appendix H RNA cluster markers of WNN-clustered CD8$^+$ CD45.2$^+$ chimeric subsetted populations visualised in Figure 6.4

Top 10 differentially expressed markers for each WNN-defined splenic T cell cluster from WT and Pepd$^{-/-}$ CD45.2$^+$ populations isolated respectively from recipients of WT:WT and WT:Pepd$^{-/-}$ BM as described in Figure 6.4 at a resolution of 0.6, filtered at a log2FC threshold of 0.25 and adjusted p value of 0.05. pct represents the percentage of cells where the gene is detected in the first (pct.1 – named in cluster column) or second (pct.2 – rest of cells not in cluster) group.

	gene	avg_log2FC	pct.1	pct.2	p_val_adj	cluster
1	Rps8	0.391606014	1	1	1.45E-224	0.Naive
2	Rps4x	0.372991492	1	1	1.44E-197	0.Naive
3	Rps20	0.37633219	1	1	6.06E-154	0.Naive
4	Npc2	0.453224381	0.988	0.915	1.31E-88	0.Naive
5	Igfbp4	0.729802351	0.612	0.353	7.77E-74	0.Naive
6	Cd8a	0.374288276	0.971	0.839	1.49E-47	0.Naive
7	Ramp1	0.390791231	0.498	0.288	1.09E-42	0.Naive
8	Rgcc	0.364196164	0.638	0.418	1.18E-37	0.Naive
9	Dapl1	0.570749186	0.584	0.441	6.12E-26	0.Naive
10	Gm12840	0.417063157	0.43	0.333	1.25E-10	0.Naive
11	Malat1	0.515143629	1	0.999	8.46E-67	1.Satb1+Naïve
12	Satb1	0.426718262	0.917	0.761	1.15E-24	1.Satb1+Naïve
13	Ccr7	0.45880391	0.828	0.678	1.86E-22	1.Satb1+Naïve
14	Ccr9	0.500641558	0.492	0.297	5.65E-22	1.Satb1+Naïve
15	Fam241a	0.418556309	0.606	0.417	1.04E-21	1.Satb1+Naïve
16	1700062C10Rik	0.478043859	0.141	0.047	7.01E-17	1.Satb1+Naïve
17	Il7r	0.458789199	0.861	0.739	3.06E-14	1.Satb1+Naïve
18	2810474O19Rik	0.428920847	0.713	0.578	4.84E-14	1.Satb1+Naïve
19	Tsc22d3	0.400101913	0.633	0.522	3.82E-08	1.Satb1+Naïve
20	Nfkbia	0.446694075	0.681	0.589	0.002004527	1.Satb1+Naïve
21	Ly6c2	2.38963116	0.96	0.288	1.48E-277	2.Ly6c2+CEM
22	Samd3	0.754539602	0.481	0.061	2.38E-164	2.Ly6c2+CEM
23	Cxcr3	0.795612795	0.662	0.139	1.12E-146	2.Ly6c2+CEM
24	Ctla2a	1.122410102	0.722	0.244	3.45E-112	2.Ly6c2+CEM
25	Il2rb	1.026344714	0.781	0.328	5.80E-99	2.Ly6c2+CEM
26	Bcl2	0.982441049	0.889	0.606	1.55E-72	2.Ly6c2+CEM
27	Ctsw	0.681585974	0.887	0.615	1.09E-52	2.Ly6c2+CEM
28	Ms4a4c	0.749539537	0.773	0.44	9.49E-50	2.Ly6c2+CEM
29	Il7r	0.709030786	0.922	0.737	1.23E-41	2.Ly6c2+CEM
30	Klrk1	0.651746578	0.298	0.094	5.68E-34	2.Ly6c2+CEM
31	Myb	1.45189072	0.41	0.042	3.19E-152	3.CEM
32	Id3	1.430037815	0.628	0.25	1.57E-68	3.CEM
33	Slamf6	1.192932609	0.819	0.514	2.39E-54	3.CEM

34	Smc4	1.06532758	0.894	0.752	1.15E-44	3.CEM
35	Ptms	0.691466892	0.367	0.133	7.99E-32	3.CEM
36	Pou2f2	0.81723587	0.543	0.27	2.39E-29	3.CEM
37	Clec2d	0.674691006	0.848	0.675	1.33E-24	3.CEM
38	Izumo1r	0.673584806	0.34	0.153	3.91E-19	3.CEM
39	Gpr183	0.970984071	0.476	0.321	3.56E-12	3.CEM
40	Slamf7	0.732796549	0.229	0.113	9.27E-08	3.CEM
41	Gzmk	2.657370307	0.866	0.059	0	4.Exhausted effector
42	Ctla2a	2.588588119	0.857	0.254	1.10E-162	4.Exhausted effector
43	Ccl5	3.421774777	0.997	0.792	1.40E-157	4.Exhausted effector
44	Nkg7	2.018662005	1	0.932	6.67E-152	4.Exhausted effector
45	Cxcr3	1.539312937	0.71	0.158	1.11E-148	4.Exhausted effector
46	S100a6	2.525653358	0.869	0.301	1.65E-146	4.Exhausted effector
47	Ccr2	1.442545209	0.455	0.052	1.71E-141	4.Exhausted effector
48	Itga4	1.934379345	0.938	0.566	1.40E-119	4.Exhausted effector
49	S100a10	1.442212063	0.991	0.966	1.99E-109	4.Exhausted effector
50	Lgals1	1.509040461	0.903	0.495	1.59E-89	4.Exhausted effector
51	Rpl23a	0.479333363	1	0.999	3.26E-53	5.CD25+Naïve
52	Malat1	0.476685284	1	0.999	4.20E-22	5.CD25+Naïve
53	Satb1	0.368072079	0.924	0.776	4.76E-09	5.CD25+Naïve
54	Myh9	0.316695921	0.934	0.861	2.77E-08	5.CD25+Naïve
55	Rapgef6	0.340753909	0.92	0.815	2.82E-07	5.CD25+Naïve
56	Macf1	0.365969979	0.788	0.653	1.41E-05	5.CD25+Naïve
57	Mycbp2	0.393665409	0.844	0.697	1.66E-05	5.CD25+Naïve
58	Map4k4	0.345398874	0.712	0.536	1.92E-05	5.CD25+Naïve
59	Kcnq1ot1	0.407369391	0.618	0.492	0.006860626	5.CD25+Naïve
60	Utrn	0.332464335	0.76	0.634	0.010431241	5.CD25+Naïve
61	Zeb2	2.630378379	0.808	0.036	0	6.Terminal effector
62	Cx3cr1	2.166234843	0.716	0.037	0	6.Terminal effector
63	Klrk1	2.636421167	0.745	0.086	8.08E-200	6.Terminal effector
64	Klre1	2.061656208	0.529	0.053	1.75E-145	6.Terminal effector
65	Gzma	4.386126939	0.625	0.104	5.09E-125	6.Terminal effector
66	Lgals1	2.852153408	0.986	0.502	3.99E-118	6.Terminal effector

67	Ahnak	2.180086549	0.928	0.324	1.01E-115	6.Terminal effector
68	Ccl5	3.034031237	1	0.797	1.54E-103	6.Terminal effector
69	S100a6	2.310219226	0.889	0.315	4.82E-99	6.Terminal effector
70	Id2	2.103193553	0.88	0.448	2.62E-75	6.Terminal effector
71	Klrg1	1.741135255	0.556	0.041	2.22E-86	7.KLRG1hi effector
72	Zeb2	1.70386535	0.514	0.066	2.22E-44	7.KLRG1hi effector
73	S100a4	2.275086107	0.653	0.133	3.26E-39	7.KLRG1hi effector
74	Ahnak	1.985876677	0.861	0.345	1.07E-27	7.KLRG1hi effector
75	S100a6	1.927579737	0.833	0.335	9.56E-24	7.KLRG1hi effector
76	Lgals1	2.230556533	0.889	0.52	2.79E-22	7.KLRG1hi effector
77	Ikzf2	2.305840631	0.431	0.119	1.83E-14	7.KLRG1hi effector
78	Capg	1.704545771	0.389	0.122	7.11E-10	7.KLRG1hi effector
79	Itgb1	1.868657597	0.569	0.266	1.49E-09	7.KLRG1hi effector
80	Gzma	1.774685171	0.306	0.126	0.012879503	7.KLRG1hi effector

Appendix I Differential gene expression analysis between CD45.2^{+} chimeric splenic CD8^{+} effector populations, 4.Exhausted effector and 6.Terminal effector as visualised in Figure 6.4D

Seurat-defined differential expression of genes between chimeric CD45.2^{+} effector populations, 4.Exhausted effector and 6.Terminal effector isolated respectively from recipients of C57BL/BJ WT:WT and WT:Pepd$^{-/-}$ BM and subjected to scRNA-Seq in combination with ADT-antibody labelling as described in Figure 6.4 at a resolution of 0.6. Results were filtered at a threshold of a log2FC of 0.25 and p-adjusted value of 0.05. pct.1 represents 4.Exhausted Effector and pct.2 represents 6.Terminal Effector.

	avg_log2FC	pct.1	pct.2	p_val_adj
Zeb2	-2.00981698	0.237	0.808	6.03E-44
Ly6c2	-2.225143016	0.206	0.779	7.74E-41
S1pr5	-1.460104785	0.016	0.457	8.78E-33
Klrk1	-1.831837356	0.255	0.745	1.18E-31
Lgals1	-1.149382205	0.903	0.986	5.96E-30
Kcnj8	-1.363657036	0.009	0.399	2.52E-28
Klrd1	-1.214163002	0.579	0.899	3.00E-26
Ctla2a	1.7395413	0.857	0.548	9.59E-26
Gzma	-3.233475049	0.212	0.625	4.37E-25
Cx3cr1	-1.313682619	0.312	0.716	1.10E-22
Itgb1	-1.261458425	0.439	0.779	1.45E-19
Gzmk	1.03574526	0.866	0.548	3.21E-19
Cxcr3	1.031824775	0.71	0.298	1.89E-17
Klf2	-0.675344664	0.956	0.995	9.14E-17
Klrc1	-1.213180516	0.159	0.5	5.78E-16
Cd3d	0.540896712	1	0.966	1.72E-13
Klre1	-1.327695309	0.202	0.529	5.27E-13
Ahnak	-0.764370512	0.763	0.928	5.53E-13
Il18rap	-0.911655788	0.252	0.572	1.81E-12
Id2	-0.973207883	0.726	0.88	2.98E-12
Igkc	1.044081624	0.38	0.067	9.34E-12
Cd27	0.734496185	0.875	0.558	1.88E-10
Dnajc15	-0.669391171	0.71	0.856	2.34E-10
Tox	0.878678743	0.623	0.284	4.81E-10
Cd28	0.720969287	0.804	0.534	1.28E-09

Cd226	-0.670341786	0.09	0.337	7.38E-09
Shisa5	0.492355743	0.988	0.952	6.78E-08
Klrg1	-0.898876003	0.199	0.452	9.18E-08
Sub1	0.545979259	0.969	0.918	2.03E-07
Rps15a	0.2607828	1	1	2.74E-07
Arl4c	-0.606098047	0.826	0.894	3.03E-07
Ms4a4b	0.348562652	1	1	1.10E-06
Vim	-0.675037717	0.72	0.885	1.19E-06
Ltb	0.623544859	0.928	0.822	1.72E-06
Klra9	-0.952128602	0.022	0.178	2.81E-06
Klrc2	-0.73067606	0.112	0.327	2.84E-06
Rpl18	0.261135777	0.997	1	3.05E-06
Tbx21	-0.665140754	0.171	0.389	4.71E-06
Ms4a6b	0.433771305	0.991	0.957	1.62E-05
Itga1	-0.534098142	0.006	0.13	1.74E-05
Fxyd5	-0.400097888	0.972	0.981	2.39E-05
Gm30211	0.448206104	0.159	0	2.62E-05
Lgals3	-0.829010446	0.227	0.447	3.38E-05
Gpr183	0.74798944	0.361	0.13	4.17E-05
Gstp3	0.522235783	0.312	0.087	4.65E-05
Gzmb	-0.620913606	0.271	0.519	6.44E-05
Sh3bgrl3	-0.374117374	0.981	0.99	0.000102605
Psmb8	0.335038183	0.978	0.952	0.000249134
Tspan3	0.542070074	0.411	0.168	0.000375957
Stard10	-0.567973841	0.146	0.327	0.0008774
Klrb1c	-0.445378805	0.006	0.106	0.001064422
Ccnd3	-0.529210808	0.67	0.798	0.001092666
Cd8b1	-0.443576628	0.935	0.928	0.001164209
Sp100	0.416700515	0.981	0.885	0.001197119
Pglyrp1	0.499550198	0.676	0.389	0.001239689
Ier3	0.633675689	0.393	0.173	0.001325376
Gabarapl2	-0.566388581	0.685	0.788	0.001367163
Sep-11	-0.610108416	0.364	0.543	0.001664515

Rap1b	-0.373265968	0.903	0.933	0.001844386
Ostf1	-0.39736481	0.819	0.918	0.002015582
Ccnd2	-0.466807568	0.769	0.856	0.002314444
Cmklr1	-0.27363645	0.006	0.101	0.002638243
Slamf6	0.630239977	0.427	0.207	0.002769638
Eomes	0.549309293	0.692	0.466	0.00301582
Lmo1	0.435404851	0.162	0.019	0.003145489
Lfng	-0.536500637	0.576	0.712	0.003168968
Ywhaq	-0.342572461	0.835	0.889	0.003415414
Reep5	-0.464481719	0.698	0.793	0.003434468
Maf	0.47961587	0.206	0.043	0.004318847
Dkkl1	-0.353909503	0.012	0.111	0.007171082
Cpne3	-0.496483513	0.118	0.284	0.007253449
Psme1	0.341556318	0.935	0.885	0.007264611
Cd5	0.557520416	0.598	0.38	0.008283152
Pacsin1	0.323519439	0.146	0.014	0.008858786
Prdx4	-0.341009658	0.025	0.135	0.009335629
Rasgef1b	0.416048757	0.181	0.034	0.011219561
Cd55	0.385589267	0.178	0.034	0.013125678
Gas7	0.443119253	0.184	0.038	0.013584667
Vmp1	0.53815214	0.555	0.317	0.015338792
Adam19	0.482603372	0.287	0.106	0.017347706
As3mt	-0.521490702	0.121	0.274	0.019973427
Ctsd	-0.352725691	0.925	0.957	0.02108454
Stmn1	-0.587021431	0.268	0.433	0.028591125
Kremen2	0.352497868	0.19	0.043	0.032039674
Rara	-0.452004294	0.171	0.327	0.033136433
Gtf2i	0.415275265	0.822	0.683	0.035560385
Trbc1	0.769646143	0.829	0.707	0.03595059
Ifngas1	0.292399458	0.131	0.014	0.047078311
Zmiz1	-0.485646112	0.212	0.38	0.048704147